TU Delft

Delft University of Technology

Thermal Shock Damage in Construction Materials

Impact and prediction of concrete and natural rocks behavior

França de Mendonça Filho, F.

DOI
10.4233/uuid:db227550-067e-4a46-8ce1-86a8ecd483f9

Publication date
2024

Document Version
Final published version

Citation (APA)
França de Mendonça Filho, F. (2024). *Thermal Shock Damage in Construction Materials: Impact and prediction of concrete and natural rocks behavior*. [Dissertation (TU Delft), Delft University of Technology]. https://doi.org/10.4233/uuid:db227550-067e-4a46-8ce1-86a8ecd483f9

Important note
To cite this publication, please use the final published version (if applicable).
Please check the document version above.

Copyright
Other than for strictly personal use, it is not permitted to download, forward or distribute the text or part of it, without the consent of the author(s) and/or copyright holder(s), unless the work is under an open content license such as Creative Commons.

Takedown policy
Please contact us and provide details if you believe this document breaches copyrights.
We will remove access to the work immediately and investigate your claim.

This work is downloaded from Delft University of Technology.
For technical reasons the number of authors shown on this cover page is limited to a maximum of 10.

THERMAL SHOCK DAMAGE IN CONSTRUCTION MATERIALS

IMPACT AND PREDICTION OF CONCRETE AND NATURAL ROCKS BEHAVIOR

THERMAL SHOCK DAMAGE IN CONSTRUCTION MATERIALS

IMPACT AND PREDICTION OF CONCRETE AND NATURAL ROCKS BEHAVIOR

Proefschrift

ter verkrijging van de graad van doctor
aan de Technische Universiteit Delft,
op gezag van de Rector Magnificus Prof. dr. ir. T.H.J.J. van der Hagen,
voorzitter van het College voor Promoties,
Monday 27, May 2024 at 15:00

door

Fernando FRANÇA DE MENDONÇA FILHO

Master of Science in Civil Engineering
Technische Universiteit Delft, Delft, Nederland,
geboren in Belém, Brazilië.

Dit proefschrift is goedgekeurd door de promotors.

Samenstelling promotiecommissie:

Rector Magnificus,	voorzitter
Dr. O. Çopuroğlu,	Technische Universiteit Delft, Promotor
Prof. dr. ir. H.E.J.G. Schlangen,	Technische Universiteit Delft, Promotor
Onafhankelijke leden:	
Prof. dr. ir. M.A.N. Hendriks,	Technische Universiteit Delft
Prof. dr. A. Noumowé,	CY Cergy Paris University
Prof. dr. A. Cwirzen,	Luleå University of Technology
Dr. ir. F.A. Veer,	Technische Universiteit Delft
Dr. K. Peterson,	University of Toronto
Prof.dr. H.M. Jonkers,	Technische Universiteit Delft (reservelid)



Keywords: Concrete spalling, thermal shock, high temperatures

Printed by: Gildeprint proefschrift

Front & Back: Cover and interior art done by Júlio Novaes Prado.

Copyright © 2024 by F.F. de M. Filho

ISBN 978-94-6496-123-2

An electronic version of this dissertation is available at
http://repository.tudelft.nl/.

To my wife, whom supported me for the entirety of this journey.

CONTENTS

Acknowledgements xi

Summary xiv

Samenvatting xvi

Listof Symbols xviii

I Introduction 1

1 General Introduction 2
- 1.1 Project introduction & motivation . . . 3
- 1.2 Problem definition . . . 4
- 1.3 Approach to research . . . 6
  - 1.3.1 Scope of the work . . . 6
  - 1.3.2 Research questions . . . 6
  - 1.3.3 Chapter outline . . . 7

2 Literature review 14
- 2.1 Concrete after high temperature exposure . . . 15
  - 2.1.1 Portland cement . . . 15
  - 2.1.2 Calcium aluminate cement . . . 18
  - 2.1.3 Other binders . . . 20
  - 2.1.4 Aggregates . . . 24
- 2.2 Concrete during high temperature exposure . . . 27
  - 2.2.1 Thermo-mechanical spalling . . . 27
  - 2.2.2 Thermo-hygral spalling . . . 28
  - 2.2.3 Recent advances and the role of fibers . . . 31
- 2.3 Concluding remarks . . . 33

II Building materials response to thermal shock 55

3 Hot spillage on CAC 56
- 3.1 Development of a spalling resistant concrete . . . 57
- 3.2 Experimental program . . . 59
  - 3.2.1 Samples and exposure . . . 59
  - 3.2.2 Powder analysis . . . 60
  - 3.2.3 Electron microscopy . . . 60
  - 3.2.4 Modelling . . . 61

3.3 Results . . . 62
3.3.1 Temperature estimation . . . 62
3.3.2 Thermogravimetric analysis . . . 64
3.3.3 X-ray diffraction . . . 66
3.3.4 Electron microscopy . . . 69
3.4 Discussion . . . 77
3.4.1 Thermo-mechanical damage . . . 77
3.4.2 Thermo-chemical alterations . . . 78
3.5 Re-hydration . . . 79
3.5.1 Materials & Methods . . . 80
3.5.2 Results & Discussion . . . 81
3.6 Conclusions . . . 85

4 Plutonic rocks as thermal shock protection 93
4.1 Plutonic rocks as building materials . . . 94
4.2 Experimental program . . . 95
4.2.1 Selected rocks . . . 95
4.2.2 X-ray diffraction . . . 95
4.2.3 Thermal gravimetric analysis . . . 96
4.2.4 Optical microscopy . . . 96
4.2.5 X-ray microtomography . . . 96
4.2.6 Thermal dilation . . . 97
4.2.7 compressive strength . . . 97
4.3 Results and discussion . . . 98
4.3.1 X-ray diffraction . . . 98
4.3.2 Thermogravimetric analysis . . . 100
4.3.3 Optical microscopy . . . 100
4.3.4 X-ray microtomography . . . 100
4.3.5 Compressive strength and thermal dilation . . . 104
4.3.6 Discussion . . . 106
4.4 Modelling . . . 107
4.5 Conclusions . . . 109

5 Concrete exposed to molten steel and slag: A case study 117
5.1 Situation . . . 118
5.1.1 Problem statement . . . 118
5.1.2 Loading cases . . . 119
5.1.3 Development of protection strategy . . . 119
5.2 Test panels design & production . . . 120
5.2.1 Materials selection & mix design . . . 120
5.2.2 Casting & installation . . . 122
5.3 Monitoring and evaluation of damage . . . 124
5.3.1 Inspections and tests . . . 124
5.3.2 On-site evaluation . . . 125
5.3.3 Optical microscopy . . . 130

5.4 Cost analysis . . . 134
5.5 Conclusions . . . 135

III Thermal shock damage prediction 139

6 Parametric analysis of concrete mix and spalling 140
6.1 Motivation and approach . . . 141
6.2 Definition of scope . . . 142
6.2.1 Mixture related features . . . 142
6.2.2 Material related features . . . 143
6.2.3 Testing related features . . . 144
6.3 Database development . . . 144
6.3.1 Data conventions . . . 146
6.3.2 Data normalisation . . . 147
6.4 Database analysis . . . 147
6.4.1 Data meta-analysis . . . 147
6.4.2 Machine learning analysis . . . 158
6.5 Conclusions . . . 164

7 The influence of pore connectivity on spalling 179
7.1 Defining pore connectivity . . . 180
7.2 Experimental methodology . . . 181
7.2.1 Mixture design . . . 181
7.2.2 Mechanical properties . . . 182
7.2.3 Spalling experiment . . . 182
7.2.4 Porosity characterization . . . 183
7.3 Results and discussion . . . 185
7.3.1 Samples properties . . . 185
7.3.2 Spalling behaviour . . . 189
7.4 Quantifying pore connectivity influence on spalling . . . 192
7.4.1 Assumptions . . . 192
7.4.2 Validation . . . 193
7.5 Discussion . . . 197
7.6 Conclusions . . . 198

IV Final considerations 207

8 Applications & Recommendations 208
8.1 Applications . . . 209
8.1.1 Factories . . . 209
8.1.2 Fire safety for tunnels . . . 210
8.1.3 Launchpads . . . 211
8.2 Recommendations for future research . . . 213
8.2.1 Prediction of spalling through analytical equation . . . 213
8.2.2 Modelling of spalling . . . 215
8.2.3 Development of high strength refractory concrete . . . 217
8.2.4 Prediction of cyclic thermal shock performance . . . 217

9 Retrospection, conclusions and final considerations **225**
9.1 Retrospection . . . 226
9.2 General conclusions . . . 227
9.3 Final considerations . . . 229

A Appendix A: Structural design of case study panels **231**
A.1 Reinforcement & stones attachment . . . 232
A.2 Hoisting . . . 235
A.2.1 Known values: . . . 235
A.2.2 Crane factors: . . . 235
A.2.3 Main loads . . . 235
A.2.4 Loads at the anchors . . . 235
A.2.5 Minimum element thickness (as defined by anchor supplier) . . . 236
A.2.6 Panels height . . . 236
A.2.7 Pull-out test . . . 236
A.2.8 Ring clutches and angle of lifting . . . 236
A.3 Conclusion . . . 238

Curriculum Vitæ **239**

List of Publications **241**

ACKNOWLEDGEMENTS

Alone– it is wonderful how little a man can do alone!
To rob a little, to hurt a little, and there is the end.

H.G. Wells, The Invisible Man

I think it is interesting that articles usually have many authors while theses are always attributed to a single person. At the time of writing of this thesis, most PhD students are expected to produce some journal papers, but only one thesis, for which he or she needs much more help and contribution than any one paper. Luckily, I had many people that helped me through this process without ever expecting recognition or something in return.

In first place, my wife, **Claudia**. Thank you for supporting me, believing I could do this and lifting me up every time I felt down. During this period we had a very dynamic life (I changed countries, you changed jobs, we bought and reformed a house and got married), and yet, you always found time to encourage me and help to cover my academic weak spots. No matter what I do after achieving the title of PhD, I'm confident it will be a good life if we are together.

Next, to my dear family, without whom I could not even come to the Netherlands in first place. Thank you **Vera** for accepting me as weird as I was and showing undoubt resolve when I decided to follow an academic path. Thank you to my late father **Fernando**, who sponsored my education and taught me strong values at an early age. Finally thank you to my sister **Alique**, without whom I would probably have grown a very different person. Your companionship and confidence were always there for me.

In the Netherlands, I can think of no one else who had as much impact in my career path as **Oğuzhan**. Be it for showing me how much I don't know about forensics of building materials, be it for helping me organizing my MSc internship, or for inviting me as a part of the Concrete Microscopy Course. Of course, the greatest impact was by later inviting me to do my PhD in the Microlab and becoming my supervisor and promoter. Working with you was a blast and I doubt I will ever have a boss with whom I agree in so many random topics. I am sure the kinship between growing in Turkey and Brazil is in big part responsible for this, and I truly hope we manage to keep in contact.

I would also like to thank my other supervisor, **Erik**. You probably don't remember, but you advised me towards getting my first job in the Netherlands, which also impacted my career choices. Later, when I returned to the Microlab, you helped tremendously with shaping my project and understanding the limitations of my findings in the context of real structures. I feel lucky I got to learn from you.

Further, I would like to recognize the contributions of two other people who also sat year after year in my progress meetings helping contextualize my ideas and plan my next

experimental campaigns. **Branko** you have always given useful advice and explained the quirks of academia to me. You even spent time helping me with my writing and experiments, which you absolutely didn't have to. I'll forever be grateful for that and all your help during my MSc. **Fred**, I have always appreciated that you were usually the first one to arrive in meetings, so we had a few minutes to talk beforehand. Your comments and remarks on my work really helped to guide some of my rougher ideas into an actual scientific endeavour. But aside from work, you are also really fun to talk to, and a relaxing time before a progress meeting is always appreciated.

While most PhD projects have a relatively slow first year, filled with literature review and preliminary experiments, I had the challenging mission of producing macro-scale test samples for our industrial case study in that first year. I have no doubt that this would either not be possible or at least not be as successful as it was without the participation of **Kuba**. I usually think that working with friends can lead to awkward situations, but in our case it functioned oh so well. However, I realise that might be a one sided view since you were the one bending steel bars while I held the table in place! But seriously man, you came in the project to save us.

In addition, there were all the nice people that helped me actually casting the big test samples besides the ones already mentioned. **Marija**, **Yadding**, **Stefan**, **Luís**, **Ydong** and **Yask**, thank you so much for your making this possible. You all helped out of camaraderie and made the elements possible. Also, my two officemates **Yu** and **Emanuelle**, who helped with the casting, but also helped with the house I bought and just the day to day mood of the office. I think our room was a very fun one to be and you guy truly went above and beyond.

But the castings definetely could not happen without the experience and help of **Maiko** and **Ton**. Maiko, you have been super fun to be around at work and outside. You were the "maestro" of our castings, and helped me with nearly everything in the Microlab and Stevinlab. Ton, you helped with all the hardest, heaviest chores. I imagine you must have been pretty tired of us occupying the sawing room and always asking for help to move giant pieces of stone, so thank you so much for helping me.

On the other side of the first year, was all the new experimental methodologies that I had to be quickly familiarized with pertaining high temperature. For this, I cannot thank **Clarissa** enough. You were always ready to help and talk about how to do any challenging experiment. Your optimism and belief that anything is simple if you have enough will to make it happen was a great kick start for my PhD.

Also thank you to **John** who helped me figure out how to make the experiments as safe as possible and how to use all the different ovens we had. And **Arjan** who helped me with the Mercury intrusion porosimetry and some missing data.

Later, when the project focus shifted towards prediction of damage, I had the pleasure of supervising **Laurens**. You were a very diligent MSc student, whom the technicians had only positive things to say about. Your experiment has been complimented not only by me, but by the reviewers of Cement and Concrete Research! No small feat during a MSc. I feel really lucky you did chose to do your project with me and Oğuzhan.

And speaking of students, I am glad I could be a part of so many interesting theses. **Priya**, your dedication, work ethic, attitude and talent all screamed "excellence" and I am very happy to see you continued your path moving towards a PhD in a good univer-

sity. I think you will be very successful in whatever you try and hope you can solve the two body problem. **Theo** and **Agatha** my Mars colonization students. I had immense fun supervising your projects. Both of you saw the end of your MSc as an opportunity to pick a very challenging topic and make it your own, which I can legitimately admire. At the end, you did real contributions to society's knowledge that really wish become useful still in our life-time.

However, maybe the biggest contributor of the project were the people in Tata Steel, who pushed this idea forward and made all this possible. Thank you **Rutger** and **Cock** for believing in this project and accepting me in the Oxystaal fabriek 2 team. I enjoyed my time getting to know the people there and understanding how it all come together to work with such efficiency. Also, a special thank to **Willem**, who helped me with several practical issues, including communication, and took time out of your already busy schedule at Tata to ensure we could discuss how this project could be useful to Tata Steel.

I would also like to thank the people that are not directly related to the project, but make everything go well on the background and often go unappreciated. People like **Jacqueline**, our section secretary that always helped me with administrative issues; **Jaap**, who also helped me with such issues and reminded me of registering my hours; and **Maria**, who helped keeping our office clean and nice.

Finally, I would like to express my appreciation for the people who had nothing to do with the project, but helped remain sane and carry on my work during a PhD and a pandemic simultaneously. **Gaby**, **Gina**, **Juan**, **Thomas**, **Lore**, **Menno** and **Arturo**, thank you for your friendship and support. Our pandemic bubble was a little bit of light in weird and difficult times. I hope our latin community in the Netherlands stays strong and we keep doing parties until we are too old to stay up late.

Erwin, **Dennis**, you guys were some of my first friends in the Netherlands and I'm so glad we managed to keep in contact for all these years. Although I have never regretted leaving France to return here, I almost regret it just to see the trip you guys were going to make there. I'm sure we will keep meeting until the day Erwin steals another cathedral and the group faces murder accusations.

And last, **Júlio** you are one of my oldest friends and we still manage to find topics to speak almost every day. We have a very solid foundation for a friendship (mostly a game franchise) and have always spent a good amount of time arguing about politics, science, religion and really anything else. You were actually one of the starting reasons why I became interested in academia and I'm still thankful for that. Also, thank you for the beautiful art in my thesis.

SUMMARY

Building materials generally perform poorly in a high temperature environment. Residential fires and fires in road tunnels are common occurrences. Furthermore, some factories have no option besides exposing their infrastructure to very high temperatures due to the nature of their operation logistics. Therefore, there is a clear need for developing structural materials that can withstand high temperatures ensuring safety during such events.

The present thesis deals with thermal shock damage in construction materials. Specifically, the first half of the thesis focuses on the development of an structural material that would fare well on severe cyclic thermal shock conditions found in a steel factory. The second half aims to improve the capacity of engineers and scientists to predict whether a concrete of a given mixture would suffer from spalling under certain heating conditions.

Initially, a review of the main effects and chemical changes caused by high temperature was performed on the conventional building materials, followed by some novel materials being currently explored by the civil engineering scientific community. This aided in the pre-selection of material to be tested at later stages. Further, existing theories concerning high temperature spalling, the causes and the main methods of mitigation were reviewed.

In Chapters 3 and 4 the binder and the stones to be used in the project were preselected and tested in conditions similar to what is present at the factory of the industrial partners. A new experimental setup had to be developed in order to match the heating conditions and perform such observations. Typical analytical chemistry and microscopy techniques were employed to study the microstructural changes in the materials, with focus on how this could affect the stress state of the concrete. Finite element modelling was used to explain some of the behaviour of the samples and predict performance on a large scale setting.

Next, the materials explored in the previous chapters were used to design four test elements that would be installed at the studied factory location. Such elements would require to follow all codes for precast concrete elements that are subjected to hoisting operations. An investigation within the factory was performed to determine all load cases during operation how these progressed in time. This aided the design of the test element, which were installed at critical locations of the factory. Two inspections were possible, one after 6 months of factory operation and one after 1 year of factory operation. The inspections showed that the test elements had a much better performance than the current method of protection used and the test was considered successful. This was considered the end of the first half of the thesis.

In the second half, instead of designing a novel experiment to improve spalling prediction capacity, first, a large performance database of concrete samples was generated through surveying numerous spalling experiments. This not only allowed for a better overview of gaps in current investigations, but also provided a considerably larger set

of data. In order to process all the data timely, machine learning algorithms were used. More than 40 properties of concrete and testing were included from over a thousand individual experiments. A gradient tree boosting classifier achieved 89% accuracy in defining if a sample would spall or not given its mixture design, physical and mechanical properties and heating conditions. One of the main observations during this endeavor was the lack of information regarding the porosity of the samples, an important microstructural property which can influence spalling considerably.

Thereafter, it was decided to design an experiment focusing on the influence of porosity in spalling. Attention was given on how porosity could be quantified in a meaningful manner, and a choice was made to focus on pore connectivity. To achieve this goal, porosity was divided between two size classes based on the resolution limitations of mercury intrusion porosimetry and X-ray microtomography, the two techniques selected to perform the quantification of pore connectivity. Once this was done, mortar samples were exposed to spalling experiments varying W/C ratio, polypropylene fibre content and heating rate. The experiment was used to create an analytical equation for spalling prediction, which was later validated with several experiments from literature. The validation achieved an accuracy of 91%.

Finally, a number of applications to this knowledge is described and recommendations are provided on which areas of this research can be further developed and how. A retrospection and several final considerations are also given in the last chapter.

SAMENVATTING

Bouwmaterialen presteren over het algemeen slecht in een omgeving met hoge temperaturen. Woningbranden en branden in wegtunnels komen veel voor. Bovendien hebben sommige fabrieken geen andere keus dan hun infrastructuur bloot te stellen aan zeer hoge temperaturen vanwege de aard van hun operationele activiteiten. Daarom is er een duidelijke behoefte aan het ontwikkelen van constructiematerialen die bestand zijn tegen hoge temperaturen en de veiligheid tijdens dergelijke evenementen garanderen.

Het huidige proefschrift gaat over schade door thermische schokken in bouwmaterialen. De eerste helft van het proefschrift richt zich concreet op de ontwikkeling van een constructiemateriaal dat goed bestand is tegen ernstige cyclische thermische schokken in een staalfabriek. De tweede helft heeft tot doel het vermogen van ingenieurs en wetenschappers te verbeteren om te voorspellen of een beton van een bepaald mengsel onder bepaalde hitte omstandigheden zou afbrokkelen.

Aanvankelijk werd een overzicht gemaakt van de belangrijkste effecten en chemische veranderingen van hoge temperaturen op conventionele bouwmaterialen, gevolgd door enkele nieuwe materialen die momenteel worden onderzocht door de wetenschappelijke gemeenschap van civieltechnische werken. Dit hielp bij de voorselectie van materialen die in latere stadia zouden worden getest. Verder werden bestaande theorieën, de oorzaken en de belangrijkste mitigatiemethoden over afbrokkeling bij hoge temperaturen beoordeeld.

In de hoofdstukken 3 en 4 werden het bindmiddel en de stenen die in het project moesten worden gebruikt vooraf geselecteerd en getest onder omstandigheden die vergelijkbaar zijn met wat aanwezig is in de fabriek van de industriële partners. Er moest een nieuwe experimentele opstelling worden ontwikkeld om de hitte omstandigheden aan te passen en waar te kunnen nemen. Typische analytische chemie- en microscopietechnieken werden gebruikt om de microstructurele veranderingen in de materialen te bestuderen, met de nadruk op hoe dit de spanningstoestand van het beton zou kunnen beïnvloeden. Eindige-elementenmodellering werd gebruikt om een deel van het gedrag van de monsters te verklaren en de prestaties op grote schaal te voorspellen.

Vervolgens zijn de in de voorgaande hoofdstukken onderzochte materialen gebruikt om vier testelementen te ontwerpen die op de te bestudeerde fabriekslocatie zouden worden geïnstalleerd. Dergelijke elementen vereisen dat alle bouwcodes worden gevolgd voor geprefabriceerde betonelementen die worden onderworpen aan hijswerkzaamheden. Er is een onderzoek binnen de fabriek uitgevoerd om van alle belasting gevallen tijdens de uitvoering te bepalen en hoe deze zich in de tijd ontwikkelden. Dit hielp bij het ontwerp van het testelement, dat op kritieke locaties in de fabriek werd geïnstalleerd. Er waren twee inspecties mogelijk, één na 6 maanden fabrieksbedrijf en één na 1 jaar fabrieksbedrijf. Uit de inspecties bleek dat de testelementen veel beter presteerden dan de huidige gebruikte beschermingsmethode en de test werd als succesvol beschouwd. Dit werd beschouwd als het einde van de eerste helft van het proefschrift.

In de tweede helft werd, in plaats van een nieuw experiment te ontwerpen om de voorspellingscapaciteit voor afbrokkeling te verbeteren, eerst een grote prestatiedatabase van betonmonsters gegenereerd door het onderzoeken van talrijke afbrokkel experimenten. Dit zorgde niet alleen voor een beter overzicht van de gaten in de huidige onderzoeken, maar leverde ook een aanzienlijk grotere set data op. Om alle data tijdig te kunnen verwerken, werd gebruik gemaakt van machine learning-algoritmen. Er zijn meer dan 40 eigenschappen van beton en testen uit meer dan duizend individuele experimenten opgenomen. Een gradiëntboomverhogende classificator behaalde een nauwkeurigheid van 89% bij het definiëren of een monster al dan niet zou afbrokkelen, gezien het mengselontwerp, de fysieke en mechanische eigenschappen en de hitte omstandigheden. Een van de belangrijkste observaties tijdens dit onderzoek was het gebrek aan informatie over de porositeit van de monsters, een belangrijke microstructurele eigenschap die het afbrokkelen aanzienlijk kan beïnvloeden.

Vervolgens werd besloten een experiment te ontwerpen dat zich richtte op de invloed van de porositeit op het afbrokkelen. Er werd aandacht besteed aan hoe porositeit op een significante manier gekwantificeerd kon worden, en er werd voor gekozen om zich te concentreren op de connectiviteit van de poriën. Om dit doel te bereiken werd de porositeit verdeeld over twee grootteklassen op basis van de resolutiebeperkingen van kwikintrusieporosimetrie en röntgenmicrotomografie, de twee technieken die werden geselecteerd om de kwantificering van de poriënconnectiviteit uit te voeren. Zodra dit was gebeurd, werden mortelmonsters blootgesteld aan afbrokkel experimenten, variërend van de W/C-verhouding, het polypropyleenvezelgehalte en de verwarmingssnelheid. Het experiment werd gebruikt om een analytische vergelijking te maken voor het voorspellen van afbrokkelen, die later werd gevalideerd met verschillende experimenten uit de literatuur. De validatie bereikte een nauwkeurigheid van 91%.

Tenslotte wordt een aantal toepassingen van deze kennis beschreven en worden aanbevelingen gedaan over welke gebieden van dit onderzoek verder ontwikkeld kunnen worden en hoe. In het laatste hoofdstuk worden tevens een terugblik en enkele slotoverwegingen gegeven.

List of Symbols

ζ	Optimum length of fibres
i	Inter-aggregate spacing
d_{agg}	Mean diameter of coarse aggregates
N_c	Critical number of fibres per cubic centimeter
N	Number of fibres per cubic centimeter
ΔT	Temperature gradient
C_1	Constant related to material capacity of enduring thermal shock
σ_f	Ultimate tensile strength of material
E	Young's modulus
α	Coefficient of thermal expansion
k	Thermal conductivity
h	Heat transfer coefficient between a given material and the medium
H	Volume of specimen divided by its heated surface
Bi	Biot number
P_v	Water vapour pressure
T	Temperature
PPI	Polypropylene index
φ	Dosage of fibres
l	length of fibres
d	Fibres diameter
$APPI$	Adjusted polyporpylene index
ρ	density of material
T_m	Melting point
A	Area of cross-section
R	Roundness parameter
P	Perimiter
f_{c_t}	Compressive strength at time t
t	Time in which experiment was performed
η	Constant dependent of curing type
τ	Constant dependent of cement type
$f_{c_{28}}$	Compressive strength at 28 days
f_{ctm}	Mean tensile strength
f_{ck}	Design compressive strength
f_{cm}	Mean compressive strength

E_{00}	Young's modulus of mixtures containing 0.00% fibre content by volume
E_{05}	Young's modulus of mixtures containing 0.05% fibre content by volume
E_{10}	Young's modulus of mixtures containing 0.10% fibre content by volume
f_{t00}	Flexural strength of mixtures containing 0.00% fibre content by volume
f_{t05}	Flexural strength of mixtures containing 0.05% fibre content by volume
f_{t10}	Flexural strength of mixtures containing 0.10% fibre content by volume
AC	Air content
φ_S	Saturation degree of material
HR	Heating rate
$\Lambda_{(MIP)}$	Connectivity of micro-pores in cement
$\Lambda_{(XCT)}$	Connectivity of macro-pores in cement
E_{cm}	Mean Young's modulus
P_{adj}	Polypropylene index divided by air content
F_1	Constant fitted for equation 8.1
F_2	Constant fitted for equation 8.1
F_3	Constant fitted for equation 8.1
Ω	Influence of properties in the minimum PPI as per equation 8.1
Ξ	Influence of f_{ck} in the minimum PPI depending of concrete class
d_{tot}	Total sample thickness
σ_{TOT}	Total spalling stress
σ_{TMM}	Fraction of spalling stress caused by the thermo-mechanical mechanism
σ_{THM}	Fraction of spalling stress caused by the thermo-hygral mechanism
κ	Stiffness matrix
δ_{TMM}	Displacement matrix
β	Experimentally determined constant

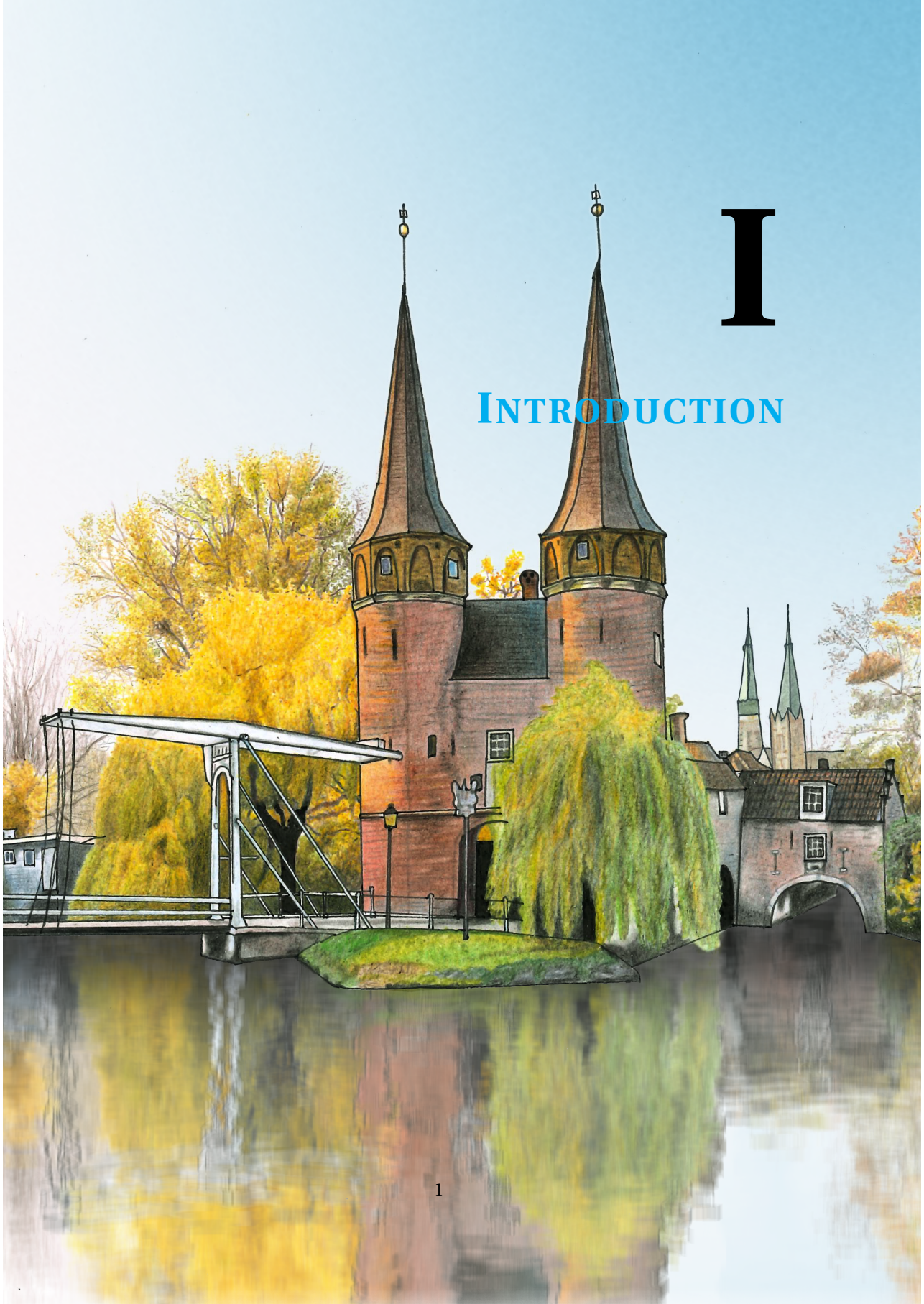

I

Introduction

1

General Introduction

If science ceases to be a rebellion against authority,
then it does not deserve the talents of our brightest children.

Freeman Dyson, The Scientist as Rebel

Logic and truth are two very different things,
but they often look the same to the mind that's performing the logic.

Theodore Sturgeon, More Than Human

This chapter introduces the PhD project of this thesis and the motivation behind it. The general problem of thermal shock in building materials is addressed and the scope of the thesis is described. The research questions and sub-questions are defined and the outline of the book is shown.

1.1. PROJECT INTRODUCTION & MOTIVATION

SUSTAINABLE development has been adopted by many countries as the ideal mode of progress since the decade of 1990s, and became an increasingly important goal with time [1]. A recent report from the Intergovernmental Panel on Climate Change (IPCC) [2] further reinforced the importance in sustainability based on the predicted consequences of carrying on with current practices. Within this context, it is only natural that attention is turned to the construction industry, which is responsible for 39% of energy-related carbon dioxide emissions [3]. The high environmental impact is due the scale of many projects in this industry (such as hydroelectric dams, planned cities, railways, airports) and the requirements for such in terms of raw materials and transportation energy. Thus, the challenge remains.

As most modern constructions are made of concrete [4], many strategies to decrease the related environmental impact by the construction industry have been researched [5–9]. However, most approaches are related to the replacement of cement by other materials, which do not address the impacts caused by transportation, demolition, waste, use of aggregates, etc. In this context, a lot of effort is currently directed to the use of recycled aggregates, which address the demolition waste and mining of natural aggregates issues. The Netherlands has set the goal of using all produced recycled aggregates within the decade of 2030 [10]. On the other hand, recent research [11] pointed to the increase in durability of constructions as the best road to sustainable buildings. Indeed, Mora [12] affirms that even a small increase in the life span of a structure far surpasses the sustainable advantages of using replacement cementitious materials.

Most structures are designed to last at least 50 years, however, the actual service-life is dependent on the combination of material, structural and environment factors. Decades of effort were directed to the correct prediction of chloride, CO_2 or sulfate ingress in concrete [13–18]. Although a lot of attention is paid on the service life prediction, thermal shock damage remains a notable exception. In such cases, the service life is often considered to end as soon as the first event occurs. In addition, structures made with high performance concrete, which have a usually much longer service-life span, have an inferior response to thermal shock than common concrete[19–23].

These are not rare events, more than 300 thousand residential fires are reported in the United States per year [24], with Europe reporting more than 2 million fires per year [25]. While most buildings are designed with fire evacuation safety protocols, other structures present a much higher risk for safety, such as tunnels. Figure 1.1 shows the incidence of fires in road tunnels caused by vehicles in different countries. Finally, a number of factory and industrial buildings (e. g. steel, aluminium, petro-chemical, cement, ceramics and aero-space industry buildings) have no option besides expose its infrastructure to daily thermal shock events due their particular operation logistics.

Aside from the threat for human life, this presents a clear problem from the sustainable point of view, requiring materials and energy to be employed constantly for rebuilding efforts. In the case of factories, it is also a financial burden, as the reconstruction often demands pausing the production activities. For this reasons, this project attempted to better understand the evolution of damage in porous cementitious materials caused by thermal shock in order to enhance the service life prediction of affected structures. Using the understanding of the main damage mechanisms, a collaboration with a steel

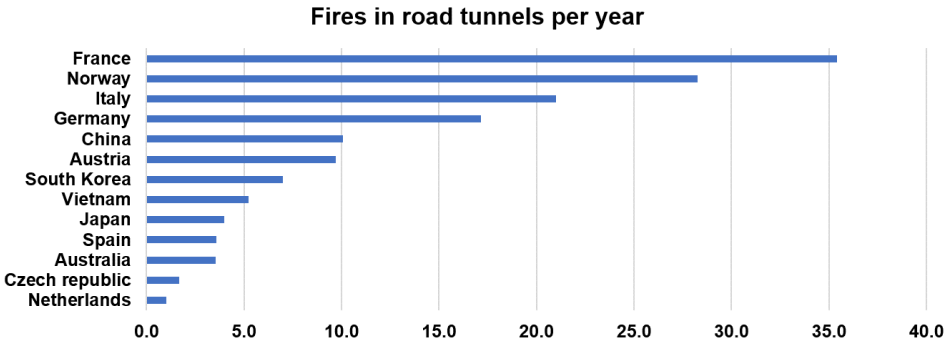

Figure 1.1: Average occurrence of fires in road tunnels for different countries, data extracted from [26–28].

factory allowed for the test of mixture designs at critical locations in the factory as a case study.

1.2. PROBLEM DEFINITION

Considering what was stated above, why do building codes prioritize designs of evacuation plans over designing fire resistant structures? Long exposure to fire decreases the mechanical properties of all conventional building materials (see Figure 1.2), which eventually elevates the risk of collapse. Steel and concrete are the two materials that fare the best, however, steel is designed with a small material factor [29] and its characteristic high thermal conductivity [30] decreases the time the structure can withstand. On the other hand, concrete structures use a much higher safety factor [31], bigger volume, and posses a thermal conductivity 100 times smaller than steel [32], representing the safest design choice during fires.

However, concrete doesn't always follow the trend shown in Figure 1.2, the actual behaviour is shown in Figure 1.3, in which a large discrepancy of performances in high temperature is observed. Indeed, for some of the analysed mixtures, the resistance was zero at 400°C, a relatively low temperature. This could be due the large influence that type of aggregates and mix design induce in the reaction of concrete to high temperatures [38]. In more extreme cases, parts of the structure might violently expel pieces of concrete at relatively early stages of the fire. This process is called spalling [39]. At the time of writing, there were no available methods to predict if a concrete member would spall based on its mixture design, thus, fire safety measures would have to be relied on as an active measure to minimize the consequences of fire. The causes for degradation of mechanical properties and spalling are discussed in detail in Chapter 2.

In addition, while most durability issues in concrete occur over the course of years or decades, fire attacks are one time events. For chloride ingress or carbonation, for example, the observation of progress in structures allowed for the development of equations estimating the evolution of these over time [40, 41]. Because most structures are not equipped with sensors, the data on fire damage mostly comes from examinations after the fact [42–45]. Furthermore, laboratory simulations are usually not good at reproduc-

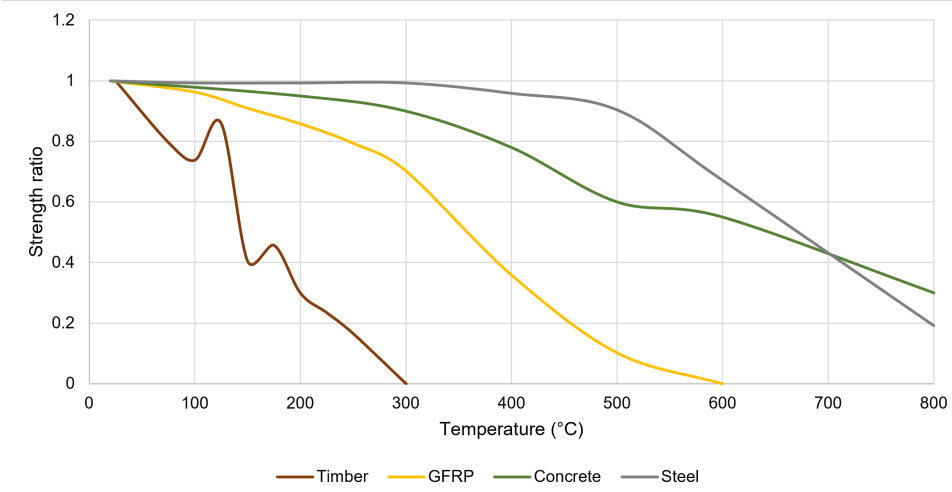

Figure 1.2: Comparison of different building materials under high temperature, data extracted from [33–37].

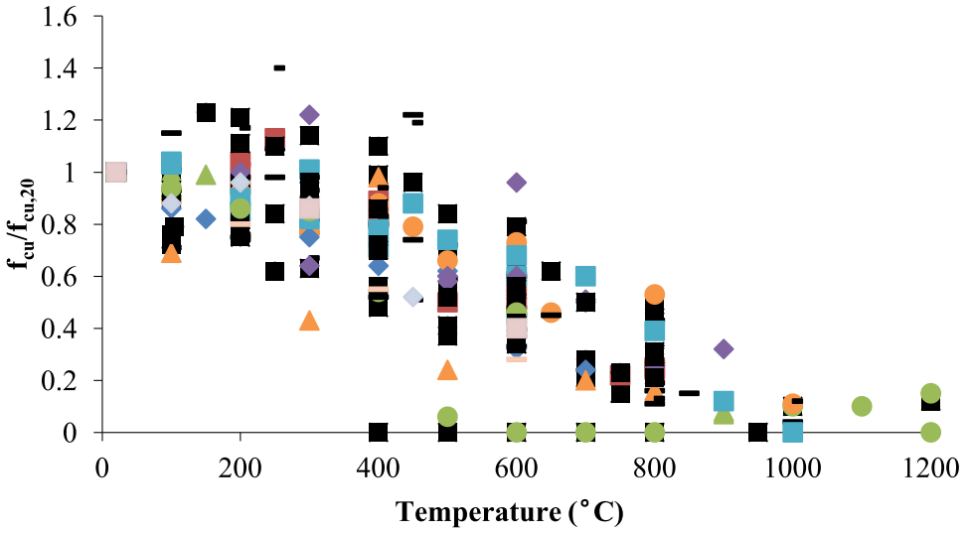

Figure 1.3: Ratio between compressive strength at 20°C and a given temperature for several concrete mixtures, picture from [35].

ing the exact effects of the event on concrete (this is discussed in Chapters 3 and 7). Thus, this makes it one of the less understood forms of damage to concrete structures, despite its relatively frequent occurrence.

1.3. APPROACH TO RESEARCH

1.3.1. SCOPE OF THE WORK

This thesis focuses on thermal shock events in concrete. However, thermal shock can define at least four different types of processes:

1. A room temperature body suddenly being heated;
2. A room temperature body suddenly being cooled;
3. A heated body suddenly being cooled;
4. A cooled body suddenly being heated.

Still, in civil engineering, the first case is the most interesting, as it represents the events leading to concrete spalling due to fire or hot spillage. As such, this thesis focuses on concrete as it would be used in conventional structures, with average temperature of 10^oC to 20^oC, suddenly receiving an unusually high thermal load of at least 500^oC. Consequently, all the mentions of "spalling" in the text refer to high temperature spalling.

Further, the service-life prediction of structures post thermal shock events would require an in-depth study of the de-hydration/re-hydration cycles happening within the binder over a long period of time. This is briefly discussed in Chapter 3, but it is not a major point of investigation in this work. Likewise, cyclic thermal loads were also not studied. The present thesis focus on the design of concrete destined to suffer a thermal load and the prediction of its behaviour after a single instance.

Finally, the project aimed at the study of concrete in the material level. Further considerations would be necessary to extend the conclusions to application at the structural level and this is addressed in Chapters 4, 7, 8 and 9.

1.3.2. RESEARCH QUESTIONS

The fundamental question of this research was if a spalling proof structural material could be designed for industrial applications. However, considering the needs of the industry (discussed in Chapter 5, the research question was divided into two simpler questions:

1. Which materials and proportion can produce a spalling resistant concrete respecting the logistics constraints of application in a typical pyro-processing facility?
2. Given a certain mixture design and composition of concrete, is it possible to predict if spalling will occur under expected thermal loading?

The first research question focuses on many engineering aspects of the problem and the direct application in a steel factory, as such, the following sub-questions were considered:

1.1 Can oven heating simulate the reaction of concrete to spilled molten steel?

1.2 What W/C ratio would perform better in conditions usually found in steel factories?

1.3 Could plutonic rocks act as a protection layer to the concrete receiving high temperature spills?

1.4 Would a hybrid concrete/stone design perform better than monolithic concrete?

1.5 What is the durability of the proposed solution?

While the second research question focused on many open points of the scientific endeavor to understand spalling. This generated the following sub-questions:

2.1 Which are the key physical or mechanical properties governing the occurrence of spalling on concrete?

2.2 Why are spalling results so inconsistent across different laboratories?

2.3 How much loading and confinement affect the material behaviour towards spalling?

2.4 How can the contribution of concrete porosity be quantified?

2.5 Can pore connectivity be quantified and used as a spalling predictor?

1.3.3. CHAPTER OUTLINE

The thesis has been divided into nine chapters under four parts, as demonstrated in Figure 1.4. The first part introduces all necessary foreknowledge to the reader for the reminder of the text. This is divided into the first chapter, which introduces the PhD project that generated the present thesis and the second chapter, which provides a brief literature review of the reactions of concrete binders and aggregates to high temperatures, and a somewhat more extensive literature review of the scientific work already carried in the field of spalling of concrete.

The second part of the thesis is entitled "Building materials response to thermal shock" and focuses on answering the first research question and its sub-questions. Within this part are the third, fourth and fifth chapters. The third chapter describes a series of analysis made on calcium aluminate cement as the main binder for the manufacturing of spalling resistant concrete. Further, the experimental approach actually submits samples to molten slag spillage with the same parameters found at the facilities of the industrial partner. Chapter 4 studies the behaviour of dunite and microgabbro as natural refractory materials and the possibility of application in civil engineering structures. Chapter 5 describes the full case study in a steel factory, including the application of the knowledge gained from Chapters 3 and 4 in test elements installed at the facility.

The third part of the thesis is entitled "Thermal shock damage prediction" and focuses on the second main research question and its sub-questions. Chapter 6 describes the creation of a large database of concrete spalling experiments and its analysis in order to study relevant properties and main source of experimental discrepancies in this

field. Further, a number of machine learning algorithms are used for an attempt to predict spalling behaviour using the aforementioned database. Chapter 7 focuses on pore connectivity as a main parameter for spalling prediction and offers a way of quantifying this property. An experimental campaign is used as basis for the development of an analytical equation to predict spalling in concrete samples.

Part four has the final considerations of the thesis. It includes one chapter exploring the possible applications of the work performed and the thoughts of the author on the most important aspects to be pursued by future work. Chapter 9, the last chapter, contains general conclusions not given by a single chapter, the answers of the research questions and some final considerations.

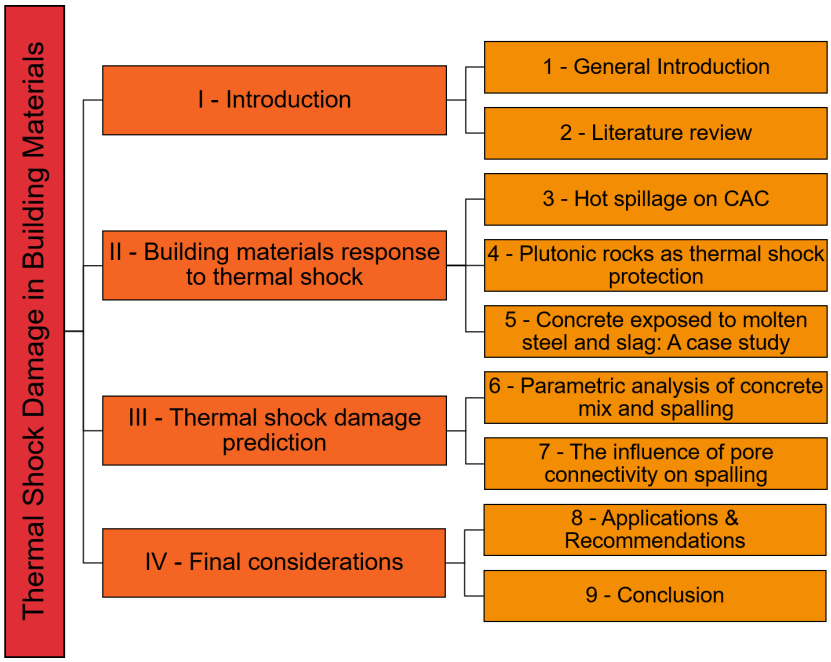

Figure 1.4: Outline of thesis.

BIBLIOGRAPHY

[1] Sharachchandra M. Lélé. "Sustainable development: A critical review". In: *World Development* 19.6 (1991), pp. 607–621. ISSN: 0305-750X. DOI: https://doi.org/10.1016/0305-750X(91)90197-P. URL: http://www.sciencedirect.com/science/article/pii/0305750X9190197P.

[2] M.R. Allen et al. "Framing and Context". In: *Global Warming of 1.5^{o}C. An IPCC Special Report on the impacts of global warming of 1.5^{o}C above pre-industrial levels and related global greenhouse gas emission pathways, in the context of strengthening the global response to the threat of climate change, sustainable development, and efforts to eradicate poverty*. Ed. by V. Masson-Delmotte et al. In Press, 2018. URL: https://www.ipcc.ch/sr15/chapter/chapter-1/.

[3] *WorldGBC Annual Report 2016 \17*. Tech. rep. World Green Building Council, 2017. URL: https://www.worldgbc.org/news-media/worldgbc-annual-report-201617.

[4] Bjørn Lomborg. *The Skeptical Environmentalist: Measuring the Real State of the World*. Cambridge University Press, 2001. DOI: 10.1017/CBO9781139626378.

[5] Mariam Abdulkareem, Jouni Havukainen, and Mika Horttanainen. "How environmentally sustainable are fibre reinforced alkali-activated concretes?" In: *Journal of Cleaner Production* 236 (2019), p. 117601. ISSN: 0959-6526. DOI: https://doi.org/10.1016/j.jclepro.2019.07.076. URL: http://www.sciencedirect.com/science/article/pii/S0959652619324151.

[6] Peter A. Adesina and Festus A. Olutoge. "Structural properties of sustainable concrete developed using rice husk ash and hydrated lime". In: *Journal of Building Engineering* 25 (2019), p. 100804. ISSN: 2352-7102. DOI: https://doi.org/10.1016/j.jobe.2019.100804. URL: http://www.sciencedirect.com/science/article/pii/S2352710219302955.

[7] Kamel Mohamed Rahla, Ricardo Mateus, and Luís Bragança. "Comparative sustainability assessment of binary blended concretes using Supplementary Cementitious Materials (SCMs) and Ordinary Portland Cement (OPC)". In: *Journal of Cleaner Production* 220 (2019), pp. 445–459. ISSN: 0959-6526. DOI: https://doi.org/10.1016/j.jclepro.2019.02.010. URL: http://www.sciencedirect.com/science/article/pii/S0959652619303890.

[8] O. Damdelen. "Investigation of 30% recycled coarse aggregate content in sustainable concrete mixes". In: *Construction and Building Materials* 184 (2018), pp. 408–418. ISSN: 0950-0618. DOI: https://doi.org/10.1016/j.conbuildmat.2018.06.149. URL: http://www.sciencedirect.com/science/article/pii/S0950061818315460.

[9] Sevket Can Bostanci. "Use of waste marble dust and recycled glass for sustainable concrete production". In: *Journal of Cleaner Production* 251 (2020), p. 119785. ISSN: 0959-6526. DOI: https://doi.org/10.1016/j.jclepro.2019.119785. URL: http://www.sciencedirect.com/science/article/pii/S0959652619346554.

[10] "Betonakkoord". In: (2018). Netherlands, available at https://www.betonakkoord.nl, visited 27-08-2022.

[11] Beatriz Palacios-Munoz et al. "Sustainability assessment of refurbishment vs. new constructions by means of LCA and durability-based estimations of buildings lifespans: A new approach". In: *Building and Environment* 160 (2019), p. 106203. ISSN: 0360-1323. DOI: https://doi.org/10.1016/j.buildenv.2019.106203. URL: http://www.sciencedirect.com/science/article/pii/S0360132319304135.

[12] Eduardo Peris Mora. "Life cycle, sustainability and the transcendent quality of building materials". In: *Building and Environment* 42.3 (2007), pp. 1329–1334. ISSN: 0360-1323. DOI: https://doi.org/10.1016/j.buildenv.2005.11.004. URL: http://www.sciencedirect.com/science/article/pii/S0360132305004737.

[13] Mark Alexander and Hans Beushausen. "Durability, service life prediction, and modelling for reinforced concrete structures – review and critique". In: *Cement and Concrete Research* 122 (2019), pp. 17–29. ISSN: 0008-8846. DOI: https://doi.org/10.1016/j.cemconres.2019.04.018. URL: http://www.sciencedirect.com/science/article/pii/S0008884619301656.

[14] Xianming Shi et al. "Durability of steel reinforced concrete in chloride environments: An overview". In: *Construction and Building Materials* 30 (2012), pp. 125–138. ISSN: 0950-0618. DOI: https://doi.org/10.1016/j.conbuildmat.2011.12.038. URL: https://www.sciencedirect.com/science/article/pii/S095006181100715X.

[15] Branko Šavija and Mladena Luković. "Carbonation of cement paste: Understanding, challenges, and opportunities". In: *Construction and Building Materials* 117 (2016), pp. 285–301. ISSN: 0950-0618. DOI: https://doi.org/10.1016/j.conbuildmat.2016.04.138. URL: http://www.sciencedirect.com/science/article/pii/S0950061816306936.

[16] Chaofan Yi, Zheng Chen, and Vivek Bindiganavile. "A non-homogeneous model to predict the service life of concrete subjected to external sulphate attack". In: *Construction and Building Materials* 212 (2019), pp. 254–265. ISSN: 0950-0618. DOI: https://doi.org/10.1016/j.conbuildmat.2019.03.318. URL: http://www.sciencedirect.com/science/article/pii/S0950061819308177.

[17] Maria Inês Serralheiro, Jorge de Brito, and Ana Silva. "Methodology for service life prediction of architectural concrete facades". In: *Construction and Building Materials* 133 (2017), pp. 261–274. ISSN: 0950-0618. DOI: https://doi.org/10.1016/j.conbuildmat.2016.12.079. URL: http://www.sciencedirect.com/science/article/pii/S0950061816320049.

[18] Woubishet Zewdu Taffese and Esko Sistonen. "Machine learning for durability and service-life assessment of reinforced concrete structures: Recent advances and future directions". In: *Automation in Construction* 77 (2017), pp. 1–14. ISSN: 0926-5805. DOI: https://doi.org/10.1016/j.autcon.2017.01.016. URL: http://www.sciencedirect.com/science/article/pii/S0926580517300559.

[19] Jie Zhao et al. "A meso-level investigation into the explosive spalling mechanism of high-performance concrete under fi re exposure". In: *Cement and Concrete Research* 65 (2014), pp. 64–75. ISSN: 0008-8846. DOI: 10.1016/j.cemconres.2014.07.010. URL: http://dx.doi.org/10.1016/j.cemconres.2014.07.010.

[20] Jie Zhao et al. "Numerical analysis of heating rate effect on spalling of high-performance concrete under high temperature conditions". In: *Construction and Building Materials* 152 (2017), pp. 456–466. ISSN: 0950-0618. DOI: 10.1016/j.conbuildmat.2017.07.023. URL: http://dx.doi.org/10.1016/j.conbuildmat.2017.07.023.

[21] Xiangwei Liang et al. "Development of ultra-high performance concrete with high fire resistance". In: *Construction and Building Materials* 179 (2018), pp. 400–412. ISSN: 09500618. DOI: 10.1016/j.conbuildmat.2018.05.241.

[22] L Missemer et al. "Fire spalling of ultra-high performance concrete : From a global analysis to microstructure investigations". In: *Cement and Concrete Research* 115.April 2018 (2019), pp. 207–219. ISSN: 0008-8846. DOI: 10.1016/j.cemconres.2018.10.005. URL: https://doi.org/10.1016/j.cemconres.2018.10.005.

[23] Shamsad Ahmad et al. "Mechanical properties of steel fiber-reinforced UHPC mixtures exposed to elevated temperature: Effects of exposure duration and fiber content". In: *Composites Part B: Engineering* 168.December 2018 (2019), pp. 291–301. ISSN: 13598368. DOI: 10.1016/j.compositesb.2018.12.083. URL: https://doi.org/10.1016/j.compositesb.2018.12.083.

[24] *Residential Building Fire Trends (2010-2019)*. Tech. rep. Federal Emergency Management Agency, 2021. URL: https://www.usfa.fema.gov/downloads/pdf/statistics/fire-estimate-summary-series.pdf.

[25] J. R. Hall S. V. Sokolov P. Wagner. *Report No 10 of Centre of Fire Statistics of CTIF*. Tech. rep. International Association of Fire and Rescue Services, 2006. URL: https://fdocuments.net/document/ctif-fire-statistics.html?page=1.

[26] *Technical Report 2016 R35 – Experience with significant incidents in road tunnels*. Tech. rep. PIARC – World Road Association, 2016. URL: http://www.piarc.org.

[27] Rui Ren et al. "Statistical analysis of fire accidents in Chinese highway tunnels 2000–2016". In: *Tunnelling and Underground Space Technology* 83 (2019), pp. 452–460. ISSN: 0886-7798. DOI: https://doi.org/10.1016/j.tust.2018.10.008. URL: https://www.sciencedirect.com/science/article/pii/S0886779817311458.

[28] Nigel Casey. "Fire incident data for Australian road tunnels". In: *Fire Safety Journal* 111 (2020), p. 102909. ISSN: 0379-7112. DOI: https://doi.org/10.1016/j.firesaf.2019.102909. URL: https://www.sciencedirect.com/science/article/pii/S0379711218305265.

[29] *EN 1993-1-1 Eurocode 3: Design of steel structures - Part 1-1: General rules and rules for buildings*. EN. Brussels: CEN, 2020.

[30] Rafał Wyczółkowski, Vazgen Bagdasaryan, and Barbara Tomczyk. "Modelling of effective thermal conductivity of a packed bed of steel bars with the use of chosen literature models". In: *Composite Structures* 282 (2022), p. 115025. ISSN: 0263-8223. DOI: https://doi.org/10.1016/j.compstruct.2021.115025. URL: https://www.sciencedirect.com/science/article/pii/S026382232101446X.

[31] *EN 1992-1-1 Eurocode 2: Design of concrete structures – Part 1-1: General rules and rules for buildings*. EN. Brussels: CEN, 2011.

[32] Khaled S. AlQdah. "Effect of using natural and local environment contents on the thermal conductivity of building materials; case in Medina, Saudi Arabia". In: *Case Studies in Thermal Engineering* 28 (2021), p. 101597. ISSN: 2214-157X. DOI: https://doi.org/10.1016/j.csite.2021.101597. URL: https://www.sciencedirect.com/science/article/pii/S2214157X21007607.

[33] Henri Kuronen, Esko Mikkola, and Simo Hostikka. "Tensile strength of wood in high temperatures before charring". In: *Fire and Materials* 45.7 (2021), pp. 858–865. DOI: https://doi.org/10.1002/fam.2813. eprint: https://onlinelibrary.wiley.com/doi/pdf/10.1002/fam.2813. URL: https://onlinelibrary.wiley.com/doi/abs/10.1002/fam.2813.

[34] İlker Bekir Topçu and Burak IşIkdağ. "The effect of cover thickness on rebars exposed to elevated temperatures". In: *Construction and Building Materials* 22.10 (2008), pp. 2053–2058. ISSN: 0950-0618. DOI: https://doi.org/10.1016/j.conbuildmat.2007.07.026. URL: https://www.sciencedirect.com/science/article/pii/S0950061807002097.

[35] Qianmin Ma et al. "Mechanical properties of concrete at high temperature—A review". In: *Construction and Building Materials* 93 (2015), pp. 371–383. ISSN: 0950-0618. DOI: https://doi.org/10.1016/j.conbuildmat.2015.05.131. URL: https://www.sciencedirect.com/science/article/pii/S0950061815006765.

[36] Fatih Mehmet Özkal et al. "Mechanical properties and bond strength degradation of GFRP and steel rebars at elevated temperatures". In: *Construction and Building Materials* 184 (2018), pp. 45–57. ISSN: 0950-0618. DOI: https://doi.org/10.1016/j.conbuildmat.2018.06.203. URL: https://www.sciencedirect.com/science/article/pii/S0950061818316106.

[37] Auro Cândido Marcolan Júnior and Poliana Dias de Moraes. "Probabilistic model for determining the failure time of steel-to-timber connections with multiple dowel-type fasteners exposed to fire". In: *Fire Safety Journal* 133 (2022), p. 103646. ISSN: 0379-7112. DOI: https://doi.org/10.1016/j.firesaf.2022.103646. URL: https://www.sciencedirect.com/science/article/pii/S0379711222001230.

[38] C.A. Britez and C.N. Costa. "Ações do Fogo nas Estruturas de Concreto". In: *Concreto: Ciência e Tecnologia*. Ed. by G.C. Isaia. São Paulo: IBRACON, 2011. Chap. 29, pp. 1029–1068.

[39] F. W. PRESTON and H. E. WHITE. "OBSERVATIONS ON SPALLING*". In: *Journal of the American Ceramic Society* 17.1-12 (1934), pp. 137–144. DOI: https://doi.org/10.1111/j.1151-2916.1934.tb19296.x. eprint: https://ceramics.onlinelibrary.wiley.com/doi/pdf/10.1111/j.1151-2916.1934.tb19296.x. URL: https://ceramics.onlinelibrary.wiley.com/doi/abs/10.1111/j.1151-2916.1934.tb19296.x.

[40] L. Bertolini. *Materiais De Construçao: Patologia / Reabilitaçao / Prevençao*. Oficina de Textos, 2006. ISBN: 9788579750106. URL: https://books.google.nl/books?id=rmk8YgEACAAJ.

[41] L. Bertolini et al. *Corrosion of Steel in Concrete: Prevention, Diagnosis, Repair*. Wiley, 2013. ISBN: 9783527651719. URL: https://books.google.nl/books?id=7B9sug5DDHkC.

[42] B. Georgali and P.E. Tsakiridis. "Microstructure of fire-damaged concrete. A case study". In: *Cement and Concrete Composites* 27.2 (2005). Cement and Concrete Research in Greece, pp. 255–259. ISSN: 0958-9465. DOI: https://doi.org/10.1016/j.cemconcomp.2004.02.022. URL: https://www.sciencedirect.com/science/article/pii/S0958946504000307.

[43] Chia-Chi Cheng et al. "Detecting the interfacial bonding of concrete-filled steel tube columns after fire by two stress wave-based methods – A case study". In: *Case Studies in Construction Materials* 17 (2022), e01399. ISSN: 2214-5095. DOI: https://doi.org/10.1016/j.cscm.2022.e01399. URL: https://www.sciencedirect.com/science/article/pii/S2214509522005319.

[44] Di Qin et al. "A comprehensive review on fire damage assessment of reinforced concrete structures". In: *Case Studies in Construction Materials* 16 (2022), e00843. ISSN: 2214-5095. DOI: https://doi.org/10.1016/j.cscm.2021.e00843. URL: https://www.sciencedirect.com/science/article/pii/S2214509521003582.

[45] Ahmed Aseem et al. "Structural health assessment of fire damaged building using non-destructive testing and micro-graphical forensic analysis: A case study". In: *Case Studies in Construction Materials* 11 (2019), e00258. ISSN: 2214-5095. DOI: https://doi.org/10.1016/j.cscm.2019.e00258. URL: https://www.sciencedirect.com/science/article/pii/S221450951830336X.

2

LITERATURE REVIEW

Even as a youngster, though, I could not bring myself to believe that if knowledge presented danger, the solution was ignorance.

Isaac Asimov, The Caves of Steel

That is the problem with ignorance. You can never truly know the extent of what you are ignorant about.

Adrian Tchaikovsky, Children of Time

This chapter reviews the current scientific knowledge on the behaviour of concrete during and after exposure to high temperatures. The state after exposure is presented first because it deals with the changes in chemistry and allows for the presentation of the main binders used for concrete at the time of writing. A brief review of the influence of aggregates is also provided. Afterwards, when presenting the behaviour of concrete during high temperature, spalling is introduced and discussed in terms of the two leading theories explaining the damage mechanism. Finally, a brief explanation of the action of fibers against high temperature is also offered.

BUILDING materials are affected by high temperatures in mainly two different ways, the first being the change of its inherent properties due to the new equilibrium state of its components. This is viewed mostly as a static phenomenon, in which the maximum temperature achieved determines the new properties. It should be mentioned that the properties after cooling are not equal to the properties during heating. However, as most literature only focus on residual properties, this chapter mentions this category of papers in opposition to mechanical testing during exposure to high temperatures. The second effect is the crack development often combined with violent detachment of material pieces, this is a dynamic effect linked not only to the maximum temperature, but to the rate in which the material is heated. This chapter offers a brief review of the current knowledge on concrete in high temperature environments dividing the main aspects under the two mentioned situations.

2.1. CONCRETE AFTER HIGH TEMPERATURE EXPOSURE

2.1.1. PORTLAND CEMENT

The vast majority of cement used for construction is Portland cement (PC), indeed, its market size has been evaluated at US$3.99 billions [1]. This is mainly due to its very low price per ton while offering high quality and versatility of application, making it the default choice of the industry [2]. However, this is a product developed to be used in ambient temperatures and outside of this range it requires special measures [3–5]. While concrete is composed of more than just cement, this section focuses on individual component behaviour while the next section discusses concrete as a whole during heating.

To understand the reaction of hydrated cement to high temperature, it is necessary to look at all the phases that compose it. Prior to hydration, Portland cement is usually made of ground clinker, gypsum, and varying amounts of pozzolanic additions such as blast furnace slag and fly ash. Table 2.1 contains a typical composition of Portaland cement type CEM I.

Table 2.1: A typical oxide composition (wt. %) of CEM I 42.5 R as determined by Lu et al. (2019) [6].

CaO	SiO_2	Al_2O_3	Fe_2O_3	MgO	K_2O	Na_2O	TiO_2	P_2O_5	Mn_2O_3	SO_3	LOI	Cl^-	IR
64.4	20.4	5.4	2.6	1.4	0.77	0.22	0.29	0.14	0.07	2.7	1.87	0.02	1.04

LOI = Loss on ignition, IR = Insoluble residue.

The clinker is composed of four main phases [7]: $3CaO \cdot SiO_2$ (in cement notation: C_3S), commonly referred to as alite; $2CaO \cdot SiO_2$ (in cement notation: C_2S), commonly referred to as belite; $3CaO \cdot Al_2O_3$ (in cement notation: C_3A), commonly referred to as aluminate or tricalcium aluminate; and $4CaO \cdot Al_2O_3 \cdot Fe_2O_3$ (in cement notation: C_4AF), commonly referred to as tetracalcium aluminoferrite. These are usually produced up to 1450^oC and consequently are very resistant against high temperatures [8].

Because cement chemistry deals with complex oxides regularly, a specific notation was developed, called cement chemist notation. All the equations describing cement reactions in this thesis, including the results of experiments, were written using standard cement chemist notation. For clarity, Table 2.2 contains the main substances and their cement notation. Although the exact composition of C-S-H can vary considerably and is

still in discussion [9–12], it will adopted as in Table 2.2 within this chapter for simplicity sake.

Table 2.2: Explanation of cement chemist notation [13].

Substance	Composition	Cement chemist notation
Calcium oxide	CaO	C
Silicon dioxide	SiO_2	S
Aluminium oxide	Al_2O_3	A
Ferric oxide	Fe_2O_3	F
Sulfur (VI) oxide	SO_3	$\overline{S}$
Carbon dioxide	CO_2	$\overline{C}$
Water	H_2O	H
Portlandite	$Ca(OH)_2$	CH
Calcium silicate hydrate	$3CaO \cdot 2SiO_2 \cdot 3H_2O$	$C_3S_2H_3$ or $C-S-H$

When Portland cement is mixed with water, the two silicate phases hydrate to create the main load bearing components (Equations 2.1 and 2.2), while the pozzolanic additions often have their contribution at a later time, described by Equation 2.3 [2].

$$2C_3S + 6H \rightarrow C-S-H + 3CH \tag{2.1}$$

$$2C_2S + 4H \rightarrow C-S-H + CH \tag{2.2}$$

$$CH + pozzolan + H \rightarrow C-S-H \tag{2.3}$$

The hydrated phases are generated at room temperature, or some degrees higher due to the heat of hydration [14, 15]. Thus, these are not as resistant to high temperatures, and can decompose much earlier. Indeed, portlandite and calcium silicate hydrate lose the chemically bound water between 300°C and 700°C and become lime and calcium silicates, respectively [16].

Further, a considerable portion of PC based concrete will carbonate during its service life [17]. This can convert the two main hydration products, as well as the unhydrated clinker phases into calcium carbonate, as described in Equations 2.4, 2.5, 2.6 and 2.7 [18]. The impact of these reactions in concrete is outside of the scope of this work, however, $CaCO_3$ is another component of concrete with weak resistance to high temperatures, releasing its carbon dioxide molecule at 750°C (Equation 2.8) [19].

$$CH + \overline{C} \rightarrow C\overline{C} + H \tag{2.4}$$

$$C-S-H + 3\overline{C} \rightarrow C\overline{C}-S-H \tag{2.5}$$

$$C_2S + 2\overline{C} + nH \rightarrow SH_n + 2C\overline{C} \tag{2.6}$$

$$C_3S + 3\overline{C} + nH \rightarrow SH_n + 3C\overline{C} \tag{2.7}$$

$$C\overline{C} \rightarrow C + \overline{C} \tag{2.8}$$

While the changes in binder composition are well understood, the exact effect of these on the mechanical properties and durability of the concrete are less so. This is due to a couple of reasons: First, the response of concrete to high temperate is a combination of each binder and each type of aggregate, resulting in several hundreds of possibilities [20]. Second, the reaction of concrete during heating has other effects that influence its mechanical properties and durability [21]. This is discussed in Section 2.2.

Currently, the Eurocode [22] takes a conservative approach of estimating that any concrete will lose most of its load bearing capacity at 600°C, which does not take the mixture design of concrete into account. Ma et al. (2015) [23] reviewed the mechanical properties of several concrete specimens under different temperatures and found that the ones with lower water-cement ratio conserve their properties better (provided they can withstand the heating period). Further, calcareous aggregates were found to perform much better than siliceous aggregates, fly ash and blast furnace slag were considered helpful while silica fume showed to be disadvantageous. Figure 2.2 summarizes the mechanical properties for typical concretes investigated at a large range of temperatures.

Memon et al. (2019) [16] tried to review the durability impact of high temperature exposure on concrete. The researchers found that this type of exposure irreversibly compromises the durability of most concretes through the coarsening of their microstructure and decomposition of aggregates. Figure 2.1 shows the changes in porosity and pore mean diameter at different temperatures.

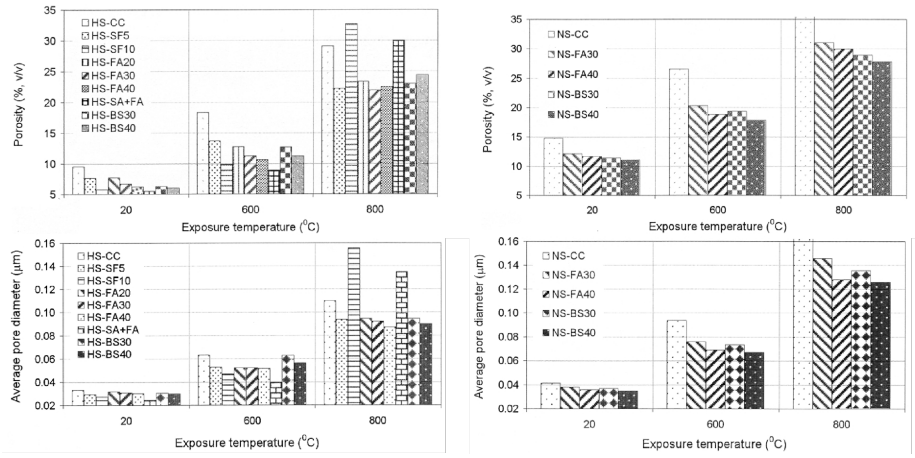

Figure 2.1: Changes in porosity and pore mean diameter as determined through mercury intrusion porosimetry, adapted from [24]. (a) Porosity in high strength concrete; (b) Porosity in normal strength concrete; (c) Mean pore diameter in high strength concrete; (d) Mean pore diameter in normal strength concrete.

Although PC based concrete is known to behave poorly against high temperature [2, 20], most engineers still chose this binder to design concrete solutions in high temperature environments. This is because other building materials are either weaker (e. g. steel), more brittle (e. g. ceramics), or economically not viable (e. g. Mg-alloys) at very high temperatures. For these applications, the field of refractory materials was developed.

2.1.2. CALCIUM ALUMINATE CEMENT

The industry standard binder for refractory concrete is calcium aluminate cement or CAC [25]. This was a cement developed in the 1908 to compete with Portland cement variants [26], however it has never become as popular mainly because of its higher cost (caused by the higher manufacturing temperature of 1650 ^{o}C) [27]. Notwithstanding, its market share has been estimated at US$500 millions, which makes it the second most used type of cement [28].

This type of cement has a much higher variability in its composition when compared to Portland cement. This is because increasing the amount of alumina in the cement can increase its high temperature resistance while sacrificing the mechanical properties proportionally [25]. Table 2.3 shows typical compositions of CACs with medium or high alumina contents. The clinker is mostly produced of three phases: Monocalcium aluminate (cement notation = CA); calcium dialuminate (cement notation = CA_2); and dodecacalcium hepta-aluminate (cement notation = $C_{12}A_7$).

Table 2.3: Oxide composition (wt. %) for CAC50 and CAC70, the number describes the minimum alumina content [29].

	CaO	SiO_2	Al_2O_3	Fe_2O_3	MgO	TiO_2	SO_3	K_2O	Na_2O
CAC50	37.00	4.80	53.00	1.30	-	3.00	-	-	-
CAC70	29.00	0.20	70.00	0.10	0.40	-	-	-	-

As with Portland cement, CAC also relies on hydration reactions to develop the mechanical properties of concrete. These reactions are described by Equations 2.9, 2.10, 2.11 [7], 2.12 and 2.13 [26]. However, after hydration, a second set of reactions occur in the cement, changing the calcium aluminate hydrates from their meta-stable forms (CAH_{10}, C_2AH_8) to their stable hydrogarnet form (C_3AH_6), as shown in Equations 2.14 and 2.15 [30]. This is called conversion and is a densification of the hydration products that renders a coarser microstructure [31]. To avoid durability problems, an upper limit of 0.40 for the water-cement ratio has been established, allowing for the conversion to occur without problems in cases where CAC is used for standard concrete in structures [26].

$$CA + 10H \rightarrow 2CAH_{10} \tag{2.9}$$

$$2CA + 11H \rightarrow C_2AH_8 + AH_3 \tag{2.10}$$

$$3CA + 12H \rightarrow C_3AH_6 + 2AH_3 \tag{2.11}$$

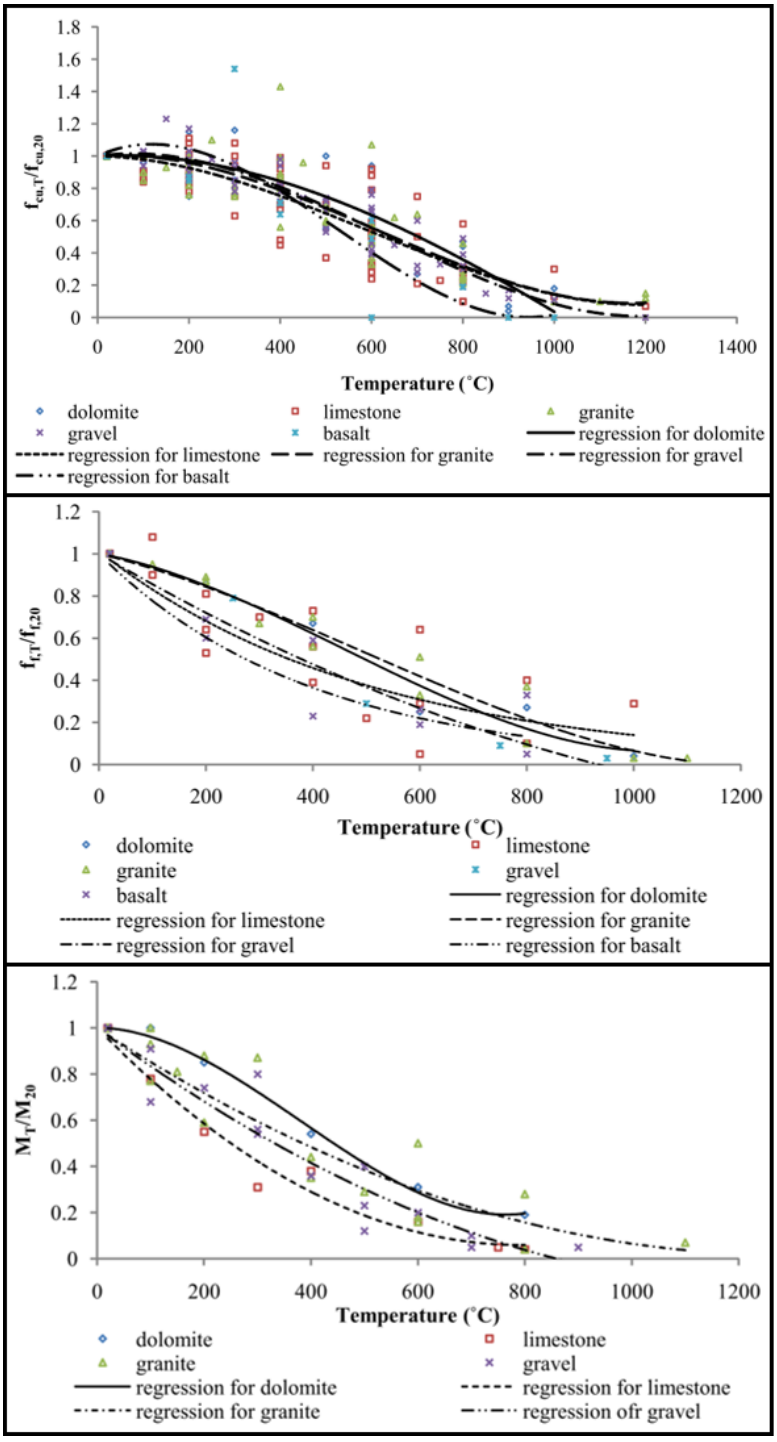

Figure 2.2: Residual mechanical properties of concrete exposed to different temperatures, adapted from [23]. Top: compressive strength; middle: flexural strength; bottom: elastic modulus.

$$C_{12}A_7 + 69H \rightarrow 6CAH_{10} + AH_3 + 6CH \tag{2.12}$$

$$C_{12}A_7 + 51H \rightarrow 6C_2AH_8 + AH_3 \tag{2.13}$$

$$3CAH_{10} \rightarrow C_3AH_6 + 2AH_3 + 18H \tag{2.14}$$

$$3C_2AH_8 \rightarrow 2C_3AH_6 + AH_3 + 9H \tag{2.15}$$

The end product is a concrete that is very resistant to heat (provided aggregates have also been selected with this intent), which retains mechanical properties much better than Portland cement. From room temperature to 200°C, the conversion reactions take place [26], the material even improves its properties up to 500°C [29]. However, from about 500°C to 1000°C, loss of the chemically bound water on the stable products occur, linearly decreasing the properties at a slower pace than in PC [32]. These reactions follow Equations 2.16 [33] and 2.17 [34]. The dehydration of C_2AH_8 follow the same path of its conversion, shown in Equation 2.15.

$$2CAH_{10} \rightarrow C_2AH_8 + AH_3 + 9H \tag{2.16}$$

$$7C_3AH_6 \rightarrow C_{12}A_7 + 9CH + 32H \tag{2.17}$$

Above 1000°C, formation of monocalcium aluminate, calcium dialuminate will create a network of sintered products. Above 1400°C, calcium hexa-aluminate (CA_6) will also be integrated to this network. Such changes dramatically improve the mechanical properties of the material, surpassing the values of the sound concrete [35].

Regarding durability, calcium aluminate cement is naturally more durable than Portland cement in a number of situations, since it was developed to be a sulphate resisting cement [2, 36], Figure 2.3 shows a comparison of different durability aspects for CAC and PC. At high temperatures, the durability of CAC-based concrete heavily depends on its mixture design [37]. Vejmelková et al. (2018) [38] showed an example of concrete made with CAC70 and basalt aggregates that still presented excellent mechanical properties and durability, even after exposure to temperatures of 1000°C.

2.1.3. OTHER BINDERS

Because of the intense drive in society towards sustainable solutions, the construction sector is exploring the use of several replacements to Portland cement [41–43]. These new binders are either based on supplementary cementitious materials (SCMs) or a variation of the calcium-silica-alumina composition of the other binders already discussed, Figure 2.4 shows a composition comparison between such materials.

Most novel binders have not been thoroughly investigated regarding their resistance to high temperatures, however, an examination of their main hydration products allow for estimations of behaviour.

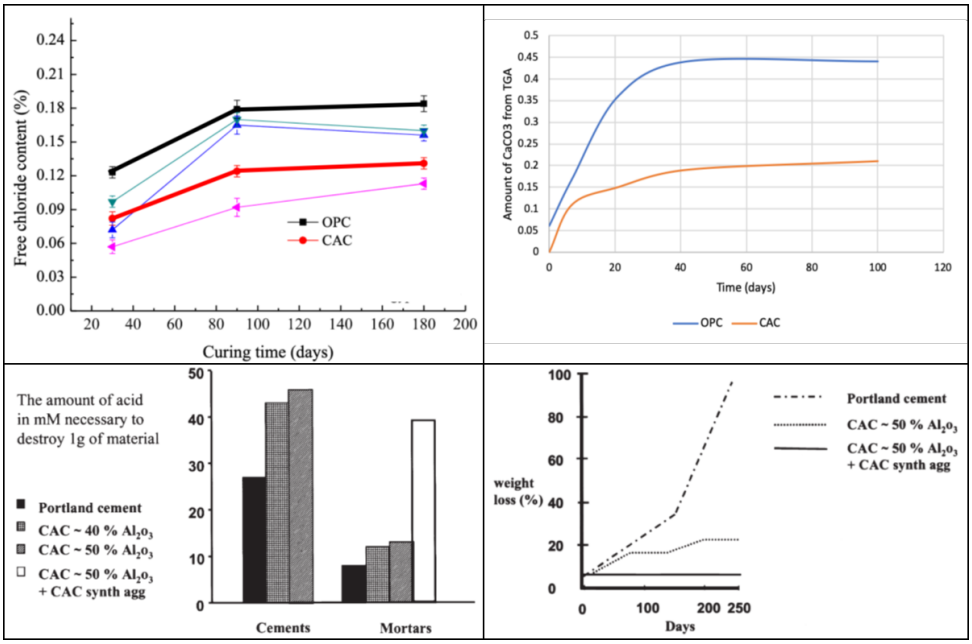

Figure 2.3: Comparison of durability between CAC and OPC. Top left: Free chloride content on samples cured in simulated sea water, adapted from [39]. Top right: Calcium carbonate content after samples being stored in 100% CO_2 atmosphere for several days, adapted from [40]. Bottom left: Amount of acid necessary to destroy 1 g of material, extracted from [27]. Bottom right: Loss of weight caused by biogenic attack, extracted from [27].

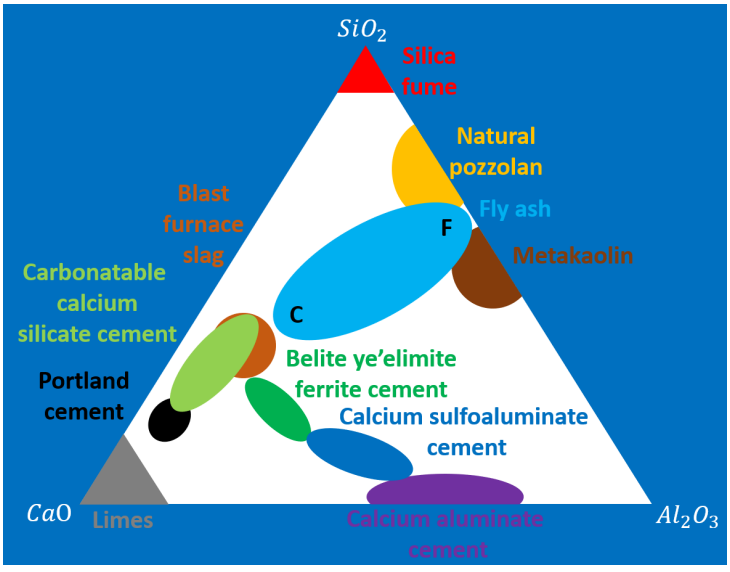

Figure 2.4: Approximate composition of different construction binders and SCMs

- **Calcium sulpho-aluminate cement (CSC):** The main hydration product is ettringite ($C_3A\overline{S}_3H_{32}$) [44], which starts decomposing at 80°C [45] and loses about a third of it mass at 190°C [46], thus, very unstable at high temperatures.
- **High belite cement:** The main reaction products are the same as Portland cement, however, the higher amount of belite causes a greater content of $C-S-H$ and less CH [42]. Therefore, it is about as effective as Portland cement at high temperatures.
- **Belite-ye'elimite-ferrite (BYF) cement:** This is a hybrid between PC and CSC, with hydration products initially based on $C-S-H$ and ettringite, however, the aluminium hydroxide dissolves to also form straetlingite (C_2ASH_3) [47]. As expected, this cement has a thermal stability in between PC and CSC.
- **Carbonated Portland cement:** These are based on the carbonation of PC and follow the explanation about Equation 2.8.
- **Carbonatable calcium silicate cement:** Although these are composed of different calcium silicates than PC [43], the main reaction products are polymorphs of $C\overline{C}$ [48], which also lose their CO_2 molecule at 750°C, and therefore, their structural stability.

Conversely, one notable alternative to Portalnd cement that has already been extensively studied are alkali-activated binder systems. These harden through the reaction of an amorphous alumino-silicate precursor with an alkali reagent (often a mix of $NaOH$ and Na_2SiO_3 solutions), forming a three-dimensional zeolitic framework that does not include water in its structure [49–51]. Two recent review articles [52, 53] were published regarding the behaviour of concrete produced with such binders when subjected to high temperatures. The reviews find that, if designed accordingly, these materials are capable to retain a considerable portion of mechanical properties up to 800°C. It cannot replace CAC to produce refractories due to its high thermal expansion, but it is a viable alternative to PC applications.

Besides calcium based cements, the construction industry has recently turned focus to magnesia based cements. Walling & Provis (2016) [54] conducted a comprehensive review of this class of cements and their potential to replace current cements in construction. The main candidates and their high temperature behaviour are presented below:

Magnesium carbonate cements

Magnesium oxide can form a number of carbonates and hydroxycarbonates as shown in Table 2.4. However, most strategies involve the formation of magnesite or nesquehonite for structural applications. While the former can be obtained dry (Equation 2.18), the latter requires a hydration step (Equations 2.19 and 2.20). Comparatively, $MgCO_3$ is less resistant to high temperatures than $CaCO_3$, losing its CO_2 molecule at temperatures higher than 600°C [55]. Similarly, nesquehonite goes through thermal decomposition between 440°C and 550°C [56], thus, the cement should perform worse than PC in thermal shock events.

$$MgO + CO_2 \rightarrow MgCO_3 \tag{2.18}$$

Table 2.4: Reaction products from MgO with water and CO_2 [54].

Mineral	Composition	Density (g/cm^3)
Brucite	$Mg(OH)_2$	2.38 [57]
Magnesite	$MgCO_3$	3.01 [58]
Nesquehonite	$MgCO_3 \cdot 3H_2O$	1.85 [59]
Lansfordite	$MgCO_3 \cdot 5H_2O$	1.70 [60]
Artinite	$Mg_2(CO_3)(OH)_2 \cdot 3H_2O$	2.03 [61]
Hydromagnesite	$Mg_2(CO_3)_4(OH)_2 \cdot 4H_2O$	2.25 [62]
Dypingite	$Mg_2(CO_3)_4(OH)_2 \cdot 5H_2O$	2.15 [63]
Huntite	$CaMg_3(CO_3)_4$	2.70 [64]

$$MgO + H_2O \rightarrow Mg(OH)_2 \tag{2.19}$$

$$Mg(OH)_2 + CO_2 + 2H_2O \rightarrow MgCO_3 \cdot 3H_2O \tag{2.20}$$

Magnesium phosphate cements

Acid phosphates have been used for cementation for several decades [65]. Magnesium phosphate cements (MPC) are usually based on the reaction of magnesia with ammonium to form a magnesium phosphate salt. Table 2.5 summarizes the most common salts formed in MPCs, with Equation 2.21 [66] describing the formation of the most common one (struvite). Because this is a very fast and exothermic reaction, retardants are often used, with borate being the most popular. Several formulations for Magnesium phosphate refractories have been developed and used for linings and bricks [67], however, these are either too expensive or have a too low pH for replacement of PC [54].

Table 2.5: Reaction products from MgO in MPCs [54].

Mineral	Composition
Struvite	$NH_4MgPO_4 \cdot 6H_2O$
Newberyite	$MgHPO_4 \cdot 3H_2O$
Hannayite	$(NH_4)_2Mg_3H_4(PO_4)_4 \cdot 8H_2O$
Schertelite	$(NH_4)_2Mg_3H_2(PO_4)_2 \cdot 4H_2O$
Dittmarite	$NH_4MgPO_4 \cdot H_2O$
Struvite-K	$MgKPO_4 \cdot 6H_2O$

$$MgO + NH_4H_2PO_4 + 5H_2O \rightarrow NH_4MgPO_4 \cdot 6H_2O \tag{2.21}$$

Magnesium silicate hydrate cements

This is a less studied system, in which instead of producing a magnesium silicate clinker, MgO and some highly reactive silica (often silica fume) are combined in-situ to form the final $M-S-H$ gel. These cements are excellent at high temperatures [68–70], maintaining good mechanical properties up to 1500°C [71, 72]. It is also possible to achieve very high compressive strength (> 120 Mpa [73]) by forming the minerals in

Table 2.6. The two main deterrents for the use of these cements in replacement of PC is the pH (between 9.5 and 10.5 [74]) and the lack of research in upscaling. As of the writing of this thesis, some researchers [75–80] argue that basalt rebars could replace steel as reinforcement to move construction towards the use of more sustainable concrete. If this becomes the new standard, magnesium silicate hydrate cements might become suitable as PC replacement.

Table 2.6: Minerals linked to $M-S-H$ gel [54].

Mineral	Group	Formulation
Lizardite	Serpentine	$Mg_3(Si_2O_5)(OH)_4$
Antigorite	Serpentine	$Mg_3(Si_2O_5)(OH)_4$
Chrysotile	Serpentine	$Mg_3(Si_2O_5)(OH)_4$
Sepiolite	Phyllosilicate	$Mg_4(Si_6O_{15})(OH)_2 \cdot 6H_2O$
Saponite	Phyllosilicate	$Ca_{0.25}(Mg,Fe)_3((Si,Al)_4O_{10})(OH)_2 \cdot nH_2O$
Talc	Phyllosilicate	$Mg_3(Si_4O_{10})(OH)_2$

Magnesium oxychloride & oxysulfate cements

These cements take advantage of the known reaction of magnesia with magnesium chloride or magnesium sulfate in water, these combine to form phases with the general composition of $xMg(OH)_2 \cdot yMgCl_2 \cdot zH_2O$ or $xMg(OH)_2 \cdot yMgSO_4 \cdot zH_2O$ [54]. However, the actual reaction products are very difficult to control and both of these classes have very low durability to water [81–83]. Therefore, these are not expected to replace PC.

2.1.4. AGGREGATES

Aggregates compose most of concrete in volume, yet they are often overlooked for being considered inert. However, these are very important for the dimensional stability and elastic modulus of concrete [84]. In refractory technology, aggregates are even more important, consisting of up to 95% of the material in mass [25]. Indeed, even if CAC is used, the aggregates might still govern the behaviour of the concrete against high temperature [37]. Although the importance of these components is known [85, 86], aggregates are frequently neglected in high temperature research.

Yang et al. (2019) [87] conducted a study on ultra-high performance concrete (UHPC) in which some mixtures used coarse aggregates and others contained only fine aggregates. The conclusion of the study pointed to an overall improved performance of concrete on high temperatures caused by coarse aggregates. However, Heo et al. (2012) [88] claim the contribution of coarse aggregates to be more complex, as the coarse particles interact with polymeric fibres, limiting their paths. This study found that aggregate size results in an inter-aggregate spacing that governs the optimum fiber length to control concrete spalling during heating, as shown in Equation 2.22. The role of fibers is discussed in Section 2.2.3.

$$\zeta = (i + d_{\text{agg}}) \left(\frac{N_c}{N} \right)^{\frac{1}{3}} \tag{2.22}$$

In which: ζ is the optimum length of fibres, i is the inter-aggregate spacing, d_{agg} is the mean diameter of the coarse aggregates, N_c is the critical number, and N is the number of fibres per cubic centimeter. The precise process to determine the inter-aggregate spacing, mean diameter and critical number can be found in the same paper [88]. Li et al. (2019) [89] found similar results, in which larger aggregates show synergy with polypropylene fibres in the protection of concrete at high temperatures. This was attributed to the different thermal dilation of the aggregates with respect to the mortar paste, which enhances connectivity on the micro-crack network.

The thermal dilation of coarse aggregates is usually determined by their chemical composition, which is often unreported or poorly described in papers. Typically, concrete researchers divide aggregates between calcareous and siliceous [90–93], because there are known problems related to siliceous aggregates at high temperatures. Namely, some siliceous aggregates break up at 350°C, while quartz changes from its α phase into its β phase at 573°C, which results in great volume expansion [94, 95].

Nevertheless, this naming convention is insufficient for high temperature studies. Indeed, Maier et al. (2020) [96] points out how the mineralogical composition variability of these two classes hinders the study of high temperature concrete due to lack of data. Figure 2.5 shows the reaction of different types of aggregates at high temperatures and demonstrates how within calcareous aggregates there are several maximum safe temperatures. In general, most researchers agree that quartz-based aggregates should be avoided [23, 97], but disagree on specific rocks. For example, Heo et al. (2011) [98] acknowledges that granite behaves poorly against high temperatures in concrete, while Ali et al. (2018) [99] claim that the difference in performance between granite and basalt only occurs in small samples and structure sized elements behave the same with either aggregate type.

Finally, the impact of recycled aggregates in high temperature resistance of concrete has been gaining attention. Cree et al. (2013) [100] conducted a review of concrete properties after fire exposure using recycled brick, glass and concrete aggregates (RBA, RGA and RCA, respectively). The researchers found that concretes using RBA and RCA usually do not suffer spalling, but highlighted the studies were conducted with laboratory graded materials, in opposition to real rubble, thus the recycled bricks contained no mortar. Zegardło et al. (2018) [101] demonstrated mixtures of concrete using CAC and recycled aggregate from sanitary ceramic waste that could maintain its compressive strength after being exposed to temperatures as high as 1000°C, commenting on the porous structure of the ceramic as an additional vapour pressure reducing mechanism. However, a more recent study from Fernandes et al. (2022) [102] found that the replacement of natural aggregates with recycled ones increased the likelihood of spalling. The authors noted that the increase in porosity from RCA could also cause an increase in total moisture, which is harmful during the heating of concrete. Yet, the same study also cautions that these conclusions were based on specific aggregates (natural or otherwise) composition, and should not be carelessly extrapolated.

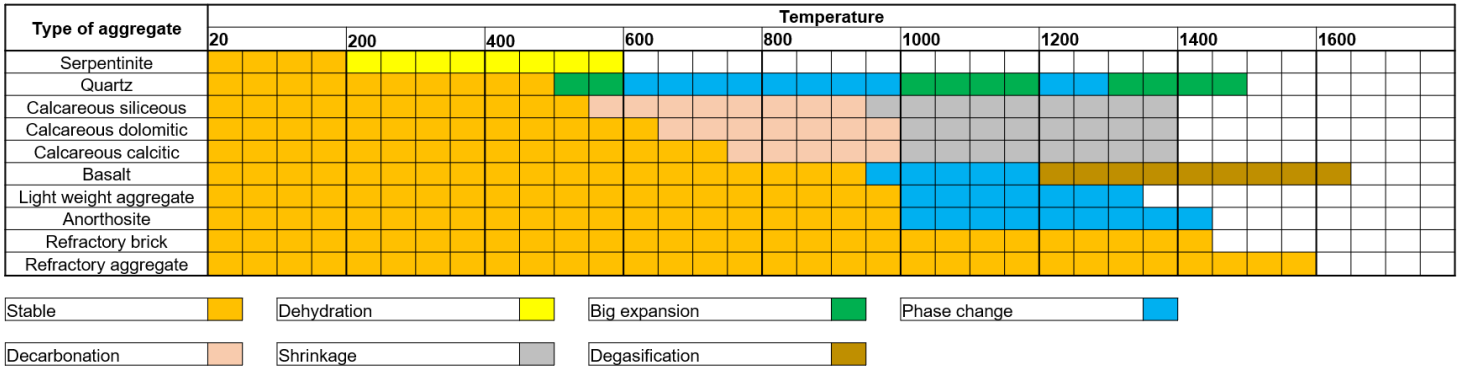

Figure 2.5: Behaviour of different types of aggregates at high temperatures, adapted from [20].

2.2. CONCRETE DURING HIGH TEMPERATURE EXPOSURE

The main concern regarding concrete after a thermal shock event (such as a fire or a industrial spillage) is to access its structural soundness through determining the remaining mechanical properties. On the other hand, during this type of event, the main concern is to avoid the material to violently expel pieces due to spalling. This is a big danger for people in the vicinity and can greatly accelerate the collapse of the structure. However, despite having observed the phenomenon nearly a century ago [103], the engineering community still struggles to predict and avoid spalling [104–106].

This is due the high speed, high complexity, multi-scale nature of this phenomenon. In addition, concrete is a highly heterogeneous material [36, 107], which also affects the spalling behaviour. Much attention has been given to the changes in water-to-binder ratio (w/b) causing otherwise high performance materials to become more fragile to thermal shock [108–112]. However, changes in type and content of cement [113, 114], type and size of aggregate [87, 89, 115], and type and dosage of fibres [116–118] also affect the material capacity to withstand sudden thermal gradients. As the material properties have been explained in the previous section, the present section focuses on the physical mechanisms of spalling.

2.2.1. THERMO-MECHANICAL SPALLING

Initially, spalling was explained through the development of tensile stresses orthogonal to the face of heating caused by thermal gradients [119, 120] (see Figure 2.6). This was named as the thermo-mechanical mechanism (TMM) of spalling, which considered the element as an homogeneous solids and was also present in other materials (e. g. metals and glass) [121]. In the following year, Lu & Fleck (1998) [122] expanded the TMM theory to include thermal shocks in both directions (hot materials being cooled and cold materials being heated); thermal shocks involving different mediums; the difference between materials with the damage governed by tensile strength and the ones governed by toughness; and a merit index to compare materials resistance to thermal shock. In the same paper, the authors proposed Equation 2.23 to describe the minimum temperature gradient a material has to be submitted to start developing cracks. This equation is for the case of a cold material being heated, governed by tensile strength (e. g. most concrete spalling cases), the other forms are also described in the mentioned paper [122].

$$\Delta T = C_1 \cdot \frac{\sigma_f}{E \cdot \alpha} \cdot \frac{k}{h \cdot H} \tag{2.23}$$

In which ΔT is the temperature gradient to which the material is subjected (K), C_1 is a constant, σ_f is the tensile strength of the material (N/m^2), E is the elastic modulus (N/m^2), α is the coefficient of thermal expansion ($1/K$), k is the thermal conductivity ($W/m/K$), h is the heat transfer coefficient between the material and the medium ($W/m^2/K$) and H is the volume of the sample divided by the heated surface (m). The third term of the equation is the inverse of the Biot number ($Bi = h \cdot H/k$), which is a non-dimensional heat transfer coefficient. A Biot number equal to zero would mean perfect thermal insulation, while a value tending to infinity would represent perfect heat transfer. As mentioned, this allows for the creation of a merit index for materials subjected to thermal shock, which the authors of Equation 2.23 presented in Figure 2.7.

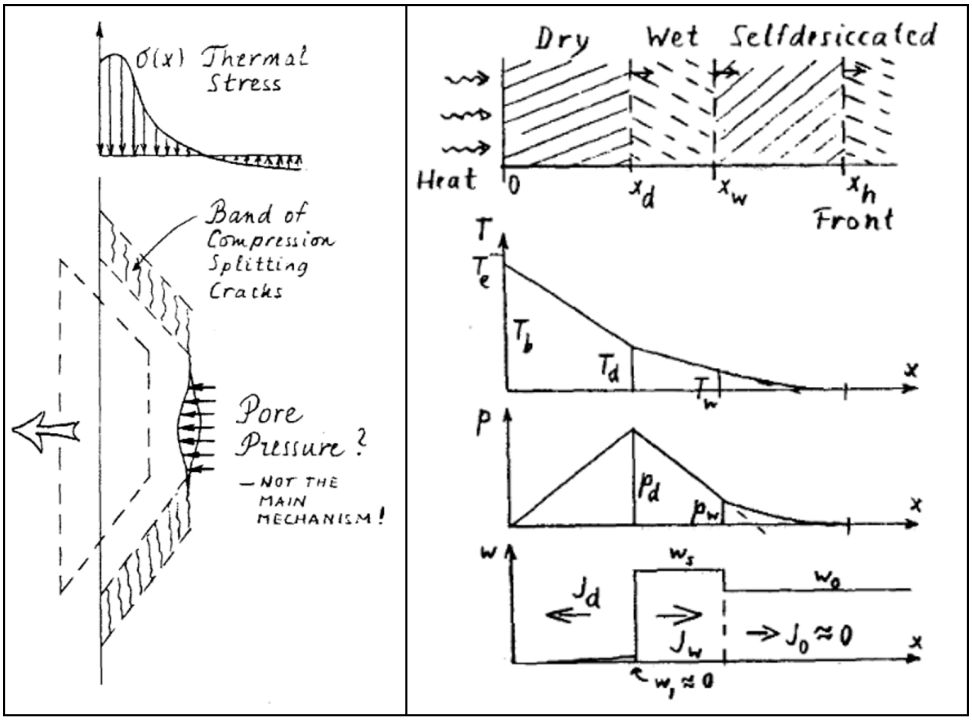

Figure 2.6: Left: Proposed mechanism of explosive spalling in a concrete wall. Right: Profiles of temperature (T), pressure (p) and moisture content (w) in a heated concrete wall. Source: Bazant (1997) [120].

However, this was found to correlate poorly with the experiments [123, 124]. Given this theory, a higher thermal gradient would cause higher stresses, but some experiments identified a critical zone for spalling between 180°C and 240°C [125]. Further, a concrete designed with higher tensile strength and less porosity (causing the thermal conductivity to increase) should perform better against thermal shock. But these changes usually result in a much worse behaviour of concrete [110, 126, 127]. Finally, concretes with similar properties would present opposite behaviours when submitted to the same heating procedures [128]. Eventually, this was attributed to differences in microstructure not taken into account, as the pressure developed in the pores during the exit of water (see Figure 2.6 right) seemed to have a greater effect than previously imagined [129]. For this reason, an alternative mechanism was proposed.

2.2.2. THERMO-HYGRAL SPALLING

The competing theory is called "moisture clog spalling" [130], in which the heating of a concrete face caused the moisture within the skin to evaporate. If the heating proceds, the evaporation front moves inward and vapour acumulates in porous zones. Eventually, vapour would not be able to migrate through a saturated front, causing the buildup of pore pressure there until spalling. This concept is sketched in Figure 2.8. This theory was later renamed as the Thermo-Hygral Mechanism (THM) of spalling.

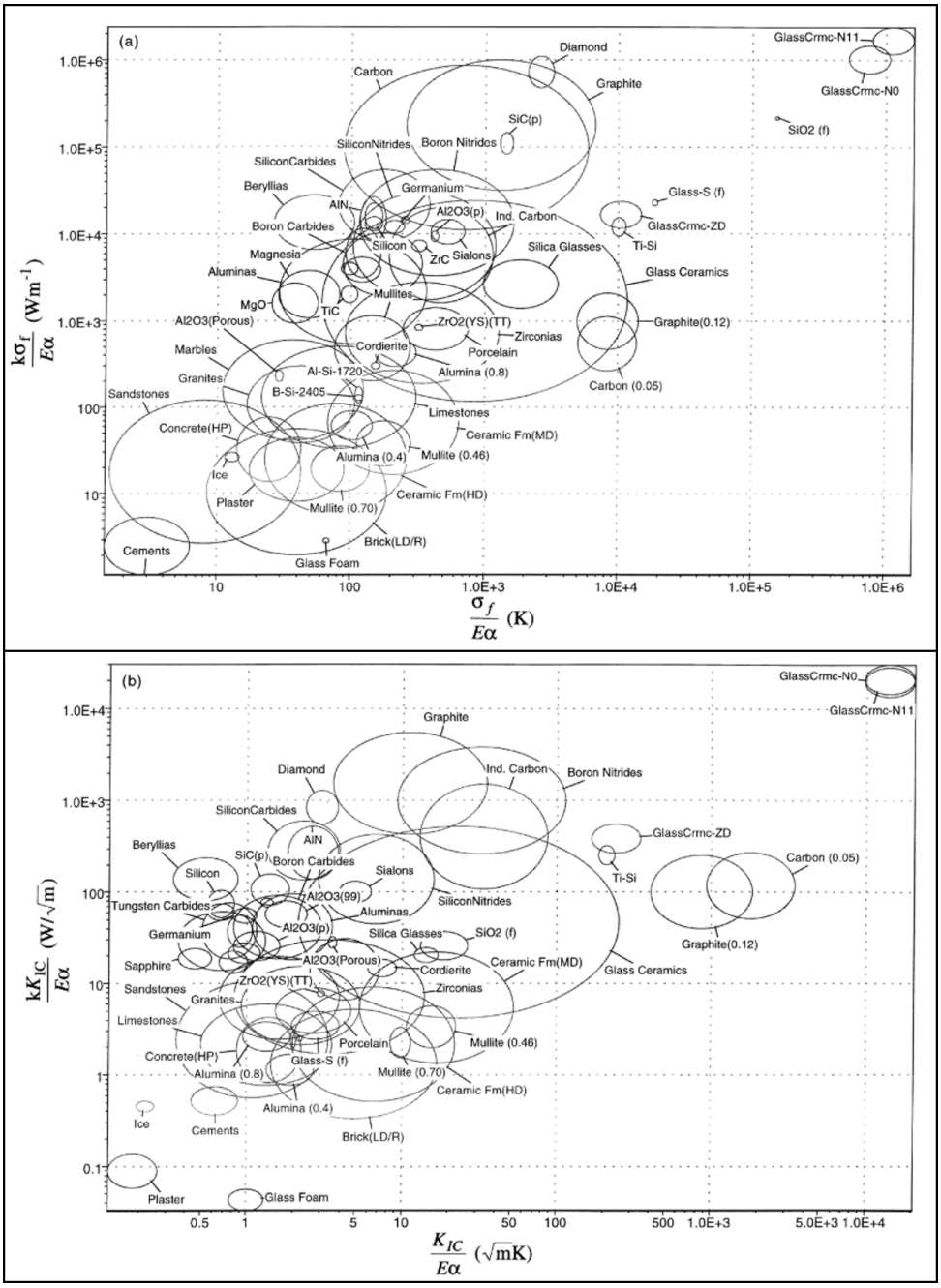

Figure 2.7: Top: Merit indices for strength governed failure at low Bi versus strength governed failure at high Bi values. Bottom: Merit indices for toughness governed failure at low Bi versus toughness governed failure at high Bi values Source: Lu & Fleck (1998) [122].

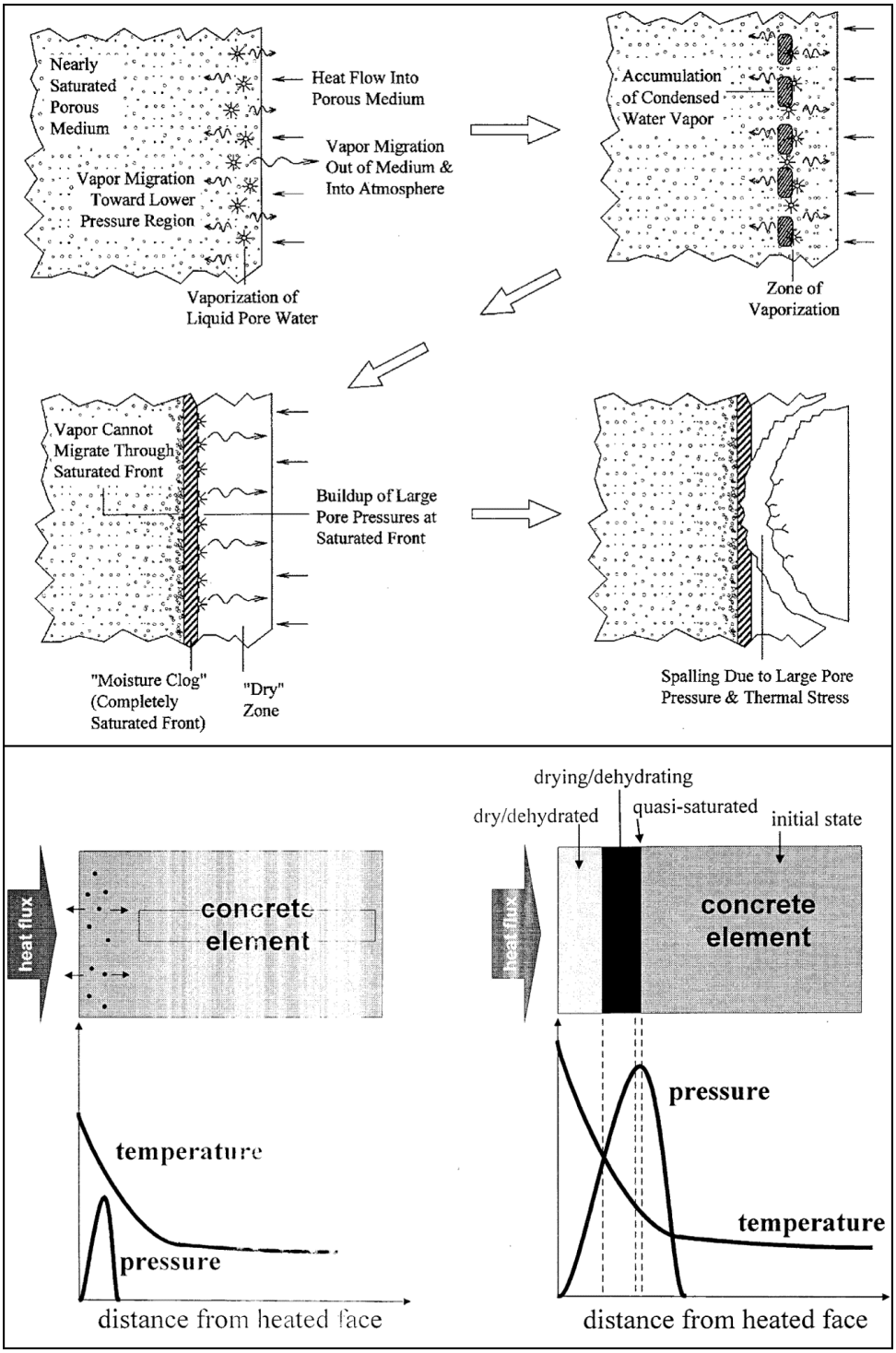

Figure 2.8: Conceptual mechanisms of moisture clog spalling. Top: Steps leading to spalling from Consolazio et al. (1998) [130]. Bottom: Build up of stresses from Kalifa et al. (2000) [125].

During the heating of samples, at 100°C, evaporation is replaced by ebullition, which drastically increases the rate of water loss within the material [131]. It was assumed that the escape of vapor becomes ruled by water vapor pressure, which has an exponential relationship to temperature described by Equation 2.24 [132], in which P_v is pressure in Pascal and T is temperature in K. Thus, the pressure development inside the material is dependent on temperature, but also on the amount of remaining water, which itself depends on the initial moisture state and heating rate. When combining this knowledge with thermogravimetric experiments, it was found that the unexplained critical temperature range described in the previous section roughly correlates to when the vapour pressure exceeds the typical tensile strength of samples [133]. This concept is illustrated in Figure 2.9. The different behaviour of samples with similar properties and same heating conditions was also explained by these studies, as the spalling was due to their differences in moisture content [128, 134].

$$P_v = exp\left(23.22 - \frac{3841.22}{T - 45.00}\right) \tag{2.24}$$

Since high strength concrete holds less water than normal strength concrete, there was still one issue to be explained. Because the pressure development within the material is inversely proportional to the maximum flow of water vapor, it is generally accepted that a more porous microstructure is less susceptible to this form of spalling [135]. This was further studied by using a single mixture design and varying the packing coefficient to choose the gradation of the aggregates, the study revealed that better packing leads to more severe spalling [136].

This theory clearly had merits, but presented a challenge for engineers to predict concrete behaviour.The TMM could be implemented by finite element methods (FEM) and the stresses derived from thermal strains. Meanwhile, the stresses caused by the THM would require the coupling of water transport with vapour expansion and a nearly perfect knowledge of the pore structure of the concrete being tested. Kalifa et al. (2000) [125] proposed an experimental setup with pressure and temperature sensors at different depths of a sample, in addition to the usual thermogravimetric measurements. This method provided a way to measure pore pressure at varying locations and was used in several future studies [129, 137–141].

2.2.3. RECENT ADVANCES AND THE ROLE OF FIBERS

Recently, Li et al. (2021) [142] reviewed several studies using the pore pressure investigation technique proposed in Kalifa et al. (2000) [125]. The review found that although this method is useful to prove positive correlations between pore pressure buildup and compressive strength, moisture content, heating rate and lateral confinement, it still fails to provide accurate quantitative estimations of spalling occurrence or damage level. This is, in part, attributed to the lack of standardization of test setup, with several parameters such as tube filler and gage head considerably changing the pressure values measured.

Currently, concrete spalling is hypothesized to happen due to the summation of the stresses generated by both TMM and THM, with the governing mechanism depending on the moisture content. For a sufficiently dry concrete, the THM becomes negligible and spalling only occurs through the TMM [87]. On the other hand, the thermo-hygral

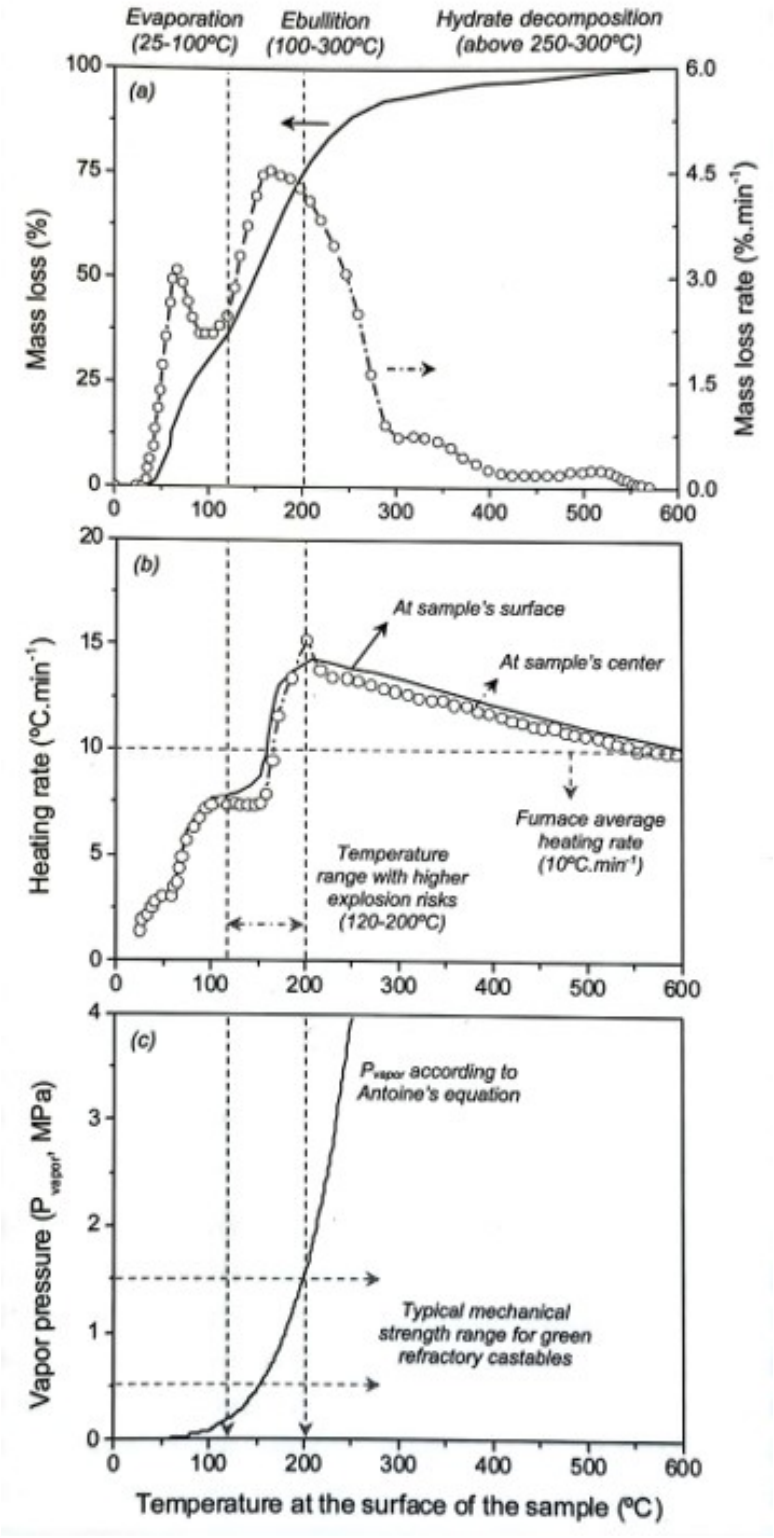

Figure 2.9: Top: Mass loss of sample at different temperatures. Middle: Heating rate difference between sample center and surface. Bottom: Vapor pressure development according to Equation 2.24. Experiments from [133], image from [25]

mechanism always suffers from thermo-mechanical stresses developed during heating [143, 144], thus it cannot be studied individually [105].

Another consensus was on the importance of fibres in the mixture design of concrete that would possibly be submitted to high temperatures. In particular, sufficient dosage of polypropylene (PP) has been found to avoid spalling even in extreme cases, such as ultra high strength concrete mixtures [110, 111, 145]. The advantages of this addition have been confirmed by several works [146–150], due to their capacity of increasing the intrinsic permeability of concrete when heated [151]. The capacity of these fibers to melt in low temperatures, allow for their partial exit, leaving empty tunnels, facilitating vapor transport [152]. Figure 2.10 provides information on the fibre melting point, influence in permeability and mechanism at high temperatures.

However, because it is still not possible to accurately estimate the vapor escape pressure, the exact dosage of polypropylene for a given mixture design remains unknown. Many researchers proposed a method to estimate the fibres needed for concrete [88, 154–156], but this field is still open for discussion. Besides polypropylene, several other types of fibers have been attempted to improve spalling resistance, with their mechanism mostly dependent on the base material. Other polymeric fibres (e. g. nylon, PET, PVA, polyamide) work similarly to PP, but their higher melting point decreases usefulness [154, 157]. Natural fibers (e. g. jute, flax, cellullose) usually shrink and burn instead of melting [117, 118, 157], thus, also providing new channels to increase permeability.

Steel fibres, on the other hand, act as local reinforcement against the stresses caused by the TMM, requiring more energy for the crack growth [91]. In general, this is a strategy used less often, as most experiments have a THM governed spalling. Nevertheless, some researchers [89, 158, 159] found synergy in the combination of PP and steel fibres, allowing for a concrete even more resistant to spalling. Few other fibres have been studied to arrest the thermo-mechanical mechanism (e. g. carbon, rubber), but not enough studies have been published for definite conclusions on their contribution [16, 160].

2.3. CONCLUDING REMARKS

Both the behaviour of concrete during exposure to high temperature and the residual properties afterwards vary considerably because of the heterogeneity of the material and its very large differences in composition. The residual properties are assumed based on the combination of binder and aggregates as explained in Section 2.1. However, observing Figure 2.2, it is evident that the prediction remains inaccurate. Further, the residual properties are only relevant if the material does not suffer from spalling, which cannot be predicted at the time of writing of this thesis.

Thus, the prediction of damage caused by spalling is lacking in literature. Because of that, no single experiment or even review study contains reliable guidelines of how to design a concrete mixture that would not suffer from spalling under specific conditions and further would retain certain mechanical properties after the exposure to high temperature.

In addition, most spalling experiments are conducted in small samples [108–110, 161–167], even though a clear size effect is present [168] and both, the TMM and the THM are worse in bigger samples [169]. This is due to a number of reasons (e. g. bigger thermal and moisture gradients in full size concrete members, lack of restraints and

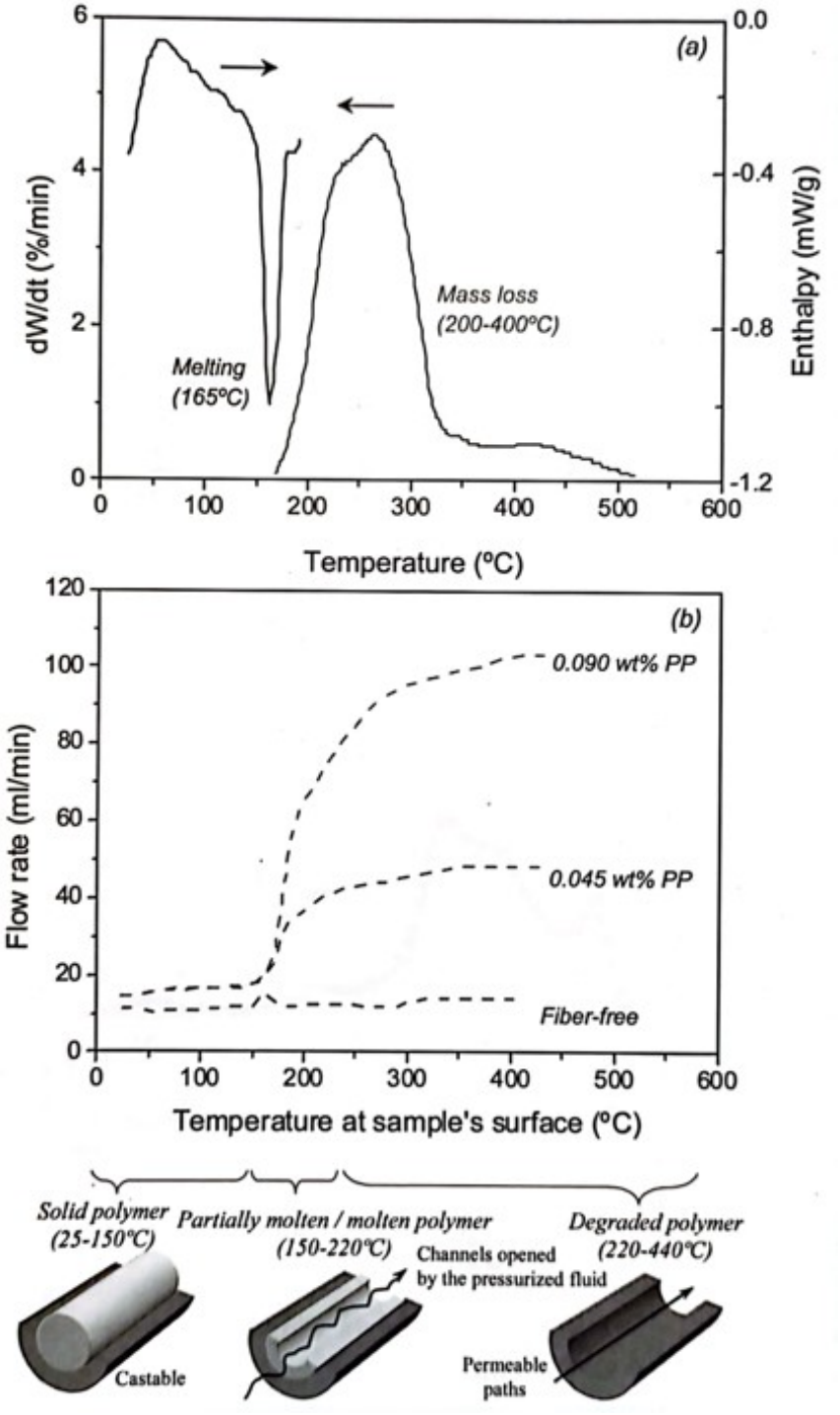

Figure 2.10: Top: Thermal analysis of polypropylene fibres. Middle: Flow rate trend for samples with and without PP fibres. Bottom: Assumed behaviour of PP fibres during heating. Experiments from [153], image from [25].

loads in small samples, different forms of heating for laboratory experiments), but poses a important challenge regarding how to extrapolate published results to actual structures. This was being studied at the time of writing of this thesis [140, 160, 170], but is likely to go on as a challenge unless a fundamental way of estimating pore structure and consequent pressure development is proposed.

BIBLIOGRAPHY

[1] *Portland Cement Market – Global Industry Analysis and Forecast (2022-2027)*. Tech. rep. Maximize Market Research PVT LTD, 2022.

[2] P.K. Mehta and P.J.M. Monteiro. *Concrete: Microstructure, Properties, and Materials*. McGraw Hill professional. McGraw-Hill Education, 2006. ISBN: 9780071462891. URL: https://books.google.nl/books?id=3j5EAQAAIAAJ.

[3] H.F.W Taylor, C Famy, and K.L Scrivener. "Delayed ettringite formation". In: *Cement and Concrete Research* 31.5 (2001), pp. 683–693. ISSN: 0008-8846. DOI: https://doi.org/10.1016/S0008-8846(01)00466-5. URL: https://www.sciencedirect.com/science/article/pii/S0008884601004665.

[4] Florian Deschner et al. "Effect of temperature on the hydration of Portland cement blended with siliceous fly ash". In: *Cement and Concrete Research* 52 (2013), pp. 169–181. ISSN: 0008-8846. DOI: https://doi.org/10.1016/j.cemconres.2013.07.006. URL: https://www.sciencedirect.com/science/article/pii/S0008884613001671.

[5] C. Romero Rodríguez et al. "Fundamental investigation on the frost resistance of mortar with microencapsulated phase change materials". In: *Cement and Concrete Composites* 113 (2020), p. 103705. ISSN: 0958-9465. DOI: https://doi.org/10.1016/j.cemconcomp.2020.103705. URL: https://www.sciencedirect.com/science/article/pii/S0958946520302122.

[6] Z.C. Lu et al. "Characterization data of reference cement CEM I 42.5 R used for priority program DFG SPP 2005 "Opus Fluidum Futurum – Rheology of reactive, multiscale, multiphase construction materials"". In: *Data in Brief* 27 (2019), p. 104699. ISSN: 2352-3409. DOI: https://doi.org/10.1016/j.dib.2019.104699. URL: https://www.sciencedirect.com/science/article/pii/S2352340919310546.

[7] H. Ideker J. et al. "Calcium Aluminate Cements". In: *Lea's Chemistry of Cement and Concrete*. Ed. by P.C. Hewlett and M. Liska. Oxford: Butterworth-Heinemann, 2019. Chap. 13, pp. 713–782.

[8] A.F. Battagin and I.L.S. Battagin. "The Portland Cement in Brazil (in Portuguese)". In: *Materiais de Construção Civil*. Ed. by G.C. Isaia. SãO Paulo: IBRACON, 2010. Chap. 24, pp. 761–790.

[9] D.L. Rayment and A.J. Majumdar. "The composition of the C-S-H phases in portland cement pastes". In: *Cement and Concrete Research* 12.6 (1982), pp. 753–764. ISSN: 0008-8846. DOI: https://doi.org/10.1016/0008-8846(82)90039-4. URL: https://www.sciencedirect.com/science/article/pii/0008884682900394.

[10] G.K. Sun, J. Francis Young, and R. James Kirkpatrick. “The role of Al in C–S–H: NMR, XRD, and compositional results for precipitated samples”. In: *Cement and Concrete Research* 36.1 (2006), pp. 18–29. ISSN: 0008-8846. DOI: https://doi.org/10.1016/j.cemconres.2005.03.002. URL: https://www.sciencedirect.com/science/article/pii/S0008884605000840.

[11] Sara Bahafid et al. “Effect of the hydration temperature on the microstructure of Class G cement: C-S-H composition and density”. In: *Cement and Concrete Research* 95 (2017), pp. 270–281. ISSN: 0008-8846. DOI: https://doi.org/10.1016/j.cemconres.2017.02.008. URL: https://www.sciencedirect.com/science/article/pii/S000884616303l2X.

[12] Mohammadreza Izadifar et al. “Correlation between Composition and Mechanical Properties of Calcium Silicate Hydrates Identified by Infrared Spectroscopy and Density Functional Theory”. In: *The Journal of Physical Chemistry C* 123.17 (2019), pp. 10868–10873. DOI: 10.1021/acs.jpcc.8b11920. eprint: https://doi.org/10.1021/acs.jpcc.8b11920. URL: https://doi.org/10.1021/acs.jpcc.8b11920.

[13] S. Mindess and J.F. Young. *Concrete*. Prentice-Hall civil engineering and engineering mechanics series. Prentice-Hall, 1981. ISBN: 9780131671065. URL: https://books.google.nl/books?id=%5C_7tRAAAAMAAJ.

[14] William Lerch and Robert Herman Bogue. *The heat of hydration of portland cement pastes*. Portland Cement Association at the National Bureau of Standards, 1934.

[15] P. Livesey, A. Donnelly, and C. Tomlinson. “Measurement of the heat of hydration of cement”. In: *Cement and Concrete Composites* 13.3 (1991). Special Issue on Blended Cements, pp. 177–185. ISSN: 0958-9465. DOI: https://doi.org/10.1016/0958-9465(91)90018-D. URL: https://www.sciencedirect.com/science/article/pii/095894659190018D.

[16] Shazim Ali Memon et al. “Durability of sustainable concrete subjected to elevated temperature – A review”. In: *Construction and Building Materials* 199 (2019), pp. 435–455. ISSN: 0950-0618. DOI: https://doi.org/10.1016/j.conbuildmat.2018.12.040. URL: https://www.sciencedirect.com/science/article/pii/S0950061818330204.

[17] Dwarakanath Ravikumar et al. “Carbon dioxide utilization in concrete curing or mixing might not produce a net climate benefit”. In: *Nature Communications* 12.1 (2021), pp. 1–13. ISSN: 20411723. DOI: 10.1038/s41467-021-21148-w. URL: http://dx.doi.org/10.1038/s41467-021-21148-w.

[18] M.A. Peter et al. “Competition of several carbonation reactions in concrete: A parametric study”. In: *Cement and Concrete Research* 38.12 (2008), pp. 1385–1393. ISSN: 0008-8846. DOI: https://doi.org/10.1016/j.cemconres.2008.09.003. URL: https://www.sciencedirect.com/science/article/pii/S0008884608001555.

[19] Kohobhange S.P. Karunadasa et al. “Thermal decomposition of calcium carbonate (calcite polymorph) as examined by in-situ high-temperature X-ray powder diffraction”. In: *Journal of Physics and Chemistry of Solids* 134 (2019), pp. 21–28. ISSN: 0022-3697. DOI: https://doi.org/10.1016/j.jpcs.2019.05.023. URL: https://www.sciencedirect.com/science/article/pii/S0022369719301970.

[20] C.A. Britez and C.N. Costa. “Ações do Fogo nas Estruturas de Concreto”. In: *Concreto: Ciência e Tecnologia*. Ed. by G.C. Isaia. São Paulo: IBRACON, 2011. Chap. 29, pp. 1029–1068.

[21] M. Hedayati et al. “A comprehensive review of spalling and fire performance of concrete members”. In: *Electronic Journal of Structural Engineering* 15.1 (2015), pp. 8–34. ISSN: 14439255.

[22] *EN 1992-1-2 Eurocode 2: Design of concrete structures - Part 1-2: General Rules – Structural fire design*. EN. Brussels: CEN, 2008.

[23] Qianmin Ma et al. “Mechanical properties of concrete at high temperature—A review”. In: *Construction and Building Materials* 93 (2015), pp. 371–383. ISSN: 0950-0618. DOI: https://doi.org/10.1016/j.conbuildmat.2015.05.131. URL: https://www.sciencedirect.com/science/article/pii/S0950061815006765.

[24] Chi-Sun Poon et al. “Comparison of the strength and durability performance of normal- and high-strength pozzolanic concretes at elevated temperatures”. In: *Cement and Concrete Research* 31.9 (2001), pp. 1291–1300. ISSN: 0008-8846. DOI: https://doi.org/10.1016/S0008-8846(01)00580-4. URL: https://www.sciencedirect.com/science/article/pii/S0008884601005804.

[25] Ana Da Luz, M.A.L. Braulio, and Victor Pandolfelli. *F.I.R.E. Compendium Series - Refractory Castable Engineering*. Göller Verlag, Mar. 2015, p. 734. ISBN: ISBN 978-3-87264-004-8.

[26] J. Bensted. “Calcium Aluminate Cements”. In: *Structure and performance of cements*. Ed. by J. Bensted and P. Barnes. London: CRC Press, 2002. Chap. 13, pp. 114–139.

[27] Karen L. Scrivener, Jean-Louis Cabiron, and Roger Letourneux. “High-performance concretes from calcium aluminate cements”. In: *Cement and Concrete Research* 29.8 (1999), pp. 1215–1223. ISSN: 0008-8846. DOI: https://doi.org/10.1016/S0008-8846(99)00103-9. URL: https://www.sciencedirect.com/science/article/pii/S0008884699001039.

[28] *Calcium Aluminate Cement Market Size By Product (2020-2026)*. Tech. rep. Report ID: GMI4855. Global Market Insights Inc., 2020. URL: https://www.gminsights.com/industry-analysis/calcium-aluminate-cement-market.

[29] N.K. Lee et al. “Microstructural investigation of calcium aluminate cement-based ultra-high performance concrete (UHPC) exposed to high temperatures”. In: *Cement and Concrete Research* 102 (2017), pp. 109–118. ISSN: 0008-8846. DOI: https://doi.org/10.1016/j.cemconres.2017.09.004. URL: https://www.sciencedirect.com/science/article/pii/S0008884617301825.

[30] H. M. Son et al. “Effect of nano-silica on hydration and conversion of calcium aluminate cement”. In: *Construction and Building Materials* 169 (2018), pp. 819–825. ISSN: 09500618. DOI: 10.1016/j.conbuildmat.2018.03.011. URL: https://doi.org/10.1016/j.conbuildmat.2018.03.011.

[31] Guoqing Geng et al. “Nanometer-Resolved Spectroscopic Study Reveals the Conversion Mechanism of CaO·Al2O3·10H2O to 2CaO·Al2O3·8H2O and 3CaO·Al2O3·6H2O at an Elevated Temperature”. In: *Crystal Growth & Design* 17.8 (2017), pp. 4246–4253. DOI: 10.1021/acs.cgd.7b00553. eprint: https://doi.org/10.1021/acs.cgd.7b00553. URL: https://doi.org/10.1021/acs.cgd.7b00553.

[32] Emmanuel Nonnet, Nicolas Lequeux, and Philippe Boch. “Elastic properties of high alumina cement castables from room temperature to 1600°C”. In: *Journal of the European Ceramic Society* 19.8 (1999), pp. 1575–1583. ISSN: 0955-2219. DOI: https://doi.org/10.1016/S0955-2219(98)00255-6. URL: https://www.sciencedirect.com/science/article/pii/S0955221998002556.

[33] Valentin Antonovič et al. “The Effect of Temperature on the Formation of the Hydrated Calcium Aluminate Cement Structure”. In: *Procedia Engineering* 57 (2013). Modern Building Materials, Structures and Techniques, pp. 99–106. ISSN: 1877-7058. DOI: https://doi.org/10.1016/j.proeng.2013.04.015. URL: https://www.sciencedirect.com/science/article/pii/S1877705813007455.

[34] Feng Wang et al. “Effect of Colloidal Silica on the Hydration Behavior of Calcium Aluminate Cement”. In: *Materials* 11.10 (2018). ISSN: 1996-1944. DOI: 10.3390/ma11101849. URL: https://www.mdpi.com/1996-1944/11/10/1849.

[35] Yulong Wang et al. “Microstructure evolution during the heating process and its effect on the elastic properties of CAC-bonded alumina castables”. In: *Ceramics International* 42.9 (2016), pp. 11355–11362. ISSN: 0272-8842. DOI: https://doi.org/10.1016/j.ceramint.2016.04.058. URL: https://www.sciencedirect.com/science/article/pii/S0272884216304539.

[36] A.M. Neville. *Properties of Concrete*. Pearson, 2011. ISBN: 9780273755807. URL: https://books.google.nl/books?id=TdfewmQ-cMIC.

[37] Wasim Khaliq and Hammad Anis Khan. “High temperature material properties of calcium aluminate cement concrete”. In: *Construction and Building Materials* 94 (2015), pp. 475–487. ISSN: 09500618. DOI: 10.1016/j.conbuildmat.2015.07.023. URL: http://dx.doi.org/10.1016/j.conbuildmat.2015.07.023.

[38] Eva Vejmelková et al. “High temperature durability of fiber reinforced high alumina cement composites”. In: *Construction and Building Materials* 162 (2018), pp. 881–891. ISSN: 09500618. DOI: 10.1016/j.conbuildmat.2018.01.076.

[39] Guoxin Li et al. “Study on the resistance to seawater corrosion of the cementitious systems containing ordinary Portland cement or/and calcium aluminate cement”. In: *Construction and Building Materials* 157 (2017), pp. 852–859. ISSN: 09500618. DOI: 10.1016/j.conbuildmat.2017.09.175. URL: https://doi.org/10.1016/j.conbuildmat.2017.09.175.

[40] S. Goñi, M. T. Gaztañaga, and A. Guerrero. “Role of cement type on carbonation attack”. In: *Journal of Materials Research* 17.7 (2002), pp. 1834–1842. ISSN: 08842914. DOI: 10.1557/JMR.2002.0271.

[41] Caijun Shi, A. Fernández Jiménez, and Angel Palomo. “New cements for the 21st century: The pursuit of an alternative to Portland cement”. In: *Cement and Concrete Research* 41.7 (2011). Special Issue: 13th International Congress on the Chemistry of Cement, pp. 750–763. ISSN: 0008-8846. DOI: https://doi.org/10.1016/j.cemconres.2011.03.016. URL: https://www.sciencedirect.com/science/article/pii/S0008884611000925.

[42] Ellis Gartner and Tongbo Sui. “Alternative cement clinkers”. In: *Cement and Concrete Research* 114 (2018). Report of UNEP SBCI WORKING GROUP ON LOW-CO2 ECO-EFFICIENT CEMENT-BASED MATERIALS, pp. 27–39. ISSN: 0008-8846. DOI: https://doi.org/10.1016/j.cemconres.2017.02.002. URL: https://www.sciencedirect.com/science/article/pii/S000888461630775X.

[43] Caijun Shi, Bo Qu, and John L. Provis. “Recent progress in low-carbon binders”. In: *Cement and Concrete Research* 122 (2019), pp. 227–250. ISSN: 0008-8846. DOI: https://doi.org/10.1016/j.cemconres.2019.05.009. URL: https://www.sciencedirect.com/science/article/pii/S0008884619301838.

[44] Khadim Ndiaye, Martin Cyr, and Stéphane Ginestet. “Durability and stability of an ettringite-based material for thermal energy storage at low temperature”. In: *Cement and Concrete Research* 99 (2017), pp. 106–115. ISSN: 0008-8846. DOI: https://doi.org/10.1016/j.cemconres.2017.05.001. URL: https://www.sciencedirect.com/science/article/pii/S0008884616306202.

[45] Yukie Shimada and J.Francis Young. “Thermal stability of ettringite in alkaline solutions at 80 °C”. In: *Cement and Concrete Research* 34.12 (2004), pp. 2261–2268. ISSN: 0008-8846. DOI: https://doi.org/10.1016/j.cemconres.2004.04.008. URL: https://www.sciencedirect.com/science/article/pii/S0008884604001632.

[46] Yuke Lou et al. “Influence of synthesis methods on ettringite dehydration”. In: *Journal of Thermal Analysis and Calorimetry* 135.4 (Feb. 2019), pp. 2031–2038. ISSN: 1588-2926. DOI: 10.1007/s10973-018-7391-8. URL: https://doi.org/10.1007/s10973-018-7391-8.

[47] Barbara Lothenbach et al. “Hydration of Belite-Ye’elimite-Ferrite cements: thermodynamic modeling”. In: *14th International Conference on the Chemistry of Cement*. Chinese Ceramic Society & China Building Materials Academy. Beijing, China: Chinese Ceramic Society & China Building Materials Academy, Oct. 2015.

[48] Warda Ashraf and Jan Olek. “Carbonation behavior of hydraulic and non-hydraulic calcium silicates: potential of utilizing low-lime calcium silicates in cement-based materials”. In: *Journal of Materials Science* 51.13 (July 2016), pp. 6173–6191. ISSN: 1573-4803. DOI: 10.1007/s10853-016-9909-4. URL: https://doi.org/10.1007/s10853-016-9909-4.

[49] Joseph Davidovits. “Properties of Geopolymer Cements”. In: vol. 1. Oct. 1994, pp. 131–149.

[50] R.V.R. San Nicolas, B. Walkley, and J.S.J. van Deventer. “7 - Fly ash-based geopolymer chemistry and behavior”. In: *Coal Combustion Products (CCP's)*. Ed. by Tom Robl, Anne Oberlink, and Rod Jones. Woodhead Publishing, 2017, pp. 185–214. ISBN: 978-0-08-100945-1. DOI: https://doi.org/10.1016/B978-0-08-100945-1.00007-1. URL: https://www.sciencedirect.com/science/article/pii/B9780081009451000071.

[51] Navid Ranjbar et al. “Hardening evolution of geopolymers from setting to equilibrium: A review”. In: *Cement and Concrete Composites* 114 (2020), p. 103729. ISSN: 0958-9465. DOI: https://doi.org/10.1016/j.cemconcomp.2020.103729. URL: https://www.sciencedirect.com/science/article/pii/S0958946520302353.

[52] Qifeng Song, Ming-Zhi Guo, and Tung-Chai Ling. “A review of elevated-temperature properties of alternative binders: Supplementary cementitious materials and alkali-activated materials”. In: *Construction and Building Materials* 341 (2022), p. 127894. ISSN: 0950-0618. DOI: https://doi.org/10.1016/j.conbuildmat.2022.127894. URL: https://www.sciencedirect.com/science/article/pii/S0950061822015677.

[53] Tawzia Manzoor, Javed Ahmad Bhat, and Asif H. Shah. “Performance of geopolymer concrete at elevated temperature A critical review”. In: *Construction and Building Materials* 420 (2024), p. 135578. ISSN: 0950-0618. DOI: https://doi.org/10.1016/j.conbuildmat.2024.135578. URL: https://www.sciencedirect.com/science/article/pii/S0950061824007190.

[54] Sam A. Walling and John L. Provis. “Magnesia-Based Cements: A Journey of 150 Years, and Cements for the Future?” In: *Chemical Reviews* 116.7 (2016). PMID: 27002788, pp. 4170–4204. DOI: 10.1021/acs.chemrev.5b00463. eprint: https://doi.org/10.1021/acs.chemrev.5b00463. URL: https://doi.org/10.1021/acs.chemrev.5b00463.

[55] William Roderick Eubank. “Calcination Studies of Magnesium Oxides”. In: *Journal of the American Ceramic Society* 34.8 (1951), pp. 225–229. DOI: https://doi.org/10.1111/j.1151-2916.1951.tb11644.x. eprint: https://ceramics.onlinelibrary.wiley.com/doi/pdf/10.1111/j.1151-2916.1951.tb11644.x. URL: https://ceramics.onlinelibrary.wiley.com/doi/abs/10.1111/j.1151-2916.1951.tb11644.x.

[56] J. Lanas and J.I. Alvarez. “Dolomitic lime: thermal decomposition of nesquehonite”. In: *Thermochimica Acta* 421.1 (2004), pp. 123–132. ISSN: 0040-6031. DOI: https://doi.org/10.1016/j.tca.2004.04.007. URL: https://www.sciencedirect.com/science/article/pii/S004060310400139X.

[57] Fuming Jiang, Sergio Speziale, and Thomas Duffy. “Single-crystal Elasticity of Brucite, Mg(OH)2, to 15 Gpa by Brillouin Scattering”. In: *American Mineralogist - AMER MINERAL* 91 (Nov. 2006), pp. 1893–1900. DOI: 10.2138/am.2006.2215.

[58] E. N. Maslen, V. A. Streltsov, and N. R. Streltsova. “X-ray study of the electron density in magnesite $MgCO_3$”. In: *Acta Crystallographica Section B* 49.6 (Dec. 1993), pp. 980–984. DOI: 10.1107/S0108768193006615. URL: https://doi.org/10.1107/S0108768193006615.

[59] G. Giester, C. L. Lengauer, and B. Rieck. “The crystal structure of nesquehonite, MgCO3 · 3H2O, from Lavrion, Greece”. In: *Mineralogy and Petrology* 70.3 (Dec. 2000), pp. 153–163. ISSN: 1438-1168. DOI: 10.1007/s007100070001. URL: https://doi.org/10.1007/s007100070001.

[60] R. J. Hill, J. H. Canterford, and F. J. Moyle. “New data for lansfordite”. In: *Mineralogical Magazine* 46.341 (1982), pp. 453–457. DOI: 10.1180/minmag.1982.046.341.08.

[61] M. Akao and S. Iwai. “The hydrogen bonding of artinite”. In: *Acta Crystallographica Section B* 33.12 (Dec. 1977), pp. 3951–3953. DOI: 10.1107/S0567740877012576. URL: https://doi.org/10.1107/S0567740877012576.

[62] M. Akao and S. Iwai. “The hydrogen bonding of hydromagnesite”. In: *Acta Crystallographica Section B* 33.4 (Apr. 1977), pp. 1273–1275. DOI: 10.1107/S0567740877005834. URL: https://doi.org/10.1107/S0567740877005834.

[63] Gunnar Raade. “Dypingite, a new hydrous basic carbonate of magnesium, from Norway”. In: *American Mineralogist* 55.9-10 (Oct. 1970), pp. 1457–1465. ISSN: 0003-004X. eprint: https://pubs.geoscienceworld.org/msa/ammin/article-pdf/55/9-10/1457/4250073/am-1970-1457.pdf.

[64] George T. Faust. “Huntite, Mg3Ca(CO3)4 A new mineral*”. In: *American Mineralogist* 38.1-2 (Feb. 1953), pp. 4–24. ISSN: 0003-004X. eprint: https://pubs.geoscienceworld.org/msa/ammin/article-pdf/38/1-2/4/4245406/am-1953-4.pdf.

[65] A. D. Wilson. “The chemistry of dental cements”. In: *Chem. Soc. Rev.* 7 (2 1978), pp. 265–296. DOI: 10.1039/CS9780700265. URL: http://dx.doi.org/10.1039/CS9780700265.

[66] Yuantao Liu et al. “Experimental research on properties and microstructures of magnesium-iron phosphate cement”. In: *Construction and Building Materials* 257 (2020), p. 119570. ISSN: 0950-0618. DOI: https://doi.org/10.1016/j.conbuildmat.2020.119570. URL: https://www.sciencedirect.com/science/article/pii/S0950061820315750.

[67] R.W. Limes and P. David. *Basic refractory compositions for intermediate temperature zones*. U.S. Patent 3 285 758, May 1965.

[68] Yu Zhang et al. “Enhanced formation of magnesium silica hydrates (M-S-H) using sodium metasilicate and caustic magnesia in magnesia castables”. In: *Ceramics International* 43.12 (2017), pp. 9110–9116. ISSN: 0272-8842. DOI: https://doi.org/10.1016/j.ceramint.2017.04.058. URL: https://www.sciencedirect.com/science/article/pii/S0272884217306661.

[69] Yu Zhang, Yawei Li, and Yajie Dai. "Formation of magnesium silicate hydrate in the Mg(OH)2-SiO2 suspensions and its influence on the properties of magnesia castables". In: *Ceramics International* 44.17 (2018), pp. 21365–21373. ISSN: 0272-8842. DOI: https://doi.org/10.1016/j.ceramint.2018.08.190. URL: https://www.sciencedirect.com/science/article/pii/S0272884218322648.

[70] Yu Zhang et al. "Temperature-dependent rehydration of magnesium silicate hydrate (M-S-H): Development of no-cement binder through MD/DFT validation". In: *Ceramics International* 48.5 (2022), pp. 7063–7070. ISSN: 0272-8842. DOI: https://doi.org/10.1016/j.ceramint.2021.11.265. URL: https://www.sciencedirect.com/science/article/pii/S0272884221036877.

[71] Bjørn Myhre, Cecilie Ødegård, and Heidi Feldborg. "Periclase castables based on the bond MgO–SiO2–H2O: Properties and current status". In: *INREFCON (5th India International Refractories Congress) in Bhubaneswar, India*. 2002.

[72] B Zhu et al. "Proceedings of the Unified International Technical Conference on Refractories (UNITECR 2013)". In: (2014).

[73] B. Sandberg and T. Mosberg. "Use of Elkem Microsilica in binder systems for ultra-low cement castables and basic, "cement-free" castables." In: *Ceramic Transactions: Advances in Refractories Technology*. Ed. by R. E. Fisher. Westerville, OH: American Ceramic Society, 1989. Chap. 4, pp. 245–258.

[74] Tingting Zhang, CR Cheeseman, and LJ Vandeperre. "Development of low pH cement systems forming magnesium silicate hydrate (MSH)". In: *Cement and Concrete Research* 41.4 (2011), pp. 439–442.

[75] Marianne Inman, Eythor Rafn Thorhallsson, and Kamal Azrague. "A Mechanical and Environmental Assessment and Comparison of Basalt Fibre Reinforced Polymer (BFRP) Rebar and Steel Rebar in Concrete Beams". In: *Energy Procedia* 111 (2017). 8th International Conference on Sustainability in Energy and Buildings, SEB-16, 11-13 September 2016, Turin, Italy, pp. 31–40. ISSN: 1876-6102. DOI: https://doi.org/10.1016/j.egypro.2017.03.005. URL: https://www.sciencedirect.com/science/article/pii/S187661021730022X.

[76] Elisabetta Monaldo, Francesca Nerilli, and Giuseppe Vairo. "Basalt-based fiber-reinforced materials and structural applications in civil engineering". In: *Composite Structures* 214 (2019), pp. 246–263. ISSN: 0263-8223. DOI: https://doi.org/10.1016/j.compstruct.2019.02.002. URL: https://www.sciencedirect.com/science/article/pii/S0263822318342259.

[77] Ahmed H. Ali et al. "Durability performance and long-term prediction models of sand-coated basalt FRP bars". In: *Composites Part B: Engineering* 157 (2019), pp. 248–258. ISSN: 1359-8368. DOI: https://doi.org/10.1016/j.compositesb.2018.08.065. URL: https://www.sciencedirect.com/science/article/pii/S1359836818322674.

[78] Xing Zhao et al. “Experimental study on effect of resin matrix in basalt fiber reinforced polymer composites under static and fatigue loading”. In: *Construction and Building Materials* 242 (2020), p. 118121. ISSN: 0950-0618. DOI: https://doi.org/10.1016/j.conbuildmat.2020.118121. URL: https://www.sciencedirect.com/science/article/pii/S0950061820301264.

[79] Xiangke Guo et al. “Deterioration of mechanical properties of basalt/carbon hybrid FRP bars in SWSC under seawater corrosive environment”. In: *Construction and Building Materials* 317 (2022), p. 125979. ISSN: 0950-0618. DOI: https://doi.org/10.1016/j.conbuildmat.2021.125979. URL: https://www.sciencedirect.com/science/article/pii/S0950061821037119.

[80] Yong Yi et al. “Mitigating the deterioration of BFRP bars in seawater sea sand mortar by reducing alkalinity”. In: *Construction and Building Materials* 317 (2022), p. 125885. ISSN: 0950-0618. DOI: https://doi.org/10.1016/j.conbuildmat.2021.125885. URL: https://www.sciencedirect.com/science/article/pii/S0950061821036187.

[81] Hongxia Qiao et al. “The application review of magnesium oxychloride cement”. In: *Journal of Chemical and Pharmaceutical Research,* 6(5) (2014), pp. 180–185. ISSN: 0975-7384. URL: https://www.jocpr.com/articles/the-application-review-of-magnesium-oxychloride-cement.pdf.

[82] Pingping He et al. “Mechanical, durability and environmental aspects of magnesium oxychloride cement boards incorporating waste wood”. In: *Journal of Cleaner Production* 207 (2019), pp. 391–399. ISSN: 0959-6526. DOI: https://doi.org/10.1016/j.jclepro.2018.10.015. URL: https://www.sciencedirect.com/science/article/pii/S0959652618330233.

[83] Yafei Hao, Chao Li, and Fengqing Zhao. “Study on water resistance modification of magnesium oxysulfate cement”. In: *IOP Conference Series: Materials Science and Engineering* 493.1 (Mar. 2019), p. 012079. DOI: 10.1088/1757-899X/493/1/012079. URL: https://dx.doi.org/10.1088/1757-899X/493/1/012079.

[84] C.S. Neto. “Agregados Naturais, Britados e Artificiais para Concreto”. In: *Concreto: Ciência e Tecnologia*. Ed. by G.C. Isaia. São Paulo: IBRACON, 2011. Chap. 7, pp. 233–260.

[85] T Harada et al. “Strength, elasticity and thermal properties of concrete subjected to elevated temperatures”. In: *Special Publication* 34 (1972), pp. 377–406.

[86] Eike Klingsch, Andrea Frangi, and Mario Fontana. *Explosive spalling of concrete in fire. Test report*. en. Report. Zürich, 2013. DOI: 10.3929/ethz-a-010076314.

[87] Juan Yang et al. “On the explosive spalling behavior of ultra-high performance concrete with and without coarse aggregate exposed to high temperature”. In: *Construction and Building Materials* 226 (2019), pp. 932–944. ISSN: 0950-0618. DOI: https://doi.org/10.1016/j.conbuildmat.2019.07.299. URL: https://www.sciencedirect.com/science/article/pii/S0950061819319737.

[88] Young-Sun Heo et al. “Relationship between inter-aggregate spacing and the optimum fiber length for spalling protection of concrete in fire”. In: *Cement and Concrete Research* 42.3 (2012), pp. 549–557. ISSN: 0008-8846. DOI: https://doi.org/10.1016/j.cemconres.2011.12.002. URL: https://www.sciencedirect.com/science/article/pii/S0008884611003061.

[89] Ye Li et al. “Effect of aggregate size and inclusion of polypropylene and steel fibers on explosive spalling and pore pressure in ultra-high-performance concrete (UHPC) at elevated temperature”. In: *Cement and Concrete Composites* 99 (2019), pp. 62–71. ISSN: 0958-9465. DOI: https://doi.org/10.1016/j.cemconcomp.2019.02.016. URL: https://www.sciencedirect.com/science/article/pii/S0958946518306504.

[90] Josipa Bosnjak. “Explosive spalling and permeability of high performance concrete under fire: numerical and experimental investigations”. PhD thesis. University of Stuttgart, 2014.

[91] Muhammad Abid et al. “High temperature and residual properties of reactive powder concrete – A review”. In: *Construction and Building Materials* 147 (2017), pp. 339–351. ISSN: 0950-0618. DOI: https://doi.org/10.1016/j.conbuildmat.2017.04.083. URL: https://www.sciencedirect.com/science/article/pii/S0950061817307389.

[92] Wouter Botte and Robby Caspeele. “Post-cooling properties of concrete exposed to fire”. In: *Fire Safety Journal* 92.May (2017), pp. 142–150. ISSN: 03797112. DOI: 10.1016/j.firesaf.2017.06.010. URL: http://dx.doi.org/10.1016/j.firesaf.2017.06.010.

[93] T.M. Jeyashree, P.R. Kannan Rajkumar, and K.S. Satyanarayanan. “Developments and research on fire response behaviour of prestressed concrete members – A review”. In: *Journal of Building Engineering* 57 (2022), p. 104797. ISSN: 2352-7102. DOI: https://doi.org/10.1016/j.jobe.2022.104797. URL: https://www.sciencedirect.com/science/article/pii/S2352710222008105.

[94] Suha Ismail Ahmed Ali and Eva Lublóy. “Effect of elevated temperature on the magnetite and quartz concrete at different W/C ratios as nuclear shielding concretes”. In: *Nuclear Materials and Energy* 33 (2022), p. 101234. ISSN: 2352-1791. DOI: https://doi.org/10.1016/j.nme.2022.101234. URL: https://www.sciencedirect.com/science/article/pii/S2352179122001156.

[95] Scott E. Johnson et al. “The quartz phase transition: Does it drive damage and reaction in continental crust?” In: *Earth and Planetary Science Letters* 553 (2021), p. 116622. ISSN: 0012-821X. DOI: https://doi.org/10.1016/j.epsl.2020.116622. URL: https://www.sciencedirect.com/science/article/pii/S0012821X20305665.

[96] M. Maier et al. “An experimental fire-spalling assessment procedure for concrete mixtures”. In: *Construction and Building Materials* 232 (2020), p. 117172. ISSN: 0950-0618. DOI: https://doi.org/10.1016/j.conbuildmat.2019.117172. URL: https://www.sciencedirect.com/science/article/pii/S0950061819326248.

[97] Jin-Cheng Liu, Kang Hai Tan, and Yao Yao. "A new perspective on nature of fire-induced spalling in concrete". In: *Construction and Building Materials* 184 (2018), pp. 581–590. ISSN: 0950-0618. DOI: https://doi.org/10.1016/j.conbuildmat.2018.06.204. URL: https://www.sciencedirect.com/science/article/pii/S0950061818316118.

[98] Young-Sun Heo et al. "Construction application of Fibre/Mesh method for protecting concrete columns in fire". In: *Construction and Building Materials* 25.6 (2011), pp. 2928–2938. ISSN: 0950-0618. DOI: https://doi.org/10.1016/j.conbuildmat.2010.12.017. URL: https://www.sciencedirect.com/science/article/pii/S095006181000694X.

[99] A. Z. Mohd Ali, Jay Sanjayan, and Maurice Guerrieri. "Specimens size, aggregate size, and aggregate type effect on spalling of concrete in fire". In: *Fire and Materials* 42.1 (2018), pp. 59–68. DOI: https://doi.org/10.1002/fam.2457. eprint: https://onlinelibrary.wiley.com/doi/pdf/10.1002/fam.2457. URL: https://onlinelibrary.wiley.com/doi/abs/10.1002/fam.2457.

[100] D. Cree, M. Green, and A. Noumowé. "Residual strength of concrete containing recycled materials after exposure to fire: A review". In: *Construction and Building Materials* 45 (2013), pp. 208–223. ISSN: 09500618. DOI: 10.1016/j.conbuildmat.2013.04.005. URL: http://dx.doi.org/10.1016/j.conbuildmat.2013.04.005.

[101] Bartosz Zegardło, Maciej Szelag, and Paweł Ogrodnik. "Concrete resistant to spalling made with recycled aggregate from sanitary ceramic wastes – The effect of moisture and porosity on destructive processes occurring in fire conditions". In: *Construction and Building Materials* 173 (2018), pp. 58–68. ISSN: 09500618. DOI: 10.1016/j.conbuildmat.2018.04.030.

[102] Bruno Fernandes et al. "Spalling behaviour of concrete made with recycled concrete aggregates". In: *Construction and Building Materials* 344 (2022), p. 128124. ISSN: 0950-0618. DOI: https://doi.org/10.1016/j.conbuildmat.2022.128124. URL: https://www.sciencedirect.com/science/article/pii/S0950061822017895.

[103] F. W. PRESTON and H. E. WHITE. "OBSERVATIONS ON SPALLING*". In: *Journal of the American Ceramic Society* 17.1-12 (1934), pp. 137–144. DOI: https://doi.org/10.1111/j.1151-2916.1934.tb19296.x. eprint: https://ceramics.onlinelibrary.wiley.com/doi/pdf/10.1111/j.1151-2916.1934.tb19296.x. URL: https://ceramics.onlinelibrary.wiley.com/doi/abs/10.1111/j.1151-2916.1934.tb19296.x.

[104] Takeshi Morita et al. "an Experimental Study on Improvement of Spalling Behavior of High-Strength Concrete Elements Under Fire Attack". In: *Journal of Structural and Construction Engineering (Transactions of AIJ)* 66.544 (2001), pp. 171–178. DOI: 10.3130/aijs.66.171_3.

[105] Francesco Lo Monte et al. “Assessment of concrete sensitivity to fire spalling: A multi-scale experimental approach”. In: *Construction and Building Materials* 212 (2019), pp. 476–485. ISSN: 0950-0618. DOI: https://doi.org/10.1016/j.conbuildmat.2019.03.332. URL: https://www.sciencedirect.com/science/article/pii/S0950061819308402.

[106] Cristian Maluk et al. “Experimental study on the fire behaviour of fibre reinforced concrete used in tunnel applications”. In: *Fire Safety Journal* 120 (2021). Fire Safety Science: Proceedings of the 13th International Symposium, p. 103173. ISSN: 0379-7112. DOI: https://doi.org/10.1016/j.firesaf.2020.103173. URL: https://www.sciencedirect.com/science/article/pii/S037971122030134X.

[107] Pengfei Liu et al. “Uncertainty quantification of the effect of concrete heterogeneity on nonlinear seismic response of gravity dams including record-to-record variability”. In: *Structures* 34 (2021), pp. 1785–1797. ISSN: 2352-0124. DOI: https://doi.org/10.1016/j.istruc.2021.08.098. URL: https://www.sciencedirect.com/science/article/pii/S2352012421008109.

[108] Sammy Y. N. Chan, Gai-fei Peng, and John K. W. Chan. “Comparison between high strength concrete and normal strength concrete subjected to high temperature”. In: *Materials and Structures* 29.10 (Dec. 1996), pp. 616–619. ISSN: 1871-6873. DOI: 10.1007/BF02485969. URL: https://doi.org/10.1007/BF02485969.

[109] A. Noumowé et al. “High-Strength Self-Compacting Concrete Exposed to Fire Test”. In: *Journal of Materials in Civil Engineering* 18.6 (2006), pp. 754–758. DOI: 10.1061/(ASCE)0899-1561(2006)18:6(754).

[110] Sun Bei and Lin Zhixiang. “Investigation on spalling resistance of ultra-high-strength concrete under rapid heating and rapid cooling”. In: *Case Studies in Construction Materials* 4 (2016), pp. 146–153. ISSN: 2214-5095. DOI: https://doi.org/10.1016/j.cscm.2016.04.001. URL: https://www.sciencedirect.com/science/article/pii/S2214509516300304.

[111] C. Kahanji, F. Ali, and A. Nadjai. “Explosive spalling of ultra-high performance fibre reinforced concrete beams under fire”. In: *Journal of Structural Fire Engineering* 7.4 (Jan. 2016), pp. 328–348. ISSN: 2040-2317. DOI: 10.1108/JSFE-12-2016-023. URL: https://doi.org/10.1108/JSFE-12-2016-023.

[112] L Missemer et al. “Fire spalling of ultra-high performance concrete : From a global analysis to microstructure investigations”. In: *Cement and Concrete Research* 115.April 2018 (2019), pp. 207–219. ISSN: 0008-8846. DOI: 10.1016/j.cemconres.2018.10.005. URL: https://doi.org/10.1016/j.cemconres.2018.10.005.

[113] Md Miah et al. “Fire spalling of concrete: Effect of cement type”. In: *4th International Workshop on Concrete Spalling Due to Fire Exposure*. RILEM. Leipzig, Germany: RILEM, Oct. 2015.

[114] Hussein Mohammed et al. “Heat-Induced Spalling of Concrete: A Review of the Influencing Factors and Their Importance to the Phenomenon”. In: *Materials* 15.5 (2022). ISSN: 1996-1944. DOI: 10.3390/ma15051693. URL: https://www.mdpi.com/1996-1944/15/5/1693.

[115] Zhu Pan, Jay G. Sanjayan, and Daniel L.Y. Kong. "Effect of aggregate size on spalling of geopolymer and Portland cement concretes subjected to elevated temperatures". In: *Construction and Building Materials* 36 (2012), pp. 365–372. ISSN: 0950-0618. DOI: https://doi.org/10.1016/j.conbuildmat.2012.04.120. URL: https://www.sciencedirect.com/science/article/pii/S0950061812003224.

[116] Young-Sun Heo et al. "Synergistic effect of combined fibers for spalling protection of concrete in fire". In: *Cement and Concrete Research* 40.10 (2010), pp. 1547–1554. ISSN: 0008-8846. DOI: https://doi.org/10.1016/j.cemconres.2010.06.011. URL: https://www.sciencedirect.com/science/article/pii/S0008884610001596.

[117] Dong Zhang et al. "Effect of natural fibers on thermal spalling resistance of ultra-high performance concrete". In: *Cement and Concrete Composites* 109 (2020), p. 103512. ISSN: 0958-9465. DOI: https://doi.org/10.1016/j.cemconcomp.2020.103512. URL: https://www.sciencedirect.com/science/article/pii/S0958946520300032.

[118] Dong Zhang, Guan Yu Tan, and Kang Hai Tan. "Combined effect of flax fibers and steel fibers on spalling resistance of ultra-high performance concrete at high temperature". In: *Cement and Concrete Composites* 121 (2021), p. 104067. ISSN: 0958-9465. DOI: https://doi.org/10.1016/j.cemconcomp.2021.104067. URL: https://www.sciencedirect.com/science/article/pii/S0958946521001360.

[119] V. N. Aptukov. "Model of thermoviscoelastoplastic material damage application to spalling failure". In: *Fizika Goreniya i Vzryva* 22.2 (1986), pp. 244–253.

[120] Z Bazant. "Analysis of Pore Pressure, Thermal Stress and Fracture in Rapidly Heated Concrete". en. In: International Workshop on Fire Performance of High-Strength Concrete. Proceedings. Appendix B: Workshop Papers. B10, Gaithersburg, MD, 1997-02-13 1997. URL: https://tsapps.nist.gov/publication/get_pdf.cfm?pub_id=916655.

[121] D.M. Rishel, F.S. Pettit, and N. Birks. "Spalling types and mechanisms in the erosion corrosion of metals at high temperature". In: *Corrosion Science* 35.5 (1993). Advances in Corrosion and Protection, pp. 1007–1013. ISSN: 0010-938X. DOI: https://doi.org/10.1016/0010-938X(93)90319-C. URL: https://www.sciencedirect.com/science/article/pii/0010938X9390319C.

[122] T.J. Lu and N.A. Fleck. "The thermal shock resistance of solids". In: *Acta Materialia* 46.13 (1998), pp. 4755–4768. ISSN: 1359-6454. DOI: https://doi.org/10.1016/S1359-6454(98)00127-X. URL: https://www.sciencedirect.com/science/article/pii/S135964549800127X.

[123] Kristian Hertz. *Heat-induced Explosion of Dense Concretes*. English. Report no. 166. Technical University of Denmark, Department of Civil Engineering, 1984.

[124] Raymond John Connolly. "The Spalling of Concrete in Fires". In: *Aston University* (1995), p. 333.

[125] Pierre Kalifa, François-Dominique Menneteau, and Daniel Quenard. “Spalling and pore pressure in HPC at high temperatures”. In: *Cement and Concrete Research* 30.12 (2000). Papers presented at the Symposium on "Transport Properties and Microstructure of Cement-Based Systems", pp. 1915–1927. ISSN: 0008-8846. DOI: https://doi.org/10.1016/S0008-8846(00)00384-7. URL: https://www.sciencedirect.com/science/article/pii/S0008884600003847.

[126] Pierre Pimienta et al. “Behavior of UHPFRC at High Temperatures”. In: *Designing and Building with UHPFRC*. John Wiley Sons, Ltd, 2011. Chap. 40, pp. 579–600. ISBN: 9781118557839. DOI: https://doi.org/10.1002/9781118557839.ch40. eprint: https://onlinelibrary.wiley.com/doi/pdf/10.1002/9781118557839.ch40. URL: https://onlinelibrary.wiley.com/doi/abs/10.1002/9781118557839.ch40.

[127] Gai-Fei Peng et al. “Combined curing as a novel approach to improve resistance of ultra-high performance concrete to explosive spalling under high temperature and its mechanical properties”. In: *Cement and Concrete Research* 109 (2018), pp. 147–158. ISSN: 0008-8846. DOI: https://doi.org/10.1016/j.cemconres.2018.04.011. URL: https://www.sciencedirect.com/science/article/pii/S0008884617301886.

[128] Marcus Maier, Matthias Zeiml, and Roman Lackner. “On the effect of pore-space properties and water saturation on explosive spalling of fire-loaded concrete”. In: *Construction and Building Materials* 231 (2020), p. 117150. ISSN: 0950-0618. DOI: https://doi.org/10.1016/j.conbuildmat.2019.117150. URL: https://www.sciencedirect.com/science/article/pii/S0950061819326029.

[129] Pierre Kalifa, Grégoire Chéné, and Christophe Gallé. “High-temperature behaviour of HPC with polypropylene fibres: From spalling to microstructure”. In: *Cement and Concrete Research* 31.10 (2001), pp. 1487–1499. ISSN: 0008-8846. DOI: https://doi.org/10.1016/S0008-8846(01)00596-8. URL: https://www.sciencedirect.com/science/article/pii/S0008884601005968.

[130] Gary R. Consolazio, Michael C. McVay, and Jeff W. Rish. “Measurement and prediction of pore pressures in saturated cement mortar subjected to radiant heating”. In: *ACI Materials Journal* 95.5 (1998), pp. 525–536. ISSN: 0889325X. DOI: 10.14359/395.

[131] K. Oda et al. “Drying characteristics of high-dense castable”. In: *Journal of the Technical Association of Refractories* 13 (2 1989), pp. 21–28.

[132] R.C. Reid, J.M. Prausnitz, and B.E. Poling. *The Properties of Gases and Liquids*. McGraw-Hill chemical engineering series v. 10. McGraw-Hill, 1987. ISBN: 9780070517998. URL: https://books.google.nl/books?id=AcRTAAAAMAAJ.

[133] Rafael Salomão, L. Bittencourt, and Victor Pandolfelli. “Drying additives for refractory castables: Aluminum powder and polymeric fibers”. In: *Cerâmica* 54 (June 2008), pp. 259–267.

[134] F T Ramal, R Salomão, and V C Pandolfelli. “Water content and its effect on the drying behaviour of refractory castables”. In: *Refractories Applications News* 10.3 (2005), pp. 10–13. ISSN: 1537-6443.

[135] F. A. Ali, D. O'Connor, and A. Abu-Tair. "Explosive spalling of high-strength concrete columns in fire". In: *Magazine of Concrete Research* 53.3 (2001), pp. 197–204. DOI: 10.1680/macr.2001.53.3.197. eprint: https://doi.org/10.1680/macr.2001.53.3.197. URL: https://doi.org/10.1680/macr.2001.53.3.197.

[136] Rafael Salomão and Victor C. Pandolfelli. "The particle size distribution effect on the drying efficiency of polymeric fibers containing castables". In: *Ceramics International* 34.1 (2008), pp. 173–180. ISSN: 0272-8842. DOI: https://doi.org/10.1016/j.ceramint.2006.09.005. URL: https://www.sciencedirect.com/science/article/pii/S027288420600277X.

[137] Long T. Phan. "Pore pressure and explosive spalling in concrete". In: *Materials and Structures* 41.10 (Dec. 2008), pp. 1623–1632. ISSN: 1871-6873. DOI: 10.1617/s11527-008-9353-2. URL: https://doi.org/10.1617/s11527-008-9353-2.

[138] Jean-christophe Mindeguia et al. "Temperature , pore pressure and mass variation of concrete subjected to high temperature — Experimental and numerical discussion on spalling risk". In: *Cement and Concrete Research* 40.3 (2010), pp. 477–487. ISSN: 0008-8846. DOI: 10.1016/j.cemconres.2009.10.011. URL: http://dx.doi.org/10.1016/j.cemconres.2009.10.011.

[139] Robert Jansson, Lars Bostro, and Fire Technology. "The Influence of Pressure in the Pore System on Fire Spalling of Concrete". In: *Fire Technology* 46 (2010), pp. 217–230. DOI: 10.1007/s10694-009-0093-9. URL: http://dx.doi.org/10.1007/s10694-009-0093-9.

[140] Jean-Christophe Mindeguia et al. "Experimental discussion on the mechanisms behind the fire spalling of concrete". In: *Fire and Materials* 39.7 (2015), pp. 619–635. DOI: https://doi.org/10.1002/fam.2254. eprint: https://onlinelibrary.wiley.com/doi/pdf/10.1002/fam.2254. URL: https://onlinelibrary.wiley.com/doi/abs/10.1002/fam.2254.

[141] Francesco Lo Monte and Roberto Felicetti. "Heated slabs under biaxial compressive loading: a test set-up for the assessment of concrete sensitivity to spalling". In: *Materials and Structures/Materiaux et Constructions* 50.4 (2017), pp. 1–12. ISSN: 13595997. DOI: 10.1617/s11527-017-1055-1. URL: https://doi.org/10.1617/s11527-017-1055-1.

[142] Ye Li et al. "Pore pressure build-up and explosive spalling in concrete at elevated temperature: A review". In: *Construction and Building Materials* 284 (2021). ISSN: 09500618. DOI: 10.1016/j.conbuildmat.2021.122818.

[143] Yiming Zhang et al. "Fast assessing spalling risk of tunnel linings under RABT fire: From a coupled thermo-hydro-chemo-mechanical model towards an estimation method". In: *Engineering Structures* 142 (2017), pp. 1–19. ISSN: 0141-0296. DOI: https://doi.org/10.1016/j.engstruct.2017.03.068. URL: https://www.sciencedirect.com/science/article/pii/S0141029617310623.

[144] Jin-Cheng Liu and Yao Zhang. “A Simplified Model to Predict Thermo-Hygral Behaviour and Explosive Spalling of Concrete”. In: *Journal of Advanced Concrete Technology* 17.7 (2019), pp. 419–433. DOI: 10.3151/jact.17.419.

[145] Yong Du et al. “Experimental study on the spalling behaviour of ultra-high strength concrete in fire”. In: *Construction and Building Materials* 258 (2020), p. 120334. ISSN: 0950-0618. DOI: https://doi.org/10.1016/j.conbuildmat.2020.120334. URL: https://www.sciencedirect.com/science/article/pii/S0950061820323394.

[146] Cristian Maluk, Luke Bisby, and Giovanni P. Terrasi. “Effects of polypropylene fibre type and dose on the propensity for heat-induced concrete spalling”. In: *Engineering Structures* 141 (2017), pp. 584–595. ISSN: 0141-0296. DOI: https://doi.org/10.1016/j.engstruct.2017.03.058. URL: https://www.sciencedirect.com/science/article/pii/S0141029617310337.

[147] Reza Abaeian, Hamid Pesaran Behbahani, and Shahram Jalali Moslem. “Effects of high temperatures on mechanical behavior of high strength concrete reinforced with high performance synthetic macro polypropylene (HPP) fibres”. In: *Construction and Building Materials* 165 (2018), pp. 631–638. ISSN: 09500618. DOI: 10.1016/j.conbuildmat.2018.01.064. URL: https://doi.org/10.1016/j.conbuildmat.2018.01.064.

[148] G. Mazzucco, C.E. Majorana, and V.A. Salomoni. “Numerical simulation of polypropylene fibres in concrete materials under fire conditions”. In: *Computers Structures* 154 (2015), pp. 17–28. ISSN: 0045-7949. DOI: https://doi.org/10.1016/j.compstruc.2015.03.012. URL: https://www.sciencedirect.com/science/article/pii/S0045794915001029.

[149] A Bilodeau, V.K.R Kodur, and G.C Hoff. “Optimization of the type and amount of polypropylene fibres for preventing the spalling of lightweight concrete subjected to hydrocarbon fire”. In: *Cement and Concrete Composites* 26.2 (2004). Fire Resistance, pp. 163–174. ISSN: 0958-9465. DOI: https://doi.org/10.1016/S0958-9465(03)00085-4. URL: https://www.sciencedirect.com/science/article/pii/S0958946503000854.

[150] Cheon-Goo Han et al. “Performance of spalling resistance of high performance concrete with polypropylene fiber contents and lateral confinement”. In: *Cement and Concrete Research* 35.9 (2005), pp. 1747–1753. ISSN: 0008-8846. DOI: https://doi.org/10.1016/j.cemconres.2004.11.013. URL: https://www.sciencedirect.com/science/article/pii/S0008884604005101.

[151] Matthias Zeiml et al. “How do polypropylene fibers improve the spalling behavior of in-situ concrete?” In: *Cement and Concrete Research* 36.5 (2006), pp. 929–942. ISSN: 0008-8846. DOI: https://doi.org/10.1016/j.cemconres.2005.12.018. URL: https://www.sciencedirect.com/science/article/pii/S0008884605003376.

[152] X. Liu et al. “On the mechanism of polypropylene fibres in preventing fire spalling in self-compacting and high-performance cement paste”. In: *Cement and Concrete Research* 38.4 (2008), pp. 487–499. ISSN: 0008-8846. DOI: https://doi.org/10.1016/j.cemconres.2007.11.010. URL: https://www.sciencedirect.com/science/article/pii/S0008884607002931.

[153] Rafael Salomão and Victor Pandolfelli. “Drying behavior of polymeric fiber-containing refractory castables”. In: *Journal of the Technical Association of Refractories* 24 (Jan. 2004), pp. 83–87.

[154] Young-Sun Heo et al. “Critical parameters of nylon and other fibres for spalling protection of high strength concrete in fire”. In: *Materials and Structures* 44.3 (Apr. 2011), pp. 599–610. ISSN: 1871-6873. DOI: 10.1617/s11527-010-9651-3. URL: https://doi.org/10.1617/s11527-010-9651-3.

[155] Dong Zhang et al. “Effect of spatial distribution of polymer fibers on preventing spalling of UHPC at high temperatures”. In: *Cement and Concrete Research* 140 (2021), p. 106281. ISSN: 0008-8846. DOI: https://doi.org/10.1016/j.cemconres.2020.106281. URL: https://www.sciencedirect.com/science/article/pii/S0008884620315611.

[156] Jin-Cheng Liu et al. “Knowledge-enhanced data-driven models for quantifying the effectiveness of PP fibers in spalling prevention of ultra-high performance concrete”. In: *Construction and Building Materials* 299 (2021), p. 123946. ISSN: 0950-0618. DOI: https://doi.org/10.1016/j.conbuildmat.2021.123946. URL: https://www.sciencedirect.com/science/article/pii/S0950061821017062.

[157] Mitsuo Ozawa et al. “Preventive effects of polypropylene and jute fibers on spalling of UHPC at high temperatures in combination with waste porous ceramic fine aggregate as an internal curing material”. In: *Construction and Building Materials* 206 (2019), pp. 219–225. ISSN: 0950-0618. DOI: https://doi.org/10.1016/j.conbuildmat.2019.02.056. URL: https://www.sciencedirect.com/science/article/pii/S0950061819303514.

[158] N. Yermak et al. “Influence of steel and/or polypropylene fibres on the behaviour of concrete at high temperature: Spalling, transfer and mechanical properties”. In: *Construction and Building Materials* 132 (2017), pp. 240–250. ISSN: 0950-0618. DOI: https://doi.org/10.1016/j.conbuildmat.2016.11.120. URL: https://www.sciencedirect.com/science/article/pii/S095006181631889X.

[159] Ye Li, Kang Hai Tan, and En-Hua Yang. “Synergistic effects of hybrid polypropylene and steel fibers on explosive spalling prevention of ultra-high performance concrete at elevated temperature”. In: *Cement and Concrete Composites* 96 (2019), pp. 174–181. ISSN: 0958-9465. DOI: https://doi.org/10.1016/j.cemconcomp.2018.11.009. URL: https://www.sciencedirect.com/science/article/pii/S0958946517307102.

[160] Fabio P. Figueiredo et al. “Effects of Recycled Steel and Polymer Fibres on Explosive Fire Spalling of Concrete”. In: *Fire Technology* 55.5 (Sept. 2019), pp. 1495–1516. ISSN: 1572-8099. DOI: 10.1007/s10694-019-00817-9. URL: https://doi.org/10.1007/s10694-019-00817-9.

[161] M. Kanéma et al. “Spalling, Thermal, and Hydrous Behavior of Ordinary and High-Strength Concrete Subjected to Elevated Temperature”. In: *Journal of Materials in Civil Engineering* 23.7 (2011), pp. 921–930. DOI: 10.1061/(ASCE)MT.1943-5533.0000272. eprint: https://ascelibrary.org/doi/pdf/10.1061/%28ASCE%29MT.1943-5533.0000272. URL: https://ascelibrary.org/doi/abs/10.1061/%5C%28ASCE%5C%29MT.1943-5533.0000272.

[162] Yang Ju et al. “On the thermal spalling mechanism of reactive powder concrete exposed to high temperature: Numerical and experimental studies”. In: *International Journal of Heat and Mass Transfer* 98 (2016), pp. 493–507. ISSN: 00179310. DOI: 10.1016/j.ijheatmasstransfer.2016.03.033. URL: http://dx.doi.org/10.1016/j.ijheatmasstransfer.2016.03.033.

[163] Wasim Khaliq and Farhan Waheed. “Mechanical response and spalling sensitivity of air entrained high-strength concrete at elevated temperatures”. In: *Construction and Building Materials* 150 (2017), pp. 747–757. ISSN: 0950-0618. DOI: https://doi.org/10.1016/j.conbuildmat.2017.06.039. URL: https://www.sciencedirect.com/science/article/pii/S0950061817311807.

[164] Shamsad Ahmad et al. “Mechanical properties of steel fiber-reinforced UHPC mixtures exposed to elevated temperature: Effects of exposure duration and fiber content”. In: *Composites Part B: Engineering* 168.December 2018 (2019), pp. 291–301. ISSN: 13598368. DOI: 10.1016/j.compositesb.2018.12.083. URL: https://doi.org/10.1016/j.compositesb.2018.12.083.

[165] Ali Nazari et al. “Thermal shock reactions of Ordinary Portland cement and geopolymer concrete : Microstructural and mechanical investigation”. In: *Construction and Building Materials* 196 (2019), pp. 492–498. ISSN: 0950-0618. DOI: 10.1016/j.conbuildmat.2018.11.098. URL: https://doi.org/10.1016/j.conbuildmat.2018.11.098.

[166] Farhad Aslani and Lining Wang. “Fabrication and characterization of an engineered cementitious composite with enhanced fire resistance performance”. In: *Journal of Cleaner Production* 221 (2019), pp. 202–214. ISSN: 0959-6526. DOI: https://doi.org/10.1016/j.jclepro.2019.02.241. URL: https://www.sciencedirect.com/science/article/pii/S0959652619306468.

[167] Serhat Çelikten, Mustafa Sarıdemir, and İbrahim Özgür Deneme. “Mechanical and microstructural properties of alkali-activated slag and slag+fly ash mortars exposed to high temperature”. In: *Construction and Building Materials* 217 (2019), pp. 50–61. ISSN: 0950-0618. DOI: https://doi.org/10.1016/j.conbuildmat.2019.05.055. URL: https://www.sciencedirect.com/science/article/pii/S0950061819312140.

[168] G. Debicki, R. Haniche, and F. Delhomme. “An experimental method for assessing the spalling sensitivity of concrete mixture submitted to high temperature”. In: *Cement and Concrete Composites* 34.8 (2012), pp. 958–963. ISSN: 0958-9465. DOI: https://doi.org/10.1016/j.cemconcomp.2012.04.002. URL: https://www.sciencedirect.com/science/article/pii/S0958946512000637.

[169] Fabio Cardoso et al. “Scale-up effect on the drying behavior of high-alumina refractory castables”. In: *Journal of the Technical Association of Refractories* 23 (Jan. 2003), pp. 226–230.

[170] Lars Boström, Ulf Wickström, and Bijan Adl-Zarrabi. “Effect of specimen size and loading conditions on spalling of concrete”. In: *Fire and Materials* 31.3 (2007), pp. 173–186. DOI: https://doi.org/10.1002/fam.931. eprint: https://onlinelibrary.wiley.com/doi/pdf/10.1002/fam.931. URL: https://onlinelibrary.wiley.com/doi/abs/10.1002/fam.931.



II

BUILDING MATERIALS RESPONSE TO THERMAL SHOCK

3

HOT SPILLAGE ON CAC

I thought if you told people facts, they'd draw their conclusions,
and because the facts were true, the conclusions mostly would be too.
But we don't run on facts. We run on stories about things.

James S.A. Corey, Babylon's Ashes

Fact and fiction carry the same intrinsic weight in the marketplace of ideas.
Unfortunately reality has no advertising budget.

Daniel Suarez, Freedom^{TM}

This chapter explores CAC as the main component for the manufacturing of building materials resistant to molten slag spill in a steel factory. Although CAC has been thoroughly studied in oven heating experiments, the author makes a distinction between the conditions of linear heating and thermal shock through spilling of molten material. The effects of the high temperature event on the microstructure are compared in different W/C ratios and moisture states. Further, a short follow-up experiment is carried to study post-effects in the microstructure, in case re-hydration takes place after the contact with molten slag.

Parts of this chapter have been published in Materials & Design **217**, 110623 (2022) [1] and in the 17th Euroseminar on Microscopy Applied to Building Materials (2019) [2].

3.1. DEVELOPMENT OF A SPALLING RESISTANT CONCRETE

CALCIUM aluminate cement (CAC) is arguably the best binder for producing bulk concrete elements expected to be exposed to high temperatures [3–5]. As such, the literature on the use of CAC at high temperatures is vast [6–13], and this was the first material considered for the development of a mix that would be later used in the case study of a steel factory (described in Chapter 5).

However, most of the literature on concrete subjected to high temperature focus either on the slow heating of the material for study of residual properties after cooling or the fast heating of the concrete for study of its performance in a fire event (see Chapter 2). Neither of which is representative to the situation in metallurgical factories, where concrete members are repeatedly subjected to sudden contact with hot spillage of metals or metallic waste.

Because the form of exposure to high temperatures can drastically change the behaviour of concrete [14–16], this was the first criterion considered before designing an experiment to test CAC's performance with respect to high temperatures. Specifically, two parameters were taken into account: The heating and cooling regime, and the chemical species in contact with the binder during exposure to high temperatures.

Regarding the heating and cooling regime, most high temperature studies on concrete are executed by the steadily heating up samples [17–21], which would not account to mechanisms related to thermal shocks caused by high temperature spillage. Contact with molten steel or slag produces nonlinear, rapid heating followed by slow cooling while the material is in contact with the substance. Further, the direction of heating is a considerable influence on the thermal shock effect on samples [22]. Figure 3.1 shows a compilation of the main differences between the two modes of heating. In addition hot spillage has the unique situation of water evaporation through the same region of contact with high temperature product, which might cause interference. In oven heating, the escape of water is free and doesn't interfere with the heating of the samples.

Regarding the chemical species in contact with the binder during exposure to high temperatures, oven experiments only take temperature into consideration, the samples are usually in contact with atmospheric air [23–25]. In metallurgical factories, the hot spillage changes composition considerably depending on production process, which might affect interaction with the binder [26].

Accordingly, this chapter focuses on simulating the event of slag spillage in a steel factory, mimicking the case study in Chapter 5. A small amount of molten slag is poured over CAC cement samples at a similar temperature it would have during steel production. This allows a better comparison of the thermo-chemical and thermo-physical effects on the material due to the small scale and controlled environment of the experiment.

The main aim is to identify different processes taking place on samples with different saturation conditions and water to cement (W/C) ratios. To avoid further changes in the microstructure of the samples after the thermal shock, these had their hydration stopped by means of epoxy impregnation or solvent exchange right after the experiment. A finite element model was used to estimate differences in temperature gradients caused by changes in material design. Finally, a combination of electron microscopy, energy dispersive spectroscopy, thermal gravimetric analysis and X-ray diffraction was used to

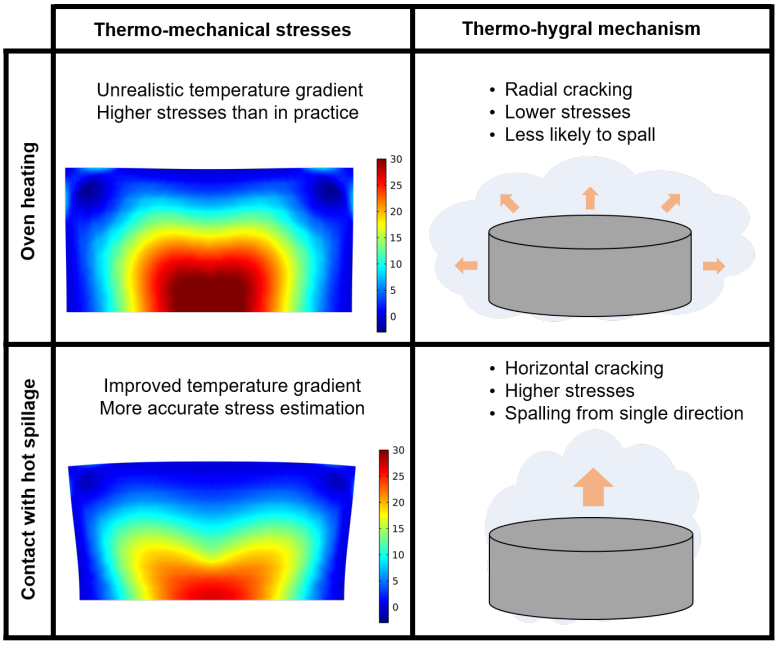

Figure 3.1: Comparison of spalling mechanisms in free samples subjected to oven heating or contact with hot spillage on the top face of sample. On the left is a finite element method simulation of the stresses generated during heating. On the right is a sketch of the preferential direction of moisture escape

investigate the microstructure and chemistry of the samples. Assumptions regarding durability and cost effectiveness can be drawn from the presented observations.

3.2. EXPERIMENTAL PROGRAM

3.2.1. SAMPLES AND EXPOSURE

Four cylindrical cement paste samples were cast in a plastic mould with the dimensions of ∅ 55 x 25 mm. Because the focus is on the interaction of molten slag with the binder phase, it was chosen to use cement paste samples, rather than mortar or concrete samples. The cement used was calcium aluminate cement Calight 50N. Normal tap water was used for the mix. Two of the samples had a W/C ratio of 0.40 and the remaining two had a W/C ratio equivalent to 0.20. To improve fluidity, MasterGlenium 51 was added as superplasticizer to the samples with the lowest W/C ratio, the quantity added was 0.4% with respect to the cement mass. The samples required no vibration. As CAC hardens considerably faster than Portland cement, only seven days are required to achieve a relatively stable microstructure with most of the hydration finished [27]. Therefore, curing a CAC mixture beyond 7 days should not have any added value. After 24 hours, the specimens were de-moulded and moved to a curing room to remain at 95% humidity and 20°C temperature for seven days.

One sample of each W/C ratio was submersed in water for 24 hours and then was exposed to molten slag. Additionally, one sample of each W/C ratio was dried for 48 hours at 40°C in an oven prior to exposure to molten slag. The samples saturated with water are herein called S2 and S4, while the samples dried in the oven are called D2 and D4. The numbers are representative of the W/C ratio, while the letters are representative of the state of the sample during the pour of slag (see Figure 3.2, top left).

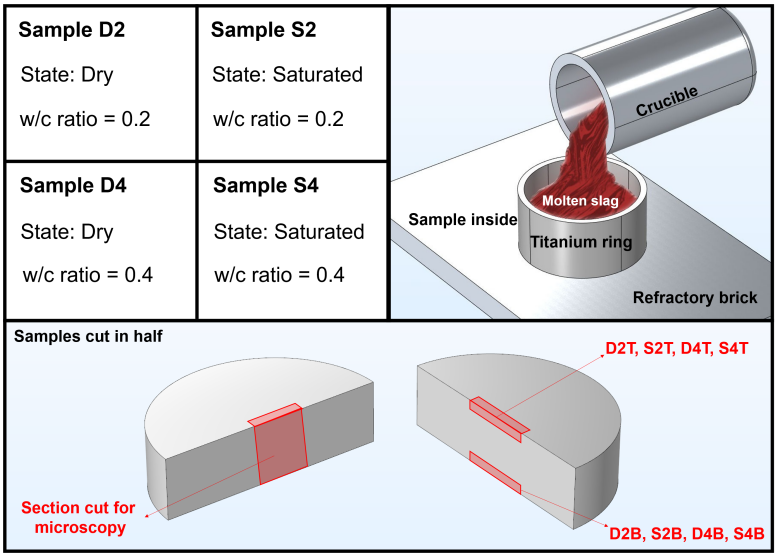

Figure 3.2: Top left: Naming convention of samples. Top right: Sketch of thermal shock experiment. Bottom: Location of analysed parts in each sample.

Table 3.1: Chemical composition of materials as determined by XRF.

Material	SiO_2	Al_2O_3	CaO	MgO	Fe_2O_3	SO_3	Na_2O	K_2O	TiO_2	P_2O_5	L.O.I.	Total
Calight 50 N	8.01	46.85	38.12	0.55	3.16	0.38	0.07	0.19	2.22	0.17	0.28	100.00
BF slag	34.40	11.53	39.17	7.81	1.42	1.6	0.23	0.58	-	-	1.15	97.89

The slag used for pouring on top of the samples was molten blast furnace slag. The composition of the slag and the cement used can be found in Table 3.1. Prior to pouring, 60 grams of slag was heated at $15^oC/m$ until 1530^oC in an alumina crucible. After 30 minutes at this temperature, the oven was opened and the crucible was removed and tilted on the samples to pour liquid slag. To keep the slag on the surface of the samples and avoid leakage to the sides, a titanium ring with an inner diameter of 55 mm and height of 35 mm was placed on top of each sample. Sample and ring were placed on top of a refractory magnesia brick for safe operation. Figure 3.2 (top right) shows a sketch of this procedure.

3.2.2. POWDER ANALYSIS

After being exposed to molten slag, the samples remained cooling for 12 hours at 20^oC and then the vitrified slag was removed and the specimens were cut in half. From one half, material was extracted from the very top (which was in contact with slag) and gently ground with an agate mortar in preparation for XRD. Prior to grinding, the material was dried through solvent exchange. Approximately 5 grams of powder from each sample was collected and kept dry until testing. Sufficient material was collected for thermogravimetric analysis (TGA) as well, these samples were designated as D2T, S2T, D4T and S4T. The same procedure was repeated for the bottom of each sample, where temperatures remained considerably lower during exposure to molten slag. Such samples were designated as D2B, S2B, D4B and S4B (see Figure 3.2, bottom).

A Bruker D8 Advance diffractometer Bragg-Brentano geometry and Lynxeye position sensitive detector was used with $CuK\alpha_{1,2}(\lambda = 0.15408nm)$ radiation for all XRD measurements. The scatter screen height was set at 5 mm height, divergence slit V12. The used voltage was 45 kV with a current of 40 mA. The spin was of the sample. All scans were performed with a 2θ angle between 10° and 130°, and a step size of 0.03°. The counting time per step was of two seconds. A combination of two software, X'Pert HighScore Plus and Jade6 was used for the spectral analysis. The standard software databases sufficed for the identification of peaks.

For the thermogravimetric analysis, a NIETZSCH STA 449 F3 Jupiter was used. Approximately 40 mg of material were used for each analysis. The mass change of samples was continuously monitored while the temperature was raised at a $10^oC/min$ rate from 40^oC to 1000^oC. In order to perform the measurements, a 1 mm^3 alumina crucible containing each sample was placed under a dry argon atmosphere with a purge rate of 50 mL/min.

3.2.3. ELECTRON MICROSCOPY

The other half of each sample was cut into 25 x 25 x 10 mm to allow a surface containing both, top and bottom of the original cylinders. Each specimen was then vacuum impregnated with epoxy resin. The impregnated specimen surfaces were ground using SiC

Table 3.2: Minerals used for standard based X-ray microanalysis quantification.

Element	Symbol	Mineral used for correction	Chemical composition
Sodium	Na	Albite	$NaAlSi_3O_8$
Magnesium	Mg	Periclase	MgO
Aluminium	Al	Jadeite	$NaAlSi_2O_6$
Silicon	Si	Quartz	SiO_2
Sulfur	S	Anhydrite	$CaSO_4$
Potassium	K	Sanidine	$KAlSi_3O_8$
Calcium	Ca	Calcite	$CaCO_3$
Titanium	Ti	Rutile	TiO_2
Iron	Fe	Haematite	Fe_2O_3
Oxygen	O	Oxigen was determined by stoichiometry	

grinding papers with increasing mesh number from #320 up to #1200. Next diamond pastes of 9 μm, 3 μm, 1 μm and 1/4 μm were used for polishing until a scratch-free surface was achieved in SEM-BSE imaging at about x1000 magnification. Between each grinding and polishing step, the samples faces were washed with ethanol, then small particles were detached using ultrasonic bath for 1 minute and finally the surface was gently dried using compressed air.

The polished sections were analyzed using BSE (backscattered electron) imaging and energy dispersive x-ray spectroscopy (EDS). The microscope used was a QUANTA^{TM} FEG 650 from Thermo Scientific^{TM} equipped with a field emission gun and concentric backscatter detector. The samples were analysed under high vacuum, with a take-off angle of 34.6° and sample to detector distance of 10 mm. The detector was a SUTW (sapphire) with a calibrated resolution of 132 eV, the accelerating voltage was set at 15 kV for all EDS measurements and the deadtime remained at approximately 10%. The beam current was constantly measured through a picoammeter. At times, several Electron micrographs were stitched for a better field of view of the samples, all stitching was performed digitally using the algorithm proposed by Preibisch et at (2009) in [28]. The presented atomic ratios are the average of tens of points taken at hydration products on the same section of a sample.

The interaction volume between the microscope beam and Portland cement phases are known [29], however, the same cannot be said for CAC phases. For this reason, it was opted to perform a Monte Carlo simulation of electrons trajectory in solids with low beam energy through the software CASINO_v2. The density for the CAC phases were extracted from literature [30, 31]. After acquisition all EDS spectra were corrected using ZAF algorithm with the aid of NIST DTSA-II software [32]. The quantification of mass and atomic percentages was standard based, using the minerals shown in Table 3.2.

3.2.4. MODELLING

For the estimation of the temperature gradients in each sample, a finite element (FE) software was used. Solid Mechanics and Heat transfer in Porous Media bundles of COMSOL®5.3 were coupled through thermal expansion multi-physics. A geometry was created to mirror each sample lying on top of a Mg refractory brick with molten slag on top of it contained by the used titanium rings. The thickness of the slag corresponded to the thickness observed post cooling. Two probe points were created, one 500 μm beneath the surface of the sample (top) and one 500 μm above the interface with the MgO brick

(bottom). The geometry is shown in Figure 3.3 (top).

A triangular mesh was used with adaptive refinement during all calculations. The time steps were taken in logarithmic scales to range from 0.0001 minutes to 100 minutes, at which point cooling was nearly complete. The sample was modeled as a porous, linear elastic material and at room temperature, with its expansion constrained by the titanium ring. Because the sample was just placed on top of the refractory brick, the connection in the model as considered a roller connection, with no restriction to horizontal displacement. All components were considered to be at 22.5^oC at the beginning of the simulation with exception of the slag, which was modelled at 1500^oC. A small amount of convective heat flux was added to simulate the air convection in the laboratory during the cooling phase. Further, the temperature estimation was later used to simulate the stress and strain in each sample. In order to improve the computation time, only one quarter of the samples was used for the mechanical simulations and symmetry was imposed in both cut faces. As the simulations required several properties as input, these were provided based on a different experiment, discussed in Section 3.5.1.

The simulations considered the water content and different W/C ratios of the samples as differences in relative humidity of the pore network, vapour permeability and porosity of the material assigned to the simulated sample. The slag was modelled as a poured liquid that changes phase during cooling. The transition from liquid to solid was modelled at 1350^oC with a transition interval of 80^oC and latent heat of transition equivalent to 294 kJ/kg in accordance to Kashiwaya (2010) [33].

3.3. RESULTS

3.3.1. TEMPERATURE ESTIMATION

The goal of the FE simulations was to estimate the temperature distribution in the samples during the pouring of slag. Because of the small size of the specimens, the use of multiple thermo-couples presented many practical difficulties. Figure 3.3 (bottom) shows the evolution of temperature at the top and at the bottom of each sample.

While the slag is poured at a temperature close to 1500^oC, a large amount of heat is quickly dissipated due to the escape of water in the same direction of contact with the spillage. Radial contact with the titanium ring and general emissivity of slag at high temperatures also contribute for initial loss of heat. The results show that the maximum temperature does not vary considerably between the top of samples, but rather the duration which this temperature is sustained. Denser samples have better thermal conductivity [34], thus, absorb more heat from the molten slag. This was observed looking at samples D2 and S2, that remain at high temperatures for longer. Because samples with higher W/C ratio possess more capillary pores, there is more water and air to act as thermal insulation, which would delay the heat transfer from the molten material to the samples. Such delay occurs in combination with the faster cooling of slag, which explains the shorter time for which the top region of the samples remain at maximum temperature. Conversely, air is more insulating than water and the saturated samples remain at high temperatures for shorter time. This is because upon contact with the slag, saturated samples quickly release most of the water, causing the molten pour to bubble during the first seconds, while the dry samples simply start absorbing the heat upon

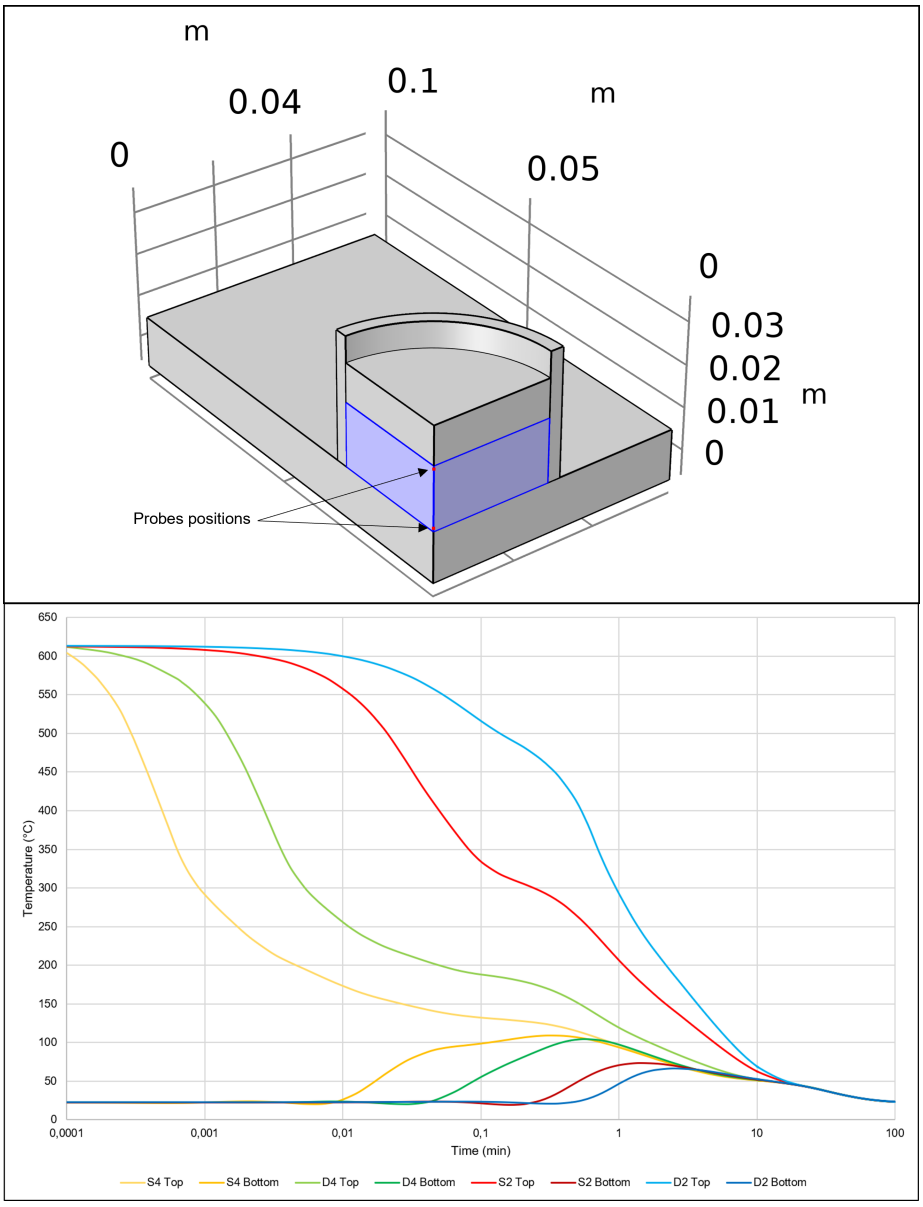

Figure 3.3: Top: Simulated geometry, with cement sample in blue and probe points for temperature estimation in red. Bottom: Estimated temperatures at red points in each sample based on FEA simulations.

contact with the slag. This is seen by looking at the slags after the experiment, in Figure 3.4.



Figure 3.4: Example of slags after cooling on top of CAC samples. Left: Slag cooled on top of a dry sample. Right: Slag cooled on top of a saturated sample.

Yet, the absorbed heat seems to be more readily dissipated by the samples with lower W/C ratio, as can be inferred by the steeper slope of the temperature vs time curves of S2T and D2T. This should also be explained by the lower amount of air acting as insulation. The described effect can be observed by the trends in the temperature evolution at the bottom, which shows samples with W/C ratio of 0.40 reaching more than 100^oC, while the remaining specimen have a maximum of 70^oC.

3.3.2. THERMOGRAVIMETRIC ANALYSIS

The thermal gravimetric analysis showed the presence of three zones of interest for all 8 samples, albeit at different magnitudes (Figure 3.5). The first zone is located between 100^oC and 200^oC; the second zone is adjacent to the first, between 200^oC and 350^oC; and the last zone of interest is between 700^oC and 800^oC degrees. Table 3.3 shows the loss due to slag spillage at the top of the samples, with respect to the values measured at the bottom of each respective sample in correspondence of the observed peaks.

Table 3.3: Decrease in peak minimum between powder collected from the top and from the bottom of each sample.

Sample	Peak 1	Peak 2	Peak 3
D2	29%	84%	16%
S2	27%	79%	-3%
D4	34%	71%	17%
S4	7%	39%	-18%

The peaks at the first zone are likely a convolution of the decomposition of two phases, CAH_{10} (usually with wide peaks around 125^oC [35]) and C_2AH_8 (usually with wide peaks around 190^oC [8]). These two phases are the hydration products with most attached water molecules found in CAC, and the first ones to decompose. All but one sample show a significant decrease in mass loss correspondence between the peaks of the top and the bottom region of the samples. Which points to dehydration of the mentioned phases during the spillage experiment. Sample S4 is the exception, these phases seem to have remained relatively at the same ratio for top and bottom. In Figure 3.3, it was shown that

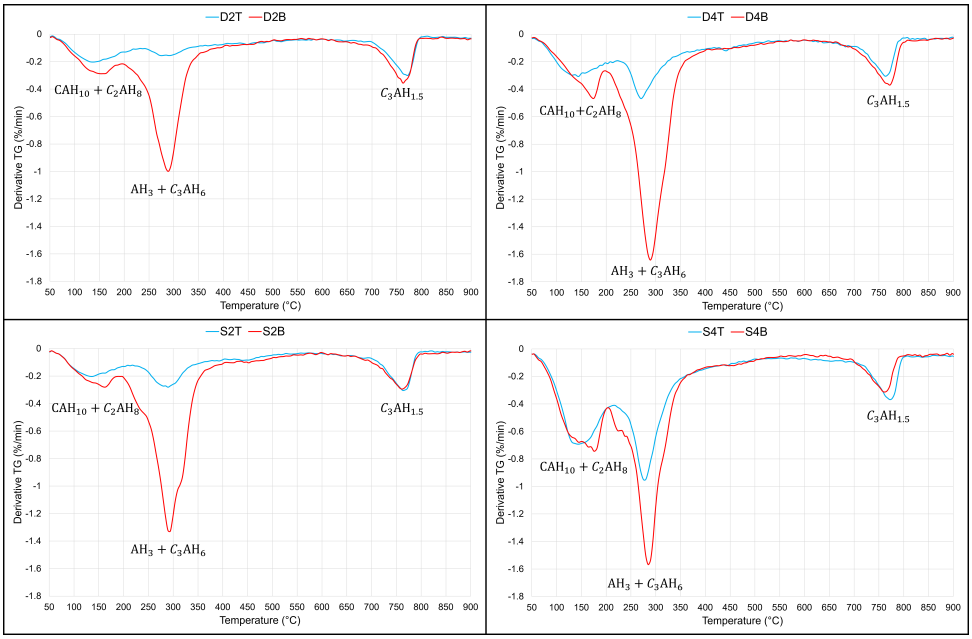

Figure 3.5: Derivative thermogravimetric analysis of samples comparing top and bottom composition.

sample S4 is the case that allows for the fastest heat transfer compared to other samples, which likely caused the bottom to reach the dehydration temperature of CAH_{10}. Furthermore, the peaks from the bottom part in samples D4 and S4 were skewed towards 200°C, while the peaks for the top part were not. Because this is only seen in samples D4 and S4, it is presumably caused by the imperfect dehydration of CAH_{10} (following equation 2.16) during the contact with molten slag. Which results in the increase of the amount of C_2AH_8. As sample S2 is presumed to have reached slightly higher temperatures than sample D2 at their respective bottoms (on Figure 3.5), it is also noticeable on the DTG results that sample S2 has a slight skew toward the same side as samples D4 and S4.

Correspondingly, the peaks in the second zone of interest are also likely to be the combination of two decomposed phases. Namely, AH_3 shows dehydration around 260°C [8] and C_3AH_6 between 280-310°C [35]. This is somewhat expected, since the dehydration of C_2AH_8 generates C_3AH_6 and AH_3 (equation 2.15).

As the temperatures at the bottom of the samples were unlikely to have reached values close to the dehydration of the two mentioned products, samples D2, S2 and D4 show a clear difference with respect to the curves obtained from material at the top of the samples.

Comparing only the curves for the top of the samples, it is apparent that sample with W/C ratio of 0.40 present a greater mass loss. This is likely due the higher amount of water during hydration, which allows for the formation of more CAH_{10} and eventually its conversion to C_3AH_6. This also holds when comparing the dry samples to their respec-

Table 3.4: Chemically bound water for top and bottom samples as calculated from TGA analyses.

Sample	Position	W/C ratio	State	Chemically bound water (%)
D2T	Top	0.20	Dry	7.3
S2T	Top	0.20	Saturated	8.4
D4T	Top	0.40	Dry	11.1
S4T	Top	0.40	Saturated	19.4
D2B	Bottom	0.20	Dry	14.4
S2B	Bottom	0.20	Saturated	17.3
D4B	Bottom	0.40	Dry	21.2
S4B	Bottom	0.40	Saturated	22.8

tive saturated pairs. Thus, the greatest peak between 100°C and 200°C in sample S4T is accompanied by the greatest peak between 200°C and 350°C in the same sample.

In a calcium aluminate cement paste, the dehydration peak between 700°C and 800°C is attributed to the conversion of $C_3AH_{1.5}$ to mayenite [36]. As the temperatures in the samples are predicted to not have surpassed 700°C, the difference between curves from the bottom of the samples and from the top is small. However, the formation of the intermediary phase $C_3AH_{1.5}$ is assumed to happen in relatively high pressure environments [37]. Although the samples were unconfined, it is believed that all specimens suffered from high capillary pressure due rapid vapour expansion during contact with the molten material. Furthermore, the dry samples present greater mass loss in correspondence with the peaks in the curves respective to their bottoms, implying lower pressure at the top, possibly due to cracking or fast water escape. On the other hand, the peaks magnitudes for both saturated samples were higher on the top than the bottom. This is likely due the higher amount of water present in the sample and its route of escape, causing a higher pore pressure environment.

The loss of chemically bound water is displayed in Table 3.4. The TGA results were in good agreement with the FE simulations, validating the initial assumption of fast cooling of slag from 1500°C to 600°C. As expected, sample S4T had almost as much chemically bound water as its counterpart (sample S4B), supporting the hypothesis of the water evaporation protecting the sample prior to the heating caused by slag. The other samples (D2T, S2T and D4T) all showed roughly half of the amount of chemically bound water in comparison with the bottom counter samples.

3.3.3. X-RAY DIFFRACTION

The results of XRD for samples with W/C ratio of 0.20 are presented in Figure 3.6 and the remaining samples in Figure 3.7. As expected, the peaks corresponding to unhydrated particles remain constant, with CA as the main phase and CA_2 and CA_4 in smaller amounts. Although CA_4 is not as common in CAC as the two other phases, it can be often found in higher purity cements [38].

Next, gibbsite is present in all bottom spectra, but absent on all spectra from the top of the samples. In addition, most hydrogarnet peaks are strongly decreased between top and bottom scans, with the exception of sample S4. Calcium aluminate decahydrate peaks were absent in all samples but S4, presumably because of the small quantity and

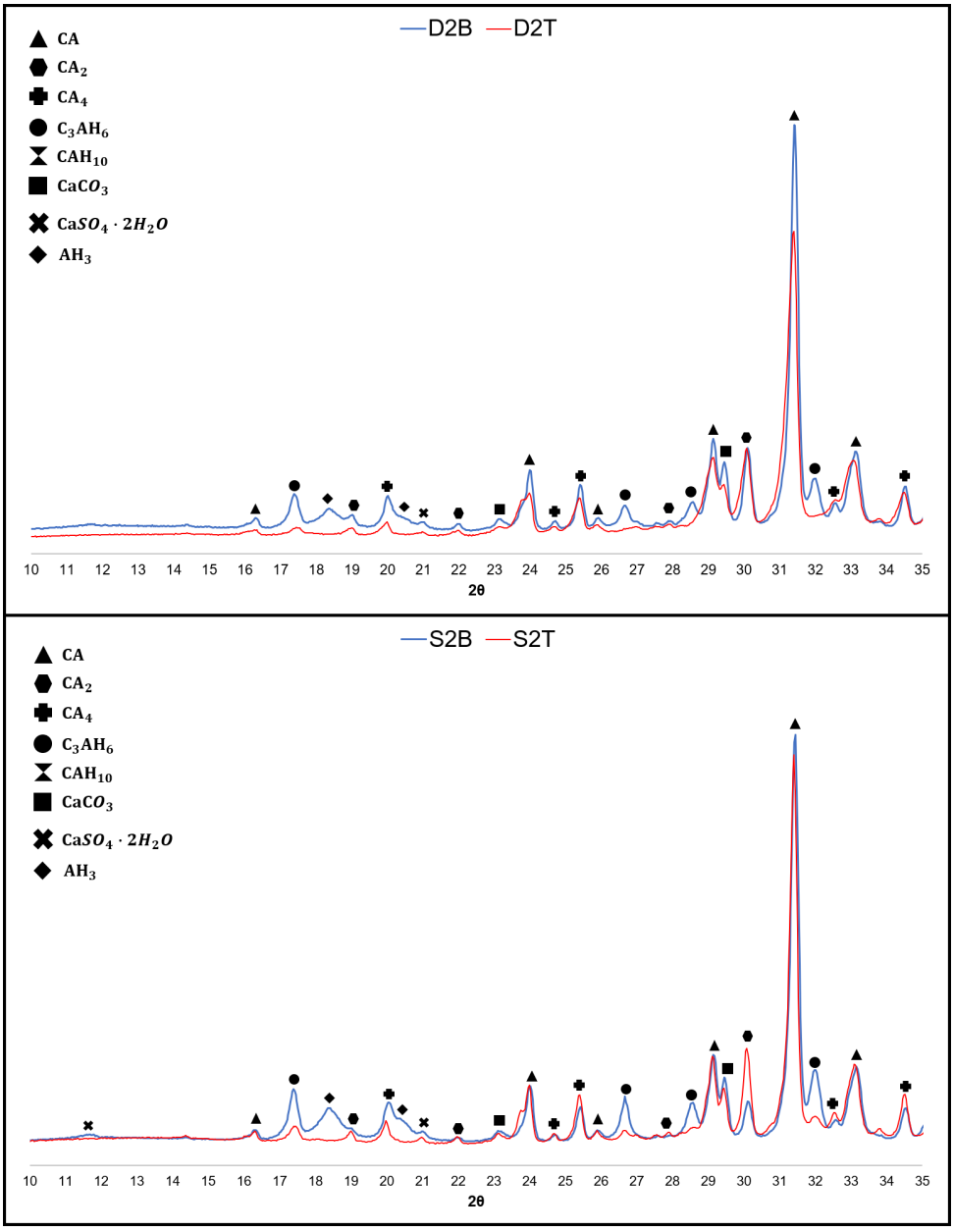

Figure 3.6: X-ray diffraction results for W/C=0.20 samples comparing top and bottom composition.

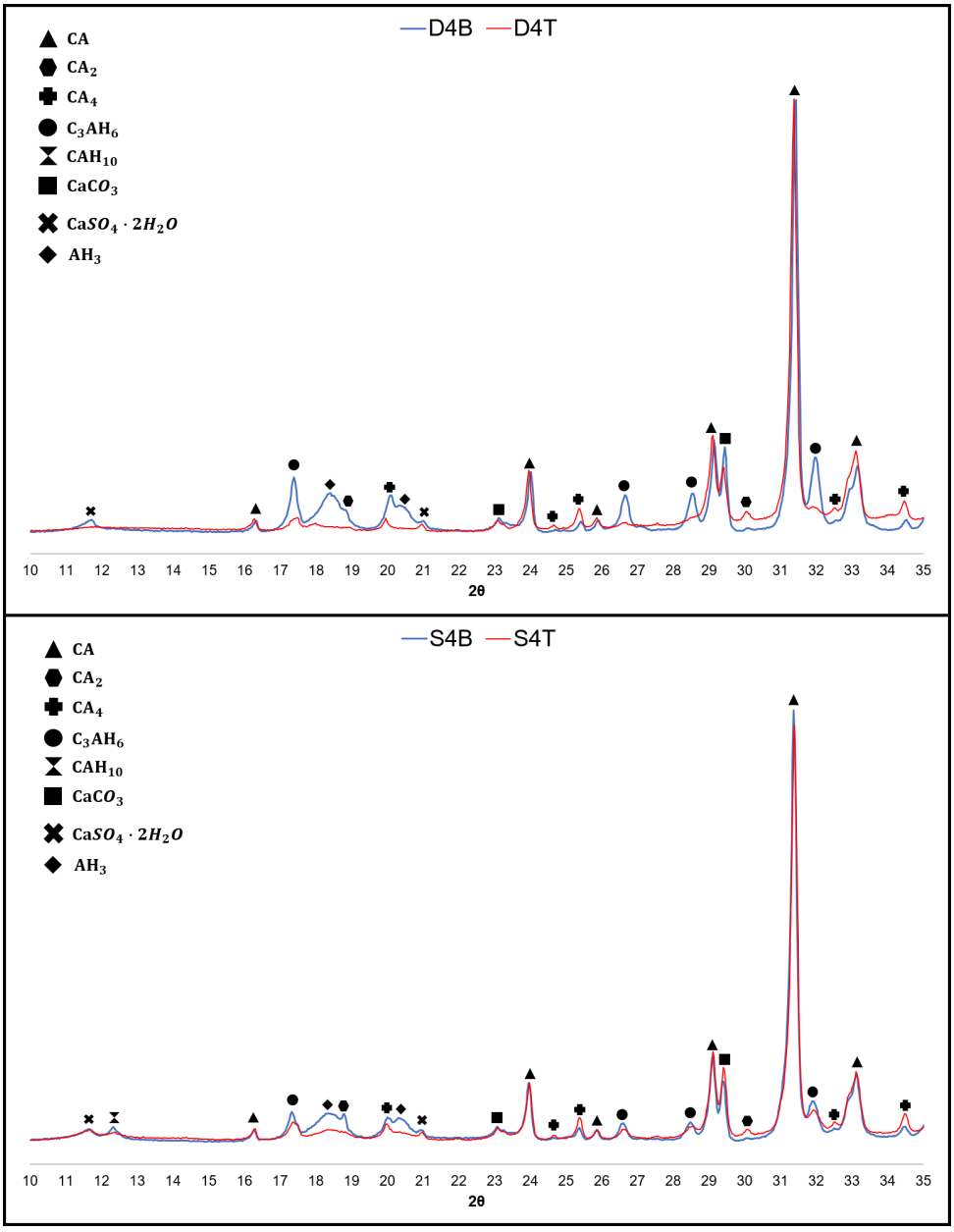

Figure 3.7: X-ray diffraction results for W/C=0.40 samples comparing top and bottom composition.

background noise. Alternatively, CAH_{10} can lose crystalinity through partial conversion, this is a solid state decomposition in which the phase will slowly (at the studied temperatures) convert to C_2AH_8 [39]. The characteristic peak for C_2AH_8 falls outside of the range studied. These results present a strong correlation with the thermogravimetric analysis, including the stronger remaining peaks of CAH_{10} on sample S4, as it will be discussed later.

Gypsum has an overlapping decomposition temperature with CAH_{10}, thus can be easily missed in the DTG results. However, trace quantities were found in the XRD spectra. These are notably present in samples S2B and D4B, albeit absent in samples S2T and D4T. Which is to be expected due the comparatively easy dehydration of this phase. Likewise, trace amounts of calcite were also detected.

3.3.4. ELECTRON MICROSCOPY

CASINO_V2 SIMULATIONS

The results for the simulations are shown in Figures 3.8 and 3.9. The volumes of interaction are slightly smaller than for Portland cement at 15 kV. The diameter of all volumes are about 1.5 μm to 2.5 μm, while the depth is between 2 μm and 3 μm. As expected, the unhydrated products and hydrogarnet have smaller interaction volumes, while CAH_{10} has the biggest interaction volume. These volumes were taken into consideration when choosing the location for the microprobe analyses.

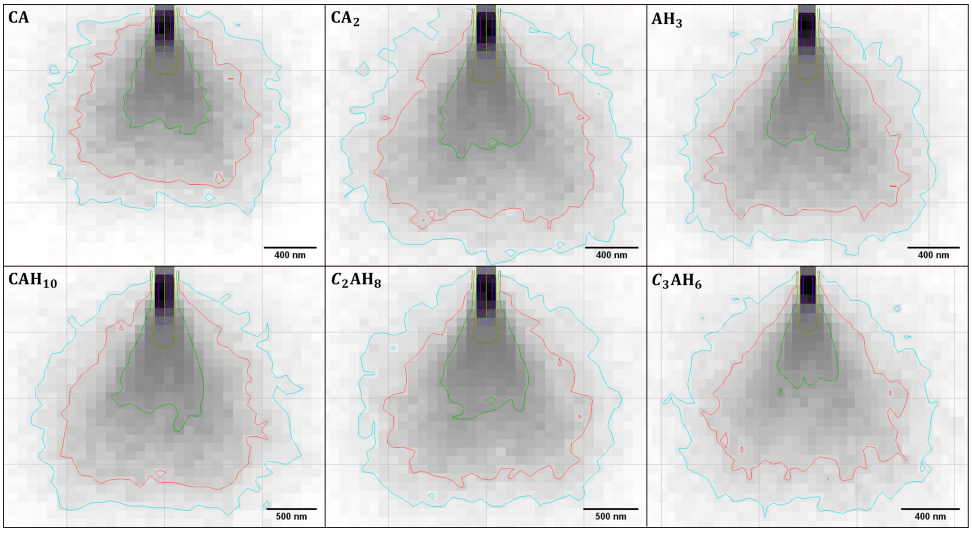

Figure 3.8: Results of vertical profiles (with respect to sample surface orientation) of electron-solid interaction volume for most common CAC phases. The gray scales represent density of electrons. The colored lines describe how many electrons reach a determined area, purple means 90%, dark blue means 75%, yellow means 50%, green means 25%, red means 10% and cyan means 5%.

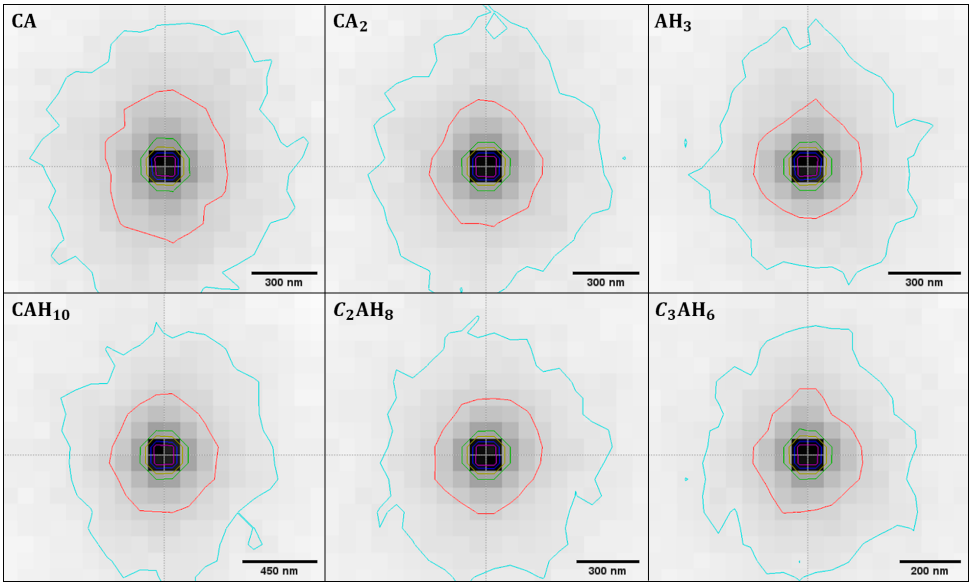

Figure 3.9: Results of horizontal profiles (with respect to sample surface orientation) of electron-solid interaction volume for most common CAC phases. The gray scales represent density of electrons. The colored lines describe how many electrons reach a determined area, purple means 90%, dark blue means 75%, yellow means 50%, green means 25%, red means 10% and cyan means 5%.

SAMPLE D2

This sample presented a dramatic change in phases characteristic size from top to the bulk of the sample. This effect was visible only in the first millimetres of the surface, becoming homogeneous after 2 mm. Figure 3.10 shows this disparity.

The top of Figure 3.10a) corresponds to the face of the sample onto which molten slag was poured. This effect is present over the entire width of the sample. Within the first 500 μm from the top, the phases are mostly between 0.5 μm and 2 μm in diameter and never above 5 μm. Between 500 μm deep and 1 mm, the phases become bigger, with unhydrated particles between 5 μm and 20 μm. After a millimetre the sample starts to present average particle sizes similar to its bulk, with some unhydrated particles bigger than 50 μm. Besides the difference in particle sizes, bright grey phases occur at the top right of Figure 3.10a) and 3.10b). Finally, there is a clear decrease in unhydrated grains size and occurrence from the first 1000 μm of the sample. This specimen displayed a comparatively simpler chemistry than the others.

Analysing the composition of the sample, the EDS spectra taken from the bright phases consistently displayed higher Ca/Al and Si/Al ratios than in any other zones of the sample. Further, siliceous hydrogarnet's (C_3ASH_6) approximate density is of 2.83 g/cm^3 [40], while CAH_{10}, C_2AH_8 and C_3AH_6 densities are 1.74 g/cm^3 [41], 1.95 g/cm^3 [40] and 2.53 g/cm^3 [40], respectively. Thus, the bright gray value phases are likely siliceous hydrogarnet.

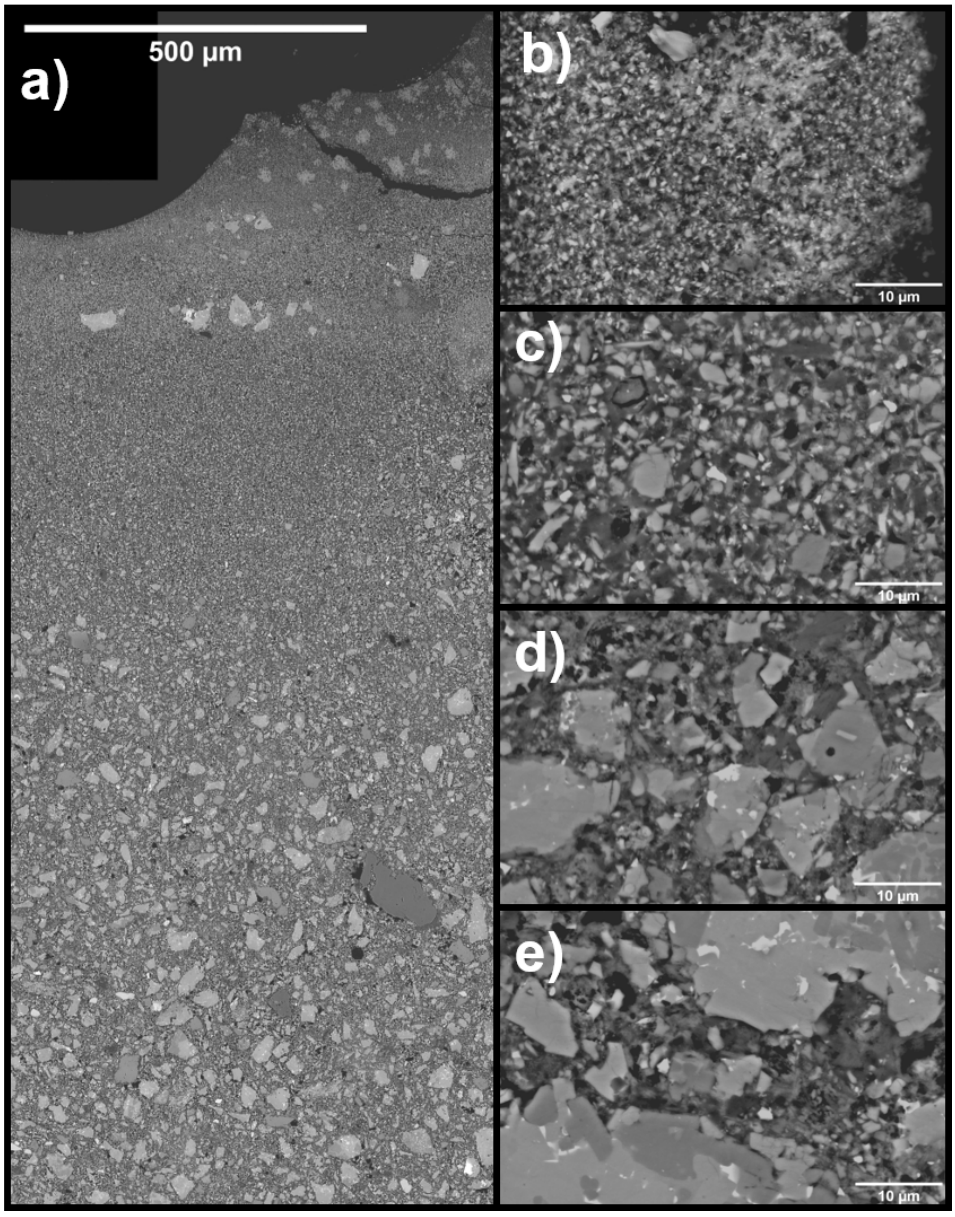

Figure 3.10: Sample D2; a) Sample overview composed of stitched micrographs; b) Electron micrograph of particles size at the very top of the sample; c) Electron micrograph at 400 μm from the surface; d) Electron micrograph ate 800 μm from the surface; e) Electron micrograph at 1500 μm from the surface.

SAMPLE S2

This sample presents no signs of the chemical changes observed on the previous one. Rather, the major effects seem to have been physical, in the form of cracks formed parallel to the surface exposed to slag spillage (see Figure 3.11, left). This crack pattern was observed throughout the top three millimetres of the sample on the entire area prepared for SEM.

When compared to the phases at the bottom of the sample, the top of the sample seems to have few differences. The average atomic composition remained similar independent of depth. Although, some needle like structures were observed exclusively in this sample, as seen in Figure 3.11, right. The needles in the top right of the figure display the same gray values and EDS spectra than CAH_{10}, which might indicate rehydration took place during the cooling of the sample. On the bottom right of the figure, the needles also present similar composition, with the distinction of high amounts of potassium. Indeed, in certain spectra, the atomic amount of K surpassed Ca. This could be a sign of replacement of calcium to form alkaline aluminate hydrates as it is known to precipitate at higher pH through the reaction in equation 3.1 [42]. However, this was rarely found in the sample and the characteristic peaks were absent in XRD analysis, hence posed a minor effect.

$$CAH_{10} + KH \leftrightarrow CH + KAH_6 + 4H \tag{3.1}$$

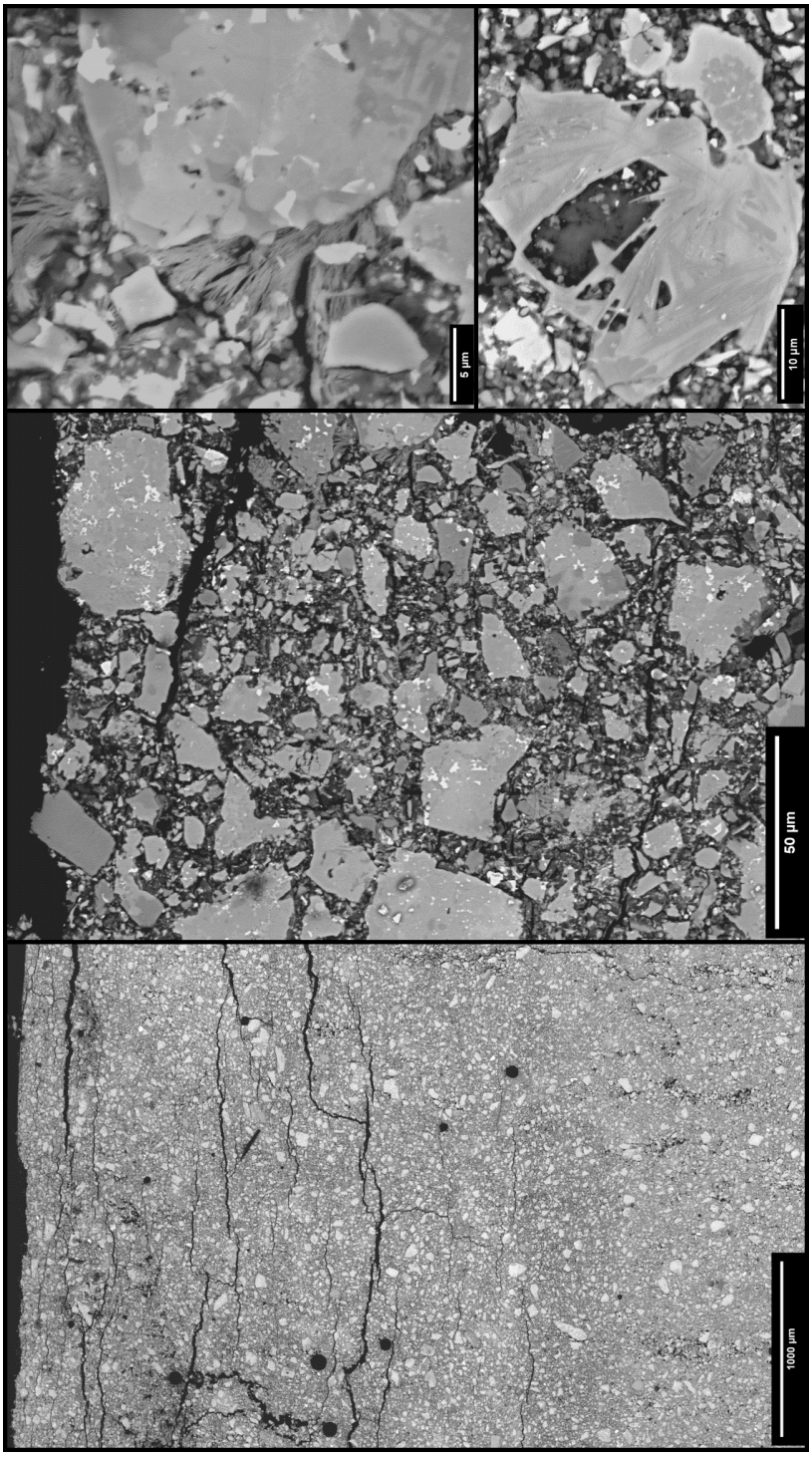

Figure 3.11: Sample S2; Left: overview of sample and surface cracking; Center: display of sample main phases; Right: needle-like structures.

SAMPLE D4

A sample overview at different scales is shown in Figure 3.12. There was considerably less cracking in this sample in comparison with the previous one. Further, most cracks were perpendicular to the surface and extended only through the first millimetre from the top.

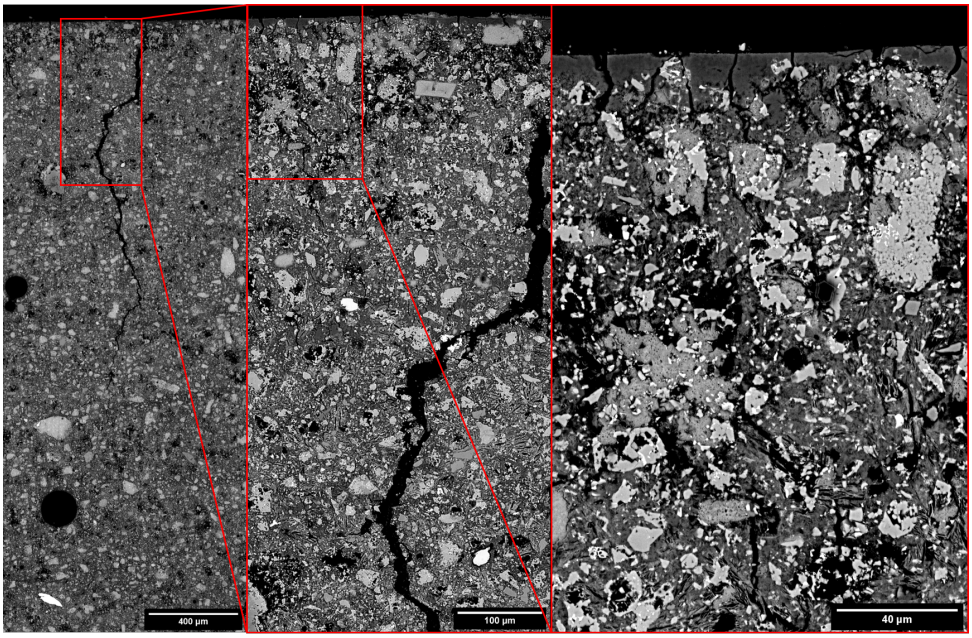

Figure 3.12: Sample D4; Left: Sample overview composed of stitched micrographs; Center: Zoomed in image of the red square present in left image; Right: Zoomed in image of the red square present in center image.

Along the entire surface of the sample there was a layer of 5 μm to 30 μm of a dark phase with an intricate microcracking pattern. This can be observed in Figure 3.12 center and right. The composition of this phase is consistent with gibbsite, however, its low backscattering coefficient points to AH_3 gel rather than its crystalline correspondent. Because this phase is seen predominantly at the top of the sample, it is likely that it is not a product of hydration or conversion, but of the decomposition of the main components of the cement, which also produce AH_3 (see equations 2.16 and 2.15).

Beneath this layer, the composition of the main binding phases resembles CAH_{10} and C_2AH_8, however, partially dehydrated. This is observed by the proportional difference in oxygen detection and higher amount of voids in comparison with the bulk of the sample. The phases with higher backscattering coefficients than AH_3 and CAH_{10}, but lower than the unhydrated particles, are very rich in calcium and present few of the other elements. This could possibly be explained by the dehydration of C_3AH_6 forming portlandite, as in equation 2.17.

Although the change in size and occurrence of unhydrated grains is not noticeable in this sample, an increase in voids around such grains was detected. The remaining

unhydrated grains demonstrated a very high concentration of Si, which might indicate the dehydration of C_3ASH_6 rather than C_3AH_6.

SAMPLE S4

Finally, an overview of sample's S4 microstructure can be seen in Figure 3.14. It did not show significant cracking, despite being the sample with the most water. It also did not show differences in the unhydrated grains.

As in the last sample, the same consistent 5 μm to 30 μm layer of AH_3 gel is present. The gel is mixed with other phases between unhydrated grains for more 30 μm to 100 μm. Past this layer, there is a well defined porous zone with 90 μm to 230 μm of thickness. The composition of this porous zone, once again, has a much higher Ca/Al atomic ratio than in the rest of the sample. After that, the sample displays very little difference to phase composition and distribution present at the bottom.

ATOMIC RATIOS

Besides the localised effects, the bulk chemistry of the hydration products was investigated in the samples taking the average composition of tens of EDS points near the top and near the bottom of each sample. Figure 3.13 shows the summarized results for Ca/Al and Si/Al ratios.

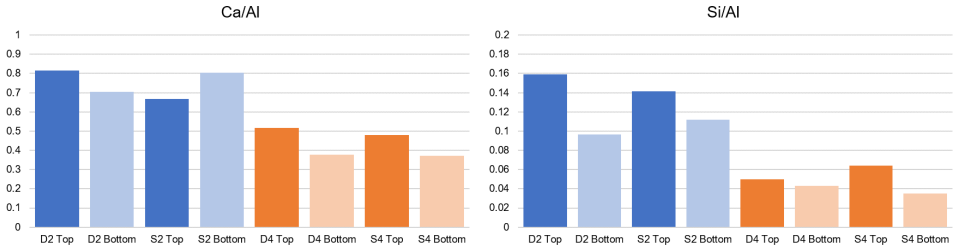

Figure 3.13: Atomic ratios of samples as of measured by the average of EDS points.

Both Ca/Al and Si/Al atomic ratios are higher in samples with lower W/C ratio, independent of pre-treatment to receive slag or the region of the sample being studied. This is likely due the higher amount of AH_3 in the samples with 0.40 of W/C ratio. Greater availability of water during hydration at room temperature can also allow for more production of AH_3 [5]. The higher temperatures estimated for these samples could further force conversion, which produces more AH_3 [6]. Finally, both samples D4 and S4 also had plenty of AH_3 gel in its surface.

Additionally, the Si/Al ratio is always higher at the top of the samples than at the bottom. Looking at table 3.1, the cement samples represent an environment saturated in Ca (the main component of the used slag), but undersaturated in Si, the second most abundant element in the molten material. Although literature is scarce for the exact conditions of this experiment, the diffusion of Ca and Si in calcium aluminosilicate slags under ultra high temperatures has been studied [43, 44], which is somewhat comparable. Thus, it is possible that silicon diffused into the cement paste in a first moment, when the slag still had a temperature over 1000°C.

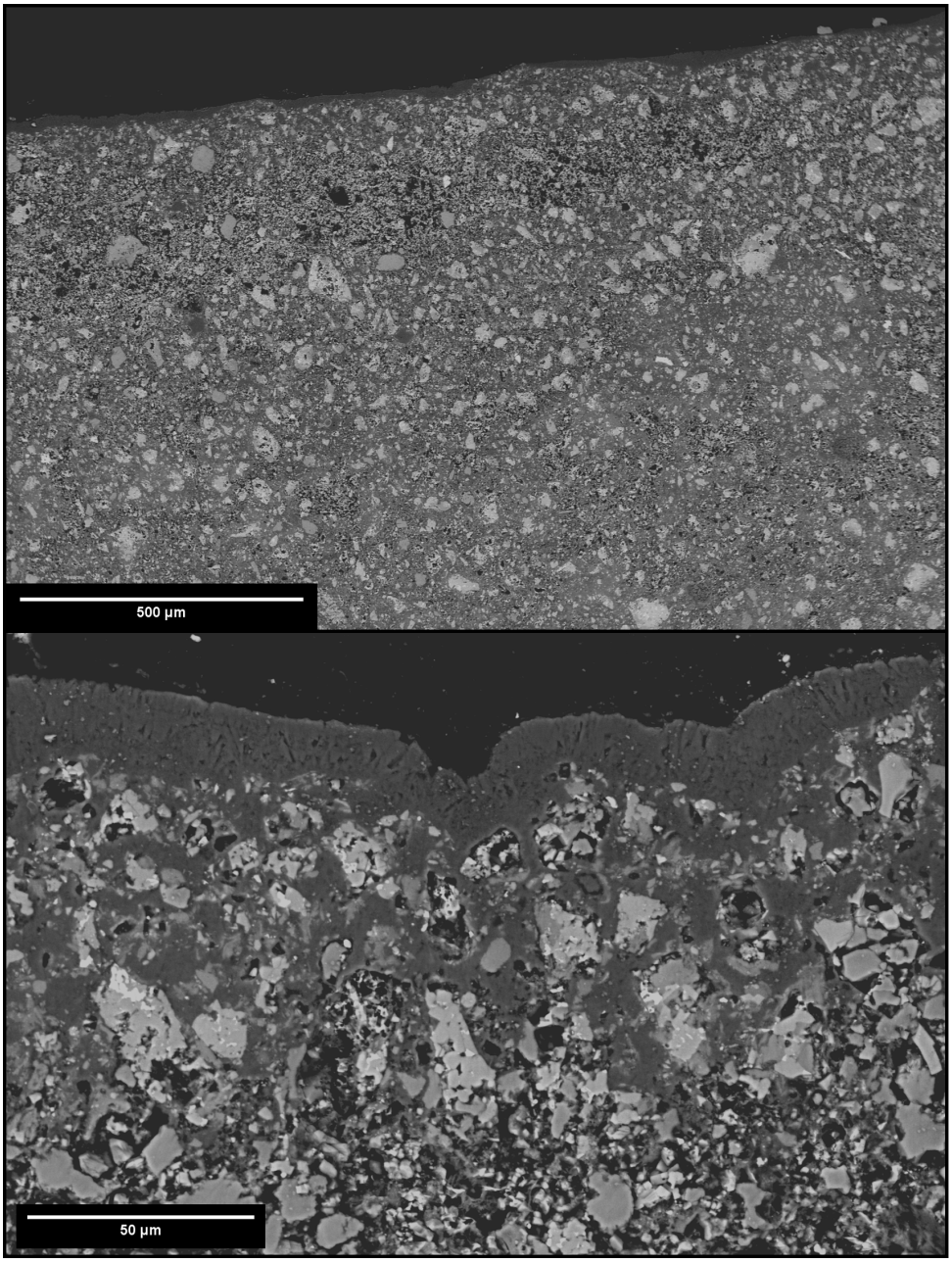

Figure 3.14: Sample S4; Top: stitched overview of sample surface; Bottom: Zoomed view of sample surface.

3.4. DISCUSSION

3.4.1. THERMO-MECHANICAL DAMAGE

The biggest physical modifications were observed in samples S2 and D4, in the form of cracking in the face receiving the molten slag. However, these two samples present opposite forms of cracking. Sample S2 displayed horizontal fracture parallel to the plane of heating by the slag, while sample D4 had vertical cracks, orthogonal to the plane being heated. This can be explained by the temperature gradient and consequent strain distribution within the cement paste.

The maximum volumetric strain for both samples occurred between 0.1 and 1 minute. Looking at this interval of time in Figure 3.3, the temperatures at the top and bottom of sample D4 had less than 100°C of difference, while sample S2 was mostly heated at the top, with the bottom still at room temperature, causing a gradient of about 300°C . Figure 3.15 shows the simulated strain fields of both samples at 0.2 minutes after the exposure.

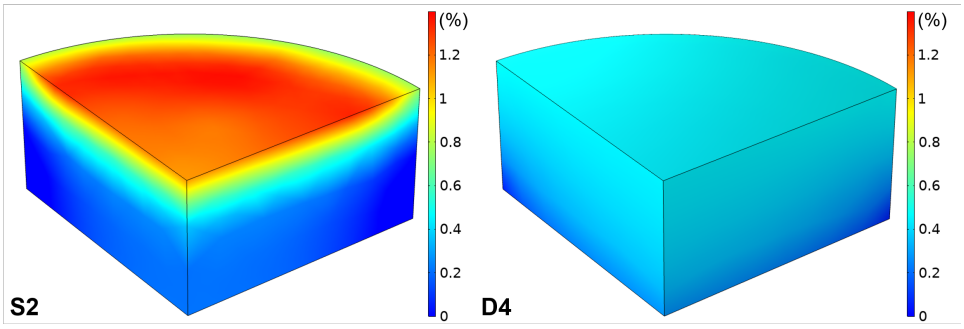

Figure 3.15: Simulated volumetric strains (%) for samples S2 and D4 at 0.2 minutes.

Sample D4 had a well distributed strain field, with the higher temperatures at the top causing typical dilation cracks (one example present in Figure 3.12). Sample S2 had a very sharp difference in strain between the top millimeter and the bottom of the sample given by the poor temperature distribution at that moment in time. Such acute difference can localised tensile stresses, contributing to horizontal cracking. However, sample D2 had a similar strain field without displaying cracking, as seen by comparing Figures 3.10 and 3.11. This is possibly due to the contribution of the moisture state of the samples. While D2 was dry and had only chemically bound water released (at a much higher temperature), sample S2 had a considerable amount of physically bound water evaporating almost instantly after exposure to the molten slag. The vapour expansion caused elevated stresses through the well known thermo-hygral damage mechanism explained in Chapter 2 and the summation of these with the shear stresses caused by the thermal dilation are believed to be responsible for the horizontal cracks. Regarding sample S4, it is clear that the temperature gradient (and ergo the stress and strain fields) were milder, given the physically bound water being able to quickly escape and act as a coolant agent to the molten slag.

3.4.2. THERMO-CHEMICAL ALTERATIONS

Three phenomena are dependent on the duration of heating during high temperature exposure: transformations in porosity, chemical composition and occurrence of new phases [45]. Sample D2 is estimated to have endured high temperatures at least one order of magnitude longer than all other samples, and accordingly, is the sample with most changes in porosity and composition.

Both, the conversion and dehydration reactions of the main phases generate water molecules (see equations 2.16, 2.15 and 2.17). Therefore, it is possible that the decrease of size and occurrence of unhydrated particles in sample D2 is connected to the presence of C_3ASH_6. Conceivably, dehydration of lower depths of the sample generated water propelled to escape through the top of the sample. Such water would be in the form of vapour at high pressure and high temperature. Its contact with the top portion of the sample could have caused steam curing. This would also agree with the overall decrease in porosity at the topmost layer.

As established in several investigations [3, 46–49], CA hydrates to directly form C_3AH_6 above 60^oC. However, C_3ASH_6 is found in opposition to C_3AH_6. This is due the high availability of Si, as commented on the results section. The main reason for such availability could be explained by the indirect dissolution of the slag into the cement acting as refractory. Braulio et al [50] describes a simpler system of samples also using CAC as a binder, in which the authors have shown that the dissolution of slag within the refractory and the precipitation of different products caused by it. In accordance, Figure 3.13 shows that slag predominantly contributed with the increase of Si atoms into the cement, causing an environment idealized in the scheme presented in Figure 3.16, where the concentration of silicon coming from the slag is represented by the red line, while the concentration of aluminum coming from the cement paste is represented by the blue line.

Although it is possible to form CAH_{10} at high temperatures for a short period of time, this depends on the availability of high crystalinity AH_3 [51], which was not found on the XRD results. Further, the TGA results support this conjecture given the almost flat curve of D2T with respect to CAH_{10}, C_2AH_8, C_3AH_6 and AH_3.

Assuming this depicts the processes taking place at sample D2, what would explain the lack of similar products in sample S2, which also endured a relatively longer period of high temperatures? The cracking allows for prompt release of pressure and faster escape route for water, which precludes the conditions necessary for steam curing as hypothesized in the previous sample. In accordance, TGA and XRD peaks are notably larger for sample S2, displaying the presence of remaining C_3AH_6 and possibly CAH_{10}. The lack of chemical complexity found by SEM EDS investigation would further agree.

While samples D2 and S2 can be seen as two extreme cases in terms of either thermo-mechanical or thermo-chemical chemical alterations, sample D4 is somewhat of a middle ground. The thermo-hygral mechanism depends on the amount of water, tensile strength and heating rate [52]. This sample contained less physically bound water than sample S2 and also a lower tensile capacity due its higher W/C ratio [53]. As a result, cracking occurred mildly and chemical changes were less pronounced. However, a zone of amorphous AH_3 was identified at the very top of the sample. The higher porosity zone beneath the top of the sample points to dehydration of phases, which would also provide

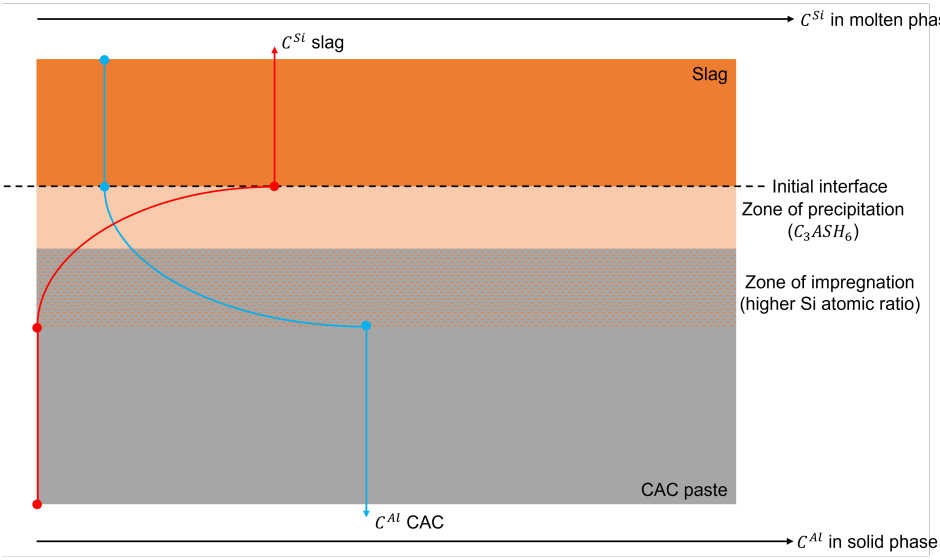

Figure 3.16: Scheme of the indirect dissolution taking place on the samples during the contact with molten slag (adapted from sketch in Poirier & Rigaud [26]).

water availability for upper layers. As cracking was less distributed, this could provide a less severe environment, in which residual water binds with available aluminum ions to generate the upper layer.

Sample S4 displayed the least estimated exposure in time at very high temperatures, quickly reaching ~ 150°C, in agreement with the large peaks for hydration products present in the results of XRD and TGA. Further, as the sample that presented longer bubbling of slag, its direct contact was slightly delayed. This resulted in a structure similar to sample D4 in terms of an upper layer of amorphous AH_3 followed by a porous zone. But, with less evident changes.

However, for the same W/C ratio, sample S4 had more physically bound water, so it should suffer more damage from evaporation. Yet, the sample remained undamaged. The combination of faster cooling of the slag by the water released on this sample and the very short time at temperatures above 200°C, caused a much smoother heating rate and strain field in comparison to sample D4. Such decrease, should be enough to avoid damage [25, 54].

3.5. RE-HYDRATION

In addition to the experiment above, a short re-hydration experiment was performed. This is because subsequent contact with air humidity after high temperature exposure further modifies the composition of the cement paste [55]. The effects of re-hydration on the pore network and mechanical properties of concrete are critical to the design of durable systems under repeated exposure to high temperatures, as well as assessing the remaining quality of damaged structures. Yet such effects remain poorly understood.

Thus, a short experimental trial was performed to study CAC as a protection layer to structural concrete made with ordinary Portland cement (OPC), which is configuration similar to the case study discussed in Chapter 5.

3.5.1. MATERIALS & METHODS

Small scale slabs were prepared containing two layers, one of approximately three years old OPC based concrete and one of CAC mortar. For the OPC concrete, cubic samples of 10 cm sides were sawn to 3 cm height. These samples had a W/C ratio, cement content and aggregate maximum size of 0.45, 355 kg/m^3 and 32 mm, respectively. The cement used was CEM III/B 42,5 N and all samples were cured in a fog room at RH>95% for 28 days. For the layer of CAC mortar, the cement REFRO50 (ÇIMSA) was used in combination with Glenium 51 (BASF), the mix proportions for cement, aggregate, water and super plasticizer were 1:1.35:0.2:0.004. The composition of REFRO50 can be found in Table 3.5.

Table 3.5: Chemical composition of REFRO50 as determined by XRF.

SiO_2	Al_2O_3	CaO	MgO	Fe_2O_3	SO_3	Na_2O	K_2O	TiO_2	P_2O_5	L.O.I.
6.2	50.0	38.8	0.8	2.7	0.2	0.3	–	4.0	–	0.3

The OPC based concrete was saturated with dry surface during the casting of the CAC mortar. Subsequently, the sample was moved to a curing chamber for 27 days. The sample was then dried in an oven at 40°C for one week before the execution of the experiment. At first, 40 grams of blast furnace slag were weighted in an alumina crucible and placed in an oven to be heated at a rate of 15°C/min until 1530°C. The composition of the used slag is found in Table 3.1. The temperature was held for 30 minutes to guarantee liquification of the slag, then the oven was opened and the molten material was poured on top of the sample at the orange area in Figure 3.18. To avoid leakage and concentrate the pour in place, a titanium ring was fixed with cement paste on top of the sample prior to the experiment.

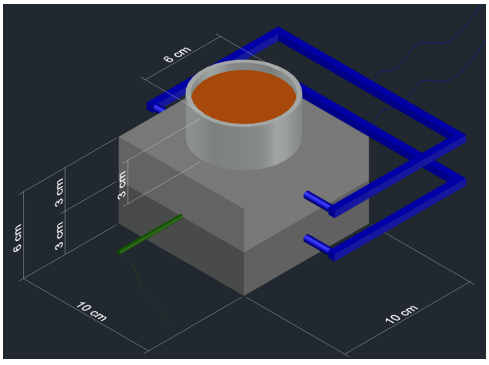

Figure 3.17: Scheme of sample dimensions and experimental setup. In dark gray is the concrete sample, in light gray is CAC sample cast on top of it, in orange is the slag poured inside the titanium ring, in green is a thermocouple between the layers of the material and in blue are extensometers.

During the experiment, the temperature between the two layers of the slab was monitored through a thermocouple capable of enduring high temperatures, further, the dilation of each layer was recorded through the use of extensometers attached to the sample. All measurements had a rate of once per second over two hours, after which the slag and sample cooled down and could be handled. In order to estimate temperature through the entire sample without drilling several times, the temperature recorded through the thermocouple was used as validation for a FEM model used in COMSOL®5.3.

After the experiment, the sample was first cut in half, then one half was sawn into 30 x 20 x 10 mm specimen parallel to the height of the sample. This half was then vacuum impregnated with epoxy resin and further ground and polished until a flat surface was achieved. Finally, a 10 nm layer of conducting carbon coating was placed on the top of the polished surface using a Leica EM CEDO030 carbon evaporator. The other half had the sawn face sealed with aluminum tape and was moved to a curing room where it was cured for one week. Thereafter, the second half was also prepared for microanalysis. The polished sections were analyzed through the use of BSE and EDS following the same procedure and standards of the experiment described prior to this.

3.5.2. RESULTS & DISCUSSION

The temperature evolution at the OPC/CAC interface can be observed in Figure 3.18, together with the model estimation. It is clear the model was very accurate at this estimation. Further, Figure 3.19 also displays the deformation of both layers.

The effect of pouring molten slag on the surface of the sample can be observed in its microstructure for the first 1.5 mm of the sample as shown in Figure 3.19. There are several shrinkage cracks and a clear refinement of the unhydrated grains to the point of mixing with hydration products in components smaller than 1 μm. This is similar to the observed in samples D2 and D4 from the previous experiment, which was expected as the sample was dry at the moment of exposure to the molten slag.

EDS performed on the products between the unhydrated grains showed that the composition had a significant increase in the amount of magnesium and silica in comparison with the reference sample. The main phase remained CAH_{10}, but the Si/Ca atomic ratio increased from 0.1 to 1.0, which could points to the same hypothesis argued in the previous experiment discussion. This observation is corroborated by the distribution of Mg. The magnesium quantified in the surface of the sample is ten times higher than when millimeters deep with respect to the face that was in contact with molten slag.

For the sample that went through re-curing, the regions near the surface presented a very complex microstructure, as it can be seen in Figure 3.20 a), which included the surface coated with a layer of CAH_{10} embedded in amorphous alumina gel (AH_3) and $CaCO_3$ from atmospheric carbonation of the calcium aluminates. Instead of the zone with very fine components, an extremely porous zone was observed, in which most of the unhydrated grains seem to have been completely consumed leaving only CAH_{10}, then an area in which the CA and CA_2 grains present a smaller granulometry, and finally a seemingly unaffected area, after 1 mm depth. Further, many of the cracks were filled by AH_3 and in smaller volume by CAH_{10} and SiO_2, this can be observed at the bottom of Figure 3.20 a) and in Figure 3.20 d).

The composition of the hydration products presented increased Mg content, while

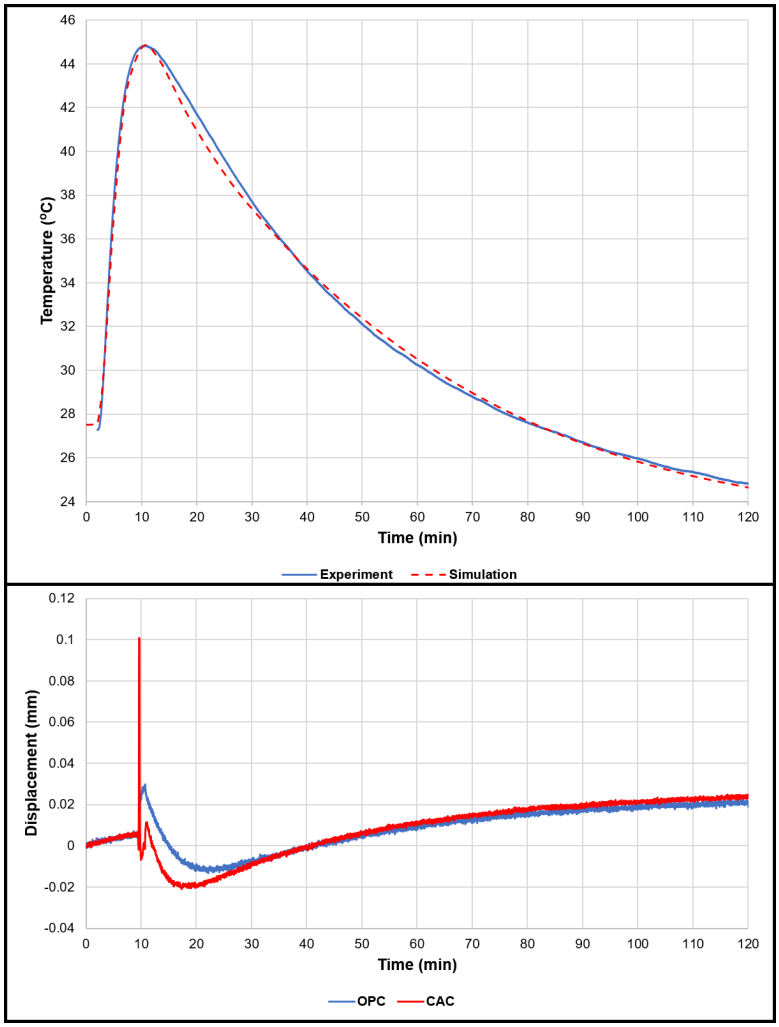

Figure 3.18: Top: temperature evolution at the interface between the two material layers. Bottom: Horizontal deformation of each layer during the experiment.

Figure 3.19: Microstructure of sample after cooling of molten slag; a) Stitching of approximately the first 2 mm of sample surface, the face which had contact with slag is on the right side of the micrograph; b) Microstructure of the sample on unaffected area, similar to that of reference sample; c) Microstructure of the sample on transition area, at approximately 400 μm of the surface; d) Microstructure of the sample near the surface affected by the pouring of slag.

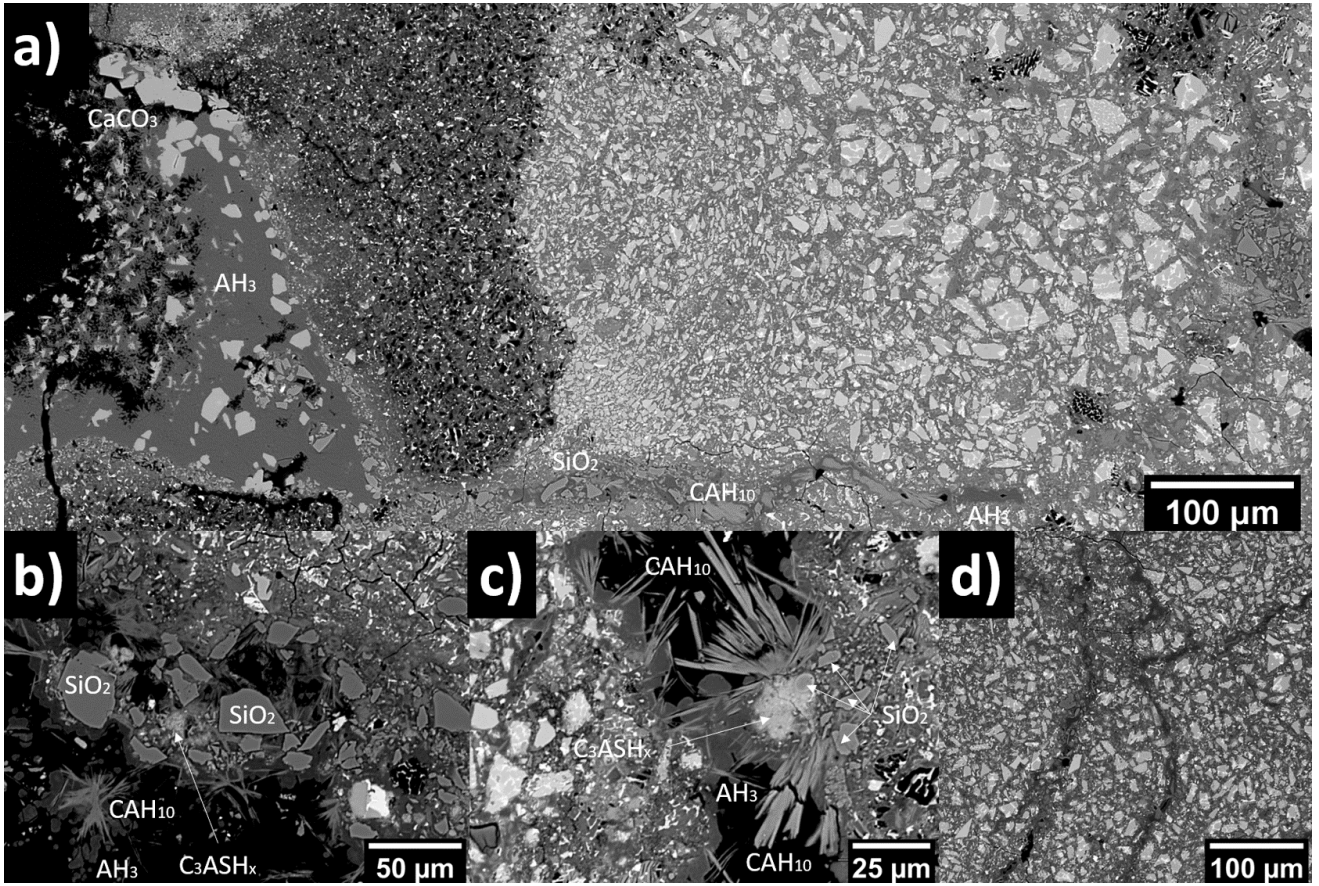

Figure 3.20: Microstructure of sample after one week in a curing room; a) Stitching of the first millimeter of sample surface, the face which had contact with slag is on the left side of the picture; b) Surface area containing silica precipitations; c) Cracked zone highlighting the needle like morphology of CAH_{10}; d) Zone with microcracks filled by AH_3.

the amount of Si dropped to values equivalent to the reference sample. The decrease in amount of silicon can be explained by areas in which solid silica precipitations were identified. An example of such areas is shown in Figure 3.20 b). Inside large cracks and the surface of the sample, freshly formed calcium aluminate decahydrate can be identified by needle morphology as described in Geng et al (2017) [39], which can be seen in Figure 3.20 c).

No indication of conversion reactions was found, although some particles of C_3AH_6 were observed embedded in AH_3, those had a very high amount of Si and slight presence of sulfur. Those phases are seen in Figure 3.20 b) and c). Given their abundance in Si, it is possible that those phases were actually an analogue to Hydrogarnet ($C_3AS_{(3-x)}H_{2x}$) or even Gehlenite (C_2ASH_8) as described in the work of Hidalgo et al (2007) [56].

This experiment confirmed a number of assumptions made on Section 3.4. Slag tends to mix with the cement paste in fine unstable solid solutions. After re-curing, these solutions partially dissipate and precipitate silica rich grains. Further, other elements carried by the slag (such as magnesium) seem to remain in the paste. Although re-curing filled many cracks with hydration products, it seems to also create a very porous zone on the surface of the damaged zone, so the effects on porosity seem to be progressive.

3.6. CONCLUSIONS

Industrial hot spillage event was reproduced at laboratory scale with controlled variables in order to study its effects on the CAC-based structural material subjected to the spill. As expected, the effects on the microstructure of the material considerably differ from experiments where such materials are subjected to a uniform thermal loading i.e. oven heating.

The main processes apparently taking place on the material during contact with molten slag were:

1. The decomposition of the hydration products;
2. The escape of physically bound water, causing thermo-hydral spalling damage in some of the samples;
3. Steam curing of the surface in contact with the hot spill for non-cracked and mildly cracked samples;
4. Diffusion of Si from the slag into the binder, given enough time of contact at high temperature.

While heating samples can simulate the first effect very well, the other effects are very geometry sensitive and not comparable on different methods. As the other effects show an appreciable influence in the performance of the samples, the author believes that the novel method proposed herein to be more suited to simulate industrial events.

Furthermore, it was concluded that a W/C ratio of 0.20 would grant better durability provided the structure is sure to remain dry. If there is a risk of having a saturated structure (i. e. outdoor installation), the counter intuitive strategy of a higher W/C ratio seems to be preferable. This has only be tested to a limit of 0.40 ratio, as it is known

that higher W/C values bring different forms of durability problems due adverse effects of conversion [3, 5].

Both steam curing and Si diffusion into the material could be beneficial for the structural durability under repeated events. However, the re-hydration of the topmost layer and precipitation of silica crystals displays the opposite effect. Thus, there is a need for long-term observation of such material under thermal shock events.

Nevertheless, CAC performed well against the severe testing conditions, showing damage only on the first millimeters of material. When cast on top of an old concrete layer, it executed its function as insulation and caused no dilation problems. Therefore, it was selected for use in the case study described in Chapter 5.

BIBLIOGRAPHY

[1] F.F. Mendonça Filho et al. “Surface effects of molten slag spills on calcium aluminate cement paste”. In: *Materials Design* 217 (2022), p. 110623. ISSN: 0264-1275. DOI: https://doi.org/10.1016/j.matdes.2022.110623. URL: https://www.sciencedirect.com/science/article/pii/S0264127522002441.

[2] F.F. Mendonca Filho and O. Copuroglu. “Re-curing of calcium aluminate cements post contact with molten slag”. In: *17th Euroseminar on Microscopy Applied to Building Materials*. Ed. by K. Peterson. University of Toronto. Toronto, Canada: University of Toronto, 2019.

[3] J. Bensted. “Calcium Aluminate Cements”. In: *Structure and performance of cements*. Ed. by J. Bensted and P. Barnes. London: CRC Press, 2002. Chap. 13, pp. 114–139.

[4] P.K. Mehta and P.J.M. Monteiro. *Concrete: Microstructure, Properties, and Materials*. McGraw Hill professional. McGraw-Hill Education, 2006. ISBN: 9780071462891. URL: https://books.google.nl/books?id=3j5EAQAAIAAJ.

[5] H. Ideker J. et al. “Calcium Aluminate Cements”. In: *Lea’s Chemistry of Cement and Concrete*. Ed. by P.C. Hewlett and M. Liska. Oxford: Butterworth-Heinemann, 2019. Chap. 13, pp. 713–782.

[6] Wasim Khaliq and Hammad Anis Khan. “High temperature material properties of calcium aluminate cement concrete”. In: *Construction and Building Materials* 94 (2015), pp. 475–487. ISSN: 09500618. DOI: 10.1016/j.conbuildmat.2015.07.023. URL: http://dx.doi.org/10.1016/j.conbuildmat.2015.07.023.

[7] Yulong Wang et al. “Microstructure evolution during the heating process and its effect on the elastic properties of CAC-bonded alumina castables”. In: *Ceramics International* 42.9 (2016), pp. 11355–11362. ISSN: 0272-8842. DOI: https://doi.org/10.1016/j.ceramint.2016.04.058. URL: https://www.sciencedirect.com/science/article/pii/S0272884216304539.

[8] N.K. Lee et al. “Microstructural investigation of calcium aluminate cement-based ultra-high performance concrete (UHPC) exposed to high temperatures”. In: *Cement and Concrete Research* 102 (2017), pp. 109–118. ISSN: 0008-8846. DOI: https://doi.org/10.1016/j.cemconres.2017.09.004. URL: https://www.sciencedirect.com/science/article/pii/S0008884617301825.

[9] John F. Zapata, Maryory Gomez, and Henry A. Colorado. “High temperature cracking damage of calcium aluminate cements”. In: *Minerals, Metals and Materials Series* Part F12.52 (2018), pp. 553–563. ISSN: 23671696. DOI: 10.1007/978-3-319-72526-0_52.

[10] Eva Vejmelková et al. “High temperature durability of fiber reinforced high alumina cement composites”. In: *Construction and Building Materials* 162 (2018), pp. 881–891. ISSN: 09500618. DOI: 10.1016/j.conbuildmat.2018.01.076.

[11] Wenjing Gu et al. “Effect of particle size of calcium aluminate cement on volumetric stability and thermal shock resistance of CAC-bonded castables”. In: *Journal of Alloys and Compounds* 772 (2019), pp. 637–641. ISSN: 09258388. DOI: 10.1016/j.jallcom.2018.09.128. URL: https://doi.org/10.1016/j.jallcom.2018.09.128.

[12] Song Gao et al. “Effect of CAC content on the strength of castables at temperatures between 300 and 1000 °C”. In: *Ceramics International* 46.10, Part A (2020), pp. 14957–14963. ISSN: 0272-8842. DOI: https://doi.org/10.1016/j.ceramint.2020.03.024. URL: https://www.sciencedirect.com/science/article/pii/S0272884220306428.

[13] Peixiong Zhang et al. “Relationship between the strength and microstructure of CAC-bonded castables under intermediate temperatures”. In: *Ceramics International* 46.1 (2020), pp. 888–892. ISSN: 0272-8842. DOI: https://doi.org/10.1016/j.ceramint.2019.09.046. URL: https://www.sciencedirect.com/science/article/pii/S0272884219325751.

[14] Rodgers Bangi Mugume and Takashi Horiguchi. “Prediction of spalling in fibre-reinforced high strength concrete at elevated temperatures”. In: *Materials and Structures* 47.4 (Apr. 2014), pp. 591–604. ISSN: 1871-6873. DOI: 10.1617/s11527-013-0082-9. URL: https://doi.org/10.1617/s11527-013-0082-9.

[15] Ying Zhen Li and Haukur Ingason. “Overview of research on fire safety in underground road and railway tunnels”. In: *Tunnelling and Underground Space Technology* 81.August (2018), pp. 568–589. ISSN: 08867798. DOI: 10.1016/j.tust.2018.08.013. URL: https://doi.org/10.1016/j.tust.2018.08.013.

[16] L Missemer et al. “Fire spalling of ultra-high performance concrete : From a global analysis to microstructure investigations”. In: *Cement and Concrete Research* 115.April 2018 (2019), pp. 207–219. ISSN: 0008-8846. DOI: 10.1016/j.cemconres.2018.10.005. URL: https://doi.org/10.1016/j.cemconres.2018.10.005.

[17] Pierre Kalifa, François-Dominique Menneteau, and Daniel Quenard. “Spalling and pore pressure in HPC at high temperatures”. In: *Cement and Concrete Research* 30.12 (2000). Papers presented at the Symposium on "Transport Properties and Microstructure of Cement-Based Systems", pp. 1915–1927. ISSN: 0008-8846. DOI: https://doi.org/10.1016/S0008-8846(00)00384-7. URL: https://www.sciencedirect.com/science/article/pii/S0008884600003847.

[18] Ana Fernández-Jiménez et al. “New Cementitious Materials Based on Alkali-Activated Fly Ash: Performance at High Temperatures”. In: *Journal of the American Ceramic Society* 91.10 (2008), pp. 3308–3314. DOI: https://doi.org/10.1111/j.1551-2916.2008.02625.x. eprint: https://ceramics.onlinelibrary.wiley.com/doi/pdf/10.1111/j.1551-2916.2008.02625.x. URL: https://ceramics.onlinelibrary.wiley.com/doi/abs/10.1111/j.1551-2916.2008.02625.x.

[19] G. Debicki, R. Haniche, and F. Delhomme. “An experimental method for assessing the spalling sensitivity of concrete mixture submitted to high temperature”. In: *Cement and Concrete Composites* 34.8 (2012), pp. 958–963. ISSN: 0958-9465. DOI: https://doi.org/10.1016/j.cemconcomp.2012.04.002. URL: https://www.sciencedirect.com/science/article/pii/S0958946512000637.

[20] Izabela Hager et al. “Effect of Cement Type on the Mechanical Behavior and Permeability of Concrete Subjected to High Temperatures”. In: *Materials* 12.18 (2019). ISSN: 1996-1944. DOI: 10.3390/ma12183021. URL: https://www.mdpi.com/1996-1944/12/18/3021.

[21] Farhad Aslani and Lining Wang. “Fabrication and characterization of an engineered cementitious composite with enhanced fire resistance performance”. In: *Journal of Cleaner Production* 221 (2019), pp. 202–214. ISSN: 0959-6526. DOI: https://doi.org/10.1016/j.jclepro.2019.02.241. URL: https://www.sciencedirect.com/science/article/pii/S0959652619306468.

[22] K D Hertz. “Limits of spalling of fire-exposed concrete”. In: *Fire Safety Journal* 38 (2003), pp. 103–116.

[23] Sammy Y. N. Chan, Gai-fei Peng, and John K. W. Chan. “Comparison between high strength concrete and normal strength concrete subjected to high temperature”. In: *Materials and Structures* 29.10 (Dec. 1996), pp. 616–619. ISSN: 1871-6873. DOI: 10.1007/BF02485969. URL: https://doi.org/10.1007/BF02485969.

[24] Young-Sun Heo et al. “Critical parameters of nylon and other fibres for spalling protection of high strength concrete in fire”. In: *Materials and Structures* 44.3 (Apr. 2011), pp. 599–610. ISSN: 1871-6873. DOI: 10.1617/s11527-010-9651-3. URL: https://doi.org/10.1617/s11527-010-9651-3.

[25] N. Algourdin et al. “Influence of polypropylene and steel fibres on thermal spalling and physical-mechanical properties of concrete under different heating rates”. In: *Construction and Building Materials* 259 (2020), p. 119690. ISSN: 0950-0618. DOI: https://doi.org/10.1016/j.conbuildmat.2020.119690. URL: https://www.sciencedirect.com/science/article/pii/S0950061820316950.

[26] J. Poirier and M. Rigaud. *FIRE Compendium Series: Corrosion of refractories : the fundamentals*. F.I.R.E. compendium series. Göller Verlag, 2017. ISBN: 9783872640062. URL: https://books.google.nl/books?id=rDwqswEACAAJ.

[27] H.F.W. Taylor. *Cement Chemistry*. Thomas Telford, 1997. ISBN: 9780727725929. URL: https://books.google.nl/books?id=1BOETtwi7mMC.

[28] Stephan Preibisch, Stephan Saalfeld, and Pavel Tomancak. “Globally optimal stitching of tiled 3D microscopic image acquisitions”. In: *Bioinformatics* 25.11 (Apr. 2009), pp. 1463–1465. ISSN: 1367-4803. DOI: 10.1093/bioinformatics/btp184. eprint: https://academic.oup.com/bioinformatics/article-pdf/25/11/1463/950295/btp184.pdf. URL: https://doi.org/10.1093/bioinformatics/btp184.

[29] H.S. Wong and N.R. Buenfeld. “Monte Carlo simulation of electron-solid interactions in cement-based materials”. In: *Cement and Concrete Research* 36.6 (2006), pp. 1076–1082. ISSN: 0008-8846. DOI: https://doi.org/10.1016/j.cemconres.2006.03.006. URL: https://www.sciencedirect.com/science/article/pii/S0008884606000664.

[30] National Center for Biotechnology Information. *PubChem Compound Summary for CID 159415, Calcium aluminate*. Retrieved September 28, 2022. 2022. URL: https://pubchem.ncbi.nlm.nih.gov/compound/Calcium-aluminate.

[31] Valentin Antonovič et al. “The Effect of Temperature on the Formation of the Hydrated Calcium Aluminate Cement Structure”. In: *Procedia Engineering* 57 (2013). Modern Building Materials, Structures and Techniques, pp. 99–106. ISSN: 1877-7058. DOI: https://doi.org/10.1016/j.proeng.2013.04.015. URL: https://www.sciencedirect.com/science/article/pii/S1877705813007455.

[32] D.E. Newbury and N.W.M. Ritchie. “Performing elemental microanalysis with high accuracy and high precision by scanning electron microscopy/silicon drift detector energy-dispersive X-ray spectrometry (SEM/SDD-EDS)”. In: *Journal of Materials Science* 50 (2015), pp. 493–518. DOI: https://doi.org/10.1007/s10853-014-8685-2.

[33] Yoshiaki Kashiwaya, Tomohiro Akiyama, and Yutaro In-Nami. “Latent Heat of Amorphous Slags and Their Utilization as a High Temperature PCM”. In: *ISIJ International* 50.9 (2010), pp. 1259–1264. DOI: 10.2355/isijinternational.50.1259.

[34] Jinpeng Dai et al. “Research on influencing factors and time-varying model of thermal conductivity of concrete at early age”. In: *Construction and Building Materials* 315 (2022), p. 125638. ISSN: 0950-0618. DOI: https://doi.org/10.1016/j.conbuildmat.2021.125638. URL: https://www.sciencedirect.com/science/article/pii/S0950061821033742.

[35] K. Scrivener, R. Snellings, and B. Lothenbach. *A Practical Guide to Microstructural Analysis of Cementitious Materials*. CRC Press, 2016. ISBN: 9781351228497. DOI: https://doi.org/10.1201/b19074.

[36] Chaiwat Phrompet et al. “Optical and dielectric properties of nano-sized tricalcium aluminate hexahydrate (C3AH6) cement”. In: *Construction and Building Materials* 179 (2018), pp. 57–65. ISSN: 0950-0618. DOI: https://doi.org/10.1016/j.conbuildmat.2018.05.180. URL: https://www.sciencedirect.com/science/article/pii/S0950061818312649.

[37] M.T. Palou et al. “Hydration of high alumina cement–silica fume composite with addition of Portland cement or sodium polyphosphate under hydrothermal treatment”. In: *Journal of Thermal Analysis and Calorimetry* 113 (2013), pp. 385–394. DOI: https://doi.org/10.1007/s10973-013-3042-2.

[38] D. Fernández-González et al. “Solar synthesis of calcium aluminates”. In: *Solar Energy* 171 (2018), pp. 658–666. ISSN: 0038-092X. DOI: https://doi.org/10.1016/j.solener.2018.07.012. URL: https://www.sciencedirect.com/science/article/pii/S0038092X18306753.

[39] Guoqing Geng et al. “Nanometer-Resolved Spectroscopic Study Reveals the Conversion Mechanism of CaO·Al2O3·10H2O to 2CaO·Al2O3·8H2O and 3CaO·Al2O3·6H2O at an Elevated Temperature”. In: *Crystal Growth & Design* 17.8 (2017), pp. 4246–4253. DOI: 10.1021/acs.cgd.7b00553. eprint: https://doi.org/10.1021/acs.cgd.7b00553. URL: https://doi.org/10.1021/acs.cgd.7b00553.

[40] M. Balonis and F.P. Glasser. “The density of cement phases”. In: *Cement and Concrete Research* 39.9 (2009), pp. 733–739. ISSN: 0008-8846. DOI: https://doi.org/10.1016/j.cemconres.2009.06.005. URL: https://www.sciencedirect.com/science/article/pii/S0008884609001343.

[41] Pierre Villars (Chief Editor). *CAH10 (CaAl2[OH]8[H2O]5.4) Crystal Structure*. PAULING FILE in: Inorganic Solid Phases, SpringerMaterials (online database). 2016. URL: https://materials.springer.com/isp/crystallographic/docs/sd_1811685.

[42] S. Goñi et al. “A new insight on alkaline hydrolysis of calcium aluminate cement concrete: Part I. Fundamentals”. In: *Journal of Materials Research* 11.7 (1996), pp. 1748–1754. DOI: 10.1557/JMR.1996.0219.

[43] H. Towers and J. Chipman. “Diffusion of Calcium and Silicon in a Lime-Alumina-Silica Slag”. In: *JOM* 9 (1957), pp. 769–773. DOI: https://doi.org/10.1007/BF03377932.

[44] K. Zheng et al. “Investigation of Self-Diffusion and Structure in Calcium Aluminosilicate Slags by Molecular Dynamics Simulation”. In: *Materials Sciences and Applications* 5.2 (2014), pp. 73–80. DOI: 10.4236/msa.2014.52011.

[45] Z. Ignaszak and P. Popielarski. “Contribution to Thermal Properties of Multi-Component Porous Ceramic Materials Used in High-Temperature Processes in the Foundry Industry”. In: *Heat and Mass Transfer in Porous Media*. Ed. by J.M.P.Q. Delgado. Berlin, Heidelberg: Springer Berlin Heidelberg, 2012, pp. 187–218. ISBN: 978-3-642-21966-5. DOI: 10.1007/978-3-642-21966-5_8. URL: https://doi.org/10.1007/978-3-642-21966-5_8.

[46] R.N. Edmonds and A.J. Majumdar. “The hydration of monocalcium aluminate at different temperatures”. In: *Cement and Concrete Research* 18.2 (1988), pp. 311–320. ISSN: 0008-8846. DOI: https://doi.org/10.1016/0008-8846(88)90015-4. URL: https://www.sciencedirect.com/science/article/pii/0008884688900154.

[47] R.N. Edmonds and A.J. Majumdar. “The hydration of Secar 71 aluminous cement at different temperatures”. In: *Cement and Concrete Research* 19.2 (1989), pp. 289–294. ISSN: 0008-8846. DOI: https://doi.org/10.1016/0008-8846(89)90093-8. URL: https://www.sciencedirect.com/science/article/pii/0008884689900938.

[48] Herbert Pöllmann. “Calcium Aluminate Cements – Raw Materials, Differences, Hydration and Properties”. In: *Reviews in Mineralogy and Geochemistry* 74.1 (Jan. 2012), pp. 1–82. ISSN: 1529-6466. DOI: 10.2138/rmg.2012.74.1. eprint: https://pubs.geoscienceworld.org/msa/rimg/article-pdf/74/1/1/2948803/1_REV074C01.pdf. URL: https://doi.org/10.2138/rmg.2012.74.1.

[49] Colan E. Hughes et al. “Exploiting in-situ solid-state NMR spectroscopy to probe the early stages of hydration of calcium aluminate cement”. In: *Solid State Nuclear Magnetic Resonance* 99 (2019), pp. 1–6. ISSN: 0926-2040. DOI: https://doi.org/10.1016/j.ssnmr.2019.01.003. URL: https://www.sciencedirect.com/science/article/pii/S0926204018300936.

[50] M.A.L. Braulio et al. “Basic slag attack of spinel-containing refractory castables”. In: *Ceramics International* 37.6 (2011), pp. 1935–1945. ISSN: 0272-8842. DOI: https://doi.org/10.1016/j.ceramint.2011.02.007. URL: https://www.sciencedirect.com/science/article/pii/S0272884211000964.

[51] Barbara Lothenbach, Laure Pelletier-Chaignat, and Frank Winnefeld. “Stability in the system CaO–Al2O3–H2O”. In: *Cement and Concrete Research* 42.12 (2012), pp. 1621–1634. ISSN: 0008-8846. DOI: https://doi.org/10.1016/j.cemconres.2012.09.002. URL: https://www.sciencedirect.com/science/article/pii/S0008884612001949.

[52] Zhu Pan, Jay G. Sanjayan, and Daniel L.Y. Kong. “Effect of aggregate size on spalling of geopolymer and Portland cement concretes subjected to elevated temperatures”. In: *Construction and Building Materials* 36 (2012), pp. 365–372. ISSN: 0950-0618. DOI: https://doi.org/10.1016/j.conbuildmat.2012.04.120. URL: https://www.sciencedirect.com/science/article/pii/S0950061812003224.

[53] Amirmohamad Abolhasani, Hadi Nazarpour, and Mehdi Dehestani. “The fracture behavior and microstructure of calcium aluminate cement concrete with various water-cement ratios”. In: *Theoretical and Applied Fracture Mechanics* 109 (2020), p. 102690. ISSN: 0167-8442. DOI: https://doi.org/10.1016/j.tafmec.2020.102690. URL: https://www.sciencedirect.com/science/article/pii/S0167844220302664.

[54] Gyeongcheol Choe et al. “Effect of moisture migration and water vapor pressure build-up with the heating rate on concrete spalling type”. In: *Cement and Concrete Research* 116.August 2017 (2019), pp. 1–10. ISSN: 00088846. DOI: 10.1016/j.cemconres.2018.10.021. URL: https://doi.org/10.1016/j.cemconres.2018.10.021.

[55] Abdullah Huzeyfe Akca and Nilüfer Özyurt. “Effects of re-curing on microstructure of concrete after high temperature exposure”. In: *Construction and Building Materials* 168 (2018), pp. 431–441. ISSN: 0950-0618. DOI: https://doi.org/10.1016/j.conbuildmat.2018.02.122. URL: https://www.sciencedirect.com/science/article/pii/S0950061818303714.

[56] A. Hidalgo et al. “Microstructure of the system calcium aluminate cement-silica fume: application in waste immobilization”. In: *From Zeolites to Porous MOF Materials - The 40th Anniversary of International Zeolite Conference*. Ed. by Ruren Xu et al. Vol. 170. Studies in Surface Science and Catalysis. Elsevier, 2007, pp. 1617–1628. DOI: https://doi.org/10.1016/S0167-2991(07)81039-1. URL: https://www.sciencedirect.com/science/article/pii/S0167299107810391.

4

PLUTONIC ROCKS AS THERMAL SHOCK PROTECTION

Sometimes scientists change their minds. New developments cause a rethink. If this bothers you, consider how much damage is being done to the world by people for whom new developments do not cause a rethink.

Terry Pratchett, The Science of Discworld

a circle of Göbeklitepe stones, which looked very comtemporary even though they were based on something over ten thousand years old.

Kim Stanley Robinson, 2312

This chapter explores an alternative for damage prevention in thermal shock events by applying a surface protection to concrete instead of changing the material composition. The author studied two plutonic rocks, dunite and microgabbro for their role as such protection. A number of experiments determined the rocks physical, thermal, mechanical and optical properties and pre-heating was applied to half of the samples to study the effect of the first thermal cycle. An explanation was offered to the microstructural changes observed before and after heating and their impacts on the macro-properties of the materials. A short FEM simulation is carried to further explore the suitability of using the selected rocks as a surface cover to a concrete substrate in an industrial setting.

Parts of this chapter have been published in Materials **15**, 3490 (2022) [1].

4.1. PLUTONIC ROCKS AS BUILDING MATERIALS

ROCKS compose the oldest temples ever found, the Göbeklitepe and the Nevali Çori in south-eastern Turkey, both from 10000 BCE to 8000 BCE [2], and are still vastly used in modern constructions [3]. However, on the context of high temperatures, rocks present largely different behaviours. This is due their wide composition range and the transformations associated with each type of microstructure, as discussed in Chapter 2. As mentioned in Chapter 3, the environments being considered in the present research assumes the spill of a product (e. g. molten slag, pig iron, unrefined oil, liquid aluminium) into an ambient temperature concrete structure. In this scenario the thermal shock usually ranges from the temperature of concrete (from 5^oC to 40^oC) to the temperature of the product (from 800^oC to 1500^oC).

It has been previously pointed out that fast heating rates (such as the ones mentioned above) cause a thermo-mechanical mechanism (TMM) governed spalling in concrete [4], while slower rates are dominated by the thermo-hygral mechanism (THM) or do not spall at all [5]. The heating rate has even been found as the main difference between slow loss of strength and explosive failure for given concrete mixes [4–6]. The operating temperature of the industrial processes is set to achieve higher product quality and cannot be changed. Thus, this thesis presents the idea of using naturally refractory rocks as a surface layer protection to concrete that would be exposed to the described thermal gradients. Such overlay element would heat up and dissipate energy before the underlying concrete can be affected and later slowly transfer the warmth to the substrate structure, greatly decreasing the danger of explosive spalling.

However, a number of conditions must be met before choosing a material for such application. Because of the size of structures usually encountered in such facilities, the material would have to be available in large quantities and within reasonable geographical proximity. Furthermore, it would be desirable for it to possess similar thermal dilation to concrete at low temperatures while displaying lower strains at high temperatures. It should also be chemically stable at high temperature to allow for good durability when exposed to frequent events and possess high toughness to resist eventual impacts. Finally, compressive strength similar or superior to the used concrete would be desirable.

Due to their geological formation, plutonic rocks are the most likely candidates for high temperature applications. Given the known geological properties, availability at the time of writing of this thesis and market costs, two stones were pre-selected: dunite and micrograbbro. This chapter describes the study of these two stones as possible building material with the end goal of serving as a protection layer to the concrete in a steel factory during spillage of molten iron or slag. While this chapter focus on the properties of the stones, the details of a concrete/stone hybrid element are explored in Chapter 5.

4.2. EXPERIMENTAL PROGRAM

4.2.1. SELECTED ROCKS

Dunite was mined from the Orhaneli ophiolite, situated in the western part of the Izmir-Ankara-Erzincan Suture Zone and south of Bursa (Turkey), an area that exposes cumulates belonging to the mantle-crust transition zone [7]. This rock presented an average density of 3258 kg/m^3. Microgabbro was mined from the Alanya Massif (Turkey), a microcontinent area that possesses ductile-deformed meta-basaltic rocks [8]. This rock presented an average density of 2813 kg/m^3. Both were cut for transportation purposes. The rocks were later sub-sampled for the experiments. Figure 4.1 shows an overview of the rocks location and appearance. Prior to the experiments, half the samples were heated to a temperature of 900°C for one hour. This allows for comparison of the behaviour of the non-heated rocks against the pre-heated stones.



Figure 4.1: Geographic location where the rocks were mined (top); Pallet of dunite (bottom left); Pallet of microgabbro (bottom right).

4.2.2. X-RAY DIFFRACTION

In order to determine the mineralogical composition of the rocks, samples (in natural form and pre-heated state) were ground to fine powder and kept dry until testing through X-ray diffraction. A Bruker D8 Advance diffractometer Bragg-Brentano geometry and Lynxeye position sensitive detector was used with $CuK\alpha_{1,2}(\lambda = 1.5408\text{Å})$ radiation for all XRD measurements. The scatter screen height was set at 5 mm height, divergence slit V12. The used voltage was 45 kV with a current of 40 mA. The spin was of the sample. All scans were performed with a 2θ angle between 10° and 130°, with a step size of 0.03^o. The counting time per step was of two seconds. A combination of two softwares, X'Pert HighScore Plus and Jade6 was used for the spectral analysis. The standard software databases sufficed for peak identification. This method has been previously reported in Mendonça Filho et al (2022) [9]

4.2.3. THERMAL GRAVIMETRIC ANALYSIS

Powder samples, prepared in the same fashion as described for X-ray diffraction were used to perform thermogravimetric analysis (TGA) with the goal of understanding the chemical transformations in the rocks when heated. For the analyses, a NIETZSCH STA 449 F3 Jupiter was used. Approximately 40 mg of material was used for each analysis. The mass change of samples was continuously monitored while the temperature was raised at a $10^oC/m$ rate from 40^oC to 1000^oC. In order to perform the measurements, an 1 mm^3 alumina crucible containing each sample was placed under a dry argon atmosphere with a purge rate of 50 mL/min, as advised in Scrivener et al (2017) [10].

4.2.4. OPTICAL MICROSCOPY

To complement the results of X-ray diffraction while simulating a thermal shock event, optical microscopy was performed. For this test, plates of 80 mm of length and width, with 30 mm of depth were cut. Each plate then was exposed to 40 g of molten slag heated at 1530^oC to simulate a thermal shock event (similar to the experiment described in Chapter 3. After the exposure, the samples were allowed to cool for 12 hours, then the slag was removed and the specimens were cut in half. From the halved vertical face, petrographic thin sections were produced. For this purpose, a controlled grinding process was employed with a semi-automatic thin sectioning machine, with three diamonds rollers of 64, 46 and 16 μm. Measurements with an electronic drop indicator yielded a thickness of about 22 μm stone and about 8 μm mounting glue. A more in depth description of the sample preparation can be found in Poole and Sims (2016)[11]

The analysis was performed through a Leica DM2500P optical microscope equiped with linear and circular polarization filters. Lenses of magnification and numerical aperture equivalent to 2.5/0.07,10/0.22 and 20/0.4 respectively, were available. Plain polarized light (PPL) and cross polarized light (XPL) were used. The camera used to acquire the micrographs was a Leica DFC310FX digital camera, with a 1392x1040 resolution. Proprietary software was used for the image acquisition.

4.2.5. X-RAY MICROTOMOGRAPHY

For the quantification of different components on the rocks, cylindrical samples of non-heated dunite and microgabbro were scanned by a Phoenix Nanotom X-ray CT scanner. These samples were then heated to a temperature of 900^oC at a rate of 10 ^oC/min and re-scanned using the same equipment. The scanner is composed of a transmission type X-ray tube, a sample stage and a 3072 x 2400 flat panel detector with a pixel size of 100 μm. The transmission target uses a tungsten filament and possesses a maximum accelerating voltage of 180 kV. However, the acquisitions were performed at 120 kV. A dunite sample of 16 mm diameter was used, resulting in a spatial resolution of 8 μm/pixel. The microgabbro cylinder had a 25 mm of diameter, resulting in a spatial resolution of 13.33 μm/pixel. Different sample sizes were used because dunite presented fine cracks, that could be better analyzed using a higher spatial resolution. Meanwhile, microgabbro has relatively larger grains, which can be better studied with a larger field of view. Reconstruction was done through datos veloCt, the software provided by the equipment manufacturer. This procedure has been previously described by Rodriguez et al (2020)[12]

Bruker's DataViewer software was used for registration. The scanners of the natural

Table 4.1: Shape and dimensions of samples used for each test.

Analysis method	Sample shape	Sample dimensions (mm)
X-ray difraction	Powder	<0.01
Thermogravimetric analysis	Powder	<0.01
Optical microscopy	Rectangle mounted in glass	30 x 45 x 0.022
Compressive strength	Cube	40 x 40 x 40
Thermal dilation	Cylinder	5 x 5
Micro tomography (dunite)	Cylinder	16 x 30
Micro tomography (microgabbro)	Cylinder	25 x 40

stones could be registered to their pre-heated counterpart through true 3D registration using rigid transform, so expansion could also be detected. The post-processing of the images was performed using the freeware Fiji image analysis [13].

For dunite scans, a Gaussian blur filter (with 2 pixel radius) was used, followed by a non-local means denoising filter [14] in order to reduce noise. For phase segmentation, a classifier was trained using 3D trainable WEKA segmentation [15]. Because the segmentation of fine, crack-like phases is challenging, the authors opted to use a randomizable filtered classifier as basis for the WEKA training. For microgabbro, a median filter (with 2 pixel radius) was used, followed by the mentioned non-local means denoising filter. The segmentation of microgabbro samples was performed based on thresholding. The plugin 3D objects counter [16] was used to acquire the size distribution and diverse geometric properties of the phases after segmentation.

4.2.6. THERMAL DILATION

Cylindrical cores were extracted from non-heated dunite, pre-heated dunite, non-heated microgabbro and pre-heated microgabbro. The dimensions of these were 5 mm of diameter and varying heights between 3 and 7 mm. A Perkin Elmer TMA 4000 thermomechanical analyzer was used to determine the coefficient of thermal expansion (CTE) of the samples. The CTE was determined by heating each sample from ambient temperature (24^oC) to 800^oC at a heating rate of 2.8 ^oC/min and continuosly monitoring the strain of the samples.

4.2.7. COMPRESSIVE STRENGTH

Three cubes with 40 mm sides were tested for each rock in order to determine compressive strength according to NEN-EN 1926:2007 [17]. Samples were tested in natural state and after the pre-heating treatment. The samples were tested at a fixed loading rate of 13.5 kN/s using a a servo-hydraulic mechanical press with maximum load capacity of 5000 kN and high stability from Matest. Table 4.1 shows a review of samples shapes and dimensions for each test.

4.3. RESULTS AND DISCUSSION

4.3.1. X-RAY DIFFRACTION

The results of X-ray diffraction for dunite and microgabbro can be found in Figure 4.2. As expected, dunite was mostly composed of olivine, predominantly forsterite (Mg_2SiO_4). The best fit was found with a sample of molecular percentage of fosterite to fayelite (Fe_2SiO_4) equivalent to $Fo_{95}Fa_{05}$. Zincochromite ($ZnCr_2O_4$) was the second most abundant mineral detected although the peaks were less visible on the non-heated dunite sample. Trace amounts of chrysolite ($Mg_3(Si_2O_5)(OH)_4$) were also identified, which is common due the serpentinization of olivine [18, 19]. At 900^oC it is expected that the chrysolite will go through dehydration following equation 4.1 [20], which is confirmed by the absence of peaks on the heated dunite sample.

$$\underset{(serpentine)}{2Mg_3Si_2O_5(OH)_4} \rightarrow \underset{(forsterite)}{3Mg_2SiO_4} + \underset{(silica)}{SiO_2} + \underset{(fluid)}{4H_2O} \tag{4.1}$$

Microgabbro was found to be composed mostly of albite ($NaAlSi_3O_8$), with considerable amounts of chamosite ($(Fe,Al,Mg)_6(Si,Al)_4O_{10}(OH)_8$) and pumpellyite ($Ca_2FeAl_2(SiO_4)(Si_2O_7)(OH)_2 \cdot H_2O$) and small amounts of aluminian augite ($Ca(Mg,Fe,Al)(Si,Al)_2O_6$) and analcime ($Na(Si_2Al)O_6 \cdot H_2O$). On the pre-heated sample, the peaks for chamosite, pumpellyite and analcime were absent. For analcime, this is explained due the mineral dehydration at relatively low temperatures and pressure [21]. For pumpellyite, the dehydration occurs at even lower temperatures ($T < 300^oC$) [22], also in a single step. On the other hand, the behaviour of chamosite at higher temperatures is still in debate. Steudel et al (2016) [23] recently proposed that this can be described by the following five steps process:

1) Oxidation (100%)

$$2[MgFe(II)Al(OH)_6] \cdot [(Si_3Al)Mg_2Fe(II)O_{10}(OH)_2] \rightarrow 2[MgFe(III)Al(OH)_5(O)] \cdot [(Si_3Al)Mg_2Fe(III)O_{10}(OH)(O)] + 2H_2$$

2) Dehydroxylation of interlayer octahedral sheet

$$2[MgFe(III)Al(OH)_5(O)] \cdot [(Si_3Al)Mg_2Fe(III)O_{10}(OH)(O)] \rightarrow 2[MgFe(III)Al(O)_{2.5}(O)] \cdot [(Si_3Al)Mg_2Fe(III)O_{10}(OH)(O)] + 5H_2O\uparrow$$

3) Dehydroxylation of 2:1 layers

$$2[MgFe(III)Al(O)_{2.5}(O)] \cdot [(Si_3Al)Mg_2Fe(III)O_{10}(OH)(O)] \rightarrow 2[MgFe(III)Al(O)_{2.5}(O)] \cdot [(Si_3Al)Mg_2Fe(III)O_{10}(O)_{0.5}(O)] + H_2O\uparrow$$

4) & 5) Decomposition and Recrystallization

$$2[MgFe(III)Al(O)_{2.5}(O)] \cdot [(Si_3Al)Mg_2Fe(III)O_{10}(O)_{0.5}(O)] \rightarrow 2Mg[SiO_3] + 2MgAl_2O_4 + 2MgFe_2O_4 + 4SiO_2(amorphous)$$

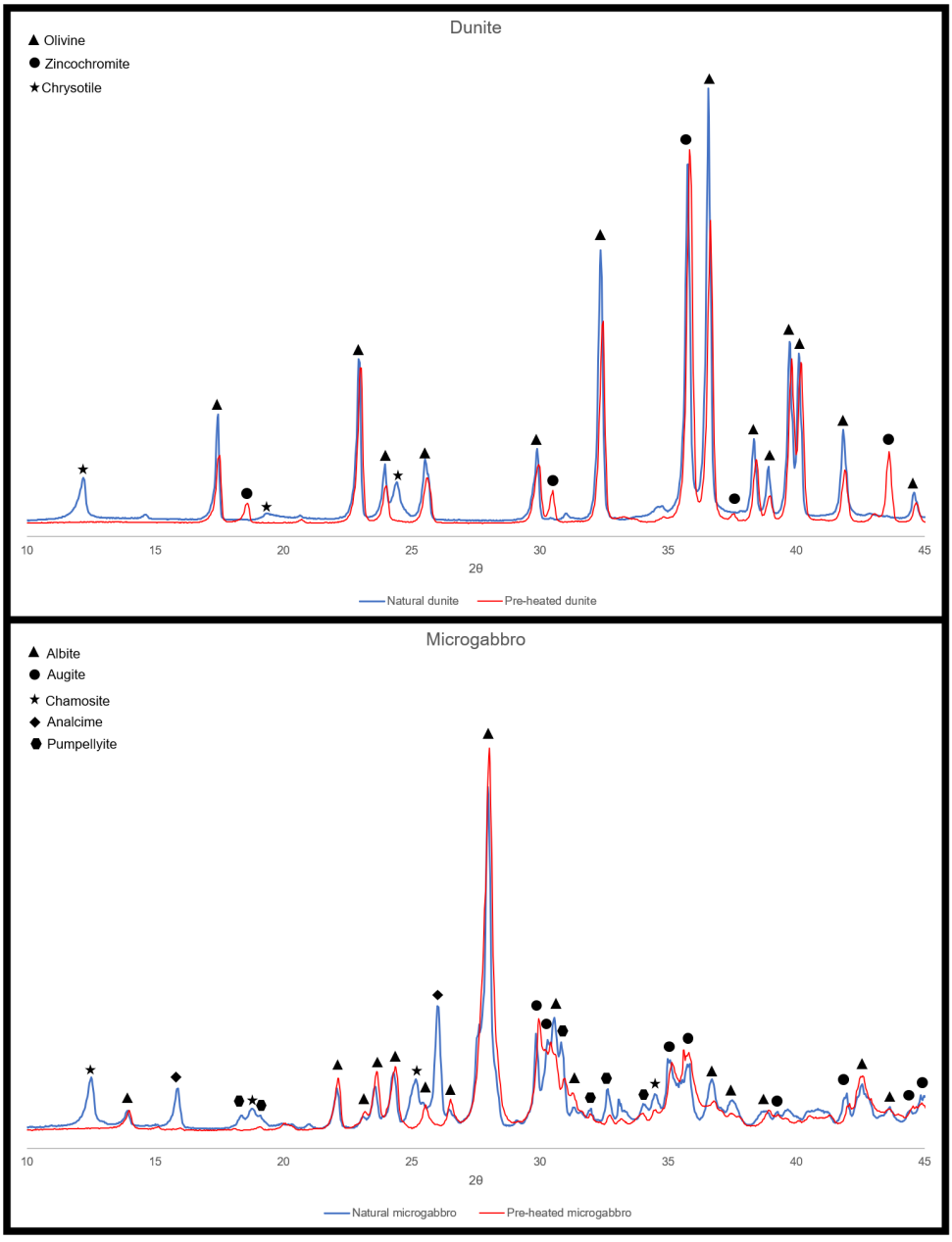

Figure 4.2: XRD results for dunite (top) and microgabbro (bottom) samples. The natural samples (in blue) are overlapped with their pre-heated counter parts(in red).

4.3.2. THERMOGRAVIMETRIC ANALYSIS

The result for the thermogravimetric analyses are presented in Figure 4.3. The small mass loss in dunite between 400°C and 700°C is attributed to the dehydration of chrysotile [24]. On the other hand, three DTG peaks were present in the results for microgabbro. The first peak, between 200°C and 450°C corresponds to analcime [25], although a very broad range of temperature, the maxima is characteristically located in the 350°C-370°C range [26]. The second peak (between 470°C and 600°C) and the third peak (between 615°C and 800°C), both belong to the thermal decomposition reactions of chamosite [27]. Pumpellyite has a characteristic dehydration peak between 150°C and 300°C [22], thus it in overlapped with analcime.

4.3.3. OPTICAL MICROSCOPY

Figure 4.4 shows several fields of view of the thin sections for all samples, based on the irregular extinction and banded structures in large crystals, the olivine portion of dunite is assumed to be strained [28]. Furthermore, considering the interference colors present in Figure 4.4 a, it can be assumed the olivine is magnesium rich [29]. The angular black features present in Figure 4.4 a and d appear opaque in plain polarized light, as these are the zincochromite phase. Figure 4.4 b highlights a strain of chrysotile in the center of the image with a dark gray fractured aspect. Embedded within the chrysotile, the brighter gray-bluish fibrous phase is antigorite, another mineral in the serpentine subgroup often identified by these features. [30].

Figure 4.4 d and e show a thin section made from the heated dunite sample, the difference in interference colors was apparent. The reason for the red-brown to dark brown colour has been previously discussed in the works of Bron [31]. The colours are caused by the occurrence of hematite, which, itself has two sources during the heating of dunite. The first being the development of dust like separations of hematite by the olivine (which develops pleochroism), this is usually seen in the periphery of the grains. The second source was serpentine, oxidating Fe^{2+} into Fe^{3+}. As expected the chrysotile suffered dehydration after heating, losing its texture and leaving just vestiges of its presence. Figure 4.4 e shows a previous site of chrysotile in the pre-heated sample.

Microgabbro displays a typical subhedral aspect with phaneritic texture in Figure 4.4 c, with pumpellyite appearent as brighter yellow and augite as deep purple. Both analcime [29] and chamosite [32] appear as opaque black, while, albite can be seen in the center right of the image marked by a typical dark grey almost extinct [33]. The difference between the non-heated sample and the heated on transmission light microscopy is rather small, with Figure 4.4 f showing only small details in inter-granular space in red.

4.3.4. X-RAY MICROTOMOGRAPHY

DUNITE

Through the registration process it was clear that after cooling, the heated samples return to their natural size, demonstrating good dimensional stability. The tomography of dunite reveals three phases (in Figure 4.5), as expected by the XRD results. In the volumetric representation of Figure 4.5, serpentine is seen white and light grey while olivine is dark grey. In the 2D slices, zincochromite is shown in white, olivine in bright grey and chrysotile in dark grey and black. The phases can be clearly distinguished due their

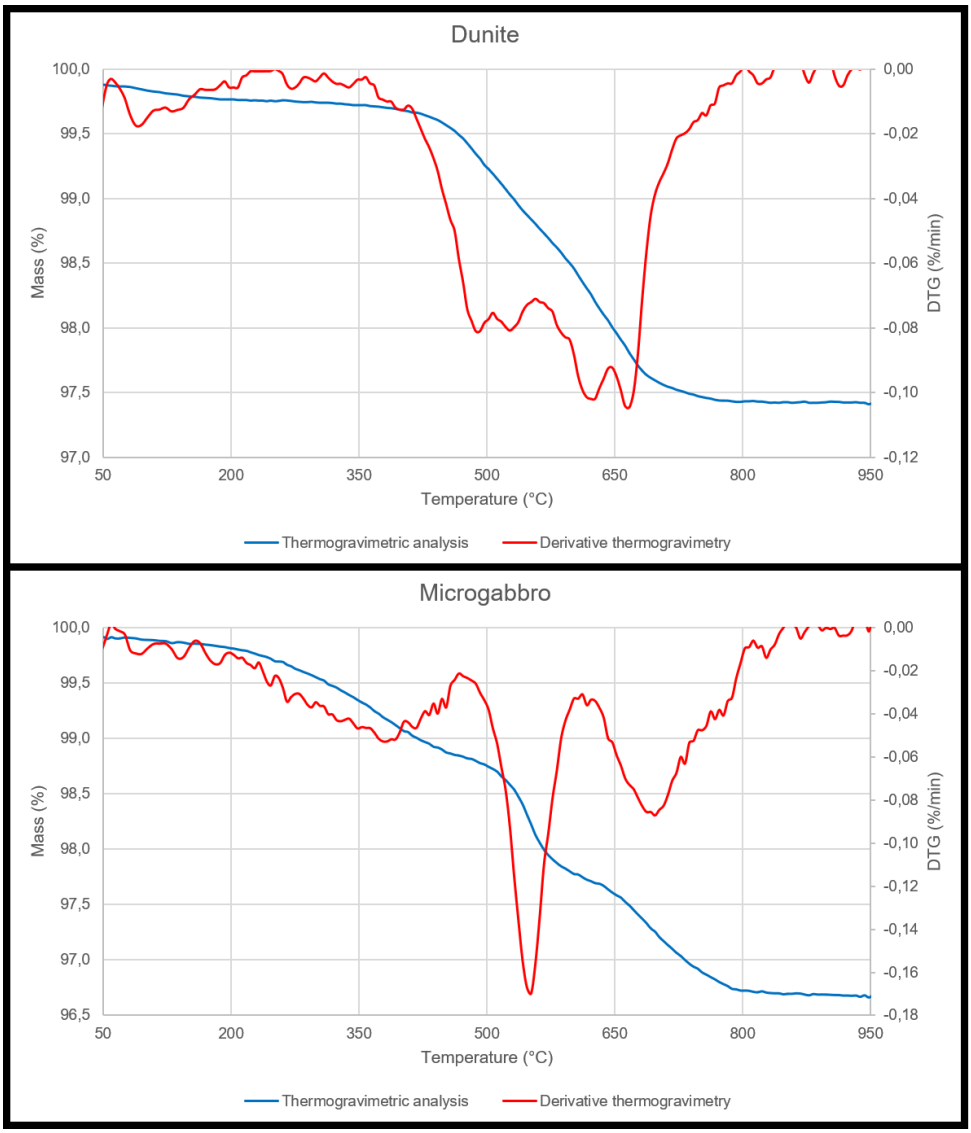

Figure 4.3: Thermogravimetric analysis results for dunite (top) and microgabbro (bottom) samples. The TGA results are seen in blue, while the DTG results are overlapped in red.

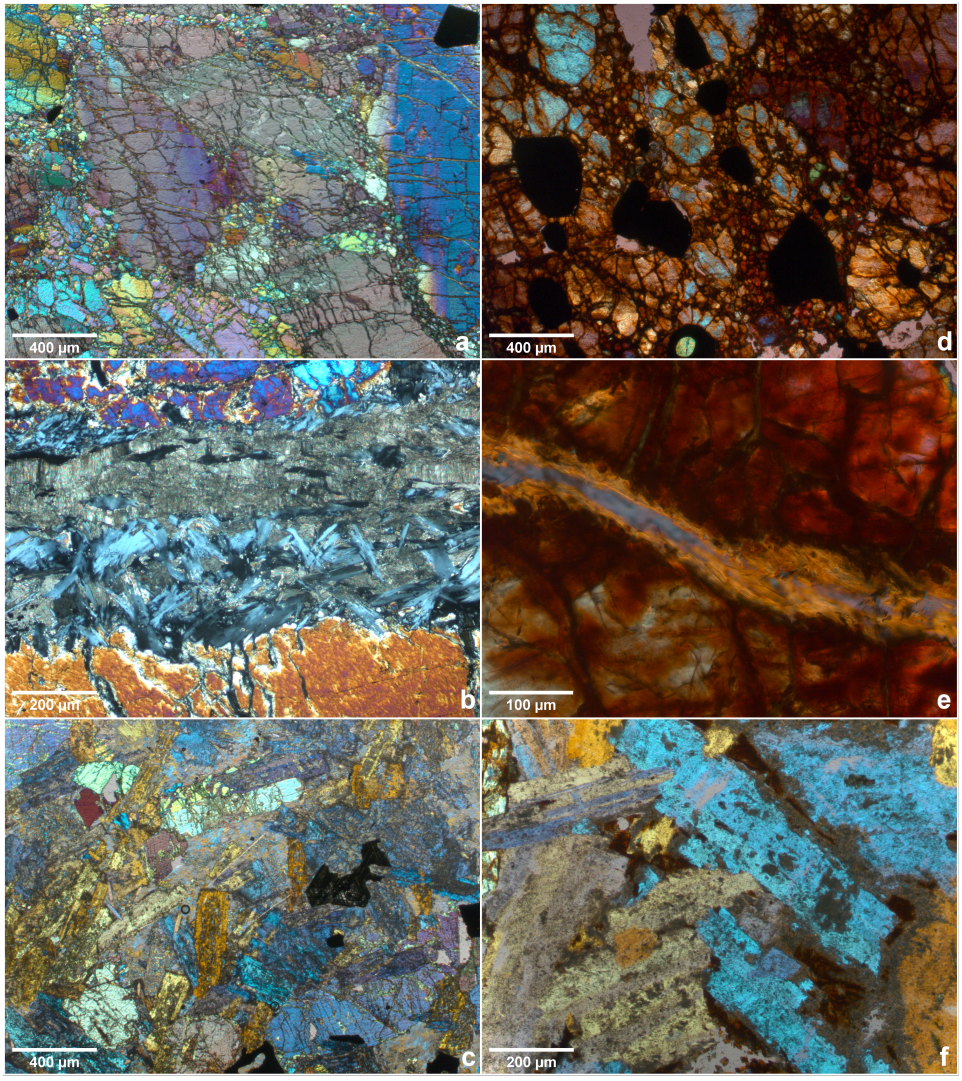

Figure 4.4: Thin sections of the samples: a) Natural dunite overview; b) Natural dunite, focus on chrysotile vein; c) Natural microgabbro overview; d) Pre-heated dunite overview; e) Pre-heated dunite, focus on chrysotile; f) Pre-heated gabbro overview.

density difference, as stated in Table 4.2.

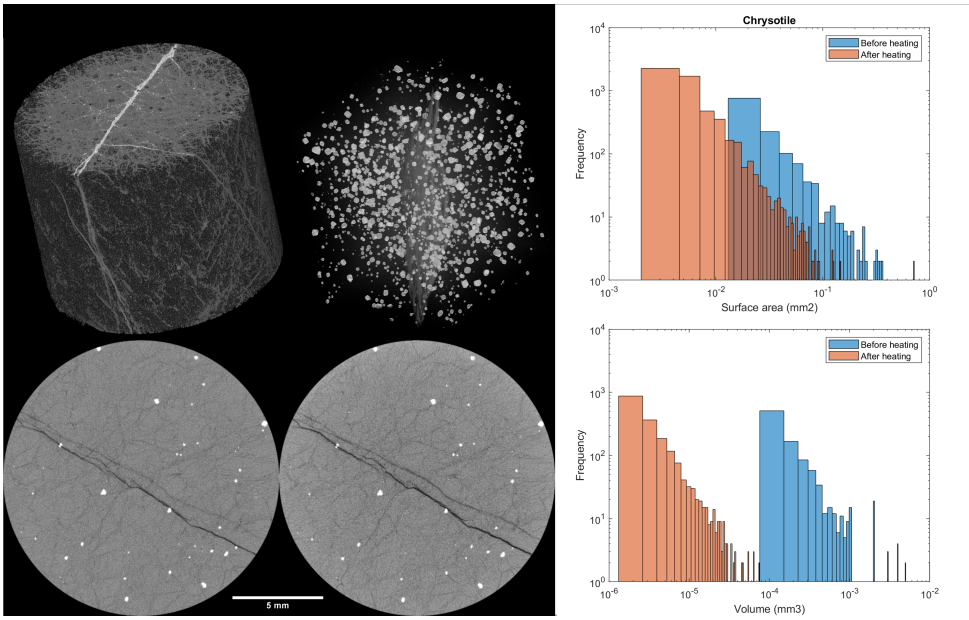

Figure 4.5: Results of dunite tomography. Top left: Representative volume studied. Top middle: Zincochromite and main serpentine vein. Bottom left: Slice of natural dunite. Bottom middle: same slice after heating treatment. Top right: Changes in chrysotile surface area before and after heating treatment. Bottom right: Changes in chrysotile volume before and after heating treatment.

According to equation 4.1, the chrysotile dark grey and black phases should be eliminated after heating, which was confirmed by the XRD results. Yet, these phases remain visible in Figure 4.5. This is because the serpentine phase was transformed into forsterite and amorphous silica. While forsterite is indistinguishable from the original olivine phase in the tomography, the silica has a density of 2.196 g/cm^3 [42] and fluid is just 1 g/cm^3. Which means the dark grey and black phases in the scans are actually the silica and fluid generated by the conversion of serpentine.

The serpentine conversion can be further inferred by the better contrast in the scan after heating (caused by the greater difference in phases density) and by the 20% decrease in dark grey phases followed by the same proportional increase in the bright grey phases. This is a volume indication of how much forsterite and silica were generated from the change in chrysotile. In accordance with the other tests, zincochromite was not affected by the heating of the sample, remaining at approximately 0.7% in volume. The summary of the segmentation results can be found in Table 4.2.

Besides total sample volume change, individual grains were investigated regarding their shift in surface area and volume. This is because the complex shape of the phases renders most geometrical measurements (i.e. diameter or bounding box) useless. Hence, only 3D information, such as the two measurements cited could be reliably compared. As zincochromite remained mostly unchanged after heating, the changes for

Table 4.2: Relative amount of phases for dunite and microgabbro as computed from CT segmentation

Phase	Density (g/cm^3)	Volume before heating (%)	Volume after heating (%)
Zincochromite	5.434 [34]	0.66	0.69
Olivine	3.287 [35]	86.44	88.77
Chrysotile	2.56 [36]	11.53	9.33
Augite	3.4 [37]	07.76	07.37
Pumpellyite	3.18 [38]		
Chamosite	3.13 [39]	31.98	29.27
Albite	2.4 [40]		
Analcime	2.3 [41]	60.26	63.36

chrysotile are displayed in Figure 4.5.

MICROGABBRO

The tomography of microgabbro only reveals three distinguishable phases (see Figure 4.6). Because the density of analcime and albite are very similar, these two phases cannot be readily differentiated based on the digital volume, these were simply segmented as the darkest phase. The bright gray phase is a combination of pumpellyite and chamosite, also not possible to discriminate. Finally the brighter phase in the slices is augite. The relative amounts and densities can be found in Table 4.2. The net transformation of pumpellyite, chamosite and analcime decreased volume of the bright gray phase by roughly 3%, which was increased in the dark grey phase. This can also be observed in differences in shape at the edges of individual grains on the tomography slices.

Analcime was indistinguishable from albite, thus, it could not be analysed. Augite was not affected by the heating treatment. However, the changes in pumpellyite and chamosite display a far larger shift in volume than in surface area (see Figure 4.6). As expected, the dehydration and dehydroxilation happened from the grain surface inward, which caused the decrease in surface area for the three phases studied (including both dunite and microgabbro). Since chrysotile has a finer and acicular habit, the surface area was affected to a greater extent than chamosite and pumpellyite for the same high temperature exposure. For the volume, much of the decrease was caused by the separation of particles, which were considered a single entity before heating, evident in all three phases. Moreover, the difference between the shift in volume and surface area was a good indication of the shape change of the particles.

4.3.5. COMPRESSIVE STRENGTH AND THERMAL DILATION

The results for compressive strength are displayed in Table 4.3. The studied dunite presented a compressive strength comparable with high performance concrete, which ensures the possibility for structural use. An increase of 77% in strength was observed after heating, pointing to a good durability for the selected application. Microgabbro compressive strength was found to be comparable with ultra-high performance concrete, however, a decrease of 14% was registered after heating. As the strength after this decrease remained superior to 160 MPa, such decrease was considered tolerable.

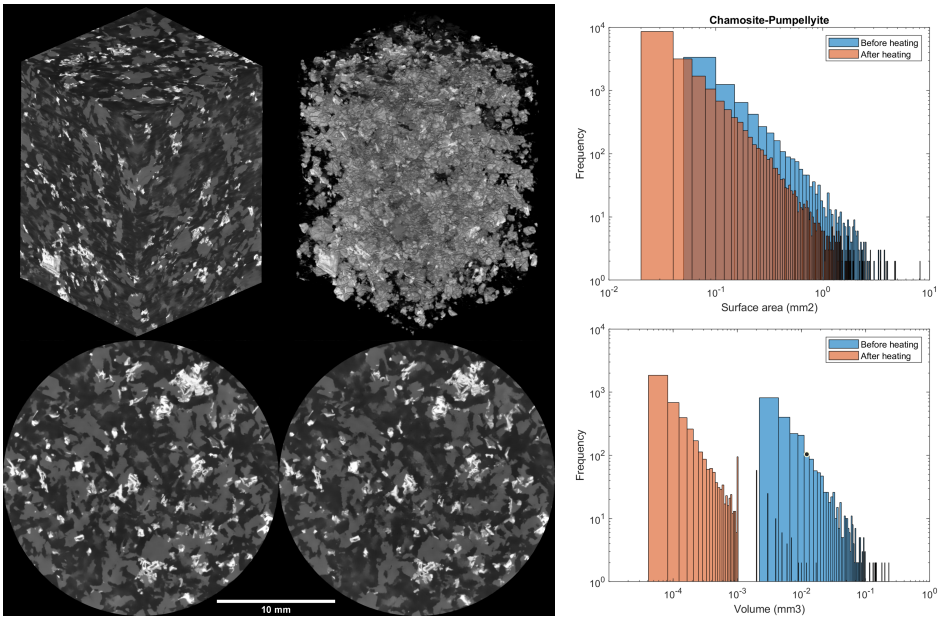

Figure 4.6: Results of microgabbro tomography. Top left: Representative volume studied. Top middle: Augite. Bottom left: Slice of natural microgabbro. Bottom middle: same slice after heating. Top right: Changes in chamosite-pumpellyite surface area before and after heating treatment. Bottom right: Changes in chamosite-pumpellyite volume before and after heating treatment.

Table 4.3: Compressive strength results for dunite and microgabbro.

Sample	Compressive strength (MPa)	Standard deviation (MPa)
Dunite	84	8.58
Dunite (heated)	149	22.46
Microgabbro	193	4.31
Microgabbro (heated)	166	2.96

Figure 4.7 shows the results for thermal dilation of the samples. Available results for normal strength [43] and high performance concrete [44] were added for comparison purposes. At temperatures beneath 100°C, all samples possess thermal strain similar to concrete, with the exception of pre-heated dunite, which presents very low dilation. Between 100°C and 500°C, natural microgabbro dilates more than an average concrete sample, while both pre-heated samples show a smaller dilation. Non-heated dunite shows a remarkably similar dilation. Above 500°C, concrete usually has a sharp increase in dilation and damage accumulation. Natural microgabbro follows the dilation increase, matching the concrete well. The other stones remain linear, displaying comparatively small expansion at high temperatures.

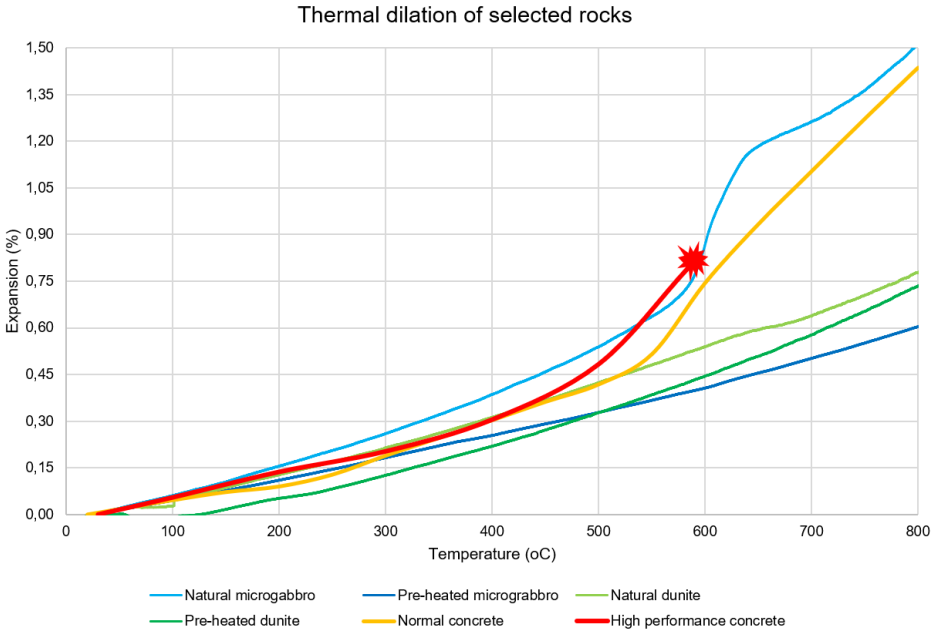

Figure 4.7: Thermal dilation of samples in natural and pre-heated state. Normal and high strength concrete dilation results are added for comparison.

Besides the increase in expansion, the difference between the expansions of non-heated and pre-heated dunite were almost linear, only diminishing at temperatures higher than 700°C. In contrast, while non-heated microgabbro presents the non-linear expansion with a sudden increase between 550°C and 650°C, the pre-heated stone presents a linear expansion with a lower rate of expansion than dunite at temperatures higher than 500°C.

4.3.6. DISCUSSION

In dunite samples, the conversion of chrysotile to forsterite and silica, as theorized in equation 4.1 and indicated in the XRD and TGA results, seem to improve both, mechanical and thermal properties of the stone. From a mechanical point of view, such results

were unexpected, as early studies showed the weakening of dunite by serpentine dehydration [45]. However, a more recent study [46] presents different conclusions, in which the absence of pore fluid (through evaporation) and even strain-hardening during distributed deformation makes the influence of serpentine on the strength ambiguous. Although the mentioned study used antigorite as a reference, similar behaviour can be expected from chrysotile. Furthermore, small amounts of antigorite were detected as seen in the optical microscopy results. Another possible contributing factor could be the filling of spaces with hematite, as observed in the previous section. Regardless of the cause, this increase in mechanical strength could be very useful for applications such as the one discussed in this and the next chapter.

Regarding the thermal dilation, both non-heated and pre-heated dunite show similar behaviour at low temperature. After 100^oC, non-heated dunite expands an average of 10% more than pre-heated dunite. This value is proportional to the amount of chrysotile in the sample, in fact, the value changes at temperatures higher than 640^oC, when chrysotile is known to start losing structural water [47]. Although the non-heated dunite thermal expansion becomes more similar to its pre-heated twin after such temperatures, the latter still displays lower expansion, due to its already reached mineral stability. This relatively stable and small thermal dilation over a range of temperatures is seen as an advantage for the use of the natural material without pre-treatment.

The small decrease in microgabbro ultimate compressive strength was likely due to the small increase in porosity in its microstructure introduced by the conversion of pumpellyite, chamosite and analcime into magnesium oxide and SiO_2 (as corroborated by the difference in particle volume shown in Figure 4.6).

Although the observations through optical microscopy and microtomography both displayed limited changes in microstructure, the change in the samples expansion caused by thermal loading was considerable. Unlike the dunite samples, the microgabbro samples presented a complex behaviour, in which the difference between the natural and the pre-heated samples starts as early as 50^oC and increases in a second degree rate up to 570^oC.

In line with the results of DTG and the findings of Caillére and Hénin [48] the steep increase in thermal expansion of the natural microgabbro between 570^oC and 640^oC was caused by the dehydroxylation of chamosite. Because of this temperature interval, it is also clear the chamosite is rich in Mg-hydroxy in its interlayer [48].

It seems clear that chamosite plays a dominant role in the thermal expansion behaviour of the studied microgabbro samples. As its full decomposition was not finished until temperatures of slightly above 800^oC [49], the performance observed in the pre-heated sample can only be expected after heating at 900^oC or above for a considerable amount of time.

4.4. MODELLING

Besides the experimental campaign, it was decided to perform a brief numerical analysis to better grasp the influence of the surface layer in the stresses caused to the substrate concrete by the temperature rise. A finite element software (COMSOL®5.3) was used to simulate the behaviour of a composite wall with a concrete substrate and a stone overlay exposed to hot spills. This analysis was performed to gain insight in the suitability of

Table 4.4: Properties for dunite and microgabbro used in FEA.

Property	Dunite	Microgabbro
Density (kg/m^3)*	3252	2799
Poisson ratio	0.27 [50]	0.21 [51]
Young's modulus (GPa)	165.82 [52]	91.55 [53]
Heat capacity (J/(kg·K))	965 [54]	980 [54]
Thermal conductivity (W/(m·K))	2.77 [55]	2.66 [56]
Coefficient of thermal expansion (1/K)*	As shown in Figure 4.7	As shown in Figure 4.7

*Measured experimentally

the pre-selected material as concrete overlay and the initial dimensions were estimated with knowledge of the case-study mentioned in Chapter 5. The simulated concrete wall had three meters in height, 10 meters in length and 50 cm in depth. The stone element was created with equal height and length, but only 10 cm deep. A spill in one quarter of the wall was designed to create a sudden thermal shock from ambient temperature up to 1000°C followed by the cooling of material based on previous research [9]. A representation of the geometry is in Figure 4.8.

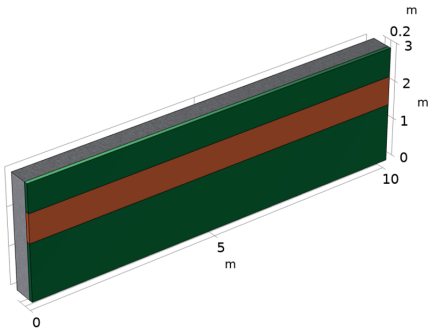

Figure 4.8: Geometry of the studied model. The concrete is represented in gray, the stone is represented in green and the region of the stone receiving the spillage of molten metal is represented in orange.

A 2D, triangular mesh with maximum element size of 3 cm was used for the FEM simulation, the elements were free to deform in the Z-direction. The wall was considered fixed in the bottom and in the back, while the top and the face with the protective stone were free. The fixed faces were also considered to have thermal insulation. This is roughly representative of a system found in a steel factory. The concrete material was considered porous while the rocks were set as solid materials. The temperature estimation was later used to couple the heat transfer and solid mechanics modules of the software for the calculation of stresses derived from the thermal expansion. While average concrete properties were used for such computations, the results of the stones analyses were fed as input. Additionally, a few properties of each stone were lacking for the model and were taken from previous researches available in literature as detailed in Table 4.4

Figure 4.9 shows the temperature development at the modeled concrete walls when

a 10 cm stone protection was used. Due to the stones capacity of energy absorption and the amount of molten material simulated, the temperature in the concrete wall layer can be kept below 100^oC, with the maximum temperature in the concrete occurring about 50 minutes after the exposure of the stone layers to the molten material. Figure 4.10 shows the stresses distribution on the cross-section of the simulated concrete walls at the 50 minutes time.

As the stresses in the concrete were derived from the rocks expansion, smaller coefficients of thermal dilation were clearly advantageous for the protection layer, even though dunite transfer more heat to the substrate. Because the concrete remains at relatively low temperatures (<200^oC), the pre-heated dunite material displays the least amount of principal stresses. In situations in which it is expected for the concrete to reach temperatures higher than 500^oC, a protection layer of stone could still secure a slower temperature increase (to avoid spalling). In this case, pre-heated microgabbro would likely perform better, given its lower thermal expansion at such temperatures. In both cases, the pre-heated material presents clear advantages against its natural counter-parts.

4.5. CONCLUSIONS

The present study proposed dunite and microgabbro as possible building materials to be used as a protective surface layer to concrete structures that are repeatedly exposed to high temperatures in industrial environments or otherwise. The main function of such surface layers would be to endure the thermal shock present in such environments and transfer the heat to the concrete at a much slower rate, reducing the risk of concrete spalling. To achieve this goals, the microstructure, mechanical properties and thermal performance of these minerals have been studied.

The main changes in dunite were caused by the dehydration of chrysotile, which provides improvements in both mechanical and thermal properties. The structural changes in microgabbro were more complex, involving the decomposition of analcime, pumpellyite and chamosite. The latter only becoming complete after 800^oC. While the ultimate compressive strength slightly decreases, its thermal expansion improves considerably after heating.

Both rocks were found to present befitting properties to their use as protection layer in industrial applications. Consequently, Chapter 5 includes the use of these rocks in test panels at a steel factory.

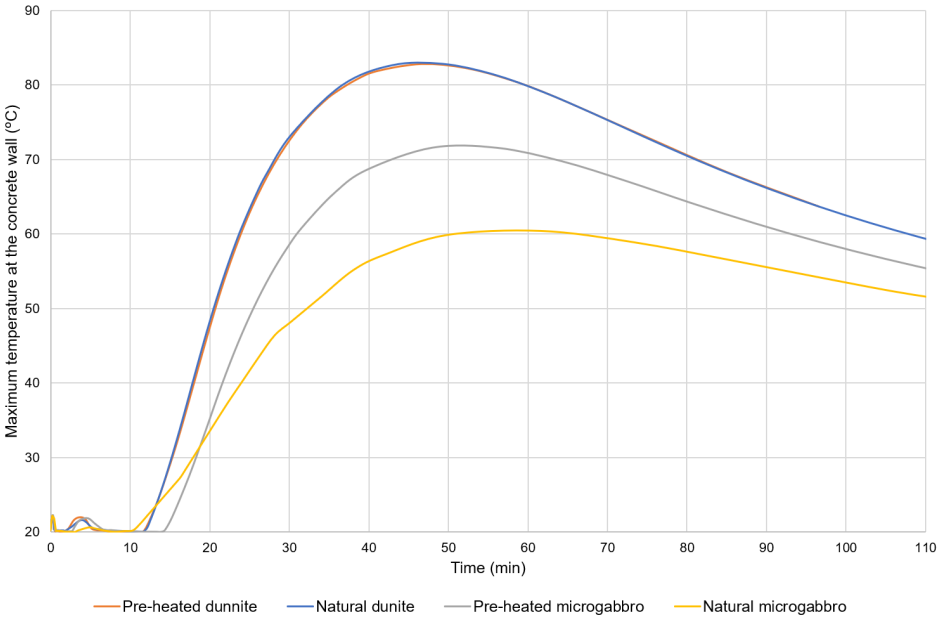

Figure 4.9: Maximum temperature reached in the concrete substrate during the heating of the surface stones.

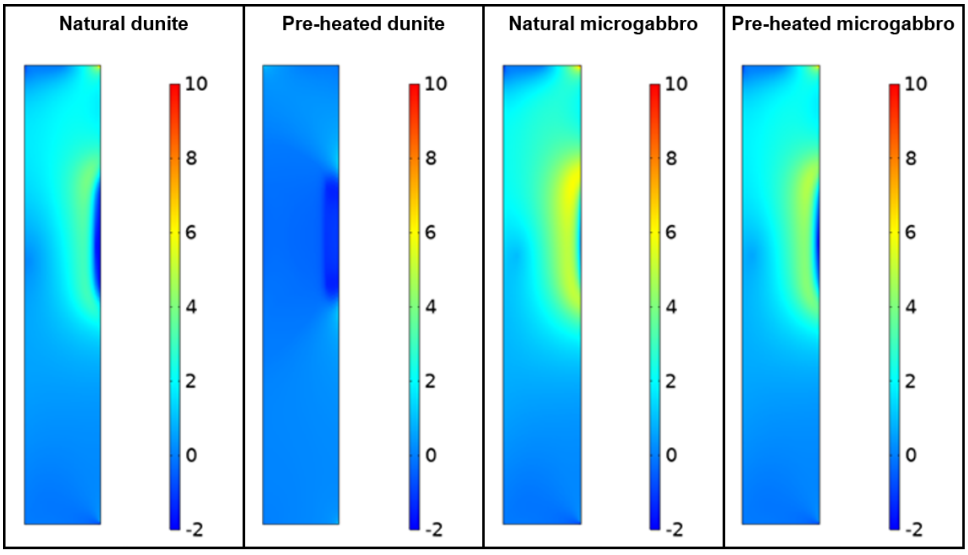

Figure 4.10: Principal stresses in simulated concrete walls at 50 minutes after hot spill exposure (scale in MPa).

BIBLIOGRAPHY

[1] Fernando França de Mendonça Filho et al. “Plutonic Rocks as Protection Layers to Concrete Exposed to Ultra-High Temperature”. In: *Materials* 15.10 (2022). ISSN: 1996-1944. DOI: 10.3390/ma15103490. URL: https://www.mdpi.com/1996-1944/15/10/3490.

[2] Marta Tobolczyk. “The World’s Oldest Temples in Göbekli Tepe and Nevali Çori, Turkey in the Light of Studies in Ontogenesis of Architecture”. In: *Procedia Engineering* 161 (2016). World Multidisciplinary Civil Engineering-Architecture-Urban Planning Symposium 2016, WMCAUS 2016, pp. 1398–1404. ISSN: 1877-7058. DOI: https://doi.org/10.1016/j.proeng.2016.08.600. URL: https://www.sciencedirect.com/science/article/pii/S1877705816328296.

[3] Bassim El Jazouli and Eleni Tsangouri. “Fire-exposed stones in constructions: Residual strength, performance loss and damage mode shift due to mineralogical transformation and micro-cracking”. In: *Engineering Geology* 302 (2022), p. 106638. ISSN: 0013-7952. DOI: https://doi.org/10.1016/j.enggeo.2022.106638. URL: https://www.sciencedirect.com/science/article/pii/S0013795222001235.

[4] Jie Zhao et al. “Numerical analysis of heating rate effect on spalling of high-performance concrete under high temperature conditions”. In: *Construction and Building Materials* 152 (2017), pp. 456–466. ISSN: 0950-0618. DOI: 10.1016/j.conbuildmat.2017.07.023. URL: http://dx.doi.org/10.1016/j.conbuildmat.2017.07.023.

[5] Gyeongcheol Choe et al. “Effect of moisture migration and water vapor pressure build-up with the heating rate on concrete spalling type”. In: *Cement and Concrete Research* 116.August 2017 (2019), pp. 1–10. ISSN: 00088846. DOI: 10.1016/j.cemconres.2018.10.021. URL: https://doi.org/10.1016/j.cemconres.2018.10.021.

[6] Ye Li et al. “Pore pressure build-up and explosive spalling in concrete at elevated temperature: A review”. In: *Construction and Building Materials* 284 (2021). ISSN: 09500618. DOI: 10.1016/j.conbuildmat.2021.122818.

[7] Ender Sarıfakıoğlu, H. Özen, and J. Winchester. “Whole Rock and Mineral Chemistry of Ultramafic-mafic Cumulates from the Orhaneli (Bursa) Ophiolite, NW Anatolia.” In: *Turkish Journal of Earth Sciences* 18 (Jan. 2009), pp. 55–83.

[8] Alastair H.F. Robertson and Osman Parlak. “Late Cretaceous-Palaeocene subduction-collision-exhumation of a microcontinent along the northern, active margin of the Southern Neotethys: Evidence from the Alanya Massif and the adjacent Antalya Complex (S Turkey)”. In: *Journal of Asian Earth Sciences* 201 (2020), p. 104467. ISSN: 1367-9120. DOI: https://doi.org/10.1016/j.jseaes.2020.104467. URL: https://www.sciencedirect.com/science/article/pii/S1367912020302601.

[9] F.F. Mendonça Filho et al. “Surface effects of molten slag spills on calcium aluminate cement paste”. In: *Materials Design* 217 (2022), p. 110623. ISSN: 0264-1275. DOI: https://doi.org/10.1016/j.matdes.2022.110623. URL: https://www.sciencedirect.com/science/article/pii/S0264127522002441.

[10] Karen Scrivener, Ruben Snellings, and Barbara Lothenbach. *A Practical Guide to Microstructural Analysis of Cementitious Materials*. 1st ed. Vol. 1. CRC Pressg, 2017.

[11] A.B. Poole and I. Sims. *Concrete Petrography: A Handbook of Investigative Techniques, Second Edition*. CRC Press, 2016. ISBN: 9781466583825. URL: https://books.google.nl/books?id=uM4dCgAAQBAJ.

[12] C. Romero Rodríguez et al. “Fundamental investigation on the frost resistance of mortar with microencapsulated phase change materials”. In: *Cement and Concrete Composites* 113 (2020), p. 103705. ISSN: 0958-9465. DOI: https://doi.org/10.1016/j.cemconcomp.2020.103705. URL: https://www.sciencedirect.com/science/article/pii/S0958946520302122.

[13] J. Schindelin et al. “Fiji: An open-source platform for biological-image analysis”. In: *Nature Methods* 9.7 (2012), pp. 676–682. DOI: https://doi.org/10.1038/nmeth.2019.

[14] Jerome Darbon et al. “Fast nonlocal filtering applied to electron cryomicroscopy”. In: *5th IEEE International Symposium on Biomedical Imaging: From Nano to Macro, Proceedings, ISBI* (May 2008), pp. 1331–1334. DOI: 10.1109/ISBI.2008.4541250.

[15] Ignacio Arganda-Carreras et al. “Trainable Weka Segmentation: a machine learning tool for microscopy pixel classification”. In: *Bioinformatics* 33.15 (Mar. 2017), pp. 2424–2426. ISSN: 1367-4803. DOI: 10.1093/bioinformatics/btx180. eprint: https://academic.oup.com/bioinformatics/article-pdf/33/15/2424/25157856/btx180.pdf. URL: https://doi.org/10.1093/bioinformatics/btx180.

[16] S. Bolte and F. P. Cordelieres. “A guided tour into subcellular colocalization analysis in light microscopy”. In: *Journal of Microscopy* 224.3 (2006), pp. 213–232. DOI: https://doi.org/10.1111/j.1365-2818.2006.01706.x. eprint: https://onlinelibrary.wiley.com/doi/pdf/10.1111/j.1365-2818.2006.01706.x. URL: https://onlinelibrary.wiley.com/doi/abs/10.1111/j.1365-2818.2006.01706.x.

[17] *NEN-EN 1926:2007 – Natural stone test methods – Determination of uniaxial compressive strength*. Standard. Delft, NL: Nederlands Normalisatie-instituut, Jan. 2007.

[18] N. G. Holm et al. "Serpentinization and the Formation of H2 and CH4 on Celestial Bodies (Planets, Moons, Comets)". In: *Astrobiology* 15.7 (2015), pp. 587–600. DOI: https://doi.org/10.1089/ast.2014.1188.

[19] Hector M. Lamadrid et al. "Effect of water activity on rates of serpentinization of olivine". In: *Nature Communications* 8.1 (2017), pp. 1–9. ISSN: 2041-1723. DOI: 10.1038/ncomms16107. URL: https://doi.org/10.1038/ncomms16107.

[20] G. W. Brindley. "Kinetics and Mechanisms of Dehydration and Recrystallization of Serpentine—I". In: *Clays and Clay Minerals* 12.1 (2017), pp. 35–47. ISSN: 1552-8367. DOI: 10.1346/CCMN.1963.0120107. URL: https://doi.org/10.1346/CCMN.1963.0120107.

[21] Giuseppe Cruciani and Alessandro Gualtieri. "Dehydration dynamics of analcime by in situ synchrotron powder diffraction". In: *American Mineralogist* 84.1-2 (Feb. 1999), pp. 112–119. ISSN: 0003-004X. DOI: 10.2138/am-1999-1-212. eprint: https://pubs.geoscienceworld.org/ammin/article-pdf/84/1-2/112/4007830/amin_84_1-2_112.pdf. URL: https://doi.org/10.2138/am-1999-1-212.

[22] Hans-Joachim Massonne and Arne P. Willner. "Phase relations and dehydration behaviour of psammopelite and mid-ocean ridge basalt at very-low-grade to low-grade metamorphic conditions". In: *European Journal of Mineralogy* 20.5 (Oct. 2008), pp. 867–879. DOI: 10.1127/0935-1221/2008/0020-1871. URL: https://doi.org/10.1127/0935-1221/2008/0020-1871.

[23] Annett Steudel et al. "Thermal behavior of chlorites of the clinochlore-chamosite solid solution series: Oxidation of structural iron, hydrogen release and dehydroxylation". In: *Applied Clay Science* 132-133 (2016), pp. 626–634. ISSN: 0169-1317. DOI: https://doi.org/10.1016/j.clay.2016.08.013. URL: http://www.sciencedirect.com/science/article/pii/S0169131716303386.

[24] Romain Lafay et al. "Mineral replacement rate of olivine by chrysotile and brucite under high alkaline conditions". In: *Journal of Crystal Growth* 347.1 (2012), pp. 62–72. ISSN: 0022-0248. DOI: https://doi.org/10.1016/j.jcrysgro.2012.02.040. URL: http://www.sciencedirect.com/science/article/pii/S0022024812001820.

[25] Eva Kuzielová et al. "Influence of hydrothermal treatment parameters on the phase composition of zeolites". In: *Journal of Thermal Analysis and Calorimetry* 1.142 (2020), pp. 37–50. DOI: 10.1007/s10973-020-09784-8. URL: https://doi.org/10.1007/s10973-020-09784-8.

[26] Ciriaco Giampaolo and Gianni Lombardi. "Thermal behaviour of analcimes from two different genetic environments". In: *European Journal of Mineralogy* 6.2 (Mar. 1994), pp. 285–290. DOI: 10.1127/ejm/6/2/0285. URL: http://dx.doi.org/10.1127/ejm/6/2/0285.

[27] M. Földvári. *Handbook of Thermogravimetric System of Minerals and Its Use in Geological Practice*. Magyar Állami Földtani Intézet alkalmi kiadványa. Geological Institute of Hungary, 2011. ISBN: 9789636712884. URL: https://books.google.nl/books?id=xpxeMwEACAAJ.

[28] W.S. MacKenzie, C.H. Donaldson, and C. Guilford. *Atlas of Igneous Rocks and Their Textures*. Longman, 1982. ISBN: 9780470273395. URL: https://books.google.nl/books?id=-itMyAR%5C_%5C_jEC.

[29] W.S. MacKenzie, W.S. MacKenzie, and C. Guilford. *Atlas of Rock-Forming Minerals in Thin Section*. A Halsted Press book. Wiley, 1980. ISBN: 9780470269213. URL: https://books.google.nl/books?id=ikgSAQAAIAAJ.

[30] Françoise Boudier, Alain Baronnet, and David Mainprice. "Serpentine Mineral Replacements of Natural Olivine and their Seismic Implications: Oceanic Lizardite versus Subduction-Related Antigorite". In: *Journal of Petrology* 51.1-2 (Aug. 2009), pp. 495–512. ISSN: 0022-3530. DOI: 10.1093/petrology/egp049. eprint: https://academic.oup.com/petrology/article-pdf/51/1-2/495/16670954/egp049.pdf. URL: https://doi.org/10.1093/petrology/egp049.

[31] V. A. Bron, I. A. Stepanova, and T. N. Kudryavtseva. "Effect of degree of serpentine formation in dunite on its properties and structure change during heating". In: *Refractories* 8.9-10 (1967), pp. 553–558. ISSN: 15739139. DOI: 10.1007/BF01288402.

[32] Antoni Camprubí and Carles Canet. "Berthierine and chamosite hydrothermal: Genetic guides in the Peña Colorada magnetite-bearing ore deposit, Mexico". In: *Earth, Planets and Space* 61.2 (2009), pp. 291–295. ISSN: 18805981. DOI: 10.1186/BF03352910.

[33] Anne Jordan Brackmann Thompson et al. *Atlas of Alteration: A Field and Petrographic Guide to Hydrothermal Alteration Minerals*. Geological Association of Canada, Mineral Deposits Division, Special Publication, 6. Geological Association of Canada, Mineral Deposits Division, 1996. ISBN: 9780919216594. URL: https://books.google.nl/books?id=49tPAQAAIAAJ.

[34] John L. Jambor et al. "New Mineral Names". In: *American Mineralogist* 73.8 (1988), pp. 927–935. ISSN: 0003-004X.

[35] W.A. Deer, R.A. Howie, and J. Zussman. *Rock-Forming Minerals: Orthosilicates, Volume 1A*. Rock-forming minerals. Geological Society, 1982. ISBN: 9781897799888. URL: https://books.google.nl/books?id=uwsIAYz7-QIC.

[36] "PubChem Compound Summary for CID 25477, Chrysotile". In: *National Center for Biotechnology Information* (2020). URL: https://pubchem.ncbi.nlm.nih.gov/compound/Chrysotile.

[37] G. Faure and T.M. Mensing. *Introduction to Planetary Science: The Geological Perspective*. Springer Netherlands, 2007. ISBN: 9781402055447. URL: https://books.google.nl/books?id=U4FZp6f6q6MC.

[38] W. Schumann. *Gemstones of the World*. Gemstones of the World. Sterling, 2009. ISBN: 9781402768293. URL: https://books.google.nl/books?id=V9PqVxpxeiEC.

[39] B. Sadler. *Light Metals 2013*. The Minerals, Metals & Materials Series. Springer International Publishing, 2017. ISBN: 9783319651361. URL: https://books.google.nl/books?id=ydIxDwAAQBAJ.

[40] M.H. Manghnani and S.I. Akimoto. *High-Pressure Research: Applications in Geophysics*. Elsevier Science, 2017. ISBN: 9781483260532. URL: https://books.google.nl/books?id=PMk3BQAAQBAJ.

[41] W.L. Pohl. *Economic Geology: Principles and Practice*. Wiley, 2011. ISBN: 9781444394863. URL: https://books.google.nl/books?id=f5vPAwAAQBAJ.

[42] W.M. Haynes. *CRC Handbook of Chemistry and Physics*. CRC Press, 2016. ISBN: 9781498754293. URL: https://books.google.nl/books?id=VVezDAAAQBAJ.

[43] Tayfun Uygunoğlu and İlker Bekir Topçu. "Thermal expansion of self-consolidating normal and lightweight aggregate concrete at elevated temperature". In: *Construction and Building Materials* 23.9 (2009), pp. 3063–3069. ISSN: 0950-0618. DOI: https://doi.org/10.1016/j.conbuildmat.2009.04.004. URL: http://www.sciencedirect.com/science/article/pii/S0950061809001159.

[44] I. Hager. "Behaviour of cement concrete at high temperature". In: *Bulletin of the Polish Academy of Sciences: Technical Sciences* 61.No 1 (2013), pp. 145–154. DOI: 10.2478/bpasts-2013-0013.

[45] Robert E. Riecker and Thomas P. Rooney. "Weakening of Dunite by Serpentine Dehydration". In: *Science* 152.3719 (1966), pp. 196–198. DOI: 10.1126/science.152.3719.196. eprint: https://www.science.org/doi/pdf/10.1126/science.152.3719.196. URL: https://www.science.org/doi/abs/10.1126/science.152.3719.196.

[46] Melodie E French, Greg Hirth, and Keishi Okazaki. "Fracture-induced pore fluid pressure weakening and dehydration of serpentinite". In: *Tectonophysics* 767 (2019), p. 228168. ISSN: 0040-1951. DOI: https://doi.org/10.1016/j.tecto.2019.228168. URL: https://www.sciencedirect.com/science/article/pii/S0040195119302756.

[47] A.K. Datta et al. "Dehydration and phase transformation in chrysotile asbestos—A radial distribution analysis study". In: *Bulletin of Materials Science* 9 (1987), pp. 103–110. URL: https://opsias.ias.ac.in/article/fulltext/boms/009/02/0103-0110.

[48] S. Caillére and S. Hénin. "Relation entre la constitution cristallochimique des phyllites et leur temperature de deshydratation application au cas des chlorites". In: *Bulletin de la Société française de céramique* 48 (1960), pp. 63–67.

[49] J. Kloprogge and R. Frost. "Thermal decomposition of Ferrian chamosite: an infrared emission spectroscopic study". In: *Contributions to Mineralogy and Petrology* 138 (2000), pp. 59–67. DOI: https://doi.org/10.1007/PL00007663.

[50] W. F. Brace. “ELASTICITY AND RIGIDITY OF ROCKElasticity and rigidity of rock”. In: *Structural Geology and Tectonics*. Berlin, Heidelberg: Springer Berlin Heidelberg, 1987, pp. 208–213. ISBN: 978-3-540-31080-8. DOI: 10.1007/3-540-31080-0_35. URL: https://doi.org/10.1007/3-540-31080-0_35.

[51] L.S. Blake. *Civil Engineer's Reference Book*. Elsevier Science, 2013. ISBN: 9781483102337. URL: https://books.google.nl/books?id=pM%5C_8BAAAQBAJ.

[52] Nikolas I. Christensen. “Elasticity of ultrabasic rocks”. In: *Journal of Geophysical Research (1896-1977)* 71.24 (1966), pp. 5921–5931. DOI: https://doi.org/10.1029/JZ071i024p05921. eprint: https://agupubs.onlinelibrary.wiley.com/doi/pdf/10.1029/JZ071i024p05921. URL: https://agupubs.onlinelibrary.wiley.com/doi/abs/10.1029/JZ071i024p05921.

[53] Petrov, Y. et al. “Structural-temporal approach for dynamic strength characterization of gabbro-diabase”. In: *EPJ Web of Conferences* 94 (2015), p. 01042. DOI: 10.1051/epjconf/20159401042. URL: https://doi.org/10.1051/epjconf/20159401042.

[54] Shahrzad Roshankhah. “Physical properties of geomaterials with relevance to thermal energy geo-systems”. PhD thesis. Georgia Institute of Technology, 2015.

[55] Aurangzeb, S. Mehmood, and A. Maqsood. “Modeling of Effective Thermal Conductivity of Dunite Rocks as a Function of Temperature”. In: *International Journal of Thermophysics* 29 (2008), pp. 1470–1479. DOI: https://doi.org/10.1007/s10765-008-0500-3.

[56] Sayyadul Arafin and Ram Singh. “Thermal and Transport Properties of Mafic and Ultramafic Rocks of Oman Ophiolite”. In: *Sultan Qaboos University Journal for Science [SQUJS]* 21 (Nov. 2016), p. 69. DOI: 10.24200/squjs.vol21iss1pp69-81.

5

CONCRETE EXPOSED TO MOLTEN STEEL AND SLAG: A CASE STUDY

All fine and simple in principle.
The details very complicated, of course.

Neal Stephenson, Fall; or, Dodge in Hell

Nothing is so painful to the human
mind as a great and sudden change.

Mary Shelley, Frankenstein

This chapter describes a case study in which a factory has continuous loss of protection concrete at a specific location and the solution currently used is compared with a couple of alternative strategies using special materials. Namely, the use of monolithic CAC based concrete and a stone-concrete hybrid have been proposed following the conclusions of Chapters 3 and 4. The design and manufacturing of test panels have been described in details. These panels have been monitored for a year and remained sound with very few loss of cross section. In comparison with the solution previously used at the location of the tests, the proposed material demonstrated superior durability. The chapter is concluded with a cost analysis to change the repair procedure, which showed the solution tested to be very attractive.

Parts of this chapter are being considered for publication in Case Studies in Construction Materials.

5.1. SITUATION

THE steel factory in which the case-study was considered had a large budget allocated for the repair of walls located in a concrete pit, beneath each of the three steel converters in the factory. Due to the confidentiality of the exact layout and equipment, it is not possible to share the technical drawings. A sketch is offered in Figure 5.1. On top of the mentioned walls are rails for the transport of a ladle that receives the molten steel, then excess slag is disposed in the pit. This process occurs about 20 times a day in each converter and spills are frequent.

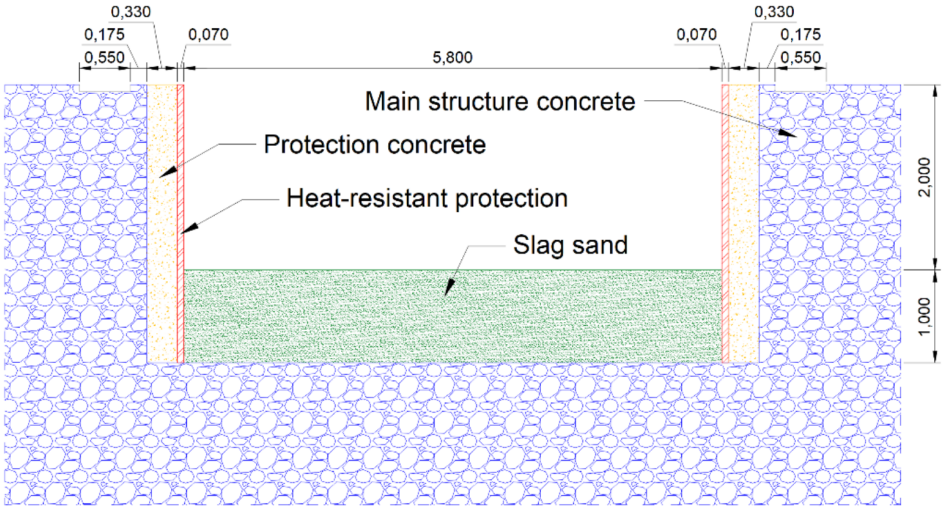

Figure 5.1: Sketch of the geometry of the cross-section of the studied area, units in m.

5.1.1. PROBLEM STATEMENT

The pit is made of Portland cement (PC) based reinforced concrete and a layer of refractory material applied to the top of the concrete. The refractory layer is usually detached relatively quickly and due to the inefficiency of PC against high temperature [1–5], the walls of the pit are constantly damaged. Because the operation of the converters is vital to the production of steel in the factory, these can only stop for repairs twice a year. The planned stops are the only moment in which the walls can be repaired and only few hours are available for this service. Often the repaired concrete is in service two or three day after casting, with no time for curing.

This is an issue for the factory operation for two reasons. The first reason is that damage is not limited to the protection concrete showed in Figure 5.1. It often reaches the main structure concrete and hinders the safe transport of the ladles to receive the molten steel. Further, constant repair of the walls is a financial burden.

5.1.2. LOADING CASES

A small investigation campaign, comprised of employee interviews, gathering of data and review of old inspection reports was conducted at the start of the project to determine the different phases of operation that could cause damage to the material in the studied location. The main causes of damage were divided into three categories:

HIGH TEMPERATURE SPILLAGE

During the blowing of oxygen in the iron inside the converters, a certain amount of slag pours over the converters. Later, while pouring the metal to the ladle, it also occurs to pour it on the walls. In both instances, the spill is at a temperature higher than 1500°C. On average, five tons of slag are spilled per cycle. This slag is different from the one used in Chapters 3 and 4, being mainly composed of iron.

IMPACT FROM BULLDOZER

As slag accumulates on the bottom of the pit, a bulldozer is remotely operated to collect this material. The operator has only a partial line of sight to the bulldozer and often hammers it against the walls attempting to collect more slag. This operation is time sensitive and the operator often prioritizes the expediency of the bulldozer.

IMPACT FROM FALLING DEBRIS

During the loading of the converters with scrap metal, some pieces fall between the converters and the opening in the 25 meters level. Such pieces are often small, but can also be as large as a cubic meter, weighting several tonnes, hitting the walls from a 20 meters drop.

5.1.3. DEVELOPMENT OF PROTECTION STRATEGY

At the start of the project, many possibilities were discussed for the protection of the walls at the pits and most time was spent with preliminary modelling of the option shown in Figure 5.2. As the investigation of damage causes proceeded, it became clear that load cases of mechanical impacts should also be considered and the design was shifted accordingly.

The main challenge for the design of a protection material was the incompatibility of the load cases. Thermal shock events can weaken the material through the differential dilation of the paste and aggregates [6], the loss of chemically bound water [7], the formation of cracks due the temperature gradients [8] and occurence of spalling [9]. Mixes with lower water-binder ratio and lower porosity are often more sensitive to thermal shock, and fail more violently [10]. Impact loads can also cause the spalling of concrete, but caused by different phenomena. Namely, the high speed nature of the loading doesn't allow for the proper energy dissipation between the paste and aggregates [11]. Usually, high performance concretes, with very high compressive strength and Young's modulus resist better against this type of damage [12]. However, such materials have very low water-binder ratio and porosity [13].

Additionally, both load cases are difficult to reproduce in small scale. Most thermal shock experiments are tested in laboratory through the heating of the material in an oven, which does not accurately reproduce the effects of a hot spill on concrete (see

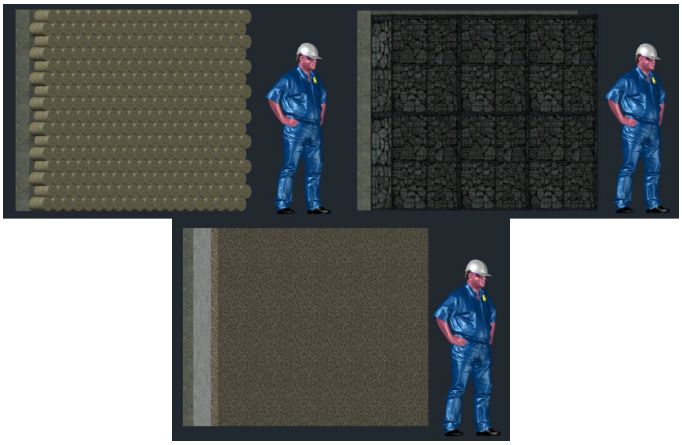

Figure 5.2: Possible thermal load protections to be applied at the location. Left: Stacked cylinders of refractory stone; Right: Gabion wall of refractory stone; Bottom: Protection composed of one layer of calcium aluminate cement concrete and one layer of refractory stone.

Chapter 3). Impact loads also suffer from size effect. The most common setup uses a split-hopkinson pressure bar, which often limits samples to the millimeter scale [14].

For these reasons, it was planned to test large scale concrete panels in-situ. The size and geometry of such elements was mostly determined by the company requirements. Initially, it was envisioned to test a series of 1 x 1 m elements. However, the company requested the elements to be 2 x 1 m for ease of installation and that the 40 cm depth was respected to keep the profile of the wall. Further, because of the uniqueness of the opportunity, it was suggested to test four elements, two of monolithic calcium aluminate cement (CAC) based concrete and two combining CAC concrete and refractory stones.(Figure 5.3). To control the production, such elements were to be produced at TU Delft facilities and then transported to the steel factory for attachment through a single steel rod. Some preliminary 2D heat dissipation simulations were performed with COMSOL®to validate the requested protection geometry. Figure 5.4 shows the results of such simulations, so an approximate estimation of the heat transfer to the structural concrete through protection layer could be performed.

5.2. TEST PANELS DESIGN & PRODUCTION

5.2.1. MATERIALS SELECTION & MIX DESIGN

The panels were produced using the calcium aluminate cement Refro50 from Çimsa (composition shown in Chapter 3). As a mineral addition, Elkem Microsilica®920E was used. To avoid spalling, polypropylene Fibremesh®150 was added. These fibers had 12 mm length and 31 μm diameter. MasterGlenium®51 was added to control fluidity.

For the panels using stone blocks, the materials for these were plutonic rocks with high refractory and mechanical properties. Half of the blocks were composed of dunite mined from Orhaneli, Bursa, Turkey; and the other half of microgabbro, from Alanya, Turkey. The characterization of these rocks and their compatibility with concrete sub-

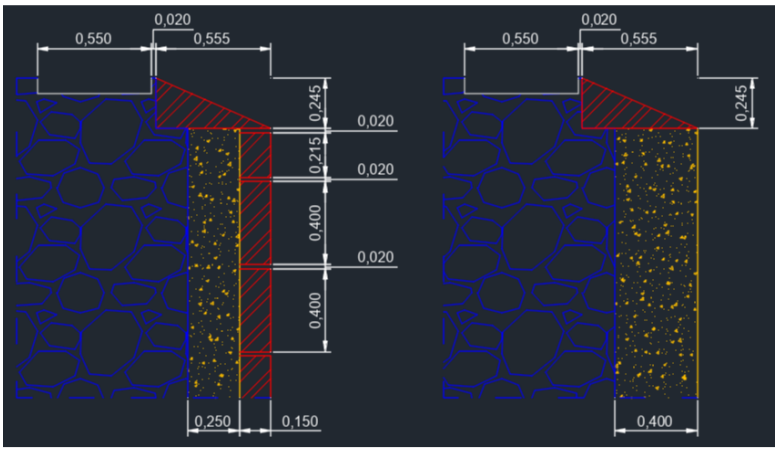

Figure 5.3: Initial conception of protection elements. Blue: Structural concrete; Yellow: CAC based concrete; Red: Refractory stone. Units in mm.

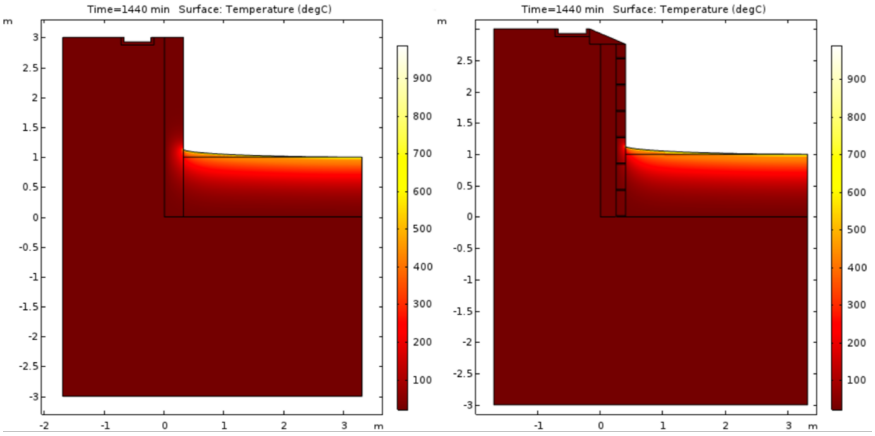

Figure 5.4: Preliminary simulations of heat dissipation capacity of requested geometry for protection elements.

jected to high temperature is present in Chapter 4.

For the aggregates, it was originally envisioned to use crushed dunite or microgabbro as sand. Because of the reinforcement density, the elements used only fine aggregate. However, it was found that the crushing of these rocks was very time-consuming and as these materials are not commercially available in this format, this solution would become costly and therefore undesirable. For this reason, it was decided to use crushed olivine sand as a good heat resisting fine aggregate. This can be purchased in bulk quantities in the Netherlands, with a $D_{\max} = 3\ mm$.

All panels used the same mix design, shown in Table 5.1.

Table 5.1: Mixture proportions the test panels, values for 1 m^3 of concrete.

C (kg)	SF (kg)	W (kg)	A (kg)	SP (kg)	PP (kg)	PPI* (-)
510	76.5	204	1530	8.67	1.35	523

C = cement, SF = silica fume, W = water, A = aggregates, SP = superplasticizer, PP = polypropylene fibres, PPI = polypropylene index.

* Calculated according to Li et al (2021) [15], this measure is discussed in Chapter 6.

5.2.2. CASTING & INSTALLATION

The monolithic panels were cast one week apart. Afterwards, the stone blocks were drilled following the specifications of Figure A.4. These were, then, placed in the bottom of the moulds with the steel pins and profiles connecting them. Styrofoam was placed between the gaps of each stone to avoid concrete from leaking during casting (see Figure 5.5). Afterwards, reinforcement was positioned with 30 mm spacers and finally the steel anchors were grouted in the open face of the stones. Because this operation required relatively precise production, there was an interval of two months between the casting of the two first panels and the two remaining ones. The concrete-stone hybrid panels were also cast one week apart from each other. All panels had the amount of superplasticizer adjusted during casting. Afterwards, the panels were kept sealed with a plastic sheet for three days. At the fourth day the panels were unsealed and the mould was removed.

During casting of the panels, the fresh mix was used for the determination of air content following the standard NEN-EN 12350-7 [16]. In addition, 12 cubes of 40 mm sides were produced using the concrete of each panel. These cubes were stored near the panels and used for testing compressive strength at the ages of 7 and 28 days. The tests were carried at a fixed loading rate of 13.5 kN/s using a a servo-hydraulic mechanical press with maximum load capacity of 5000 kN and high stability from Matest, following NEN-EN 12390-3:2019 [17]. The results for these tests are found in Table 5.2, the naming for the panels follows Figure A.3. The compressive strength of the stones was reported in Table 4.3.

One week after the casting of the final panel, all panels were hoisted at TU Delft (see Figure 5.6 and sent to the factory for installation. As expected by the calculations, there was no damage to the panels during any hoisting and movement operation and the panels arrived at the site intact. At the factory, a thin sheet of mineral wool was placed as thermal insulation between the walls and the panels. Panels 1 and 2 were placed ten



Figure 5.5: Hybrid panel being prepared for casting.

Table 5.2: Air content and compressive strength of the concrete in each panel.

		Compressive strength (MPa)	
Panel	Air content (%)	7 days	28 days
1	1.5	63.38	74.97
2	3.0	56.87	72.44
3	1.7	79.89	86.82
4	2.4	72.62	91.63

meters apart on the north wall, while panels 3 and 4 were placed facing panels 1 and 2, also ten meters apart in the south wall. The walls are six meters apart. Beside the panels, the structure of the factory was protected with the usual projected PC based concrete. The locations mentioned for the panels were predicted by the company employees as critical zones, usually presenting the highest amount of damage.



Figure 5.6: Panels being hoisted at TU Delft. Left: Panel 1. Right: Panel 4.

5.3. MONITORING AND EVALUATION OF DAMAGE

5.3.1. INSPECTIONS AND TESTS

Once the panels were installed, no further access was possible until factory operation ceased again. The plan was to evaluate the performance of the test panels against the concrete walls the factory had been using. This comparison was to be performed through three parameters:

1. Depth of protection loss: As all protections to the structure were composed of 40 cm elements, the comparative rate at which the protection thickness decrease could give a good estimation of repair needs.

2. Ultrasonic pulse velocity (UPV): Because the thermal and impact damage create a large number of cracks and voids in the internal microstructure, the propagation of mechanical waves could be used as benchmark for progressive damage.

3. Core extraction for laboratory analysis: The extraction of cores could allow for direct observation of the microstructure.

Over a period of one year, only two visits were possible due to safety protocols. Each visit had an allocated time of two hours for inspection and selection of core drilling locations. The first inspection was executed after 6 months of factory operation, and consisted of visual appreciation, ultrasound and selection of one core per panel. The UPV was determined in accordance to ISO 1920-7 [18]. However, reliable results were only found for panels 1 to 3 and north wall, the surface of panel 4 and south wall were too rough for the measurements.

Afterwards, the panels and walls were marked so each would have 50 mm diameter cores extracted for laboratory analysis. The cores were extracted 8 hours after the first inspection and immediately sealed in plastic bags. At TU Delft, petrographic thin sections for optical microscopy were produced from the cores. In particular, the very top of each core was used, as it contained the portion of material reacting with the falling molten slag and iron.

In order to produce thin sections, the cores were cut in half and the top 50 mm were carefully ground with a semi-automatic thin sectioning machine, with three diamonds rollers of 64, 46 and 16 μm. This process continued until measurements with an electronic drop indicator yielded a thickness of about 20 μm material and about 10 μm mounting glue. This followed the procedure described in Poole and Sims (2016)[19].

The thin sections were analyzed through a Leica DM2500P optical microscope equiped with linear and circular polarization filters. Lenses of magnification and numerical aperture equivalent to 2.5/0.07,10/0.22 and 20/0.4 respectively, were available. Plain polarized light (PPL) and cross polarized light (XPL) were used. The camera used to acquire the micrographs was a Leica DFC310FX digital camera, with a 1392x1040 resolution. Proprietary software was used for the image acquisition.

The other half of the cores were used to produce polished samples, these were approximately 10 x 30 x 45 mm and had their surface impregnated under vacuum with epoxy resin containing an fluorescent dye. The impregnated specimen surfaces were ground using SiC grinding papers with increasing mesh number from #320 up to #1200 in order to achieve a flat surface.

The polished sections were analyzed under UV light using the same equipment described for the thin sections. Eight micrographs were recorded for each polished section under the same illumination conditions and at 10 times magnification. The freeware Fiji image analysis [20] was used for determining the mean pixel brightness at each image and the values were then averaged for each sample.

The second inspection was executed after one year of factory operation. Unfortunately, this visit was interrupted after 40 minutes due to logistic issues of the factory. The unforeseen small duration of the second inspection, made impossible to collect UPV measurements and cores. Thus, only photographic documentation and damage depth measurements could be performed. Figure 5.7 gives a sketch of the panels location. The center is where the converter is suspended and the red dots show the locations where cores were extracted for later production of thin-sections.

5.3.2. ON-SITE EVALUATION

Table 5.3 summarizes the deterioration in both, panels and walls, after 6 months of factory operation. The 7 cm refractory layer applied to usual repair concrete was completely

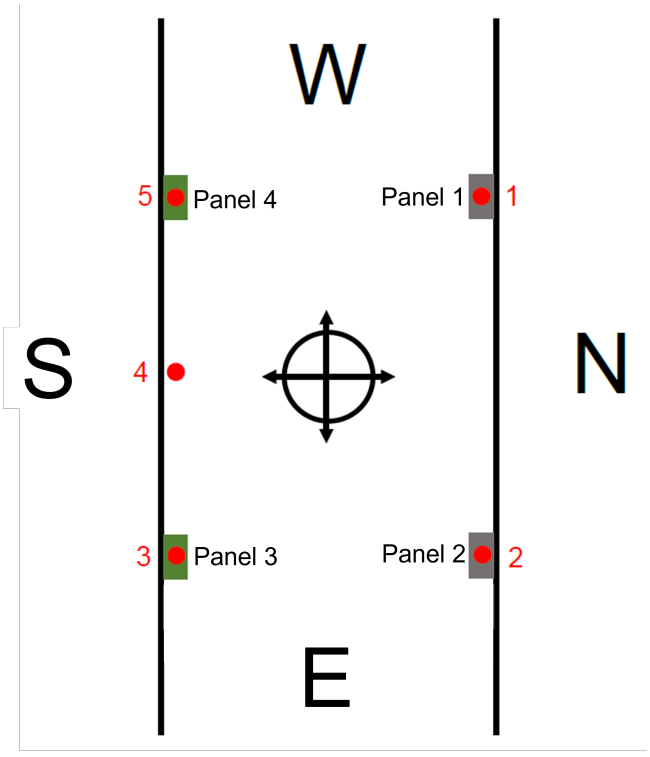

Figure 5.7: Sketch of location of panels and collected cores.

removed at the time of the first inspection. Overall depth of protection loss was present in both north and south walls. Additionally, the upper rocks in panel 4 broke, losing about half their depth. The other three panels had no overall damage, only local deterioration.

Table 5.3: Accumulated damage in panels and walls after 6 months of factory operation.

Element	Overall damage depth (cm)	Damage depth at worst location (cm)
Panel 1	0	3
Panel 2	0	5
Panel 3	0	10
Panel 4	8	15
North wall	15	40
South wall	12	40

The damage at worst location for panels 1 and 2 were very minor, amounting to only 7.5% and 12.5% of their respective total depth. Figure 5.8 shows the panels during the first inspection. The damage in panel 1 seemed to be caused by a single vertical impact. Panel 2 also seemed to present damage only at the top. In a similar fashion, the biggest damage in panel 3 was in the top stone blocks, with the bottom blocks intact. However, panel 4 showed an overall damage of approximately eight cm in all stone blocks, with few locations in which the concrete portion of the panel was already exposed. As the coloration of half the blocks in panel 4 has not changed to yellow-brownish, it indicates the damage has been predominantly from impact, not thermal shock.

The overall damage in the walls was between 10 and 15 cm, with several location in which the loss of protection was the full 40 cm, thus leaving the structural concrete exposed. Figure 5.9 shows the walls during the first inspection. The north wall had more damage than the south wall, with its protection entirely removed in the right corner of Figure 5.9, while, in the left corner, it is possible to observe exposed reinforcement. The south wall lost large portions of its protection on the bottom, which points to damage caused by the bulldozer. Further, there was a increased amount of damage in the south wall near the location of panel 4, which might indicate a extraordinary event at this area of the factory.

The results of UPV are displayed in Table 5.4. The values of pulse velocity in concrete seem to be inversely correlated to the amount of damage. Panel 3 values were extracted from a microgabbro surface, which is naturally denser than concrete, but can present increased permeability after repeated thermal events above 600^oC [21]. In addition, while microgabbro is more homogeneous from a macroscale perspective, the aggregates in concrete further decrease the wave velocity for the frequencies commonly used in UPV tests [22].

After the inspection, standard repair was performed in the walls, using a 33 cm layer of PC based concrete and 7 cm of refractory material. This had the walls damage return to zero, while the panels received no maintenance. At the time of one year after the installation of panels, a second access at the location was possible for inspection. Table 5.5 shows the deterioration in panels and walls. While the damage in the panels is the



Figure 5.8: Photographic record of state of the panels after 6 months of factory operation.

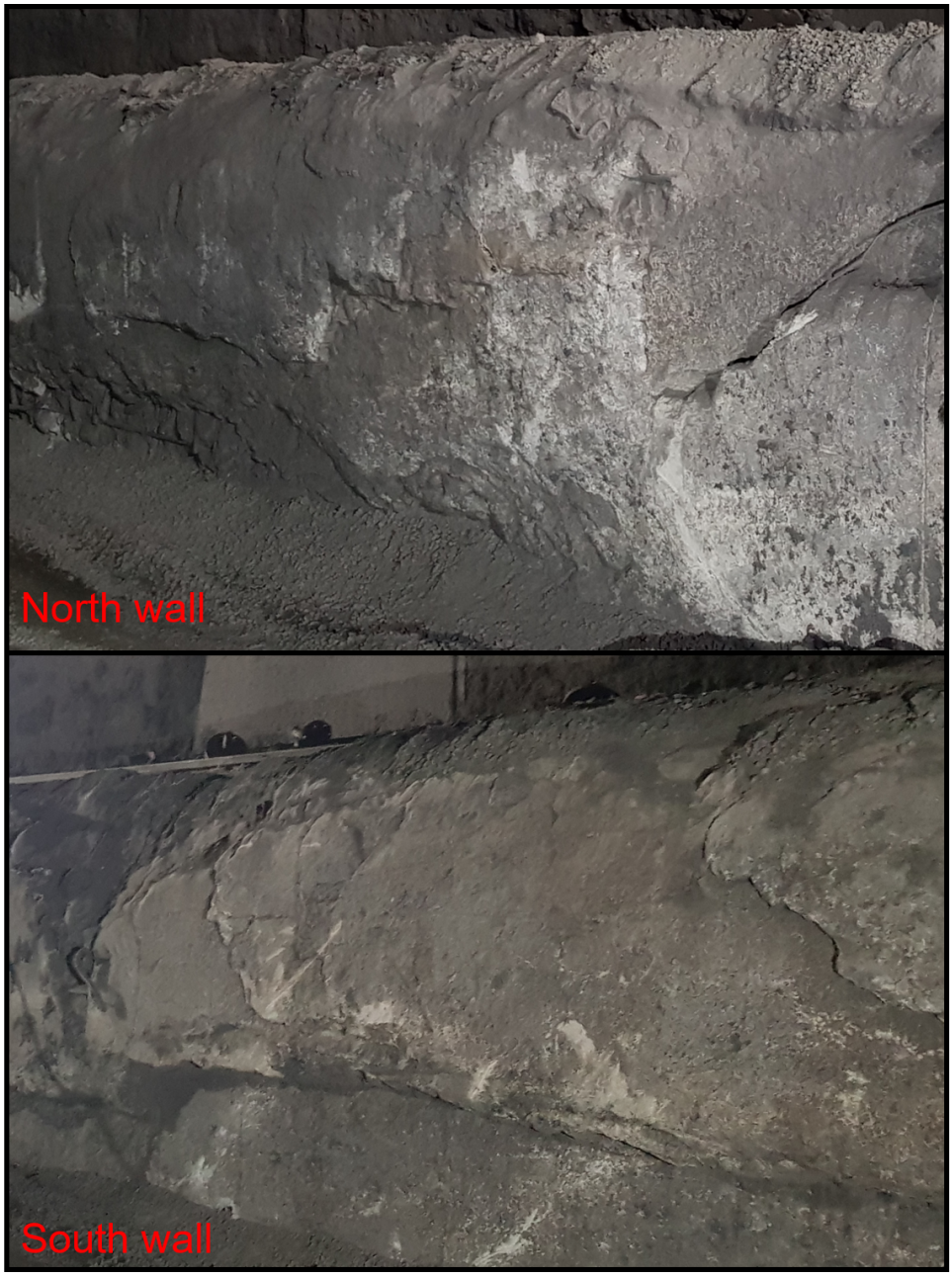

Figure 5.9: Photographic record of state of walls (reference) after 6 months of factory operation.

Table 5.4: Ultrassonic pulse velocity results.

Element	UPV (km/s)
Panel 1	1.78
Panel 2	1.59
Panel 3	2.36
Panel 4	-
North wall	1.42
South wall	-

accumulation of one year of events, the damage in the walls are only regarding 6 months of factory operation.

Table 5.5: Accumulated damage in panels and walls after 1 year of factory operation.

Element	Overall damage depth (cm)	Damage depth at worst location (cm)
Panel 1	0	5
Panel 2	0	9
Panel 3	0	15
Panel 4	8	15
North wall	10	40
South wall	8	40

The overall damage in walls decreased in this cycle, with the wall in the north side performing once more slightly worst than its counterpart. For local damage, the walls had portions of protection completely removed, leaving the structural concrete exposed again. Meanwhile the panels presented no loss in their overall protection depth, with increases only in local damage. Panels 1 and 2 had slight progression of the damage already seen in the first inspection, while panels 3 and 4 had patches in which the stones came out, leaving the concrete portion of the panels acting as protection elements.

5.3.3. OPTICAL MICROSCOPY

Analysis of the core's thin sections showed that most samples presented molten iron adhered to the top of the material. This was composed by a dense, dark red layer of iron with an average thickness of 50 μm followed by a porous, orange layer of slag with an average thickness of 125 μm. Figure 5.10 a displays an example of such layers. At the point of contact from the cement paste with the molten iron, a few micrometers can be observed with a darker coloration, pointing to infiltration of the iron in the material.

The stone samples did not show fracturing, despite the results of Table 5.3. Further, the change in coloration was only observable in thin sections, which indicates either a lower temperature ($\geq 600^{o}$C) or short exposure time to high temperatures. Microgabbro samples presented a shift from bright blue and yellow-orange coloration to darker blue and purple colors after one year in the factory. This is probably due the dehydration of

pumpellyite, occurs between 150°C and 300°C (see Chapter 4).

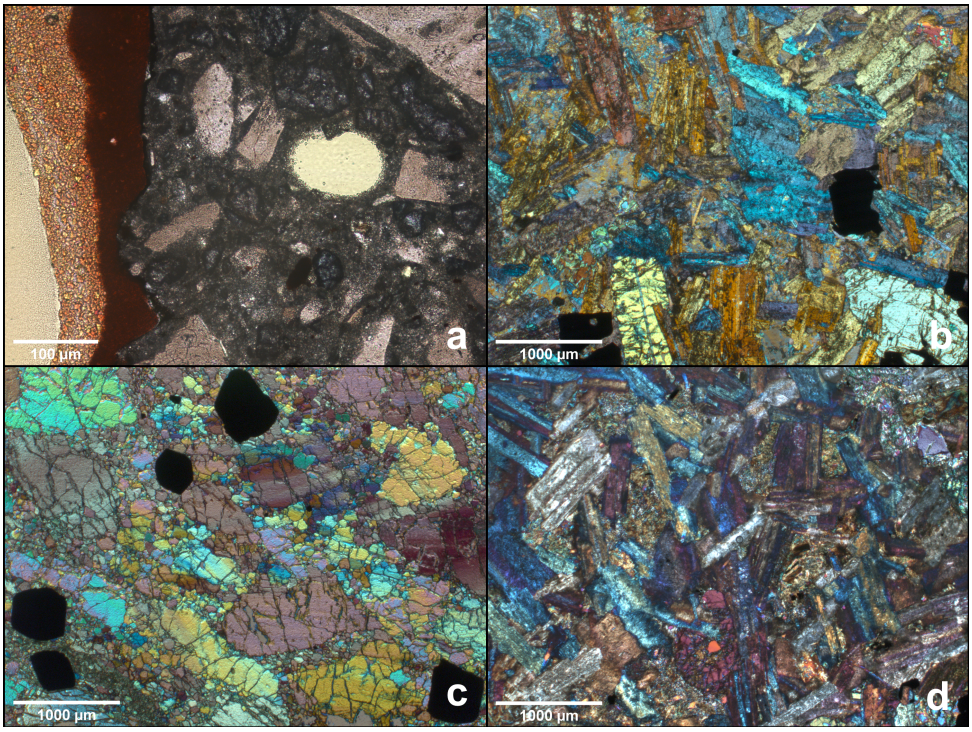

Figure 5.10: Thin sections produced from the panels. a) PPL view of molten iron layer on top of cement after 6 months of factory operation (the picture is shown in the orientation the core was extracted); b) CPL view of microgabbro before installation in factory; c) CPL view of dunite before installation in factory; d) CPL view of microgabbro after 12 months of factory operation.

The concrete samples also showed signals of exposure to high temperatures. Figure 5.11 a is composed of four micrographs stitched together to show the change in color from light brown to dark brown in the sample. This occurs due to the dehydration of CAC phases [19], and can be observed in the top 500 μm to 800 μm of all samples. In addition, the average crack width also changes from the top of the sample to the bulk. At the surface, the cracks have an opening of approximately 15μm, while lower this decreases to 5 μm to 10 μm.

Figure 5.11 b shows the interface of the refractory layer with the molten material. As in Figure 5.11 a, the average crack width is approximately 15 μm, with the very top of the sample displaying a brighter color than the bottom. It is also possible to observe some degree of infiltration of the molten material through the cracks, which may indicate a slow process of indirect dissolution taking place [23]. As this process requires sustained high temperature to occur and advances in terms of micrometers per day, it is unlikely to be the cause of damage. In comparison, Figure 5.11 c shows the conventional concrete used for protection. A bigger field of view was required to encompass the cracks, which possess an average width between 40 μm and 50 μm. It can be seen that the mix uses

much bigger aggregate grains and presents no discoloration at the top.

The interface between the usual protection material and the concrete in the underlying structure is displayed in Figure 5.11 d. Fractures are present between the two materials, however, it is not clear if this is due the transference of damage by the protection concrete or the result of core drilling vibration. Although previous laboratory studies confirmed the compatibility between the material of the panels and old concrete substrate (see Chapter 3), no interface is available since the panels were precast and later placed in front of the structural concrete.

Further, the micrograph in Figure 5.11 e uses cross polarized light to demonstrate that the concrete in the underlying structure already carbonated and uses quartzic aggregates. The aggregate type reinforces the necessity for high temperature protection while the carbonated state can actually act as an advantage, because carbonated concrete has a better heat absorption capacity [15]. However, wet repair provides a source of moisture, transferred to the underlying material through capillary absorption [24], which, in turn, causes carbonation and increases chances of reinforcement corrosion [25].

The values for mean pixel brightness can be found in Table 5.6. The value for the core extracted from the north wall is more than double of the south wall. The dye within epoxy is the main contributor for brightness increase, the amount of epoxy in each sample is proportional to the permeability of said sample, thus the north wall possessed considerably more cracks. This is in good agreement with the damages reported in Table 5.3. Additionally, the values of the panels were lower than of the cores extracted from the walls, with the notable exception of panel 2. The cause for that seems to be a high concentration of microcracks at the first millimeter of the sample, being the only bright zone of the polished section.

Table 5.6: Mean pixel brightness for UV light images of the thin sections produced from cores of the first inspection.

Element	Mean pixel brightness
Panel 1	5.46
Panel 2	13.17
Panel 3	4.92
Panel 4	5.39
North wall	23.97
South wall	9.44

Table 5.3 and 5.5 shows the least amount of damage for panels 1 and 2, followed by panels 3 and 4, with both walls sustaining the most amount of damage. However, Figures 5.10 and 5.11 only show typical marks of high temperature damage in the panels. As the cores have been extracted from locations with constant exposure to falling molten iron, it is unreasonable to consider there was no exposure to high temperatures. Which might indicate a case of survival bias.

Continuous exposure to high temperature dehydrates the outer layer of the conventional concrete. The weakened surface is, then, more prone to detach from the structure

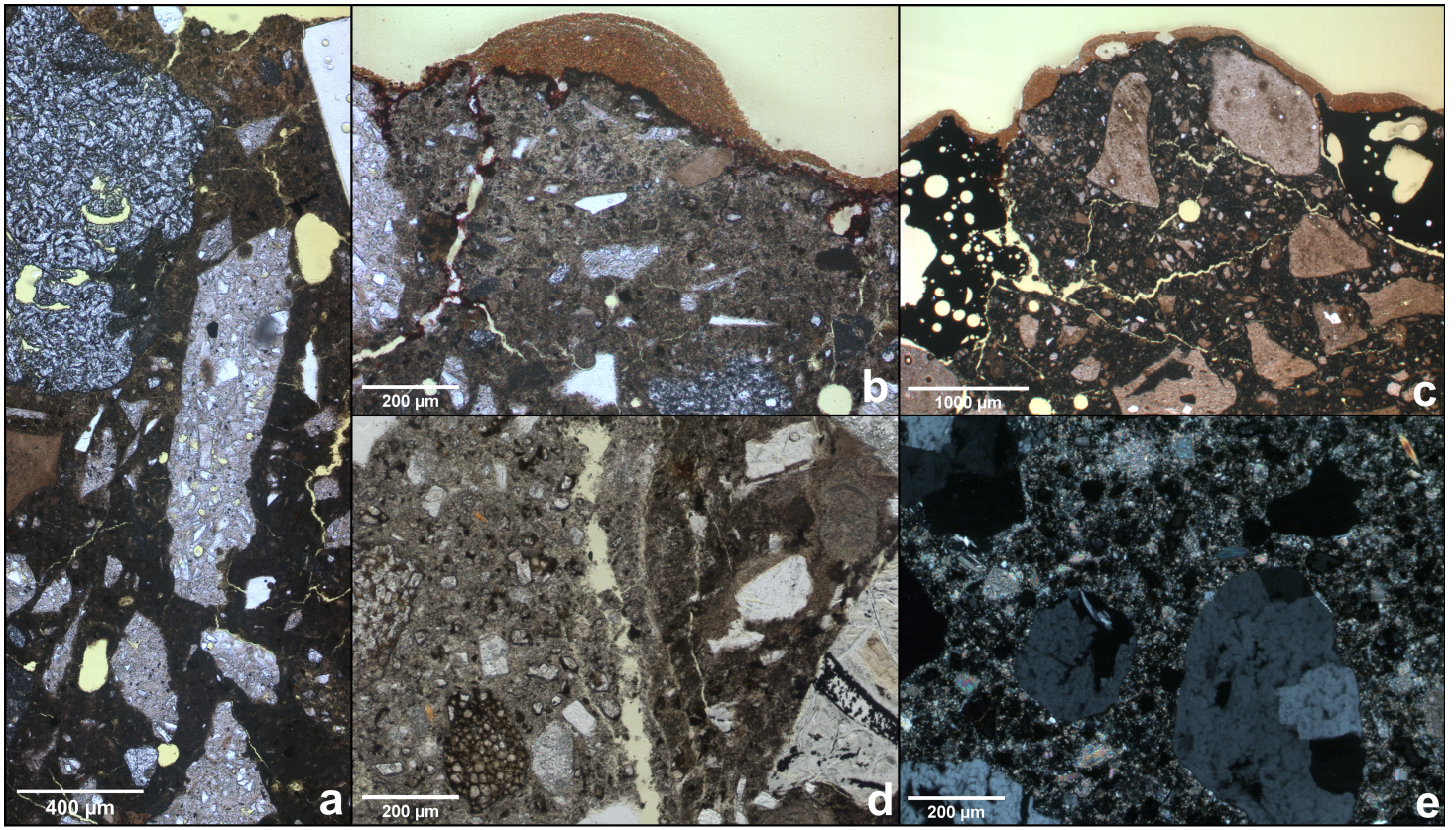

Figure 5.11: Thin sections produced from the panels. a) Stitched micrograph of PPL view of CAC subjected to the thermal load after 6 months of factory operation; b) PPL view of the same thin section with focus on the molten iron interface; c) PPL view of PC based concrete after 6 months of factory operation; d) PPL view of the interface of structural concrete and protection concrete after 12 months of factory operation; e) CPL view of structural concrete.

during the repeated impact loads. Although the stones do not spall or lose their mechanical properties at high temperatures (see Chapter 4), their natural low strain capacity and tensile strength proved insufficient for such high dynamic load, thus, also losing the material exposed to molten iron. In contrast, the use of silica fume enhances the already present capacity of CAC to retain mechanical properties at high temperature [26]. Thus, the damaged material could still withstand repeated impact and would show the marks of thermal changes in thin sections.

The thin sections revealed most damage on the initial 2 millimetres and the inspection determined only a few centimetres of damage at the location. This implies that the application of this solution in the walls could at least triple the service life before intervention is required. Although the material is more expensive than the conventional protection concrete, the increase in service life would more than compensate the initial higher price and become cost effective after the first installation. This is further explored in the next section.

5.4. COST ANALYSIS

As the panels performed much better than the usual protection, a further implementation by the company was discussed. During a meeting, it was decided that it would be the most desired option to continue with the projected concrete mode of repair, while changing the material of repair to something analogous to what was used in the test panels. Then, it was requested from TU Delft a cost analysis of such change. As the budget of operations for the studied walls is confidential, the cost analysis present in this chapter is merely comparative.

An average maintenance campaign uses a fictional value of 100x to repair the walls, with 44x used for cleaning and other services not related to the actual repair and protection of the structure. From the remaining budget, 30x is used for the application of a 33 cm concrete layer and 26x is used for the application of the 7 cm refractory layer on top of the concrete layer. This operation is repeated twice a year for each of the three converters, costing a total of 600x/year.

As the changes suggested by TU Delft focus on the use of a different material, the price for services and execution should remain the same. Mostly, the material cost and quality control of the new material are the only increases in price. A protection layer of 40 cm made entirely of concrete produced with a similar mixture to the one used in the test panels would cost approximately 52x, which is considerably more expensive than the base 30x for concrete already used at the factory. However, this would not require an extra layer of refractory material on top of it, eliminating the additional cost of 26x. This change in procedure would make the price of walls maintenance drop from 100x to 96x, if used in all converters, it would result in 576x/year.

The change in costs is not considerable. This is because while only the material costs were decreased, most of the overall costs are linked to specialized labor. Thus, the strategy of TU Delft was not to create a much cheaper material, but to reduce the amount of maintenance the walls would require. The value of 576x/year would only be true if the walls required maintenance every six months. However, the test panels did not require maintenance after one year (this would mean skipping two maintenance campaigns), and are still at the factory at the time of writing of this thesis. Below, Table 5.7 shows a

comparison taking into account that the optimised material would reduce the need of maintenance campaigns.

Table 5.7: Comparison of yearly costs for maintenance of studied walls.

Material	Maintenance frequency	Comparative cost
PC based concrete	Every 6 months	600x/year
TU Delft concrete	Every 6 months	576x/year
TU Delft concrete	Every 1.0 year	288x/year
TU Delft concrete	Every 1.5 year	192x/year
TU Delft concrete	Every 2.0 years	144x/year

Even using the most conservative approach, would estimate one maintenance campaign per year to each wall beneath the converters, the difference in budget would already be from 600x to 288x, a 52% saving. The best case scenario would be if the walls only required maintenance once every two years, which would bring the cost to 144x, a76% decrease in cost. Since the initial budget allocated for this services is considerable enough to justify the interest in this PhD project, these saving are considered major successes from the case study.

5.5. CONCLUSIONS

This chapter describes a case study in which a factory has continuous loss of protection concrete at a specific location and the solution currently used is compared with a couple of alternative strategies using special materials. Namely, the use of monolithic CAC based concrete and a stone-concrete hybrid have been proposed following the conclusions of Chapters 3 and 4. The design and manufacturing of test panels to be tested at the most severe locations in the steel factory have been described in details.

Because the access to the test area was very limited, relatively few tests could be performed and the author focused on loss of material to compare resistance and used thin section microscopy to determine the cause of damage. Analyzing the results, it seems that the combination of loads creates a positive feedback loop in which the high temperature weakens the conventional protection concrete and the impact loads remove it from the structure.

The stone-concrete type panels performed better than the usual protection, but still failed at a higher rate than expected. This was likely due the low energy distribution capacity of the stones. The monolithic concrete panels performed very well and present a viable alternative for the factory to protect its own structure. When performing a cost analysis, the material suggested by TU Delft is expected to reduce the budget allocated to the studied problem, at least, in half. For this reason, this was considered a successful case study.

BIBLIOGRAPHY

[1] B. Georgali and P.E. Tsakiridis. "Microstructure of fire-damaged concrete. A case study". In: *Cement and Concrete Composites* 27.2 (2005). Cement and Concrete Research in Greece, pp. 255–259. ISSN: 0958-9465. DOI: https://doi.org/10.1016/j.cemconcomp.2004.02.022. URL: https://www.sciencedirect.com/science/article/pii/S0958946504000307.

[2] P.K. Mehta and P.J.M. Monteiro. *Concrete: Microstructure, Properties, and Materials*. McGraw Hill professional. McGraw-Hill Education, 2006. ISBN: 9780071462891. URL: https://books.google.nl/books?id=3j5EAQAAIAAJ.

[3] C.A. Britez and C.N. Costa. "Ações do Fogo nas Estruturas de Concreto". In: *Concreto: Ciência e Tecnologia*. Ed. by G.C. Isaia. São Paulo: IBRACON, 2011. Chap. 29, pp. 1029–1068.

[4] Qianmin Ma et al. "Mechanical properties of concrete at high temperature—A review". In: *Construction and Building Materials* 93 (2015), pp. 371–383. ISSN: 0950-0618. DOI: https://doi.org/10.1016/j.conbuildmat.2015.05.131. URL: https://www.sciencedirect.com/science/article/pii/S0950061815006765.

[5] Ying Zhen Li and Haukur Ingason. "Overview of research on fire safety in underground road and railway tunnels". In: *Tunnelling and Underground Space Technology* 81.August (2018), pp. 568–589. ISSN: 08867798. DOI: 10.1016/j.tust.2018.08.013. URL: https://doi.org/10.1016/j.tust.2018.08.013.

[6] Pierre Kalifa, Grégoire Chéné, and Christophe Gallé. "High-temperature behaviour of HPC with polypropylene fibres: From spalling to microstructure". In: *Cement and Concrete Research* 31.10 (2001), pp. 1487–1499. ISSN: 0008-8846. DOI: https://doi.org/10.1016/S0008-8846(01)00596-8. URL: https://www.sciencedirect.com/science/article/pii/S0008884601005968.

[7] Jin-Cheng Liu, Kang Hai Tan, and Yao Yao. "A new perspective on nature of fire-induced spalling in concrete". In: *Construction and Building Materials* 184 (2018), pp. 581–590. ISSN: 0950-0618. DOI: https://doi.org/10.1016/j.conbuildmat.2018.06.204. URL: https://www.sciencedirect.com/science/article/pii/S0950061818316118.

[8] M. Kanéma et al. "Spalling, Thermal, and Hydrous Behavior of Ordinary and High-Strength Concrete Subjected to Elevated Temperature". In: *Journal of Materials in Civil Engineering* 23.7 (2011), pp. 921–930. DOI: 10.1061/(ASCE)MT.1943-5533.0000272. eprint: https://ascelibrary.org/doi/pdf/10.1061/\%28ASCE\%29MT.1943-5533.0000272. URL: https://ascelibrary.org/doi/abs/10.1061/%5C%28ASCE%5C%29MT.1943-5533.0000272.

[9] S. Martinovic et al. “Implementation of image analysis on thermal shock and cavitation resistance testing of refractory concrete”. In: *Journal of the European Ceramic Society* 30.16 (2010), pp. 3303–3309. ISSN: 0955-2219. DOI: https://doi.org/10.1016/j.jeurceramsoc.2010.07.041. URL: https://www.sciencedirect.com/science/article/pii/S0955221910003717.

[10] Hyoung-Seok So. “Spalling Prevention of High Performance Concrete at High Temperatures”. In: *High Performance Concrete Technology and Applications*. Ed. by Salih Yilmaz and Hayri Baytan Ozmen. Rijeka: IntechOpen, 2016. Chap. 2. DOI: 10.5772/64551. URL: https://doi.org/10.5772/64551.

[11] Hasan Yıldırım and Turan Özturan. “Impact resistance of concrete produced with plain and reinforced cold-bonded fly ash aggregates”. In: *Journal of Building Engineering* 42 (2021), p. 102875. ISSN: 2352-7102. DOI: https://doi.org/10.1016/j.jobe.2021.102875. URL: https://www.sciencedirect.com/science/article/pii/S2352710221007336.

[12] Přemysl Kheml et al. “Cratering damage of high-performance cementitious composites and conventional normal strength concrete caused by in-service projectile impact”. In: *Materials Today: Proceedings* 62 (2022). 37th Danubia Adria Symposium on Advances in Experimental Mechanics, pp. 2436–2439. ISSN: 2214-7853. DOI: https://doi.org/10.1016/j.matpr.2022.02.587. URL: https://www.sciencedirect.com/science/article/pii/S2214785322012494.

[13] A.M. Neville. *Properties of Concrete*. Pearson, 2011. ISBN: 9780273755807. URL: https://books.google.nl/books?id=TdfewmQ-cMIC.

[14] A.M. Bragov et al. “Determination of the mechanical properties of concrete using the split Hopkinson pressure bar method”. In: *Procedia Structural Integrity* 28 (2020). 1st Virtual European Conference on Fracture - VECF1, pp. 2174–2180. ISSN: 2452-3216. DOI: https://doi.org/10.1016/j.prostr.2020.11.045. URL: https://www.sciencedirect.com/science/article/pii/S2452321620307058.

[15] Yongqiang Li et al. “Chemical and mineralogical characteristics of carbonated and uncarbonated cement pastes subjected to high temperatures”. In: *Composites Part B: Engineering* 216 (2021), p. 108861. ISSN: 1359-8368. DOI: https://doi.org/10.1016/j.compositesb.2021.108861. URL: https://www.sciencedirect.com/science/article/pii/S1359836821002523.

[16] *NEN-EN 12350-7:2019 – Testing fresh concrete – Part 7: Air content – Pressure methods*. Standard. Delft, NL: Nederlands Normalisatie-instituut, June 2019.

[17] *NEN-EN 12390-3:2019 – Testing hardened concrete – Part 3: Compressive strength of test specimens*. Standard. Delft, NL: Nederlands Normalisatie-instituut, July 2019.

[18] *ISO 1920-7:2004 – Testing of concrete – Part 7: Non-destructive tests on hardened concrete*. Standard. Geneva, CH: International Organization for Standardization, 2004.

[19] A.B. Poole and I. Sims. *Concrete Petrography: A Handbook of Investigative Techniques, Second Edition*. CRC Press, 2016. ISBN: 9781466583825. URL: https://books.google.nl/books?id=uM4dCgAAQBAJ.

[20] J. Schindelin et al. "Fiji: An open-source platform for biological-image analysis". In: *Nature Methods* 9.7 (2012), pp. 676–682. DOI: https://doi.org/10.1038/nmeth.2019.

[21] C. Jones et al. "Acoustic emission and fluid permeability measurements on thermally cracked rocks". In: *Physics and Chemistry of the Earth* 22.1 (1997), pp. 13–17. ISSN: 0079-1946. DOI: https://doi.org/10.1016/S0079-1946(97)00071-2. URL: https://www.sciencedirect.com/science/article/pii/S0079194697000712.

[22] Carnot Nogueira. *Ultrasonic wave propagation in concrete: Characterization of mechanical damage and wavelet analysis of grain-size distribution*. Verlag Dr. Mller, 2009. ISBN: 978-3639182699.

[23] J. Poirier and M. Rigaud. *FIRE Compendium Series: Corrosion of refractories : the fundamentals*. F.I.R.E. compendium series. Göller Verlag, 2017. ISBN: 9783872640062. URL: https://books.google.nl/books?id=rDwqswEACAAJ.

[24] Yang Zhang et al. "Interfacial bond properties between normal strength concrete substrate and ultra-high performance concrete as a repair material". In: *Construction and Building Materials* 235 (2020), p. 117431. ISSN: 0950-0618. DOI: https://doi.org/10.1016/j.conbuildmat.2019.117431. URL: https://www.sciencedirect.com/science/article/pii/S0950061819328831.

[25] Othman Omikrine Metalssi, Abdelkarim Aït-Mokhtar, and Philippe Turcry. "A proposed modelling of coupling carbonation-porosity-moisture transfer in concrete based on mass balance equilibrium". In: *Construction and Building Materials* 230 (2020), p. 116997. ISSN: 0950-0618. DOI: https://doi.org/10.1016/j.conbuildmat.2019.116997. URL: https://www.sciencedirect.com/science/article/pii/S0950061819324390.

[26] N.K. Lee et al. "Microstructural investigation of calcium aluminate cement-based ultra-high performance concrete (UHPC) exposed to high temperatures". In: *Cement and Concrete Research* 102 (2017), pp. 109–118. ISSN: 0008-8846. DOI: https://doi.org/10.1016/j.cemconres.2017.09.004. URL: https://www.sciencedirect.com/science/article/pii/S0008884617301825.

III

THERMAL SHOCK DAMAGE PREDICTION

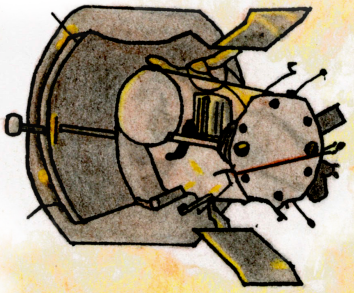

6

PARAMETRIC ANALYSIS OF CONCRETE MIX AND SPALLING

He was prepared, he thought, for any wonder. The only thing he had never expected was the utterly commonplace.

Arthur C. Clarke, 2001: A Space Odyssey

All your questions can be answered, if that is what you want. But once you learn your answers, you can never unlearn them.

Neil Gaiman, American Gods

This chapter sought to identify the main parameters influencing spalling in concrete, in order to improve prediction capacity of engineers. To achieve this goal, a large database of more than 1000 unique samples was collected from 70 publications. The database included 40 properties for each studied sample, besides information on spalling, spalling time, spalling temperature and spalling mass when available. Analysis of the database pointed to some gaps in literature and possibly disadvantageous biases in experimental design. Several machine learning algorithms were used to attempt to predict spalling from the gathered data, reaching a maximum accuracy of 89.73%. Both the database and the algorithms provided important insights that were used for the design of the experiment in the next chapter.

6.1. MOTIVATION AND APPROACH

ALTHOUGH spalling is a problem known for a long time [1], engineers still fail to predict if a concrete mixture will resist spalling during an eventual thermal shock situation [2–4]. The best solution remains to test the material in the actual location, such as done in Chapter 5. However, there are obvious disadvantages to that approach and it would be clearly more desirable to possess a tool to predict if concrete would spall or not.

The lack of prediction capacity is due the high speed, high complexity nature of this phenomenon. Besides the two mechanisms acting simultaneously (explained in Chapter 2), concrete is a highly heterogeneous material [5, 6], which also affects the spalling behaviour. A lot of attention has been given to the changes in water-to-binder ratio (w/b) causing otherwise high performance materials to become more fragile to thermal shock [7–11]. However, changes in type and content of cement [12, 13], type and size of aggregate [14–16], and type and dosage of fibres [17–19] also affect the material capacity to withstand sudden thermal gradients.

Current advances in finite element modelling (FEM) propose to couple both spalling mechanisms for accurate estimation of material behaviour [20–22]. However, these are still insensitive to mixture variation, only assuming random meso-structures. Similarly, design codes [23–27] also do not consider concrete recipe, only the dosage of polypropylene fibres, which does not represent an absolute safety value [2, 28, 29]. Thus, there is a clear need for a method of predicting the spalling behaviour of concrete, taking the materials parameters into account.

Yet, computational power hinders the application of multi-scale modelling departing from w/c ratio and aggregates PSD and content all the way to structural behaviour of a given member [30]. Further, analytical models are usually limited to a single mechanism of spalling [31, 32], or to a perfectly solid material [22, 33].

On the other hand, machine learning (ML) algorithms have emerged recently as tools to predict behaviour of very complex system without requiring perfect knowledge of the causing phenomena [34, 35], including in cementitious systems [36, 37]. The application of such algorithms in the vast available literature of concrete spalling experiments might provide useful insights in common trends and even a prediction tool for engineers.

In this chapter the author compiles a database of over one thousand concrete samples that went through concrete spalling to address the question whether the most common ML algorithms currently used are appropriate to study this form of failure. This is done by first defining the most agreed upon influencing parameters of spalling on concrete samples. Next, a database is created with peer-reviewed research that provides the minimum amount of details, conventions are created as no study presents the full amount of information of its experiment. Finally, a selection of ML algorithms was used to predict the outcome of the experiments in the database. The analyses were performed in python and the parameters for the algorithms is described. Insights are drawn from the results, particularly the graphical results from logistic regression and decision trees influence the follow-up study in Chapter 7.

6.2. DEFINITION OF SCOPE

The most commonly investigated parameters when studying concrete spalling under high temperatures are the W/C ratio, use of fibres and the compressive strength [7, 38, 39]. Although these have a influence in the behaviour, it is clear that several other parameters also play a role [40–42]. The question regarding which features to include in this type of study is complex as one of the outputs is which features are most relevant. Further, the use of too many features usually requires an exponentially larger database [43]. Finally, very few published studies include pore size distribution, adsorption and desorption isotherms, thermal conductivity, coeficient of thermal dilation or even elastic modulus. Because of that, the features included in the database had to be chosen not only by presumed significance, but also by availability.

6.2.1. MIXTURE RELATED FEATURES

As stated in the previous section, several aspects of mix design can facilitate or hinder spalling. The parameters for such designs are usually described in detail in publications, thus, it is easy to obtain the most desired features. The ones selected for this study were:

1. Type of binder;
2. Content of binder (kg/m^3);
3. Use of supplementary cementitious materials;
4. Type of supplementary cementitious materials;
5. Content of supplementary cementitious materials (kg/m^3);
6. Type of aggregates;
7. Content of aggregates (kg/m^3);
8. The maximum diameter of aggregates (mm);
9. Content of plasticizer (kg/m^3);
10. Water/binder ratio;
11. Type of fibres;
12. Content of fibres (kg/m^3);
13. Dimensions of fibres (mm);
14. Polypropylene index (PPI);
15. Adjusted polypropylene index (APPI).

The polypropylene index was a measure introduced by Li et al (2021) [41], defined by Equation 6.1, in which φ is the dosage of fibers in kg/m^3, l is the length of fibers in mm and d is the diameter of fibers in also in mm. This is a very convenient way of having a number estimating the fibres concentration in the material, which is more significant to spalling than the mere dosage [38].

$$PPI = \frac{\varphi \cdot l}{d} \tag{6.1}$$

Although this was proposed for polypropylene, other studies [44–47] show that many types of fiber can execute the same anti-spalling function. Thus, the authors propose an adjusted PP index (APPI) in Equation 6.2, ρ is density in kg/m^3 and T_m is the melting point in ^{o}C. These indices were used for any fiber addition to concrete with a melting point lower than 250°C, which is considered a critical temperature for concrete spalling [48]. If more than one type of fiber with melting point lower than 250°C was added to the sample, the PPIs were computed individually and then added.

$$APPI = \frac{\varphi \cdot l}{d \cdot \rho \cdot T_m} \tag{6.2}$$

If the cross-section of used fibers was rectangular, the diameter used for PPI and APPI was estimated based on Equation 6.3, in which A is the area of said cross-section in mm^2.

$$d = \sqrt{\frac{4 \cdot A}{\pi}} \tag{6.3}$$

6.2.2. MATERIAL RELATED FEATURES

The reporting of material properties varied considerably, with some studies only informing the age and compressive strength of concrete. Because tension is the governing stress during spalling [49, 50], preference was given to the studies that also reported any form of tensile test results. The properties that could be consistently recorded for most studies were:

1. Concrete age (days);
2. Concrete strength in compression (MPa);
3. Concrete strength in tension (MPa);
4. Concrete moisture content (%, based on mass);
5. Concrete reinforcement ratio (%, based on area).

Attempts were also made to record the concrete modulus of elasticity, air content and permeability (gas and water), however, too few of the papers have reported any of these properties.

6.2.3. TESTING RELATED FEATURES

As spalling is very affected by samples size and geometry [40, 51] and heating program [52, 53], this was also taken into account. Mostly, the details of the samples and experimental programs were well reported and could be recorded without any hindrances. The selected properties were:

1. Curing regime;
2. State of sample (dry or wet);
3. Sample shape;
4. Sample roundness;
5. Sample volume (mm^3);
6. The presence of compressive loading during test;
7. Confinement of sample during test;
8. The heating device;
9. The heating rate (^oC/min);
10. The time of heating (min);
11. The maximum temperature (^oC);
12. How long the sample remained at maximum temperature (min).

The sample roundness is defined as Equation 6.4 applied to the cross-section of the two smallest axis of a sample. Where R stands for roundness, A is the area and P is the perimeter. Thus, a cylindrical sample would have a roundness of 1, while a cube would have a value of 0.78.

$$R = \frac{4 \cdot \pi \cdot A}{P^2} \tag{6.4}$$

6.3. DATABASE DEVELOPMENT

The scientific studies used for the creation of the database are reported in Table 6.1. Preference was given to journal papers due to the higher degree of scrutiny during peer-review. Further, most documents were published in the last two decades, this is mostly due to digital availability. The number of samples in Table 6.1 refers to samples in which at least one of the parameters was changed. If all parameters were kept the same, no new entry was made, and the amount of samples that spalled or not was registered in the same entry of the database. On average, the publications contained 16 unique samples tested and a total of 70 publications was used to gather 1129 entries for the database.

Table 6.1: Literature used for the acquisition of data.

Publication	Published in	No. of samples
Kristian Hertz (1984) [54]	Report no. 166	31
Faris Ali et al (2001) [55]	Magazine of Concrete Research	2
Long T. Phan et al (2001) [56]	Materials and Structures	16
Takeshi Morita et al (2001) [2]	Journal of Structural and Construction Engineering	23
A. Bilodeau et al (2004) [57]	Cement and Concrete Composites	12
Cheon-Goo Han et al (2005) [58]	Cement and Concrete Research	24
A. Noumowé et al (2006) [8]	Journal of Materials in Civil Engineering	8
Lars Bostrom (2007) [59]	Fire and Materials	43
X. Liu et al (2008) [60]	Cement and Concrete Research	6
Long T. Phan (2008) [61]	Materials and Structures	16
M. B. Dwaikat et al (2009) [52]	Fire Technology	4
Cheon-Goo Han et al (2009) [62]	Construction and Building Materials	10
Young-Sun Heo et al (2010) [17]	Cement and Concrete Research	50
W. Z. Zheng et al (2010) [63]	Fire Safety Journal	24
Faris Ali et al (2011) [64]	Materials and Structures	6
Young-Sun Heo et al (2011) [44]	Materials and Structures	45
Mugume R. Bangi et al (2011) [65]	Cement and Concrete Research	18
Young-Sun Heo et al (2011) [66]	Construction and Building Materials	2
Zhu Pan et al (2012) [14]	Construction and Building Materials	18
Young-Sun Heo et al (2012) [28]	Materials and Structures	17
Guncheol Lee et al (2012) [45]	Construction and Building Materials	25
Young-Sun Heo et al (2012) [38]	Cement and Concrete Research	31
G. Debicki et al (2012) [40]	Cement and Concrete Composites	23
Robert Jansson (2013) [67]	Materials and Structures	28
H. Carre et al (2013) [68]	MATEC Web of Conferences	6
K. K. Sideris et al (2013) [69]	Construction and Building Materials	32
Eike Klingsch et al (2013) [70]	IBK Bericht	24
Pietro Lura et al (2014) [71]	Cement and Concrete Composites	3
Mitsuo Ozawa et al (2014) [47]	Construction and Building Materials	4
Yang Ju et al (2015) [72]	Science Bulletin	25
Young-Sun Heo et al (2015) [73]	Materials and Structures	7
Jean C. Mindeguia et al (2015) [51]	Fire and Materials	12
Steve Werner et al (2015) [74]	Fire and Materials	4
I. Rickard et al (2015) [75]	Structural Engineering: Providing Solutions to Global Challenges	28
Yining Ding et al (2016) [76]	Construction and Building Materials	7
Sun Bei (2016) [9]	Case Studies in Construction Materials	11
C. Kahanji et al (2016) [10]	Journal of Structural Fire Engineering	7
Asif H. Shah et al (2017) [77]	Construction and Building Materials	8
N. Yermak et al (2017) [78]	Construction and Building Materials	21
N. K. Lee et al (2017) [79]	Cement and Concrete Research	3
Cristian Maluk et al (2017) [29]	Engineering Structures	22
Yang Ju et al (2017) [80]	Construction and Building Materials	5
Wasim Khaliq et al (2017) [81]	Construction and Building Materials	20
Msheer H. Ali et al (2017) [82]	Engineering Science and Technology	24
Xiangwei Liang et al (2018) [83]	Construction and Building Materials	20
Gai-Fei Peng et al (2018) [84]	Cement and Concrete Research	11
Dong Zhang et al (2018) [85]	Cement and Concrete Research	2
Jin-Cheng Liu et al (2018) [86]	Cement and Concrete Composites	2
Izabela Hager et al (2018) [87]	MATEC Web of Conferences	7
Gyeongcheol Choe et al (2019) [88]	Cement and Concrete Research	8
Shamsad Ahmad et al (2019) [89]	Composites Part B: Engineering	4
Juan Yang et al (2019) [15]	Construction and Building Materials	4
Ye Li et al (2019) [90]	Cement and Concrete Composites	16
Ibrahim H. Alfahdawi et al (2019) [91]	Construction and Building Materials	40
Ye Li et al (2019) [16]	Cement and Concrete Composites	11
Fabio P. Figueiredo et al (2019) [92]	Fire Technology	23
T.M. Viana et al (2020) [93]	Construction and Building Materials	12
N. Algourdin et al (2020) [53]	Construction and Building Materials	9
M. Maier et al (2020) [94]	Construction and Building Materials	15
Young Du et al (2020) [95]	Construction and Building Materials	17
Dong Zhang et al (2020) [96]	Cement and Concrete Composites	6
Ye Li et al (2020) [97]	Construction and Building Materials	26
Jin-Cheng Liu et al (2020) [98]	Archives of Civil and Mechanical Engineering	28
Dong Zhang et al (2020) [18]	Cement and Concrete Composites	4
Marcus Maier et al (2020) [99]	Construction and Building Materials	18
Gyeongcheol Choe et al (2020) [100]	Construction and Building Materials	9
Jin-Cheng Liu et al (2021) [101]	Construction and Building Materials	54
Dong Zhang et al (2021) [102]	Cement and Concrete Research	8
Dong Zhang et al (2021) [103]	Construction and Building Materials	4
Dong Zhang et al (2021) [19]	Cement and Concrete Composites	16

6.3.1. DATA CONVENTIONS

Although the papers were chosen based on abundance of the selected data, many still lack some of the features. To account for that, a number of conventions were used. This decreases the potential precision of the algorithms, however, it was necessary to achieve at least one thousand unique entries. The conventions are found in the list below:

- If the age of samples was not specified, it was assumed to be 28 days;
- If the heating device was not specified, it was assumed to be an oven;
- When cement was referred as CEM II, it was considered CEM II/A;
- When cement was referred as CEM III, it was considered CEM III/A;
- If the cement was not specified, it was assumed to be CEM I;
- If the aggregate $D_{\max}$ was not specified, it was assumed to be 6.3 mm;
- If drying was not reported after curing, it was assumed the samples were wet;
- If the moisture content was not specified, it was assumed 4% for wet samples;
- If the moisture content was not specified, it was assumed 2% for dry samples;;
- If W/B ratio was not specified for samples with $\sigma_c > 120$ MPa, it was assumed 0.18;
- If σ_c was not specified, it was considered 40 MPa for W/B > 0.38;
- If σ_c was not specified, it was considered 60 MPa for W/B ≤ 0.38;
- If σ_c was not specified, it was considered 120 MPa for W/B < 0.28;
- If reinforcement was reported, but not the amount, it was assumed 1%;
- If loading was not specified, it was assumed the samples were unloaded;
- If curing was not specified, it was assumed the samples have been cured in air;
- If curing duration was not specified, it was assumed to be 28 days.

In the cases where compressive strength of the samples was reported at 28 days, but spalling test occurred at a different age, the strength at testing was estimated according to ACI 209-92 [104]. This follows Equation 6.5, in which η and τ are constants that change with cement and curing type as shown in Table 6.2.

$$f_{c_t} = \frac{t}{\eta + \tau \cdot t} \cdot f_{c_{28}} \tag{6.5}$$

When the tensile strength of the samples was not reported, this was estimated based on the Eurocode [105], following Equations 6.6 and 6.7.

$$f_{\text{ctm}} = 0.3 \cdot f_{\text{ck}}^{(2/3)} \leq C50/60 \tag{6.6}$$

$$f_{\text{ctm}} = 2.12 \cdot ln\left(1 + \frac{f_{\text{cm}}}{10}\right) > C50/60 \tag{6.7}$$

Table 6.2: Values for η and τ parameters of Equation 6.5.

Cement type	Cure type	η	τ
I	Moist	4	0.85
	Steam	1	0.95
III	Moist	2.3	0.92
	Steam	0.7	0.98

6.3.2. DATA NORMALISATION

In order for the machine learning algorithms to properly function, it is necessary to perform feature scaling in the database [43]. This was done through min-max normalisation for all quantitative properties, following Equation 6.8. In which x' is the normalised value of property x and $min(x)$ is the minimum value of x in the database and $max(x)$ is the maximum value of x in the database.

$$x' = \frac{x - min(x)}{max(x) - min(x)} \tag{6.8}$$

The qualitative data required another set of conventions for coding. Cement type was divided between conventional (i.e. CEM I, ASTM Type I), composite (i.e. CEM II, CEM III, ASTM Type IV) and aluminate (i.e. CAC). Pozzolanic additions were divided between fine (i.e. silica fume, nano slica) and coarse (i.e. fly ash, blast furnace slag, glass powder). The fibers were divided between polypropylene, metalic, polimeric (i.e. nylon, PET, PVA) and natural (i.e. flax, jute, cellullose). The concrete type was divided between normal strength concrete (NSC), high strength concrete (HSC) and ultra-high strength concrete (UHSC). The shape of samples was divided into 1D (i.e. beams, columns), 2D (i.e. slabs, discs) and 3D (i.e. cubes, prisms, cylinders). The heating devices were separated between devices that heat the whole sample (i.e. oven, gas furnace) and devices that heat only one face of the sample (i.e. radiant heater, blowtorch, open face oven). Aggregates were divided between quartz based (i.e. granite, sandstone), non-quartz based (i.e. limestone, basalt) and unknown for publications not specifying the composition of the aggregates. The type of curing was divided between submersed curing, placement in a curing room, sealing of sample, air curing, steam curing and drying in an oven. Loading, confinement, state (wet or dry) and spalling were considered binary values. If an experiment used 6 copies of each sample and only 2 out 6 spall, spalling was still considered to have taken place in that particular set of parameters.

6.4. DATABASE ANALYSIS

6.4.1. DATA META-ANALYSIS

Among all collected data, 48% of the samples suffered from high temperature spalling. This is a desirable amount as it shows the data has a good spread between a combination of properties that leads to either result. Figure 6.1 shows the types of additions and aggregates in the studies mentioned in Table 6.1. More than half of the samples had the addition of silica fume, fly ash or silica fume and fly ash. This is because spalling is often studied in high strength or ultra-high strength concrete. Only a little more than a quar-

ter of the samples had no mineral addition and only about 5% had the addition of blast furnace slag.

For the type of aggregates (Figure 6.2, nearly 25% was not reported. This is a considerable amount that should be noted, as this is a parameter that greatly affects the resistance of concrete to spalling [87, 94, 106], yet publications fail to report it. Half of the samples contained quartz based aggregates, while one quarter contained non-quartz based aggregates. While it is more desirable to use non-quartz based rocks, the choice of aggregate is largely determined by geographic and economic constraints [66].

Figure 6.3 displays the different types of fibres used and their incidence in the collected publications. A little more than a third of all samples did not use any fibres. About half of the samples contained a single type of fibre in the mixture design, while 15% of samples contained a combination of two types of fibres. As PP is the industry standard for increase of spalling resistance [41, 42, 107], it is the most present fibre, with more than 40% of samples containing it. Metallic and other polymeric fibres are the second most commom type, both found in about 15% of samples. Only 2.4% of samples contained natural fibers as these usually shrink and burn instead of melting [18, 19, 108].

Figure 6.4 has some of the other qualitative data regarding the samples extracted from the publication in Table 6.1. Most samples were made of concrete, with only about 20% made of mortar and less than 1% made of cement paste. However, in more than 10% of the cases, the aggregate $D_{\max}$ was not reported, making it impossible to correctly classify the sample as mortar or concrete. This is something that should be avoided in the future, as there is already evidence of the influence of this parameter on spalling [14, 16, 38, 109].

Most samples were cubes, prisms or cylinders, as these are the most common types of concrete specimens. About a quarter of the samples was shaped as a slab or disc, and only 13% was column or beam shaped. The shape of samples is proportional to the volume (seen in Figure 6.6) and the type of heating. Thus, one sided heating was only applied to about 20% of samples, with all the remaining samples going through heating in all available faces. The vast majority of samples were tested unloaded, with only 15% of samples carrying load during test. This was a well reported feature with less than 0.5% so publications not mentioned with samples were loaded or not.

Figure 6.5 displays the distribution of four mixture design parameters. Cement content has a clear peak around 425 kg of cement per cubic meter of concrete, which was expected as this is a standard dosage. However, as many publications focused on ultra-high strength concrete, a relatively high amount of samples also possess a cement content around 800 to 900 kg/m^3. Aggregate dosage had most samples with either 1450 kg/m^3 or 1750 kg/m^3, which are also very conventional dosages. Water to binder ratios varied considerably between 0.20 and 0.45 with few samples on the extreme ends of design parameters. The polypropylene index was zero for all samples without fibers. For most samples with fibres, PPI was below 1000, which is the most commonly used in real concrete mixtures. However, many researchers tried extreme values for fibre dosage, with PPIs ranging from 2000 up to even 8000.

Most of the studied samples were tested at 28 days (see Figure 6.6), even though a couple hundred samples has been tested at several months or even years. A good range of maximum temperatures has also been tried, with most studies using 600°C, 900°C

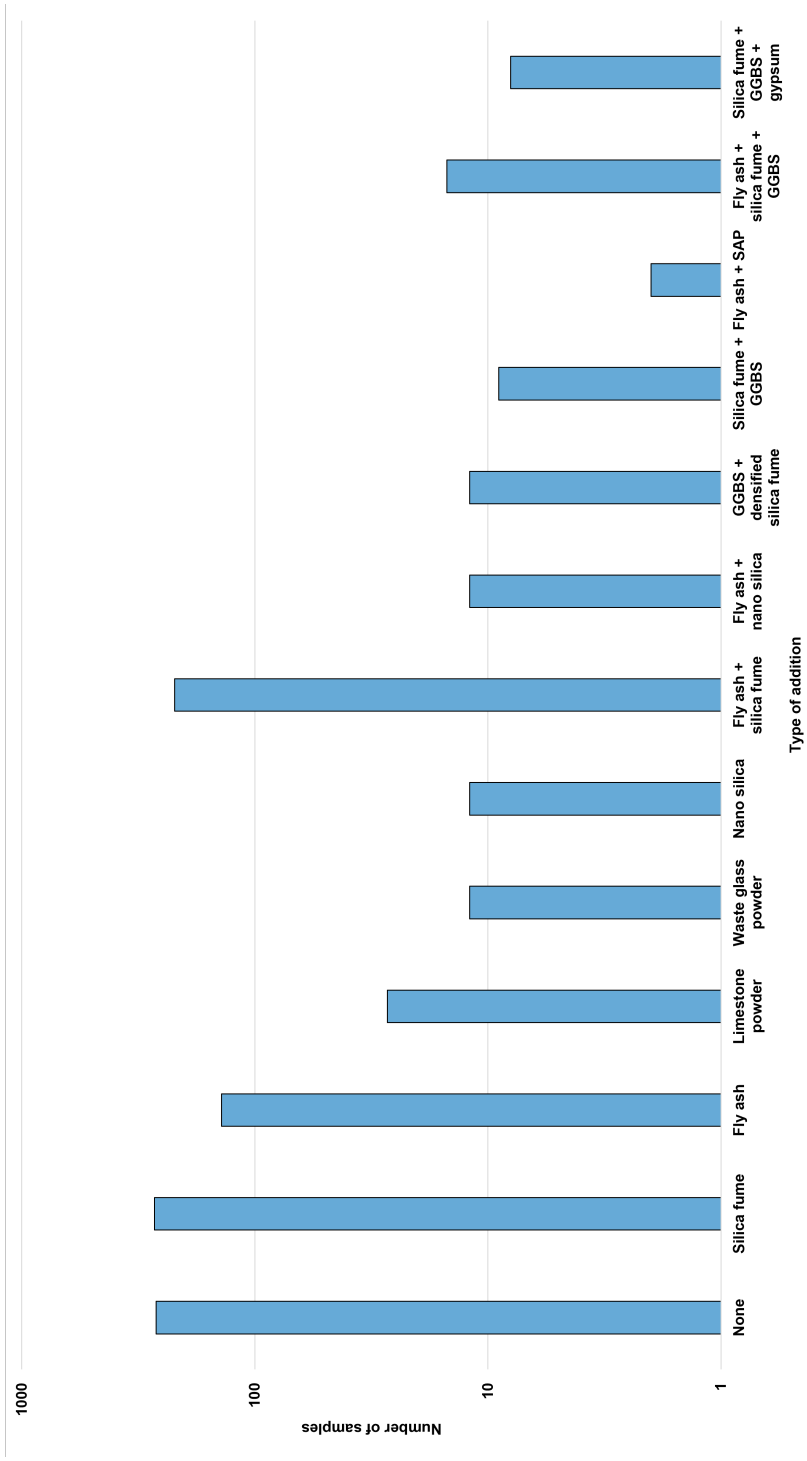

Figure 6.1: Type of mineral additions found in the consulted literature.

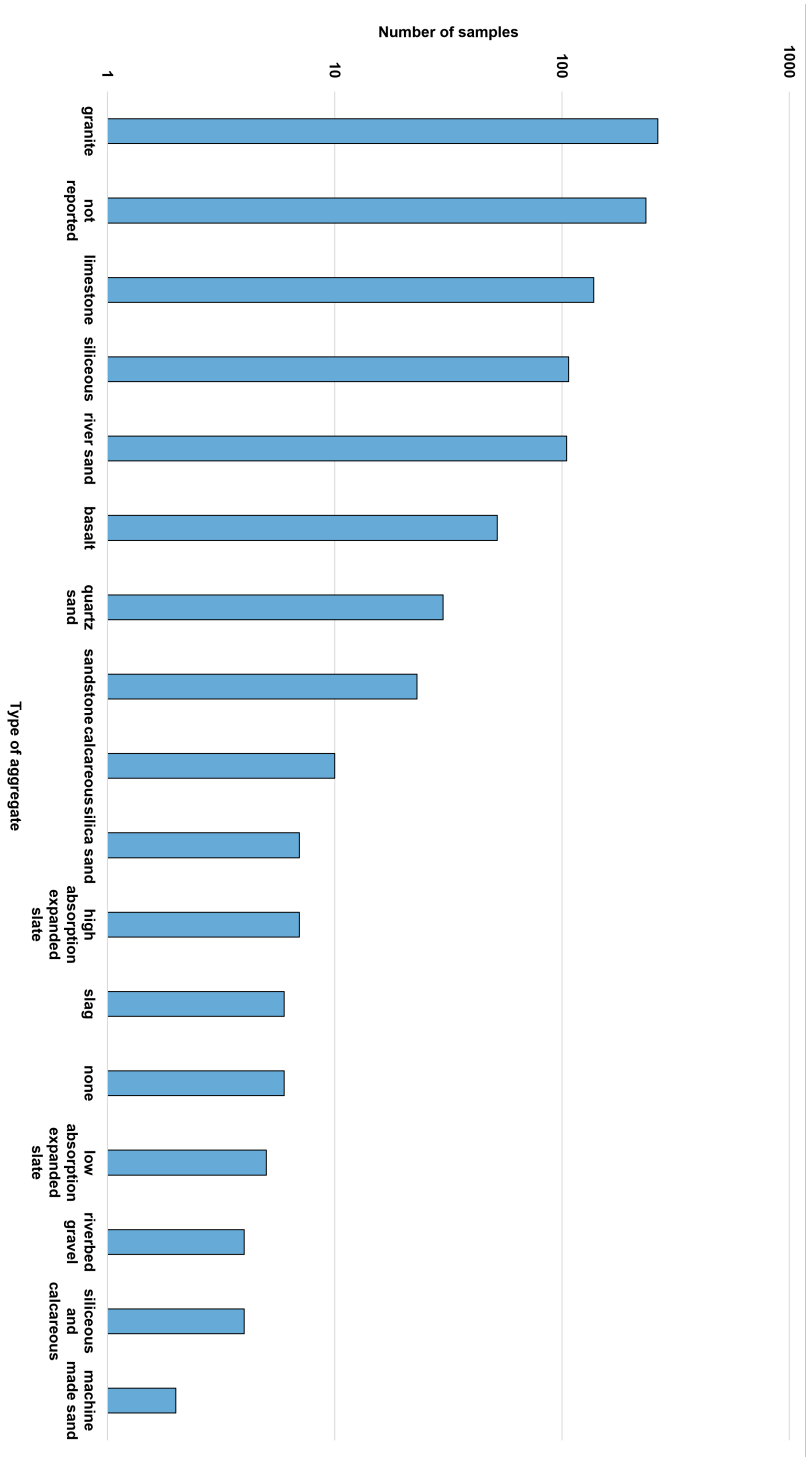

Figure 6.2: Type of aggregates found in the consulted literature.

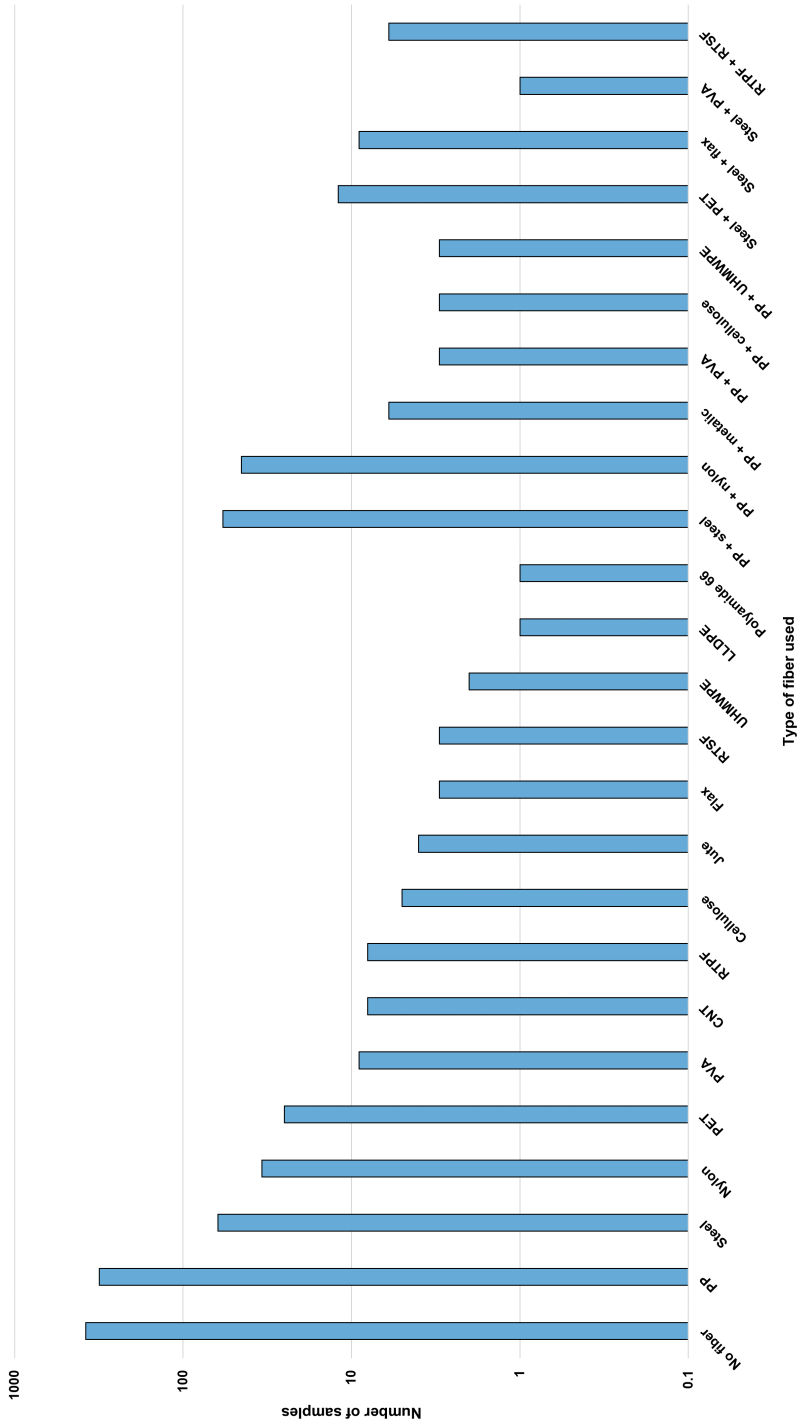

Figure 6.3: Type of fibres found in the consulted literature. PP = polypropylene, PET = polyester, PVA = polyvinilalcohool, CNT = carbon nano-tubes, RTPF = recycled tyre polymer fibre, RTSF = recycled tyre steel fibre, UHMWPE = ultra-high molecular weight polyethylene, LLDPE = linear low-density polyethylene

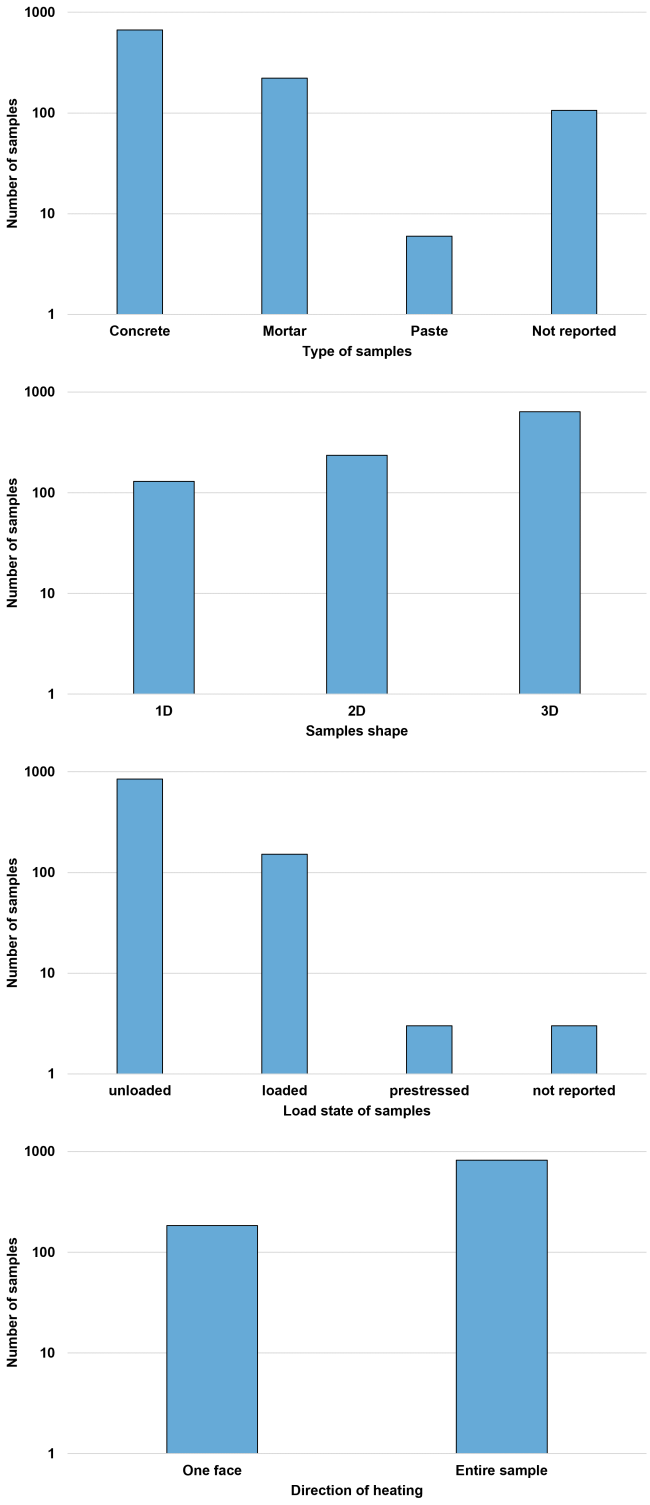

Figure 6.4: Sample and testing information extracted from the consulted literature.

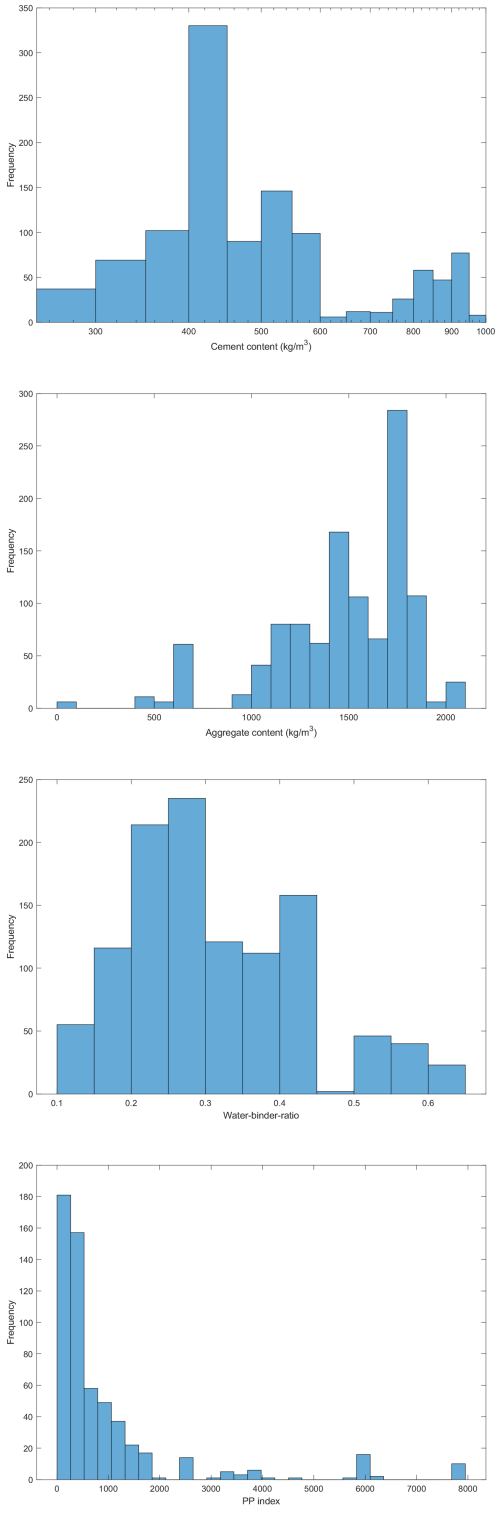

Figure 6.5: Histograms of mix design parameters found in the selected literature.

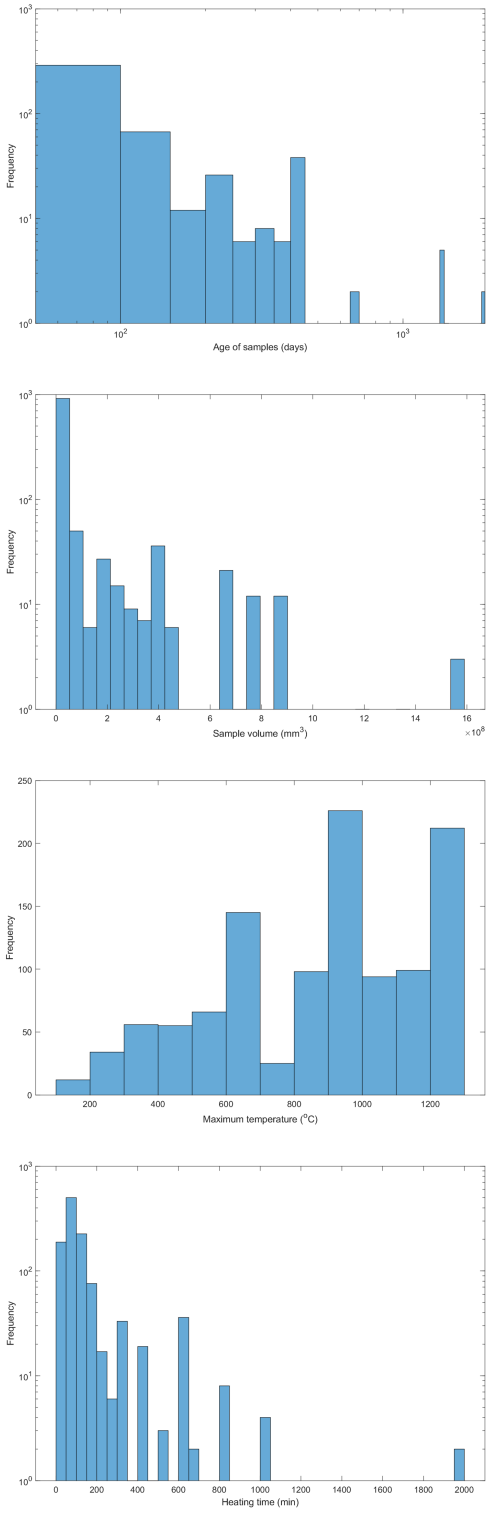

Figure 6.6: Histograms of test parameters found in the selected literature.

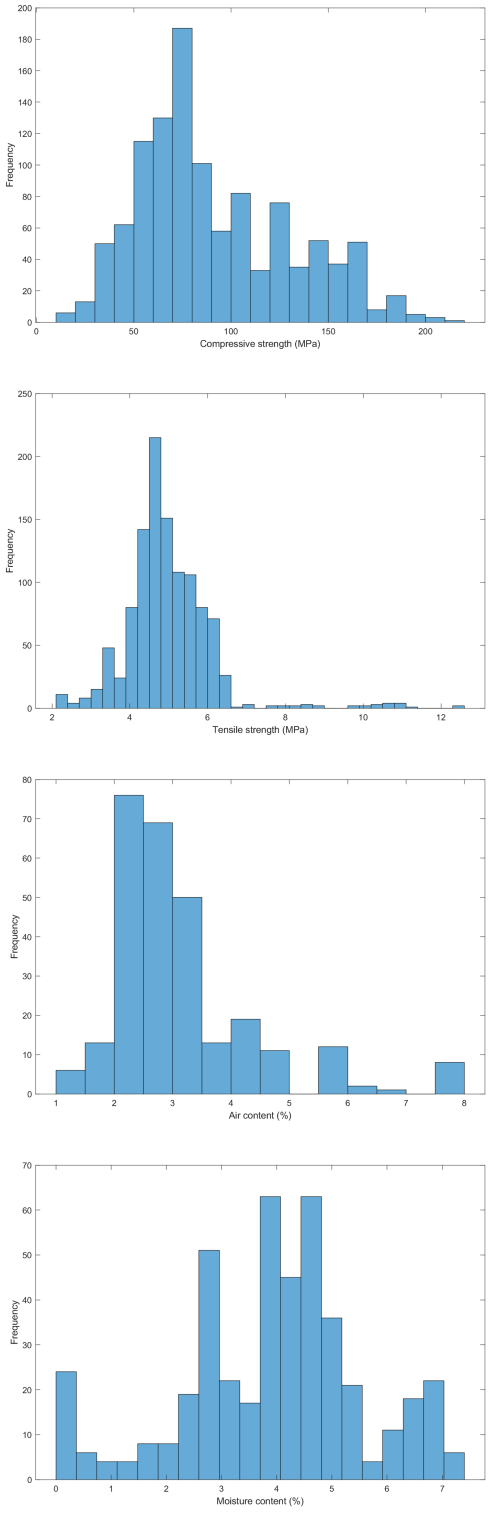

Figure 6.7: Histograms of properties of samples found in the selected literature.

or 1250°C. A clear bias towards small samples was observed in Figure 6.6, with most samples smaller than half a cubic meter. This is somewhat harmful to the understanding of spalling as most small samples are tested in ovens with heating from all direction, which is not the case in practice. Accordingly, the volume to area of heating ratio is small for most samples, again moving away from spallings cases in actual structures.

Figure 6.7 shows some of the properties of the studied samples. Most samples achieved a high compressive strength, of 75 MPa or more. This is a current problem in the study of spalling, as many researchers focus on the performance of high strength or ultra-high strength concrete. Nevertheless, spalling is a common occurrence in normal strength concrete as well [46, 52, 64], and must be understood in this material. Similarly, the tensile strength is mostly in the high end of the concrete spectrum since even samples that did not achieve high strength, were mostly reinforced with fibres. The distribution of air content, on the other hand, presented a good range, with most values in the typical zone between 2% and 4%. Similarly, the moisture content of the samples was well distributed, with most values ranging from 3% to 5%. Few samples were reported completely dry (MC < 0.5%) or completely saturated (MC > 7%).

Combining the data in Figures 6.5, 6.6 and 6.7 provides Figure 6.8, which demonstrates how the compressive strength, time of heating and polymeric fibre dosage are correlated to spalling in the studied samples. The initial observations of this image are rather obvious, shorter heating time, higher compressive strength and lower polymeric fibre content lead to spalling. However, it is also noticeable that samples with no polymeric fibres and very short time of heating are relatively resistant to spalling provided $\sigma_C \lesssim 100$ MPa. Similarly, samples with no polymeric fibre and very high strength still spall relatively less provided the heating time exceeds about 100 minutes. Polymeric fibre content presents a clear advantage, with several examples of samples with the same properties spalling or not according to the PP index. Further, mixtures with relatively high PP index (higher than 100) still suffer from spalling and follow the same trend as the samples with no fibres. Thus, for a sample with a given dosage of PP fibres, reducing the strength or increasing the heating time can avoid spalling.

It is clear that these three properties are not sufficient to address spalling in concrete. However, Bellman (2003) [110] already described several challenges in trying to analyse or even organize data in more than three dimensions, the term coined for this is "the curse of dimensionality". One of the methods to cope with this phenomenon is by regularisation of features [111], which is explored in the following section. Furthermore, this is a recurring problem in dynamic programming, and has been addressed in a number of techniques related to machine learning [112–114]. This partially motivated the author to explore machine learning as the main method of analysis for the created database.

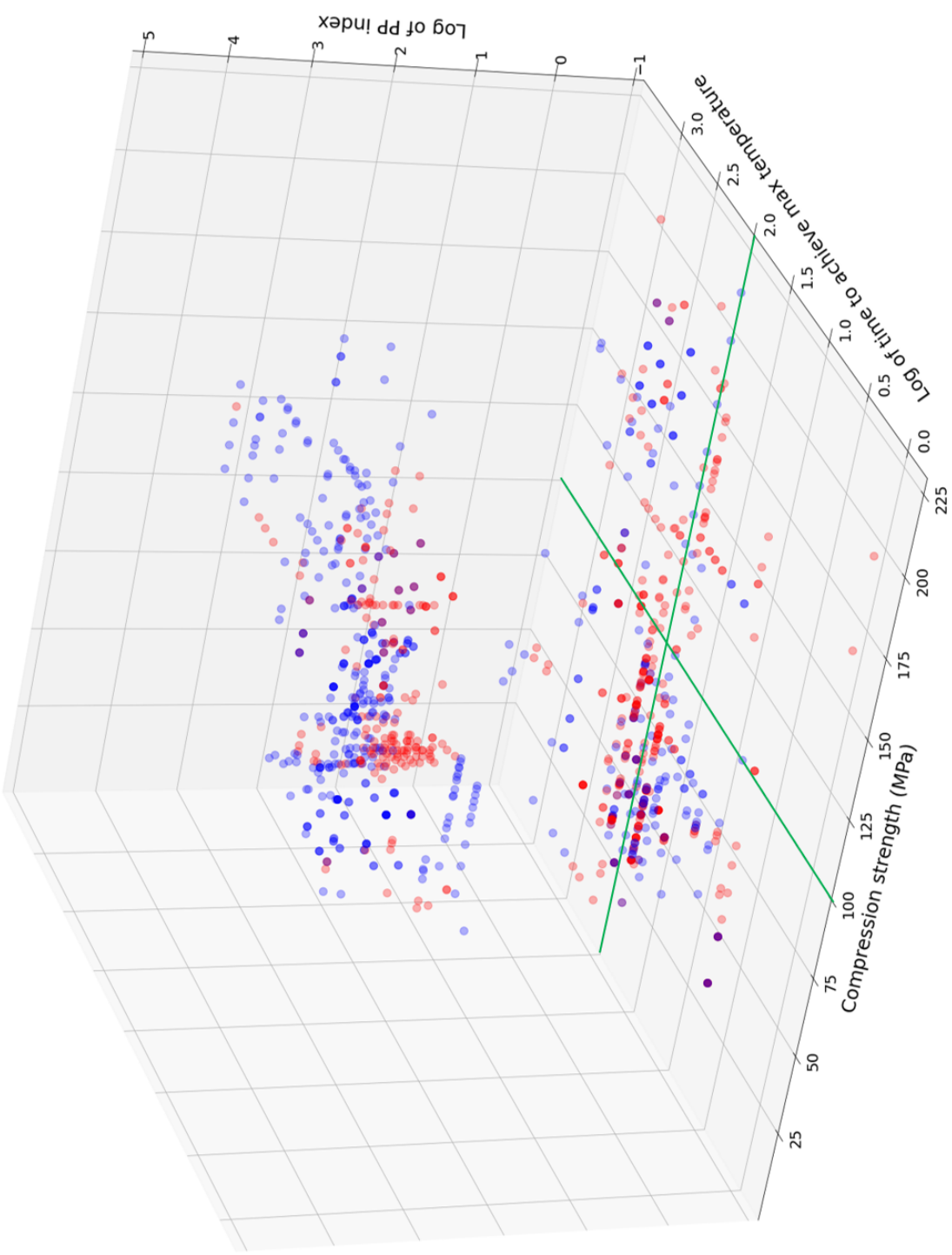

Figure 6.8: Plot of compressive strength, time of heating and polymeric fibre dosage of samples. Samples that spalled are seen in red and the remaining samples in blue, the color intensity is proportional to the amount of samples in the same coordinates.

6.4.2. MACHINE LEARNING ANALYSIS

LOGISTIC REGRESSION

All machine learning algorithms were implemented in Python 3.6.5, and had small parametric studies were performed to determine the most suitable values to use in the codes. The train-test split was 80%-20% and accuracy was determined through the "score" method from scikit-learn [115], in which it returns the total correct predictions divided by the total predictions.

The first attempt to predict the behaviour of the literature samples regarding spalling using all the selected features was through logistic regression. The best results were found with a learning rate of 0.001 and a L1 regularization of 0.7, achieving an accuracy of 77.91%. Although this is a simple method, it allows for the determination of the influence of each feature on the outcome through Lasso regularization. Figure 6.9 shows the perceived influence of each studied property according to this tool.

The polypropylene index and sample volume were the two most dominant features according to the L1 regularization. The index is shown in the negative zone as it avoids spalling, and further, all use of fibres appear as improving spalling resistance (see Chapter 2), albeit with much less efficacy than PP. Sample volume is in the positive zone as bigger samples allow for a bigger temperature gradient. The next most important features are the heating conditions. The difference between unilateral and encompassing heating was negligible, but the maximum temperature and the time to reach maximum temperature were very important. Maximum temperature is in the positive zone since the higher it is, the bigger thermal gradients are possible. Time to reach maximum temperature is in the negative zone, following the observations made in Figure 6.8, as higher times mean a much lower heating rate. All curing procedures seemed beneficial with the exception of steam curing.

Regarding the mixture parameters, measures that decrease porosity (e. g. increasing cement content use of SCMs) seem to consistently increase the chance of spalling while the opposite (increasing aggregate D_{max}, increasing aggregate/binder ratio) reduces it. As expected, the increase in moisture content also increases the chance of spalling. The most negligible features were W/B ratio, adjusted PPI, sealed curing, sample shape and roundness, volume to area of heating ratio, loading, age, tensile strength and reinforcement ratio. Since this is a technique destined to be used in independent variables [43], some features have negligible influence because other features dependent of them are attributed the significance. For example, the W/B ratio was proportional to compressive strength, which received a high significane. The same can be said for PPI and adjusted PPI; compressive strength and tensile strength; and volume and volume to area of heating ratio.

Following the identification of the least influential features, it was attempted to remove such features in order to achieve higher accuracy. However, the reduction of feature space caused the opposite effect, decreasing the accuracy of the logistic regression. Thus, it was decided to move forward with all the collected properties in the database.

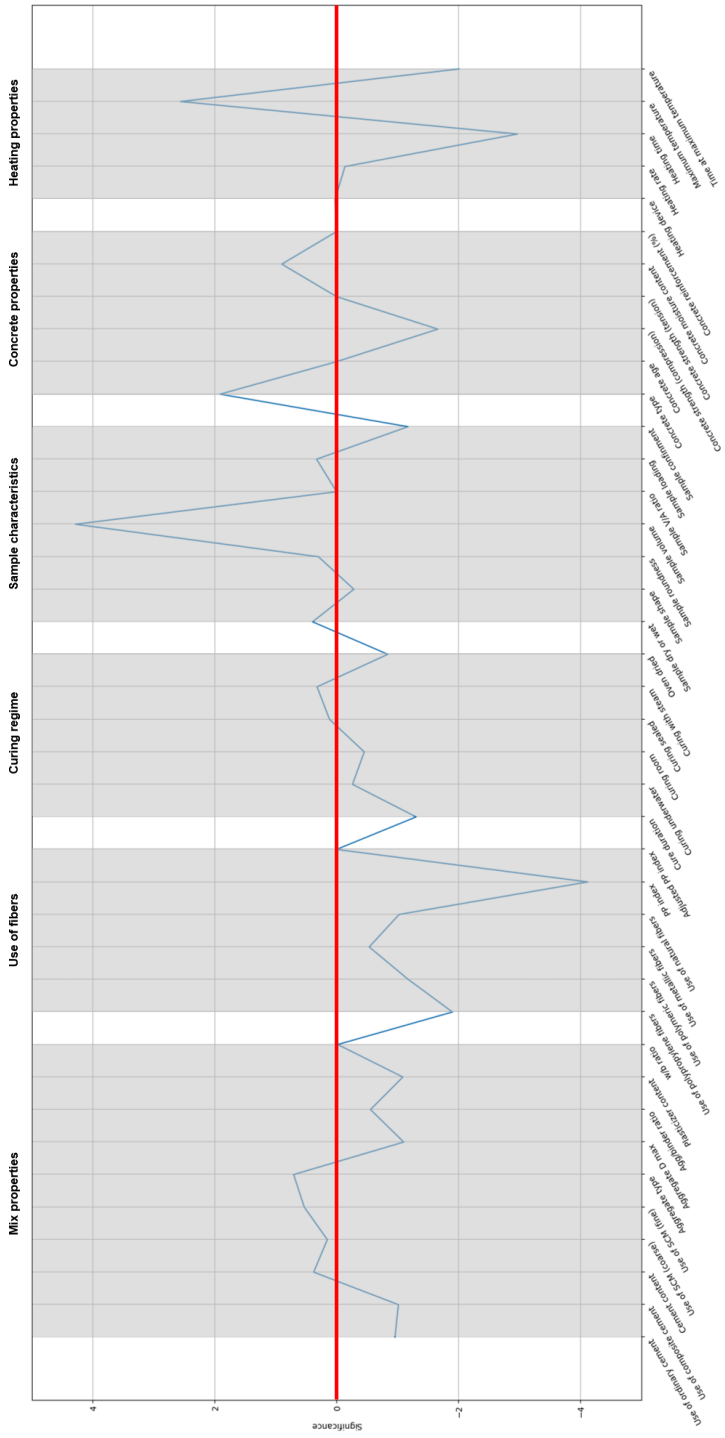

Figure 6.9: Value for weights used to estimate the importance of each feature in determing if a sample would spall through logistic regression.

DECISION TREES

Another technique that could provide insight into the classification of a sample as spalled or safe is the group of algorithms called decision trees. Specifically, a classification tree analysis pipeline was written to attempt to label the samples in the database correctly. The minimum number of samples to split an internal node was set as three after a short period of trial and error. Averaging 100 tries, the mean accuracy was 82.61%, better than logistic regression, but still lower than a desired 90%.

Figure 6.10 shows a sketch of the first 6 levels of the classification algorithm, levels 4, 5 and 6 have been divided into 4.1 to 4.4, 5.1 to 5.4 and 6.1 to 6.4 to facilitate visualization. Although the data used in the code was normalized according to Equation 6.8, the values in Figure 6.10 are shown denormalized to allow interpretation. The full decision tree had 15 levels, however, as the accuracy was below the 90% goal, it was not judged necessary to display the full decision tree.

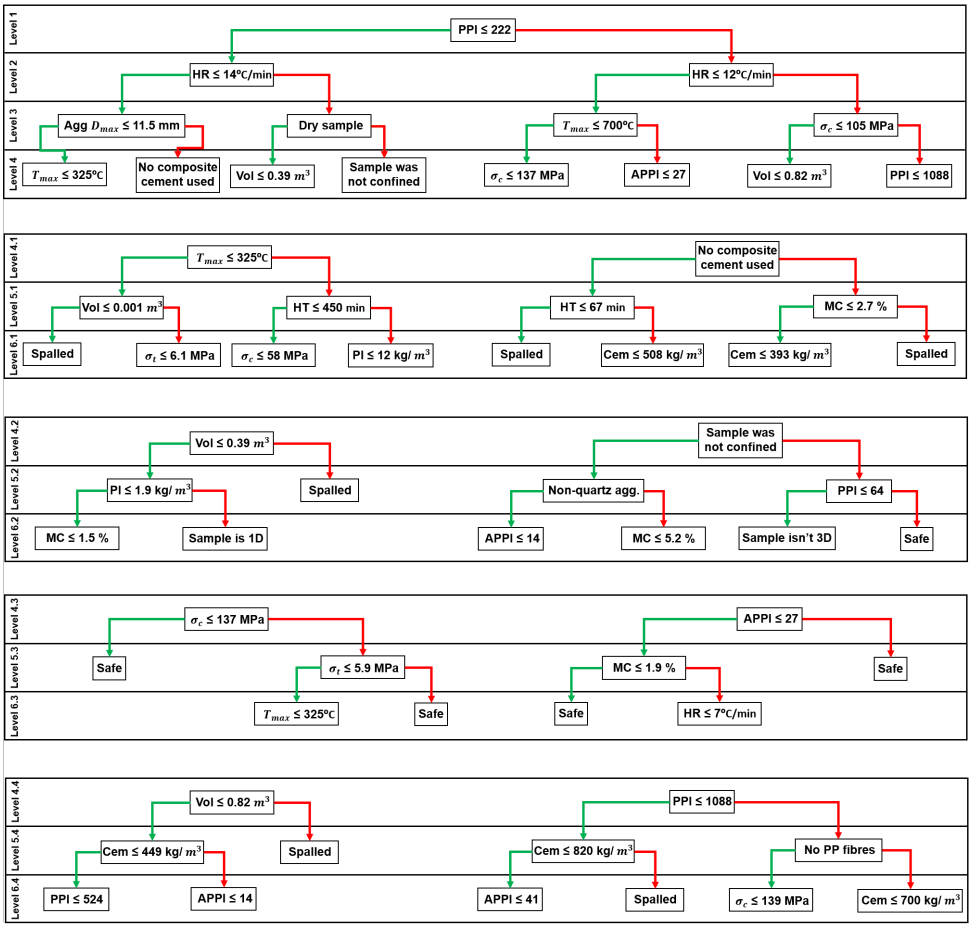

Figure 6.10: Sketch of the used decision tree by the machine learning code, green line represent true statements and red lines false statements, values are approximated.

Unsurprisingly, the polypropylene index was the first feature considered to divide samples, in accordance to what was observed through the Lasso regularization. If PP fibers of 32 μm diameter and 6 mm length were assumed, the threshold value of 222 would be equivalent to a dosage of 1.2 kg/m^3 or 0.13% in volume of concrete. However, if the used PP fibres had 32 μm diameter and 12 mm length, the necessary dosage would be only 0.6 kg/m^3 or 0.07% in volume of concrete. This shows one of the major problems with the current standards philosophy of recommending a minimum dosage of fibre.

The second feature used in the decision tree was the heating rate, a combination of two of the other biggest factors (heating time and maximum temperature) identified through the L1 regularization. Both thresholds are very similar, which might indicate a general change of behaviour of the studied samples between 10°C/min and 15°C/min. At the third level of decision, the samples with slow heating had the maximum size of aggregates or maximum temperature of heating checked. The threshold of 700°C is indicative of laboratory experiments with slow heating as the usual fire curves have a typical $T_{\max} = 1000^oC$ or higher [27, 116]. The aggregate $D_{\max}$ of 11.5 mm might be an interesting threshold to study as the literature is scarce in this area and the few papers on the topic have very limited dosage fractions [14, 16, 109]. The samples with faster heating were checked for their wetness and compressive strength (the final factor identified as critical in the previous section). Following the decision path in Figure 6.10, if a sample had low PPI and fast heating, being dry would be a major factor, as this seems to be a path governed by the THM. On the other branch, a sample with high PPI might suffer from a bigger influence of TMM, thus the decision tree checks the compressive strength, possibly as a substitute for sample ductility.

Following the left-most branch of the decision tree, Figure 6.10 shows that for CEM I (or equivalent) a heating time inferior to about an hour would mean spalling of the samples, again emphasizing the importance of heating rate. For composite cements it would judge based on the moisture content, with a relatively low threshold of 2.7%. Air cured concrete often retains more than 2% of moisture through exchange with atmosphere [101], thus, the limit value used by the ML algorithm could easily be achieved in humid regions.

On the center left branches (levels 4.2 to 6.2 in Figure 6.10), the algorithm has detected the tendency of bigger samples to spall more easily [51]. The limit of 0.39 m^3 is large for most laboratory experiments, translating into a cube of about 75 cm side, or a slab of 1.5 m sides and 18 cm depth. This, once again, shows the importance of large scale experiments as the actual structures have much larger elements, but laboratory tests assume small samples to be representative. On the other side of the same branch, the right-most path shows that a unconfined, dry sample is not expected to spall with a much smaller PPI than 222. The new PPI of 64 would mean a dosage of 0.34 kg/m^3 or 0.04% in volume of concrete, assuming PP fibers of 32 μm diameter and 6 mm length. This could be an important distinction in dosages, as inner elements require much less fibres than elements exposed to weather.

On section 4.3 to 6.3 of Figure 6.10, most branches lead to a situation in which the samples do not spall, as these are already samples with a high amount of polymeric fibres, slow heating and low maximum temperature. In case the fibres are not PP, it would require observation of the APPI, and if the sample has very high compressive strength (in

the order of about 140 MPa, it would require at least 6 MPa of tensile strength to assume resistance to spalling with relative certainty.

Finally, on the right-most branches of the decision tree (levels 4.4 to 6.4 in Figure 6.10), it is observed again the volume playing a key role. Now the identified limit was 0.82 m^3, which would be a cube with 94 cm sides or a slab with 2 m sides and 20 cm depth. On the other side of the branches it sets a new PPI threshold of 1088. This is not surprising as this is considering only sample with compressive strength superior to 105 MPa. The value of 1088 would mean 5.8 kg/m^3 of PP fibres (assuming 32 μm diameter and 6 mm length) or 0.6% in volume of concrete. Further, the cement content is also considered, with smaller contents leading to safer mixtures, presumably due to the the coarser pore structure [117].

OTHER MODELS

Several other algorithms were attempted to the same classification task. These included a Gaussian Naive Bayes classifier, support vector machine, K nearest neighbors, random forest, gradient tree boosting, histogram gradient boosting, multi-layer perceptron, and composite algorithms. For the composite classifiers, an ensemble of the four most accurate single classifiers was attempted, as well as stacking classifier, also using the four most accurate previous algorithms. A parametric study was performed in all cases trying to optimise accuracy. Table 6.3 shows the accuracy for all attempted classifiers.

Table 6.3: Accuracy achieved when classifying the database using different ML methods.

Classifier	Accuracy (%)
Logistic regression	77.91
Gaussian Naïve Bayes	70.98
Support vector machine	83.00
K nearest neighbors	85.27
Decision trees	82.61
Random forest	85.27
Gradient Tree Boosting	89.73
Histogram Gradient Boosting	86.28
Multi-layer perceptron	87.50
Ensemble	87.46
Stacking	87.05
Deep neural network	88.44

Finally, a small deep neural network was trained using Keras from TensorFlow2 [118]. The input layer had all the cases from the database used in all other ML classifiers. The number of layers and neurons in each layer was varied until an equilibrium in accuracy was found. The final shape of the network contained three hidden layers, with 800, 200 and 50 neurons, respectively. For each layer, L1 regularization of 0.0005 and L2 regularization of 0.01 were set. Between each layer, a dropout of 0.5 was set to help preventing overfitting. The learning rate was set as 0.0005 and the loss function was set as sparse categorical crossentropy. The model was run for 5000 epochs and the results are displayed in Figure 6.11.

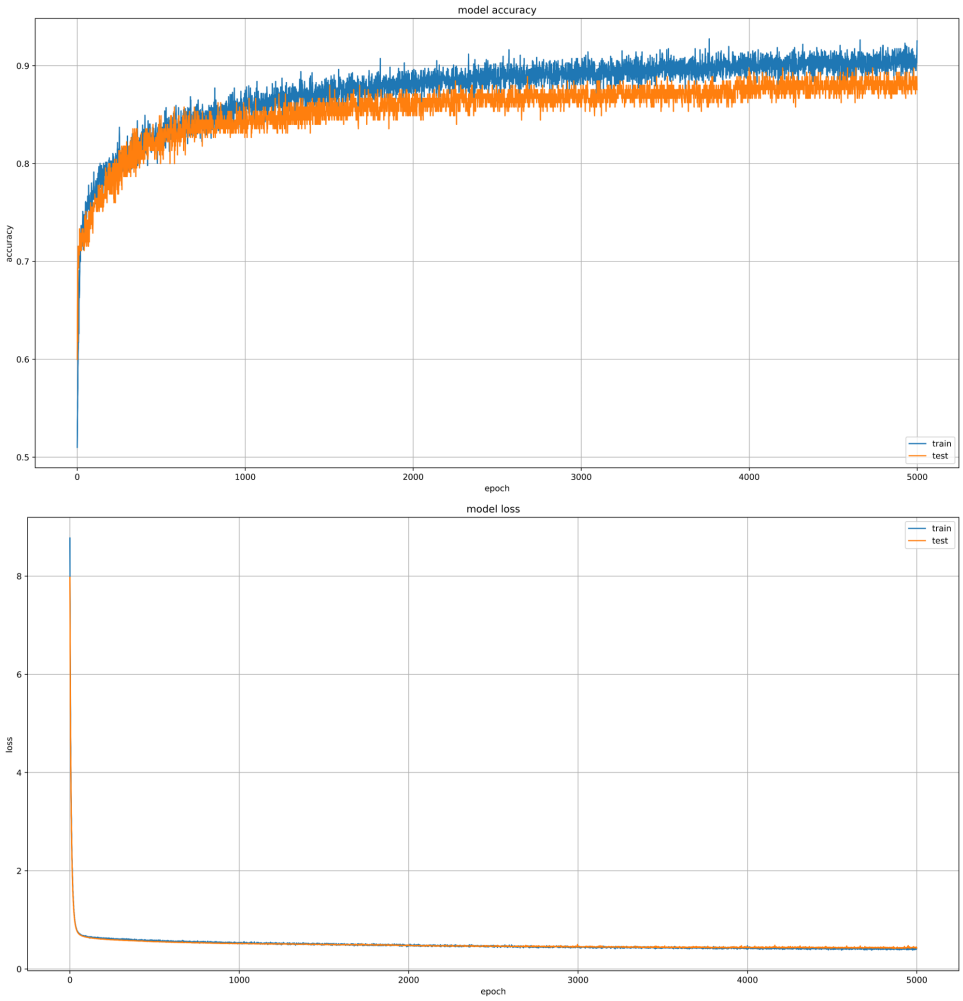

Figure 6.11: Results for accuracy and loss of deep neural network classifying the gathered database.

6.5. CONCLUSIONS

This chapter sought to identify the main parameters influencing spalling in concrete. To achieve this goal, a large database of more than 1000 unique samples was collected from 70 publications. The database included 40 properties for each studied sample besides information on spalling, spalling time, spalling temperature and spalling mass when available. Several assumptions were necessary to fill in unreported data from the publications, which decreased the accuracy of the information.

Analysis of the database pointed to some gaps in literature and possibly disadvantageous biases in experimental design. For example, most spalling tests are performed in small, unloaded samples for practical reasons, which causes a scarcity of full scale tests. Additionally, aggregate data (such as D_{max} and composition) is simply not reported, despite being proven to cause a great influence in samples resistance against spalling [14, 16, 38, 87, 94, 106, 109]. Testing of normal strength concrete is also scarce in literature, regardless of composing the vast majority of structures in danger of suffering from spalling. All of these should be considered moving forward with spalling research.

In order to use all the data collected to predict spalling, a number of machine learning classification tools were attempted. The model with keras and the gradient tree boosting were the classifiers to reach higher accuracy. Although falling short of the 90% goal, these were very close and could possibly surpass it given more time or the involvement of a programming specialist. Because the visualization of the inner workings of some of the algorithms provided further insights on the most influential parameters to determine spalling resistance of concrete samples, gradient tree boosting seems ideal for this application. A similar code to what generated Figure 6.10 could be used to reveal the decision tree paths created by this algorithm and serve as guidelines for engineers in practice.

However, some level of randomness was still observed through examples in which samples with the exact same characteristics would behave differently (i. e. one sample spalls and the other doesn't). This could be addressed in two manners, one could enlarge and improve the database until there is enough statistical redundancy that the algorithm can account for this cases. This would require a considerably larger database with at least ten thousand samples in opposition of one thousand.

The other option would be to address the poor description of the microstructure in the samples. Many of the properties present in the database, such as, w/c ratio, cement content, plasticizer dosage and compressive strength, tensile strength, dosage of PP fibres, addition of silica fume, are indirect indications of porosity and pore connectivity in the samples. No direct measurement is available as spalling research rarely includes techniques like mercury intrusion porosimetry, electron microscopy or microtomography. This might be one of the biggest omissions, as currently the ML algorithms are trying to predict spalling resistance with very incomplete information. For this reason, it was decided to dedicate the Chapter 7 of the thesis to the pursuit of the influence of porosity and pore connectivity to the phenomena of spalling.

BIBLIOGRAPHY

[1] F. W. PRESTON and H. E. WHITE. "OBSERVATIONS ON SPALLING*". In: *Journal of the American Ceramic Society* 17.1-12 (1934), pp. 137–144. DOI: https://doi.org/10.1111/j.1151-2916.1934.tb19296.x. eprint: https://ceramics.onlinelibrary.wiley.com/doi/pdf/10.1111/j.1151-2916.1934.tb19296.x. URL: https://ceramics.onlinelibrary.wiley.com/doi/abs/10.1111/j.1151-2916.1934.tb19296.x.

[2] Takeshi Morita et al. "an Experimental Study on Improvement of Spalling Behavior of High-Strength Concrete Elements Under Fire Attack". In: *Journal of Structural and Construction Engineering (Transactions of AIJ)* 66.544 (2001), pp. 171–178. DOI: 10.3130/aijs.66.171_3.

[3] Francesco Lo Monte et al. "Assessment of concrete sensitivity to fire spalling: A multi-scale experimental approach". In: *Construction and Building Materials* 212 (2019), pp. 476–485. ISSN: 0950-0618. DOI: https://doi.org/10.1016/j.conbuildmat.2019.03.332. URL: https://www.sciencedirect.com/science/article/pii/S0950061819308402.

[4] Cristian Maluk et al. "Experimental study on the fire behaviour of fibre reinforced concrete used in tunnel applications". In: *Fire Safety Journal* 120 (2021). Fire Safety Science: Proceedings of the 13th International Symposium, p. 103173. ISSN: 0379-7112. DOI: https://doi.org/10.1016/j.firesaf.2020.103173. URL: https://www.sciencedirect.com/science/article/pii/S037971122030134X.

[5] A.M. Neville. *Properties of Concrete*. Pearson, 2011. ISBN: 9780273755807. URL: https://books.google.nl/books?id=TdfewmQ-cMIC.

[6] Pengfei Liu et al. "Uncertainty quantification of the effect of concrete heterogeneity on nonlinear seismic response of gravity dams including record-to-record variability". In: *Structures* 34 (2021), pp. 1785–1797. ISSN: 2352-0124. DOI: https://doi.org/10.1016/j.istruc.2021.08.098. URL: https://www.sciencedirect.com/science/article/pii/S2352012421008109.

[7] Sammy Y. N. Chan, Gai-fei Peng, and John K. W. Chan. "Comparison between high strength concrete and normal strength concrete subjected to high temperature". In: *Materials and Structures* 29.10 (Dec. 1996), pp. 616–619. ISSN: 1871-6873. DOI: 10.1007/BF02485969. URL: https://doi.org/10.1007/BF02485969.

[8] A. Noumowé et al. "High-Strength Self-Compacting Concrete Exposed to Fire Test". In: *Journal of Materials in Civil Engineering* 18.6 (2006), pp. 754–758. DOI: 10.1061/(ASCE)0899-1561(2006)18:6(754).

[9] Sun Bei and Lin Zhixiang. “Investigation on spalling resistance of ultra-high-strength concrete under rapid heating and rapid cooling”. In: *Case Studies in Construction Materials* 4 (2016), pp. 146–153. ISSN: 2214-5095. DOI: https://doi.org/10.1016/j.cscm.2016.04.001. URL: https://www.sciencedirect.com/science/article/pii/S2214509516300304.

[10] C. Kahanji, F. Ali, and A. Nadjai. “Explosive spalling of ultra-high performance fibre reinforced concrete beams under fire”. In: *Journal of Structural Fire Engineering* 7.4 (Jan. 2016), pp. 328–348. ISSN: 2040-2317. DOI: 10.1108/JSFE-12-2016-023. URL: https://doi.org/10.1108/JSFE-12-2016-023.

[11] L Missemer et al. “Fire spalling of ultra-high performance concrete : From a global analysis to microstructure investigations”. In: *Cement and Concrete Research* 115.April 2018 (2019), pp. 207–219. ISSN: 0008-8846. DOI: 10.1016/j.cemconres.2018.10.005. URL: https://doi.org/10.1016/j.cemconres.2018.10.005.

[12] Md Miah et al. “Fire spalling of concrete: Effect of cement type”. In: *4th International Workshop on Concrete Spalling Due to Fire Exposure*. RILEM. Leipzig, Germany: RILEM, Oct. 2015.

[13] Hussein Mohammed et al. “Heat-Induced Spalling of Concrete: A Review of the Influencing Factors and Their Importance to the Phenomenon”. In: *Materials* 15.5 (2022). ISSN: 1996-1944. DOI: 10.3390/ma15051693. URL: https://www.mdpi.com/1996-1944/15/5/1693.

[14] Zhu Pan, Jay G. Sanjayan, and Daniel L.Y. Kong. “Effect of aggregate size on spalling of geopolymer and Portland cement concretes subjected to elevated temperatures”. In: *Construction and Building Materials* 36 (2012), pp. 365–372. ISSN: 0950-0618. DOI: https://doi.org/10.1016/j.conbuildmat.2012.04.120. URL: https://www.sciencedirect.com/science/article/pii/S0950061812003224.

[15] Juan Yang et al. “On the explosive spalling behavior of ultra-high performance concrete with and without coarse aggregate exposed to high temperature”. In: *Construction and Building Materials* 226 (2019), pp. 932–944. ISSN: 0950-0618. DOI: https://doi.org/10.1016/j.conbuildmat.2019.07.299. URL: https://www.sciencedirect.com/science/article/pii/S0950061819319737.

[16] Ye Li et al. “Effect of aggregate size and inclusion of polypropylene and steel fibers on explosive spalling and pore pressure in ultra-high-performance concrete (UHPC) at elevated temperature”. In: *Cement and Concrete Composites* 99 (2019), pp. 62–71. ISSN: 0958-9465. DOI: https://doi.org/10.1016/j.cemconcomp.2019.02.016. URL: https://www.sciencedirect.com/science/article/pii/S0958946518306504.

[17] Young-Sun Heo et al. “Synergistic effect of combined fibers for spalling protection of concrete in fire”. In: *Cement and Concrete Research* 40.10 (2010), pp. 1547–1554. ISSN: 0008-8846. DOI: https://doi.org/10.1016/j.cemconres.2010.

06.011. URL: https://www.sciencedirect.com/science/article/pii/S0008884610001596.

[18] Dong Zhang et al. "Effect of natural fibers on thermal spalling resistance of ultra-high performance concrete". In: *Cement and Concrete Composites* 109 (2020), p. 103512. ISSN: 0958-9465. DOI: https://doi.org/10.1016/j.cemconcomp.2020.103512. URL: https://www.sciencedirect.com/science/article/pii/S0958946520300032.

[19] Dong Zhang, Guan Yu Tan, and Kang Hai Tan. "Combined effect of flax fibers and steel fibers on spalling resistance of ultra-high performance concrete at high temperature". In: *Cement and Concrete Composites* 121 (2021), p. 104067. ISSN: 0958-9465. DOI: https://doi.org/10.1016/j.cemconcomp.2021.104067. URL: https://www.sciencedirect.com/science/article/pii/S0958946521001360.

[20] Michal Beneš and Radek Štefan. "Hygro-thermo-mechanical analysis of spalling in concrete walls at high temperatures as a moving boundary problem". In: *International Journal of Heat and Mass Transfer* 85 (2015), pp. 110–134. ISSN: 0017-9310. DOI: https://doi.org/10.1016/j.ijheatmasstransfer.2015.01.050. URL: https://www.sciencedirect.com/science/article/pii/S0017931015000587.

[21] Yiming Zhang et al. "Fast assessing spalling risk of tunnel linings under RABT fire: From a coupled thermo-hydro-chemo-mechanical model towards an estimation method". In: *Engineering Structures* 142 (2017), pp. 1–19. ISSN: 0141-0296. DOI: https://doi.org/10.1016/j.engstruct.2017.03.068. URL: https://www.sciencedirect.com/science/article/pii/S0141029617310623.

[22] Antonio Caggiano et al. "Meso-scale response of concrete under high temperature based on coupled thermo-mechanical and pore-pressure interface modeling". In: *Engineering Failure Analysis* 85 (2018), pp. 167–188. ISSN: 1350-6307. DOI: https://doi.org/10.1016/j.engfailanal.2017.11.016. URL: https://www.sciencedirect.com/science/article/pii/S135063071731107X.

[23] *EN 1992-1-2 Eurocode 2: Design of concrete structures - Part 1-2: General Rules – Structural fire design*. EN. Brussels: CEN, 2008.

[24] *DBJ/T 15-81 – Code for fire resistance design of concrete structures in buildings*. Guangdong Province, China, 2011.

[25] *ASTM E119-20 – Standard Test Methods for Fire Tests of Building Construction and Materials*. ASTM, 2020. DOI: DOI:10.1520/E0119-20.

[26] *AS 3600:2018 Sup 1 – Concrete structures – Commentary (Supplement 1 to AS 3600:2018)*. 2022. ISBN: 978-1-76113-697-9.

[27] *ISO 834-1. Fire-resistance tests – Elements of building construction – Part 1: General requirement*. 1999.

[28] Young-Sun Heo et al. “Limited effect of diameter of fibres on spalling protection of concrete in fire”. In: *Materials and Structures* 45.3 (Mar. 2012), pp. 325–335. ISSN: 1871-6873. DOI: 10.1617/s11527-011-9768-z. URL: https://doi.org/10.1617/s11527-011-9768-z.

[29] Cristian Maluk, Luke Bisby, and Giovanni P. Terrasi. “Effects of polypropylene fibre type and dose on the propensity for heat-induced concrete spalling”. In: *Engineering Structures* 141 (2017), pp. 584–595. ISSN: 0141-0296. DOI: https://doi.org/10.1016/j.engstruct.2017.03.058. URL: https://www.sciencedirect.com/science/article/pii/S0141029617310337.

[30] E.R. Gallyamov et al. “Multi-scale modelling of concrete structures affected by alkali-silica reaction: Coupling the mesoscopic damage evolution and the macroscopic concrete deterioration”. In: *International Journal of Solids and Structures* 207 (2020), pp. 262–278. ISSN: 0020-7683. DOI: https://doi.org/10.1016/j.ijsolstr.2020.10.010. URL: https://www.sciencedirect.com/science/article/pii/S0020768320303942.

[31] G. Mazzucco, C.E. Majorana, and V.A. Salomoni. “Numerical simulation of polypropylene fibres in concrete materials under fire conditions”. In: *Computers Structures* 154 (2015), pp. 17–28. ISSN: 0045-7949. DOI: https://doi.org/10.1016/j.compstruc.2015.03.012. URL: https://www.sciencedirect.com/science/article/pii/S0045794915001029.

[32] Jin-Cheng Liu and Yao Zhang. “A Simplified Model to Predict Thermo-Hygral Behaviour and Explosive Spalling of Concrete”. In: *Journal of Advanced Concrete Technology* 17.7 (2019), pp. 419–433. DOI: 10.3151/jact.17.419.

[33] Antonio Caggiano and Guillermo Etse. “Coupled thermo–mechanical interface model for concrete failure analysis under high temperature”. In: *Computer Methods in Applied Mechanics and Engineering* 289 (2015), pp. 498–516. ISSN: 0045-7825. DOI: https://doi.org/10.1016/j.cma.2015.02.016. URL: https://www.sciencedirect.com/science/article/pii/S0045782515000651.

[34] Keith T. Butler et al. “Machine learning for molecular and materials science”. In: *Nature* 559.7715 (July 2018), pp. 547–555. ISSN: 1476-4687. DOI: 10.1038/s41586-018-0337-2. URL: https://doi.org/10.1038/s41586-018-0337-2.

[35] Gus L. W. Hart et al. “Machine learning for alloys”. In: *Nature Reviews Materials* 6.8 (Aug. 2021), pp. 730–755. ISSN: 2058-8437. DOI: 10.1038/s41578-021-00340-w. URL: https://doi.org/10.1038/s41578-021-00340-w.

[36] Jonathan Lapeyre et al. “Machine learning enables prompt prediction of hydration kinetics of multicomponent cementitious systems”. In: *Scientific Reports* 11.1 (Feb. 2021), p. 3922. ISSN: 2045-2322. DOI: 10.1038/s41598-021-83582-6. URL: https://doi.org/10.1038/s41598-021-83582-6.

[37] Sławomir Czarnecki et al. “Design of a machine learning model for the precise manufacturing of green cementitious composites modified with waste granite powder”. In: *Scientific Reports* 12.1 (Aug. 2022), p. 13242. ISSN: 2045-2322. DOI: 10.1038/s41598-022-17670-6. URL: https://doi.org/10.1038/s41598-022-17670-6.

[38] Young-Sun Heo et al. “Relationship between inter-aggregate spacing and the optimum fiber length for spalling protection of concrete in fire”. In: *Cement and Concrete Research* 42.3 (2012), pp. 549–557. ISSN: 0008-8846. DOI: https://doi.org/10.1016/j.cemconres.2011.12.002. URL: https://www.sciencedirect.com/science/article/pii/S0008884611003061.

[39] Hadjira Bensalem et al. “Analysis of thermal-induced spalling tests on high to ultra-high performance concrete subjected to standard fire”. In: *Case Studies in Construction Materials* 15.July (2021), e00704. ISSN: 22145095. DOI: 10.1016/j.cscm.2021.e00704. URL: https://doi.org/10.1016/j.cscm.2021.e00704.

[40] G. Debicki, R. Haniche, and F. Delhomme. “An experimental method for assessing the spalling sensitivity of concrete mixture submitted to high temperature”. In: *Cement and Concrete Composites* 34.8 (2012), pp. 958–963. ISSN: 0958-9465. DOI: https://doi.org/10.1016/j.cemconcomp.2012.04.002. URL: https://www.sciencedirect.com/science/article/pii/S0958946512000637.

[41] Ye Li et al. “Pore pressure build-up and explosive spalling in concrete at elevated temperature: A review”. In: *Construction and Building Materials* 284 (2021). ISSN: 09500618. DOI: 10.1016/j.conbuildmat.2021.122818.

[42] T.M. Jeyashree, P.R. Kannan Rajkumar, and K.S. Satyanarayanan. “Developments and research on fire response behaviour of prestressed concrete members – A review”. In: *Journal of Building Engineering* 57 (2022), p. 104797. ISSN: 2352-7102. DOI: https://doi.org/10.1016/j.jobe.2022.104797. URL: https://www.sciencedirect.com/science/article/pii/S2352710222008105.

[43] Auélien Géron. *Hands-On Machine Learning with Scikit-Learn & TensorFlow*. OREILLY, 2017. ISBN: 9781491962299.

[44] Young-Sun Heo et al. “Critical parameters of nylon and other fibres for spalling protection of high strength concrete in fire”. In: *Materials and Structures* 44.3 (Apr. 2011), pp. 599–610. ISSN: 1871-6873. DOI: 10.1617/s11527-010-9651-3. URL: https://doi.org/10.1617/s11527-010-9651-3.

[45] Guncheol Lee et al. “Combining polypropylene and nylon fibers to optimize fiber addition for spalling protection of high-strength concrete”. In: *Construction and Building Materials* 34 (2012), pp. 313–320. ISSN: 0950-0618. DOI: https://doi.org/10.1016/j.conbuildmat.2012.02.015. URL: https://www.sciencedirect.com/science/article/pii/S095006181200092X.

[46] Rodgers Bangi Mugume and Takashi Horiguchi. “Prediction of spalling in fibre-reinforced high strength concrete at elevated temperatures”. In: *Materials and Structures* 47.4 (Apr. 2014), pp. 591–604. ISSN: 1871-6873. DOI: 10.1617/s11527-013-0082-9. URL: https://doi.org/10.1617/s11527-013-0082-9.

[47] Mitsuo Ozawa and Hiroaki Morimoto. “Effects of various fibres on high-temperature spalling in high-performance concrete”. In: *Construction and Building Materials* 71 (2014), pp. 83–92. ISSN: 0950-0618. DOI: https://doi.org/10.1016/j.conbuildmat.2014.07.068. URL: https://www.sciencedirect.com/science/article/pii/S0950061814008265.

[48] Ana Da Luz, M.A.L. Braulio, and Victor Pandolfelli. *F.I.R.E. Compendium Series - Refractory Castable Engineering*. Göller Verlag, Mar. 2015, p. 734. ISBN: ISBN 978-3-87264-004-8.

[49] Z Bazant. “Analysis of Pore Pressure, Thermal Stress and Fracture in Rapidly Heated Concrete”. en. In: International Workshop on Fire Performance of High-Strength Concrete. Proceedings. Appendix B: Workshop Papers. B10, Gaithersburg, MD, 1997-02-13 1997. URL: https://tsapps.nist.gov/publication/get_pdf.cfm?pub_id=916655.

[50] Pierre Kalifa, François-Dominique Menneteau, and Daniel Quenard. “Spalling and pore pressure in HPC at high temperatures”. In: *Cement and Concrete Research* 30.12 (2000). Papers presented at the Symposium on "Transport Properties and Microstructure of Cement-Based Systems", pp. 1915–1927. ISSN: 0008-8846. DOI: https://doi.org/10.1016/S0008-8846(00)00384-7. URL: https://www.sciencedirect.com/science/article/pii/S0008884600003847.

[51] Jean-Christophe Mindeguia et al. “Experimental discussion on the mechanisms behind the fire spalling of concrete”. In: *Fire and Materials* 39.7 (2015), pp. 619–635. DOI: https://doi.org/10.1002/fam.2254. eprint: https://onlinelibrary.wiley.com/doi/pdf/10.1002/fam.2254. URL: https://onlinelibrary.wiley.com/doi/abs/10.1002/fam.2254.

[52] M. B. Dwaikat and V. K. R. Kodur. “Fire Induced Spalling in High Strength Concrete Beams”. In: *Fire Technology* 46.1 (Apr. 2009), p. 251. ISSN: 1572-8099. DOI: 10.1007/s10694-009-0088-6. URL: https://doi.org/10.1007/s10694-009-0088-6.

[53] N. Algourdin et al. “Influence of polypropylene and steel fibres on thermal spalling and physical-mechanical properties of concrete under different heating rates”. In: *Construction and Building Materials* 259 (2020), p. 119690. ISSN: 0950-0618. DOI: https://doi.org/10.1016/j.conbuildmat.2020.119690. URL: https://www.sciencedirect.com/science/article/pii/S0950061820316950.

[54] Kristian Hertz. *Heat-induced Explosion of Dense Concretes*. English. Report no. 166. Technical University of Denmark, Department of Civil Engineering, 1984.

[55] F. A. Ali, D. O’Connor, and A. Abu-Tair. “Explosive spalling of high-strength concrete columns in fire”. In: *Magazine of Concrete Research* 53.3 (2001), pp. 197–204. DOI: 10.1680/macr.2001.53.3.197. eprint: https://doi.org/10.1680/macr.2001.53.3.197. URL: https://doi.org/10.1680/macr.2001.53.3.197.

[56] L. T. Phan, J. R. Lawson, and F. L. Davis. “Effects of elevated temperature exposure on heating characteristics, spalling, and residual properties of high performance concrete”. In: *Materials and Structures* 34.2 (Mar. 2001), pp. 83–91. ISSN: 1871-6873. DOI: 10.1007/BF02481556. URL: https://doi.org/10.1007/BF02481556.

[57] A Bilodeau, V.K.R Kodur, and G.C Hoff. “Optimization of the type and amount of polypropylene fibres for preventing the spalling of lightweight concrete subjected to hydrocarbon fire”. In: *Cement and Concrete Composites* 26.2 (2004). Fire Resistance, pp. 163–174. ISSN: 0958-9465. DOI: https://doi.org/10.1016/S0958-9465(03)00085-4. URL: https://www.sciencedirect.com/science/article/pii/S0958946503000854.

[58] Cheon-Goo Han et al. “Performance of spalling resistance of high performance concrete with polypropylene fiber contents and lateral confinement”. In: *Cement and Concrete Research* 35.9 (2005), pp. 1747–1753. ISSN: 0008-8846. DOI: https://doi.org/10.1016/j.cemconres.2004.11.013. URL: https://www.sciencedirect.com/science/article/pii/S0008884604005101.

[59] Lars Boström, Ulf Wickström, and Bijan Adl-Zarrabi. “Effect of specimen size and loading conditions on spalling of concrete”. In: *Fire and Materials* 31.3 (2007), pp. 173–186. DOI: https://doi.org/10.1002/fam.931. eprint: https://onlinelibrary.wiley.com/doi/pdf/10.1002/fam.931. URL: https://onlinelibrary.wiley.com/doi/abs/10.1002/fam.931.

[60] X. Liu et al. “On the mechanism of polypropylene fibres in preventing fire spalling in self-compacting and high-performance cement paste”. In: *Cement and Concrete Research* 38.4 (2008), pp. 487–499. ISSN: 0008-8846. DOI: https://doi.org/10.1016/j.cemconres.2007.11.010. URL: https://www.sciencedirect.com/science/article/pii/S0008884607002931.

[61] Long T. Phan. “Pore pressure and explosive spalling in concrete”. In: *Materials and Structures* 41.10 (Dec. 2008), pp. 1623–1632. ISSN: 1871-6873. DOI: 10.1617/s11527-008-9353-2. URL: https://doi.org/10.1617/s11527-008-9353-2.

[62] Cheon-Goo Han, Min-Cheol Han, and Young-Sun Heo. “Improvement of residual compressive strength and spalling resistance of high-strength RC columns subjected to fire”. In: *Construction and Building Materials* 23.1 (2009), pp. 107–116. ISSN: 0950-0618. DOI: https://doi.org/10.1016/j.conbuildmat.2008.01.011. URL: https://www.sciencedirect.com/science/article/pii/S0950061808000342.

[63] W.Z. Zheng et al. “Experimental study on concrete spalling in prestressed slabs subjected to fire”. In: *Fire Safety Journal* 45.5 (2010), pp. 283–297. ISSN: 0379-7112. DOI: https://doi.org/10.1016/j.firesaf.2010.06.001. URL: https://www.sciencedirect.com/science/article/pii/S0379711210000482.

[64] Faris Ali, Ali Nadjai, and Abid Abu-Tair. “Explosive spalling of normal strength concrete slabs subjected to severe fire”. In: *Materials and Structures* 44.5 (June 2011), pp. 943–956. ISSN: 1871-6873. DOI: 10.1617/s11527-010-9678-5. URL: https://doi.org/10.1617/s11527-010-9678-5.

[65] Mugume Rodgers Bangi and Takashi Horiguchi. “Pore pressure development in hybrid fibre-reinforced high strength concrete at elevated temperatures”. In: *Cement and Concrete Research* 41.11 (2011), pp. 1150–1156. ISSN: 0008-8846. DOI: https://doi.org/10.1016/j.cemconres.2011.07.001. URL: https://www.sciencedirect.com/science/article/pii/S000888461100192X.

[66] Young-Sun Heo et al. “Construction application of Fibre/Mesh method for protecting concrete columns in fire”. In: *Construction and Building Materials* 25.6 (2011), pp. 2928–2938. ISSN: 0950-0618. DOI: https://doi.org/10.1016/j.conbuildmat.2010.12.017. URL: https://www.sciencedirect.com/science/article/pii/S095006181000694X.

[67] Robert Jansson and Lars Boström. “Factors influencing fire spalling of self compacting concrete”. In: *Materials and Structures* 46.10 (Oct. 2013), pp. 1683–1694. ISSN: 1871-6873. DOI: 10.1617/s11527-012-0007-z. URL: https://doi.org/10.1617/s11527-012-0007-z.

[68] Carré, H. et al. “Effect of compressive loading on the risk of spalling”. In: *MATEC Web of Conferences* 6 (2013), p. 01007. DOI: 10.1051/matecconf/20130601007. URL: https://doi.org/10.1051/matecconf/20130601007.

[69] K.K. Sideris and P. Manita. “Residual mechanical characteristics and spalling resistance of fiber reinforced self-compacting concretes exposed to elevated temperatures”. In: *Construction and Building Materials* 41 (2013), pp. 296–302. ISSN: 0950-0618. DOI: https://doi.org/10.1016/j.conbuildmat.2012.11.093. URL: https://www.sciencedirect.com/science/article/pii/S0950061812009294.

[70] Eike Klingsch, Andrea Frangi, and Mario Fontana. *Explosive spalling of concrete in fire. Test report.* en. Report. Zürich, 2013. DOI: 10.3929/ethz-a-010076314.

[71] Pietro Lura and Giovanni Pietro Terrasi. “Reduction of fire spalling in high-performance concrete by means of superabsorbent polymers and polypropylene fibers: Small scale fire tests of carbon fiber reinforced plastic-prestressed self-compacting concrete”. In: *Cement and Concrete Composites* 49 (2014), pp. 36–42. ISSN: 0958-9465. DOI: https://doi.org/10.1016/j.cemconcomp.2014.02.001. URL: https://www.sciencedirect.com/science/article/pii/S0958946514000304.

[72] Yang Ju et al. “An experimental investigation of the thermal spalling of polypropylene-fibered reactive powder concrete exposed to elevated temperatures”. In: *Science Bulletin* 60.23 (2015), pp. 2022–2040. ISSN: 2095-9273. DOI: https://doi.org/10.1007/s11434-015-0939-0. URL: https://www.sciencedirect.com/science/article/pii/S2095927316302560.

[73] Young-Sun Heo, Cheon-Goo Han, and Kyoung-Min Kim. “Combined fiber technique for spalling protection of concrete column, slab and beam in fire”. In: *Materials and Structures* 48.10 (Oct. 2015), pp. 3377–3390. ISSN: 1871-6873. DOI: 10.1617/s11527-014-0406-4. URL: https://doi.org/10.1617/s11527-014-0406-4.

[74] Steve Werner and Andreas Rogge. “The effect of various fire-exposed surface dimensions on the spalling of concrete specimens”. In: *Fire and Materials* 39.5 (2015), pp. 545–556. DOI: https://doi.org/10.1002/fam.2256. eprint: https://onlinelibrary.wiley.com/doi/pdf/10.1002/fam.2256. URL: https://onlinelibrary.wiley.com/doi/abs/10.1002/fam.2256.

[75] I. Rickard et al. “Predictive testing for heat-induced spalling of concrete”. In: *Structural Engineering: Providing Solutions to Global Challenges*. International Association for Bridge and Structural Engineering (IABSE). Zurich, Switzerland: International Association for Bridge and Structural Engineering (IABSE), 2015.

[76] Yining Ding et al. “Influence of different fibers on the change of pore pressure of self-consolidating concrete exposed to fire”. In: *Construction and Building Materials* 113 (2016), pp. 456–469. ISSN: 0950-0618. DOI: https://doi.org/10.1016/j.conbuildmat.2016.03.070. URL: https://www.sciencedirect.com/science/article/pii/S0950061816303658.

[77] Asif H. Shah and U.K. Sharma. “Fire resistance and spalling performance of confined concrete columns”. In: *Construction and Building Materials* 156 (2017), pp. 161–174. ISSN: 0950-0618. DOI: https://doi.org/10.1016/j.conbuildmat.2017.08.167. URL: https://www.sciencedirect.com/science/article/pii/S0950061817317750.

[78] N. Yermak et al. “Influence of steel and/or polypropylene fibres on the behaviour of concrete at high temperature: Spalling, transfer and mechanical properties”. In: *Construction and Building Materials* 132 (2017), pp. 240–250. ISSN: 0950-0618. DOI: https://doi.org/10.1016/j.conbuildmat.2016.11.120. URL: https://www.sciencedirect.com/science/article/pii/S095006181631889X.

[79] N.K. Lee et al. “Microstructural investigation of calcium aluminate cement-based ultra-high performance concrete (UHPC) exposed to high temperatures”. In: *Cement and Concrete Research* 102 (2017), pp. 109–118. ISSN: 0008-8846. DOI: https://doi.org/10.1016/j.cemconres.2017.09.004. URL: https://www.sciencedirect.com/science/article/pii/S0008884617301825.

[80] Yang Ju et al. “Experimental investigation of the effect of silica fume on the thermal spalling of reactive powder concrete”. In: *Construction and Building Materials* 155 (2017), pp. 571–583. ISSN: 0950-0618. DOI: https://doi.org/10.1016/j.conbuildmat.2017.08.086. URL: https://www.sciencedirect.com/science/article/pii/S0950061817316781.

[81] Wasim Khaliq and Farhan Waheed. “Mechanical response and spalling sensitivity of air entrained high-strength concrete at elevated temperatures”. In: *Construction and Building Materials* 150 (2017), pp. 747–757. ISSN: 0950-0618. DOI: https://doi.org/10.1016/j.conbuildmat.2017.06.039. URL: https://www.sciencedirect.com/science/article/pii/S0950061817311807.

[82] Msheer Hasan Ali, Youkhanna Zayia Dinkha, and James H. Haido. “Mechanical properties and spalling at elevated temperature of high performance concrete made with reactive and waste inert powders”. In: *Engineering Science and Technology, an International Journal* 20.2 (2017), pp. 536–541. ISSN: 2215-0986. DOI: https://doi.org/10.1016/j.jestch.2016.12.004. URL: https://www.sciencedirect.com/science/article/pii/S2215098616308515.

[83] Xiangwei Liang et al. “Development of ultra-high performance concrete with high fire resistance”. In: *Construction and Building Materials* 179 (2018), pp. 400–412. ISSN: 09500618. DOI: 10.1016/j.conbuildmat.2018.05.241.

[84] Gai-Fei Peng et al. “Combined curing as a novel approach to improve resistance of ultra-high performance concrete to explosive spalling under high temperature and its mechanical properties”. In: *Cement and Concrete Research* 109 (2018), pp. 147–158. ISSN: 0008-8846. DOI: https://doi.org/10.1016/j.cemconres.2018.04.011. URL: https://www.sciencedirect.com/science/article/pii/S0008884617301886.

[85] Dong Zhang, Aravind Dasari, and Kang Hai Tan. “On the mechanism of prevention of explosive spalling in ultra-high performance concrete with polymer fibers”. In: *Cement and Concrete Research* 113 (2018), pp. 169–177. ISSN: 0008-8846. DOI: https://doi.org/10.1016/j.cemconres.2018.08.012. URL: https://www.sciencedirect.com/science/article/pii/S0008884617311122.

[86] Jin-Cheng Liu and Kang Hai Tan. “Mechanism of PVA fibers in mitigating explosive spalling of engineered cementitious composite at elevated temperature”. In: *Cement and Concrete Composites* 93 (2018), pp. 235–245. ISSN: 0958-9465. DOI: https://doi.org/10.1016/j.cemconcomp.2018.07.015. URL: https://www.sciencedirect.com/science/article/pii/S095894651830043X.

[87] Hager, Izabela, Mróz, Katarzyna, and Tracz, Tomasz. “Concrete propensity to fire spalling: testing and observations”. In: *MATEC Web of Conferences* 163 (2018), p. 02004. DOI: 10.1051/matecconf/201816302004. URL: https://doi.org/10.1051/matecconf/201816302004.

[88] Gyeongcheol Choe et al. “Effect of moisture migration and water vapor pressure build-up with the heating rate on concrete spalling type”. In: *Cement and Concrete Research* 116.August 2017 (2019), pp. 1–10. ISSN: 00088846. DOI: 10.1016/j.cemconres.2018.10.021. URL: https://doi.org/10.1016/j.cemconres.2018.10.021.

[89] Shamsad Ahmad et al. “Mechanical properties of steel fiber-reinforced UHPC mixtures exposed to elevated temperature: Effects of exposure duration and fiber content”. In: *Composites Part B: Engineering* 168.December 2018 (2019), pp. 291–301. ISSN: 13598368. DOI: 10.1016/j.compositesb.2018.12.083. URL: https://doi.org/10.1016/j.compositesb.2018.12.083.

[90] Ye Li, Kang Hai Tan, and En-Hua Yang. “Synergistic effects of hybrid polypropylene and steel fibers on explosive spalling prevention of ultra-high performance concrete at elevated temperature”. In: *Cement and Concrete Composites* 96 (2019), pp. 174–181. ISSN: 0958-9465. DOI: https://doi.org/10.1016/j.cemconcomp.2018.11.009. URL: https://www.sciencedirect.com/science/article/pii/S0958946517307102.

[91] Ibrahim H. Alfahdawi et al. “Influence of PET wastes on the environment and high strength concrete properties exposed to high temperatures”. In: *Construction and Building Materials* 225 (2019), pp. 358–370. ISSN: 0950-0618. DOI: https://doi.org/10.1016/j.conbuildmat.2019.07.214. URL: https://www.sciencedirect.com/science/article/pii/S0950061819318987.

[92] Fabio P. Figueiredo et al. “Effects of Recycled Steel and Polymer Fibres on Explosive Fire Spalling of Concrete”. In: *Fire Technology* 55.5 (Sept. 2019), pp. 1495–1516. ISSN: 1572-8099. DOI: 10.1007/s10694-019-00817-9. URL: https://doi.org/10.1007/s10694-019-00817-9.

[93] T.M. Viana et al. “Behaviour of ultra-high performance concretes incorporating carbon nanotubes under thermal load”. In: *Construction and Building Materials* 263 (2020), p. 120556. ISSN: 0950-0618. DOI: https://doi.org/10.1016/j.conbuildmat.2020.120556. URL: https://www.sciencedirect.com/science/article/pii/S0950061820325617.

[94] M. Maier et al. “An experimental fire-spalling assessment procedure for concrete mixtures”. In: *Construction and Building Materials* 232 (2020), p. 117172. ISSN: 0950-0618. DOI: https://doi.org/10.1016/j.conbuildmat.2019.117172. URL: https://www.sciencedirect.com/science/article/pii/S0950061819326248.

[95] Yong Du et al. “Experimental study on the spalling behaviour of ultra-high strength concrete in fire”. In: *Construction and Building Materials* 258 (2020), p. 120334. ISSN: 0950-0618. DOI: https://doi.org/10.1016/j.conbuildmat.2020.120334. URL: https://www.sciencedirect.com/science/article/pii/S0950061820323394.

[96] Dong Zhang and Kang Hai Tan. “Effect of various polymer fibers on spalling mitigation of ultra-high performance concrete at high temperature”. In: *Cement and Concrete Composites* 114 (2020), p. 103815. ISSN: 0958-9465. DOI: https://doi.org/10.1016/j.cemconcomp.2020.103815. URL: https://www.sciencedirect.com/science/article/pii/S0958946520303206.

[97] Ye Li, En-Hua Yang, and Kang Hai Tan. “Flexural behavior of ultra-high performance hybrid fiber reinforced concrete at the ambient and elevated temperature”. In: *Construction and Building Materials* 250 (2020), p. 118487. ISSN: 0950-0618. DOI: https://doi.org/10.1016/j.conbuildmat.2020.118487. URL: https://www.sciencedirect.com/science/article/pii/S095006182030492X.

[98] Jin-Cheng Liu and Zhigang Zhang. “A machine learning approach to predict explosive spalling of heated concrete”. In: *Archives of Civil and Mechanical Engineering* 20.4 (Oct. 2020), p. 134. ISSN: 1644-9665. DOI: 10.1007/s43452-020-00135-w. URL: https://doi.org/10.1007/s43452-020-00135-w.

[99] Marcus Maier, Matthias Zeiml, and Roman Lackner. “On the effect of pore-space properties and water saturation on explosive spalling of fire-loaded concrete”. In: *Construction and Building Materials* 231 (2020), p. 117150. ISSN: 0950-0618. DOI: https://doi.org/10.1016/j.conbuildmat.2019.117150. URL: https://www.sciencedirect.com/science/article/pii/S0950061819326029.

[100] Gyeongcheol Choe et al. “Influence of amorphous metallic fibers on spalling properties of high-strength concrete exposed to high temperature”. In: *Construction and Building Materials* 263 (2020), p. 120711. ISSN: 0950-0618. DOI: https://doi.org/10.1016/j.conbuildmat.2020.120711. URL: https://www.sciencedirect.com/science/article/pii/S0950061820327161.

[101] Jin-Cheng Liu et al. “Knowledge-enhanced data-driven models for quantifying the effectiveness of PP fibers in spalling prevention of ultra-high performance concrete”. In: *Construction and Building Materials* 299 (2021), p. 123946. ISSN: 0950-0618. DOI: https://doi.org/10.1016/j.conbuildmat.2021.123946. URL: https://www.sciencedirect.com/science/article/pii/S0950061821017062.

[102] Dong Zhang et al. “Effect of spatial distribution of polymer fibers on preventing spalling of UHPC at high temperatures”. In: *Cement and Concrete Research* 140 (2021), p. 106281. ISSN: 0008-8846. DOI: https://doi.org/10.1016/j.cemconres.2020.106281. URL: https://www.sciencedirect.com/science/article/pii/S0008884620315611.

[103] Dong Zhang, Yuchen Liu, and Kang Hai Tan. “Spalling resistance and mechanical properties of strain-hardening ultra-high performance concrete at elevated temperature”. In: *Construction and Building Materials* 266 (2021), p. 120961. ISSN: 0950-0618. DOI: https://doi.org/10.1016/j.conbuildmat.2020.120961. URL: https://www.sciencedirect.com/science/article/pii/S0950061820329664.

[104] *ACI PRC-209-92 Prediction of Creep, Shrinkage, and Temperature Effects in Concrete Structures*. ACI, 2002.

[105] *EN 1992-1-1 Eurocode 2: Design of concrete structures – Part 1-1: General rules and rules for buildings*. EN. Brussels: CEN, 2011.

[106] Wouter Botte and Robby Caspeele. "Post-cooling properties of concrete exposed to fire". In: *Fire Safety Journal* 92.May (2017), pp. 142–150. ISSN: 03797112. DOI: 10.1016/j.firesaf.2017.06.010. URL: http://dx.doi.org/10.1016/j.firesaf.2017.06.010.

[107] D. Cree, M. Green, and A. Noumowé. "Residual strength of concrete containing recycled materials after exposure to fire: A review". In: *Construction and Building Materials* 45 (2013), pp. 208–223. ISSN: 09500618. DOI: 10.1016/j.conbuildmat.2013.04.005. URL: http://dx.doi.org/10.1016/j.conbuildmat.2013.04.005.

[108] Mitsuo Ozawa et al. "Preventive effects of polypropylene and jute fibers on spalling of UHPC at high temperatures in combination with waste porous ceramic fine aggregate as an internal curing material". In: *Construction and Building Materials* 206 (2019), pp. 219–225. ISSN: 0950-0618. DOI: https://doi.org/10.1016/j.conbuildmat.2019.02.056. URL: https://www.sciencedirect.com/science/article/pii/S0950061819303514.

[109] Ye Li, Kang Hai Tan, and En-hua Yang. "Influence of aggregate size and inclusion of polypropylene and steel fibers on the hot permeability of ultra-high performance concrete (UHPC) at elevated temperature". In: *Construction and Building Materials* 169 (2018), pp. 629–637. DOI: 10.1016/j.conbuildmat.2018.01.105.

[110] R.E. Bellman. *Dynamic Programming*. Dover Books on Computer Science Series. Dover Publications, 2003. ISBN: 9780486428093. URL: https://books.google.nl/books?id=fyVtp3EMxasC.

[111] Vivien Cabannes et al. "Overcoming the curse of dimensionality with Laplacian regularization in semi-supervised learning". In: (2020). DOI: 10.48550/ARXIV.2009.04324. URL: https://arxiv.org/abs/2009.04324.

[112] Vladimir Pestov. "Is the k-NN classifier in high dimensions affected by the curse of dimensionality?" In: *Computers Mathematics with Applications* 65.10 (2013). Grasping Complexity, pp. 1427–1437. ISSN: 0898-1221. DOI: https://doi.org/10.1016/j.camwa.2012.09.011. URL: https://www.sciencedirect.com/science/article/pii/S0898122112006426.

[113] Amir Salimi et al. "Using a Feature Subset Selection method and Support Vector Machine to address curse of dimensionality and redundancy in Hyperion hyperspectral data classification". In: *The Egyptian Journal of Remote Sensing and Space Science* 21.1 (2018), pp. 27–36. ISSN: 1110-9823. DOI: https://doi.org/10.1016/j.ejrs.2017.02.003. URL: https://www.sciencedirect.com/science/article/pii/S1110982317300571.

[114] Lars Grüne. "Overcoming the curse of dimensionality for approximating Lyapunov functions with deep neural networks under a small-gain condition". In: *IFAC-PapersOnLine* 54.9 (2021). 24th International Symposium on Mathematical Theory of Networks and Systems MTNS 2020, pp. 317–322. ISSN: 2405-8963. DOI: https://doi.org/10.1016/j.ifacol.2021.06.152. URL: https://www.sciencedirect.com/science/article/pii/S2405896321006467.

[115] F. Pedregosa et al. “Scikit-learn: Machine Learning in Python”. In: *Journal of Machine Learning Research* 12 (2011), pp. 2825–2830.

[116] *NEN-EN 1363:1999 – Fire resistance tests – Part 1: General requirements*. Standard. Delft, NL: Nederlands Normalisatie-instituut, Aug. 1999.

[117] P.K. Mehta and P.J.M. Monteiro. *Concrete: Microstructure, Properties, and Materials*. McGraw Hill professional. McGraw-Hill Education, 2006. ISBN: 9780071462891. URL: https://books.google.nl/books?id=3j5EAQAAIAAJ.

[118] Martín Abadi et al. *TensorFlow: Large-Scale Machine Learning on Heterogeneous Systems*. Software available from tensorflow.org. 2015. URL: https://www.tensorflow.org/.

7

THE INFLUENCE OF PORE CONNECTIVITY ON SPALLING

There's no sense in being precise when you don't even know what you're talking about.

John von Neumann

Very simple was my explanation, and plausible enough – as most wrong theories are!

H.G. Wells, The Time Machine

This chapter explores the influence of pore connectivity on concrete resistance against spalling, following the conclusions of the previous chapter. First, an experiment was proposed in which the microstructure of the samples would be characterized in order to define the connectivity present in the pore space. This was divided between the connectivity in the capillary porosity, determined through mercury intrusion porosimetry and the connectivity of the macro-porosity determined through X-ray microtomography. Then, the samples went through a spalling experiment and an equation was developed to predict which samples would spall. Once the equation correctly predict the experiment, further experiments were collected from literature to validate this work. The analytical equation determines whether a given sample will suffer spalling under fast heating conditions with an accuracy higher than 91.2%.

Parts of this chapter have been accepted for publication in Construction and Building Materials.

7.1. DEFINING PORE CONNECTIVITY

FOLLOWING the conclusions of Chapter 6, it seems that the randomness attributed to spalling is in big part due to the poorly reported pore structure that governs the contribution of the THM mechanism. In the opinion of the author, the connectivity of pores is what influences the build up of stresses, rather than the volume of pores. Hence, this chapter contains a study planned to explore the influence of pore connectivity in the spalling resistance of concrete. However, as discussed in Chapter 2, pore connectivity is a loosely defined term. Further, concrete possesses pores in nearly all scales, from nanometers to centimeters (see Figure 7.1), which poses a second challenge. Surely, the connectivity within the C-S-H gel is not the same as the connectivity between honeycomb voids of a poorly compacted mass element.

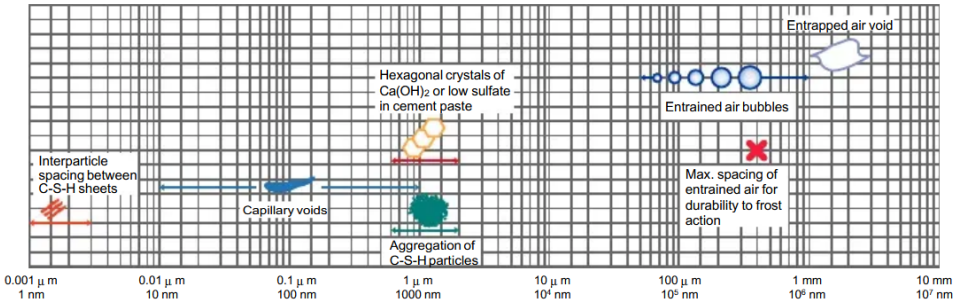

Figure 7.1: Sketch displaying the different scales of porosity present in concrete, image from Mehta & Monteiro (2006) [1].

7

In order to contour this problem, the author used the evidence gathered in Figure 6.9 as a starting point. The figure shows a great contribution of the amount of PP fibres (as measured through PPI) and W/C ratio in the resistance to spalling. These two parameters are tightly connected to the pore space within samples [2–4], and can be easily controlled in both laboratory and practice. These parameters also give a clear partition between two categories of porosity (or pore connectivity): PP fibres influence macro-pores, with a fictional diameter of several micrometers up to millimeters; W/C ratio affects micro-porosity, with diameters of several nanometers up to few micrometers. Within this chapter, porosity will be treated as a two tier system and macro-porosity and micro-porosity will be defined by the mentioned sizes of voids.

Finally, in Chapter 2 it was discussed how most spalling experiments focus on either the thermo-mechanical or the thermo-hygral contribution to the phenomenon. Because the focus of the present chapter is in the influence of pore connectivity, the experiment was deliberately planned to minimize the contribution of the TMM, so the THM could be better studied. The results showed a good correlation of the proposed connectivity measure to spalling resistance of samples. Based on these findings, the author proposes an analytical equation to predict the spalling or resistance of concrete to a given thermal load. The equation is validated using experiments from literature that include several cases outside of the parameters tested in the experimental campaign.

7.2. EXPERIMENTAL METHODOLOGY

7.2.1. MIXTURE DESIGN

All samples were cast as mortar using Portland cement type CEM I 42.5N, tap water and CEN-Norm Sand with a distribution according to NEN EN 196-1[5]. As mentioned, the two mix parameters selected as variables were the W/C ratio and polypropylene (PP) fibre content. The fibres used were Fibermesh® 150, which were 12 mm in length and 31 μm in diameter. Some mixtures presented poor workability, in which case MasterGlenium® 51 was used as superplasticizer.

A total of nine different mortar mix designs were selected (Table 7.1). The W/C ratio and fiber content (by volume) were increased between 0.30, 0.40 and 0.50 and 0.00%, 0.05% and 0.10%, respectively. For each mixture, five samples were cast in plastic cylinder moulds, with 65 mm height and 55 mm diameter. A cylindrical mould shape was chosen to highlight the contribution of the pore pressure build-up to the spalling behaviour of the samples, as edges are more prone to suffer from the TMM [6]. From the five cast samples of each mixture, three were used for spalling experiments, one for X-ray microtomography and one for mercury intrusion porosimetry. All samples were stored for 8 weeks in a fog room at 20°C and >95% RH before testing. Additionally, each mixture also had three cubes with 40 mm sides and six prisms with 40 x 40 mmm cross section and 160 mm length cast for the mechanical testing. In Table 7.1, samples were labelled using the W/C ratio as the first value, and then the PP fibre content as the second value. E.g. 40_10 is a mix design with W/C ratio 0.40 and fibre content of 0.10 % in volume.

Table 7.1: Mixture proportions of cast samples

Sample Name	C (kg)	W (kg)	A (kg)	SP (kg)	PP (%)	PPI* (-)
30_00	1	0.3	2	0.0059	0.00	0
30_05	1	0.3	2	0.0069	0.05	174
30_10	1	0.3	2	0.0094	0.10	348
40_00	1	0.4	2	0.0000	0.00	0
40_05	1	0.4	2	0.0000	0.05	174
40_10	1	0.4	2	0.0000	0.10	348
50_00	1	0.5	2	0.0000	0.00	0
50_05	1	0.5	2	0.0000	0.05	174
50_10	1	0.5	2	0.0000	0.10	348

C = cement, W = water, A = aggregates, SP = superplasticizer, PP = polypropylene fibres, PPI = polypropylene index.

* Calculated according to Li et al (2021) [7], the definition of PPI is given in the Chapter 6.

7.2.2. MECHANICAL PROPERTIES

To determine compressive strength of each mixture, three cubes with 40 mm length were tested according to NEN-EN 12390-3:2019 [8]. The samples were tested after 28 days of curing at a fixed loading rate of 13.5 kN/s using a servo-hydraulic mechanical press with maximum load capacity of 5000 kN and high stability from Matest.

For determination of flexural strength, three prisms with a cross-section of 40 x 40 mm and a length of 160 mm were tested for each mixture according to NEN-EN 12390-5:2019 [9]. The samples were tested after 28 days of curing, using a servo-hydraulic mechanical press with maximum load capacity of 5000 kN from Matest. The testing setup used a three point bending system with a centre top loading and two rollers at the bottom with a spacing of 120 mm between them. Notches of 3 mm were introduced to the bottom in the middle of each sample to ensure cracking in the middle area. Two gauges were glued to both sides of the bottom of the samples to measure the strain. Testing was done with displacement control using the crack width monitored from the applied gauges.

Due to logistic issues, only six mixtures could have the Young's modulus tested. The tests were carried out according to NEN-EN 12390-13:2021 [10]. Testing was loading-controlled with a loading rate of 0.1 kN per second (0.063 MPa/sec) using an Instron 8872. The stabilized secant modulus was measured after 3 load cycles with a maximum loading of 9 kN. Gauges were glued to all 4 sides of the samples with an initial length of 60 mm parallel to the vertical surface. Sandpaper was used to level the the top and bottom surface. For each of the six tested mixtures, three prisms with a cross-section of 40 x 40 mm and a length of 160 mm were used. The three untested mixtures were 30_05, 40_05 and 50_05. To estimate elastic moduli of these mixtures, an average of the values of the other mixtures weighted by the flexural strength was used following Equation 7.1.

$$E_{05} = \frac{\left(\frac{E_{00}}{f_{t00}} + \frac{E_{10}}{f_{t10}}\right)}{2} \cdot f_{t05} \tag{7.1}$$

Where, E_{05} is the elastic modulus of a mixture with a fibre content of 0.05%, E_{00} is the elastic modulus of a mixture with a fibre content of 0.00%, E_{10} is the elastic modulus of a mixture with a fibre content of 0.10%, f_{t00} is the flexural strength of a mixture with a fibre content of 0.00%, f_{t05} is the flexural strength of a mixture with a fibre content of 0.05% and f_{t10} is the flexural strength of a mixture with a fibre content of 0.10%.

7.2.3. SPALLING EXPERIMENT

Spalling tests were performed inside an open element HTF1700 Carbolite Furnace with an Eurotherm 3208 temperature controller. A cylindrical steel cage was placed over the samples to protect the exposed heating elements. The cage had multiple holes in all direction to allow heat flow through it (see Figure 7.2). Maximum temperature was set at 600 ^{o}C. The third parameter selected as a variable was the heating rate, a rate of either 10°C/min, 30°C/min or 50°C/min was used, with a dwell time of 30 minutes. After remaining at maximum temperature for the duration of the dwell time, the oven would be turned off and the samples cooled gradually until an internal temperature under 40 ^{o}C, at which point the samples were removed from the oven for further study. In the case of spalling before the cooling phase, the program was interrupted and the oven turned off.



Figure 7.2: Oven setup with metal cage protection over sample

7.2.4. POROSITY CHARACTERIZATION

It is generally accepted that the quantification of porosity in concrete is dependent on the technique chosen for the task [11–13]. Further, a single technique cannot cover all the range of pores in concrete while also providing 3D information about the pore network. Figure 7.3 shows the ranges for different techniques capable of identifying pore size distribution. As previously mentioned, the description of macro-porosity is a major point of interest, as fibers act in tens of micrometers to millimeter scale. Thus, X-ray microtomography (XCT) was selected to obtain a 3D rendering of the macro pores and their links. Although this technique is capable of resolve large pores, sample size becomes an issue when trying to also resolve small fibres, such as polypropylene. To bypass this issue, the author chose to use small samples for the XCT in order to visualise the fibres well, while also performing tests of air content in the mixtures as an additional measure of macro-porosity.

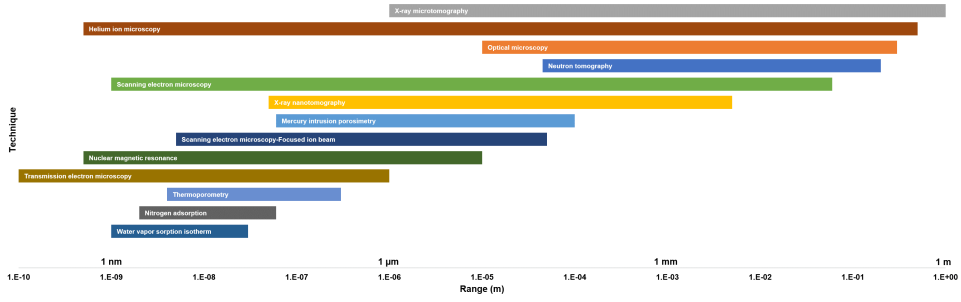

Figure 7.3: Graph displaying the range in which different techniques can be used to identify porosity in cementitious materials.

To study the capillary porosity, the author decided against image analysis through electron microscopy acquired pictures because the 2D nature of the technique hinders assumptions related to pore connectivity. Instead, it was chosen to use mercury intrusion porosimetry (MIP), as assumption regarding the connectivity of the capillary porosity are possible through the use of repeated cycles [14]. Finally, the gel porosity was not studied, as it should present negligible influence to the THM during spalling [15].

Air content tests were performed using a Form+Test Prufsysteme Air Entrainment Meter according to the standard NEN-EN 1015-7:1998 [16]. To prepare samples for mercury intrusion porosimetry, small pieces of samples were broken to a maximum size of 10 mm. Hydration was stopped using solvent exchange with isopropanol for 3 days and subsequently vacuum dryed to remove the isopropanol for 2 days. The amount of time for stopping hydration was determined based on previous work [17]. MIP was performed using a Micromeritics AutoPore IV 9500 Mercury Porosimeter. A contact angle of 141 degrees was assumed. According to the minimum and maximum applied pressures of 345 KPa and 414 MPa, respectively, the porosimeter can analyze pores with apparent diameters of 100 to 0.006 μm. The pore connectivity was determined for the mortars using Equation 7.2 from the work of Yu et al (2018) [14].

$$Pore\ connectivity\ (\%) = \left(1 - \frac{Ink\text{-}bottle\ porosity}{Total\ porosity}\right) \cdot 100 \tag{7.2}$$

Samples were acquired for microtomography by coring a cylinder with a diameter of 12 mm out of the original cast cylinders. From the cored sample the middle section was selected with a height of 20 mm. After coring they were placed in a SECADOR desiccator to stop hydration. After 5 days in the desiccator the samples were submerged in a Kalium Iodine solution, to improve the contrast for the XCT images. The solution had a concentration of 0.05M, all 9 samples were submerged in the solution and stored in airtight conditions for 2-3 days. After which, samples were removed from the solution and wrapped in plastic foil to retain the solution during the scans.

Microtomography scans were performed using a Phoenix Nanotom X-ray CT scanner. The scanner is composed of a transmission type X-ray tube, a sample stage and a 3072 x 2400 flat panel detector with a pixel size of 100 μm. The transmission target uses a tungsten filament and possesses a maximum accelerating voltage of 180 kV. However, the acquisitions were performed at 100 kV. Samples were placed at a distance of 25.99 mm from the transmission tube and 199.99 mm from the detector. A magnification of 7.69 was acquired, achieving a 6.49 μm voxel size. Reconstruction of the CT images was done through Datos VeloCT. Additionally, a median filter was applied through VGStudio Max 3.0.

The reconstructed CT images were processed using the Freeware Fiji image analysis [18]. In total 1520 images from the middle of each sample were chosen for the image stacks, which equals to a 9,87 mm sample height. Through the plugin Trainable Weka Segmentation [19], a binary stack is created containing only the pores and fibres. Subsequently, this binary stack was used in the pore analysis. A second plugin (BoneJ [20]) was used to determine the geometric properties of each individual pore detected. The data set was further treated by Matlab [21] to obtain the pore size distribution of each mixture.

Pore connectivity for macro-porosity was analysed through a tortuosity plugin [22] in ImageJ [23]. Assuming material tortuosity is inversely related to pore connectivity, a property value is acquired for the pore connectivity of large pores of the samples. The tortuosity was analyzed for each data set in the five directions of heating (because the cylinders for spalling experiments rest on top of a refractory bed inside the oven, each sample is heated only on the sides and top, not on the bottom).

7.3. RESULTS AND DISCUSSION

7.3.1. SAMPLES PROPERTIES

Table 7.2 contains the results for the mechanical properties of the samples. As expected, strength and elastic modulus decrease with increasing W/C ratio.

Table 7.2: Results obtained for mechanical properties of samples

Sample	Compressive strength (MPa)	Flexural Strength (MPa)	Elastic modulus(GPa)
30_00	76.6 ± 1.4	5.5 ± 0.3	42.8 ± 2.5
30_05	75.1 ± 2.9	5.3 ± 0.2	43.6*
30_10	77.3 ± 1.8	4.9 ± 0.3	42.9 ± 1.6
40_00	50.8 ± 5.8	3.9 ± 0.3	35.2 ± 0.8
40_05	46.0 ± 1.0	4.5 ± 0.3	39.1*
40_10	49.2 ± 1.7	4.1 ± 0.2	34.6 ± 0.8
50_00	44.9 ± 1.1	3.7 ± 0.2	30.7 ± 0.7
50_05	43.1 ± 0.2	3.6 ± 0.3	30.0*
50_10	41.3 ± 1.9	3.4 ± 0.2	28.4 ± 1.4

*Value estimated using Equation 7.1

Figure 7.4 contains a three dimensional representation of the macro-porosity and fibers of the samples as detected by XCT. The PP fibers can be observed as thin white filaments. An increase in macro-pores is observed with both, the increases in fiber content, and the decrease of W/C ratio, in accordance with the air content tests.

A combination of MIP and XCT was used to determine the pore size distribution over the entire range of interest. The results are shown in Figure 7.6 for mixture with W/C=0.30 and W/C=0.40 and Figure 7.7 for W/C=0.50.

Table 7.3 contains the results for the porosity of the samples. Given the increasing fluidity of the fresh mixtures with increasing W/C ratio, air content decreases proportionally. XCT porosity follows the same trend of air content, indeed, the Pearson correlation coefficient for these two variables is 0.95, pointing to a very strong correlation. This indicates that the small sample size for XCT does not seem to hinder the technique from correctly measuring macro-porosity. As expected, MIP porosity increased with W/C ratio and seemed insensitive to PP content.

Table 7.4 contains the estimated connectivity for micro- and macro-porosity. The values for micro-porosity were determined according to Equation 7.2, increases with W/C ratio in a similar trend to Table 7.3. Connectivity of macro-pores, as determined by computer tomography, appears to be relatively insensitive to W/C ratio variation, it increases proportionally to polypropylene fibers content. The two connectivities mea-

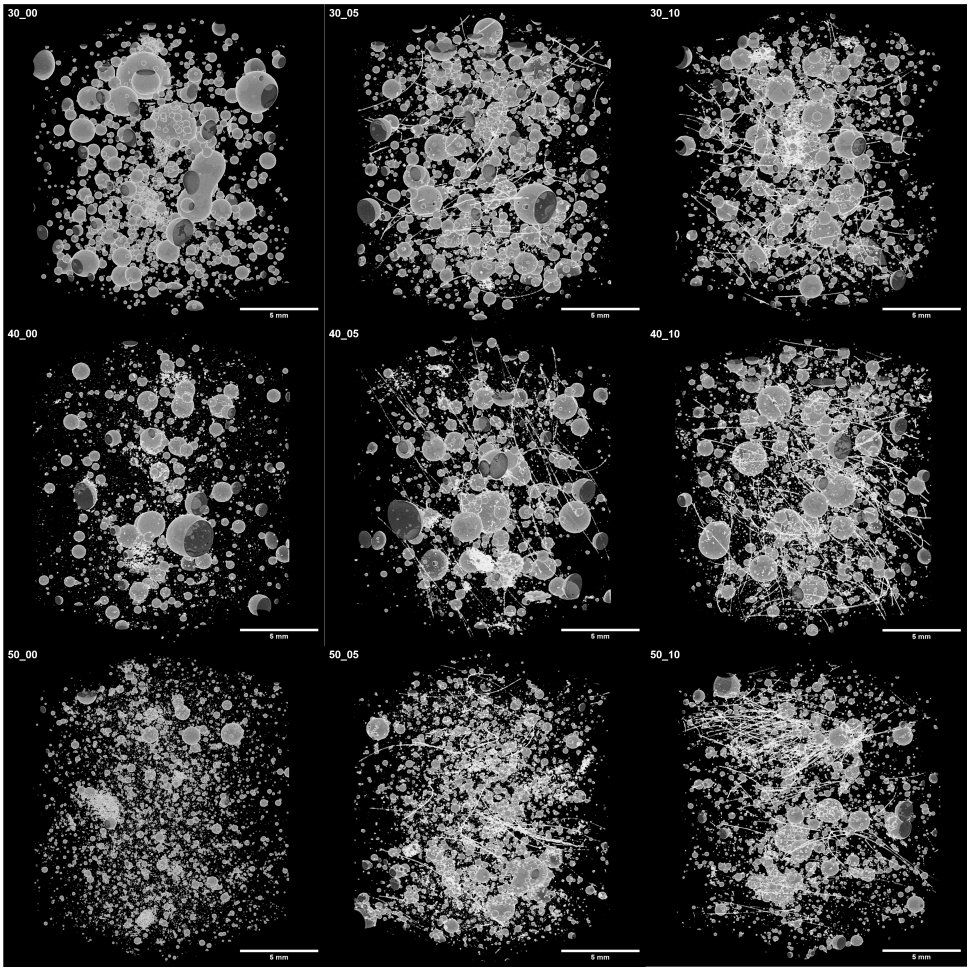

Figure 7.4: X-ray microtomography representation of macro pore volumes for each mixture.

Table 7.3: Results obtained for air content, macro-porosity as determined by XCT and micro-porosity as determined by MIP.

Sample	Air content (%)	XCT porosity (%)	MIP porosity (%)
30_00	4.8	5.11	8.26
30_05	4.3	4.20	8.13
30_10	4.1	3.15	7.79
40_00	3.0	1.91	8.80
40_05	3.4	2.84	9.77
40_10	4.6	3.34	10.22
50_00	0.8	0.46	11.43
50_05	1.8	1.11	12.01
50_10	2.2	1.39	11.80

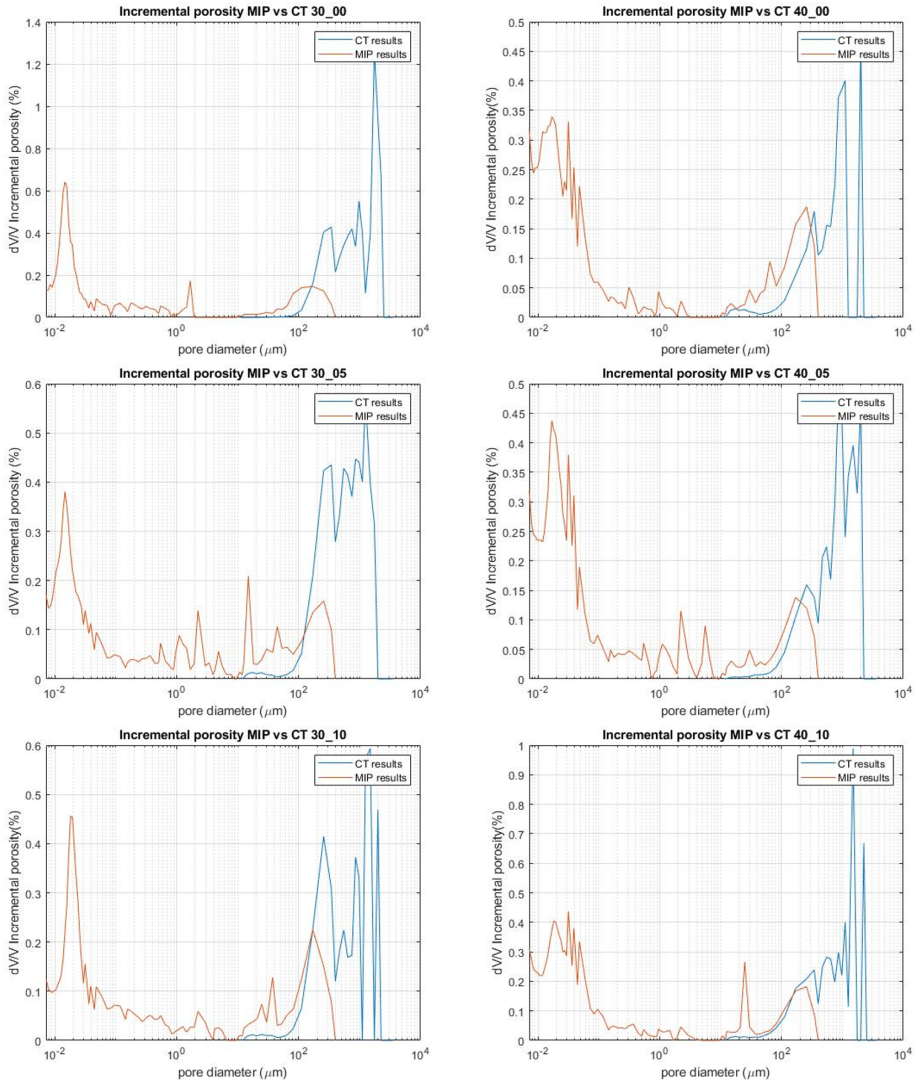

Figure 7.5: Pore size distribution for mixtures with 0.30 and 0.40 W/C ratios.

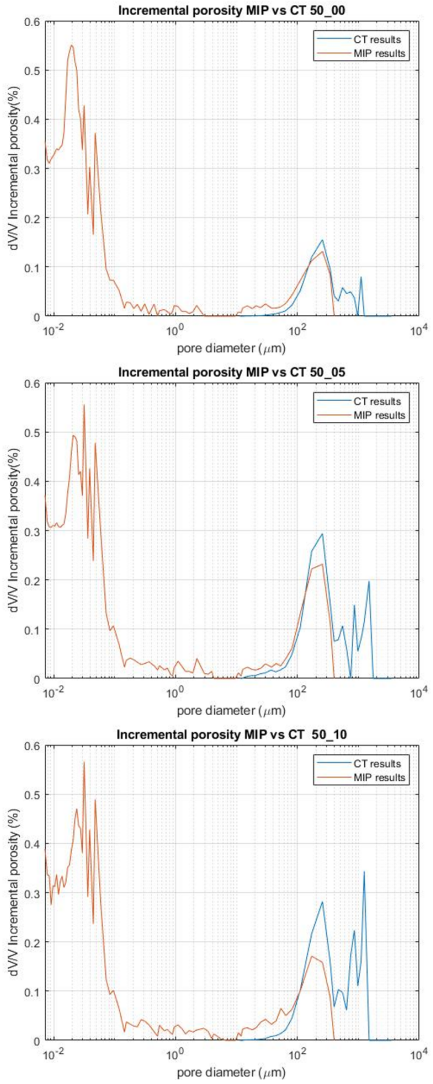

Figure 7.6: Pore size distribution for mixtures with 0.50 W/C ratio.

sures present a Pearson correlation of -0.22, which signifies a very weak correlation or no correlation at all. It was important for these values to be independent since macro and micro-porosity can vary independently in cement and concrete (see Table 7.3).

Table 7.4: Results of micro-porosity connectivity and macro-porosity connectivity of the pore space in the samples.

Sample	MIP connectivity (%)	Tomography tortuosity
30_00	24.96	1.03
30_05	25.26	1.82
30_10	32.97	3.27
40_00	38.55	1.02
40_05	36.80	1.32
40_10	38.49	1.33
50_00	48.52	1.09
50_05	45.75	1.38
50_10	47.87	1.62

7.3.2. SPALLING BEHAVIOUR

Figure 7.7 compiles the results of the spalling experiment. Although not all samples parameter combinations could be tested, other works [7, 24–26] already determined that samples with same size and mixture composition may spall with increasing heating rates. As follows, if a mixture did not spall at 50°C/min, it should not spall at a lower heating rate. Accordingly, if a mixture spalls at 10°C/min, stands to logic that it would spall at a higher heating rate.

All mixtures without polypropylene fibers suffered from spalling, regardless of heating rate or W/C ratio. Mixtures with 0.10% of PP content by volume did not suffer from spalling regardless of the W/C ratio or heating rate. The mixtures with 0.05% PP content did not spall for 0.30 W/C ratio, but did spall for 0.40 and 0.50 W/C ratios when the heating rate was increased from 10°C/min to 30°C/min (and follow the trend at 50°C/min). This disparity might seem counter intuitive since the samples with lower W/C ratio performed better, however, the actual determining factor to reduce the resistance against spalling is the concrete denser microstructure, rather than just the amount of mixture water [27–29]. In the present experiment, the low viscosity of the mixtures generated a considerably higher amount of entrapped air in the samples with W/C ratio = 0.30, as it can be observed on Table 7.3 and Figure 7.4. These are valuable data points as it indicates a higher influence of macro-porosity than micro-porosity for spalling resistance. Which is reinforced by the MIP connectivity results. In addition, all samples spalled within 10 minutes of surpassing 500°C, despite different heating rates. This might be an indication of the volume to heated area ratio influence in this heating regime.

Further, the samples displayed different degrees of spalling, depending on the amount of fibers and heating ratio. Figure 7.8 shows some examples of samples after the heating experiment. It seems the W/C ratio did not influence the size of pieces as much as the other parameters.

Mix properties		Heating rate (°C/min)		
W/C	PP (%)	10	30	50
0.30	0.00	Spalled	Spalled	Spalled
	0.05	Not tested	Sound	Sound
	0.10	Not tested	Not tested	Sound
0.40	0.00	Spalled	Not tested	Spalled
	0.05	Sound	Spalled	Spalled
	0.10	Not tested	Sound	Sound
0.50	0.00	Spalled	Not tested	Not tested
	0.05	Sound	Spalled	Spalled
	0.10	Not tested	Sound	Sound

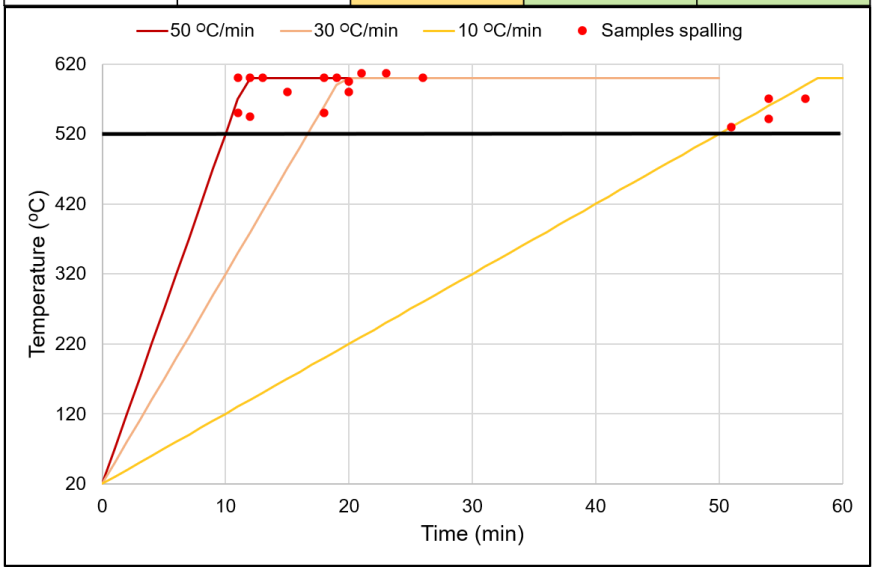

Figure 7.7: Spalling testing results. Top: Different mixtures reaction to oven heating at 10, 30 and 50°C/min. Bottom: Moment and temperature of spalling for each tested sample.

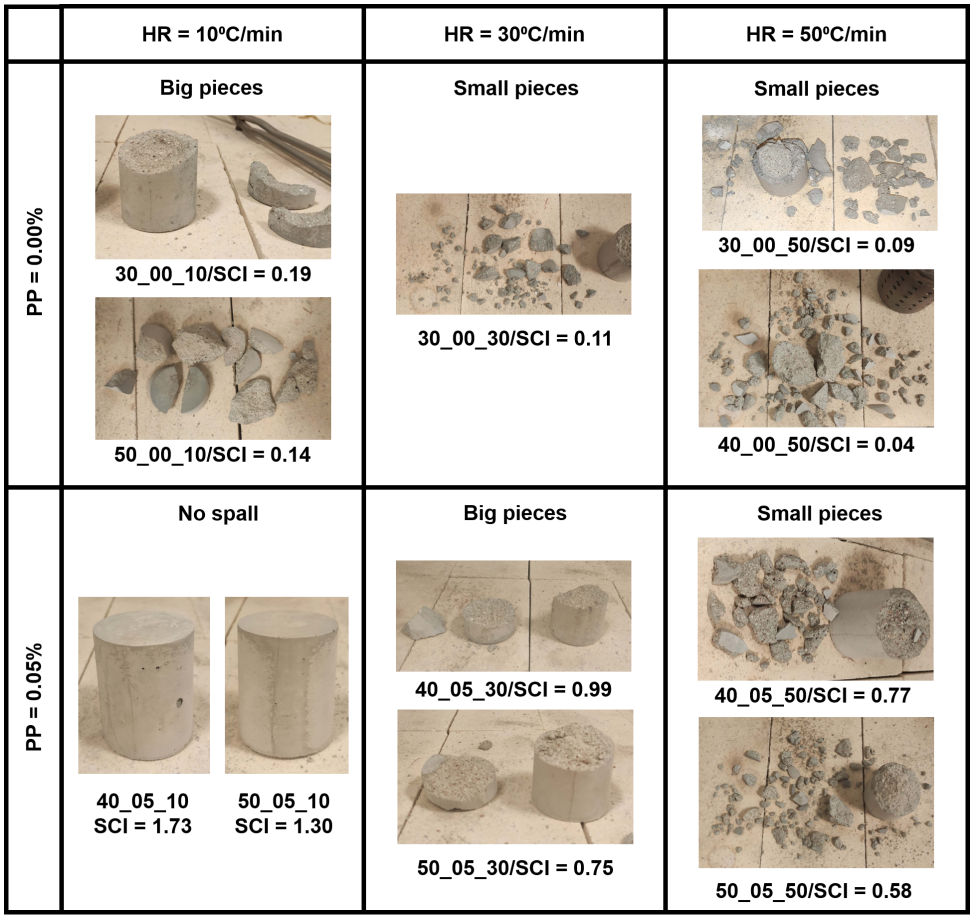

Figure 7.8: Examples of spalling intensity in selected samples (SCI is explained in Section 7.4).

7.4. QUANTIFYING PORE CONNECTIVITY INFLUENCE ON SPALLING

7.4.1. ASSUMPTIONS

As previously stated, spalling usually occurs in concrete as a combination of thermo-mechanical spalling and thermo-hygral spalling. For this work, it was assumed Equation 2.23 could describe a theoretical concrete material without porosity. Although such material is impossible, this represents a starting point for the adaptation of the work of Lu & Fleck (1998) [30] for cementitious materials. Re-writing Equation 2.23 to separate the variables based on physical meaning, it yields Equation 7.3 (same variables as Equation 2.23),in which the first term describes the contribution of the mechanical properties of the material to the resistance against thermal shock cracking, the second term describes the influence of the environment and the third term describes the contribution of the thermal properties, sample size and geometry.

$$\Delta T = \frac{\sigma_f}{E} \cdot \frac{C_1}{h} \cdot \frac{k}{\alpha \cdot H} \tag{7.3}$$

While W/C ratio is of relatively low influence for the third term [31] and no impact on the second therm, it controls the values of the first term of Equation 7.3. However, the effect of varying W/C ratio within the studied ranges seem to be negligible for the ratio between tensile strength and elastic modulus of the material. This seems intuitively wrong, since several experiments show that changing W/C ratio in cementitious materials can significantly alter the spalling resistance [31–33]. Presently, it is accepted that this is mostly caused by the lower permeability and increased brittleness of the paste [34, 35]. Both these properties are correlated to changes in capillary porosity [36, 37], which increases proportionally to the W/C ratio [38]. While brittleness addressed through the elastic modulus, changes in permeability caused by decrease of W/C ratio are unaccounted for. However, Table 7.4 shows that MIP connectivity seems proportional to changes in W/C ratio. Thus, the author proposes a variable $\Lambda_{(MIP)}$ that represents the connectivity of micro-pores based on Equation 7.2 to be added to the first term of Equation 7.3. This addition is placed on the numerator, as the increase in capillary connectivity should improve concrete resistance to spalling [14, 39].

Instead of attempting to estimate pore pressure at several scales, the author explores the THM by including the capacity of the material to allow for vapour escape. The vapour escape pressure is proportional to the thermal gradient and water mass within the sample [40]. The thermal gradient is dependent of sample size, geometry, thermal conductivity and heating rate. The sample size and geometry are already described by the variable H, as well as thermal conductivity by the variable k. Because Equation 2.23 was developed for immediate thermal shock events, heating rate still needs to be added. Using the available data set, it seems that the heating rate is inversely proportional to the square of the sample resistance to spalling. Thus, it is added in the denominator as the square root of heating rate.

The free water mass in the material can be approximated using the amount of macro-porosity and saturation level of the concrete. The authors included the variable AC as the air content and φ_S as the saturation degree. For a mix with same permeability, in-

creasing saturation degree seems to make spalling much more likely [41], as intuitively inferred by the higher amount of water vapor in need to escape, thus φ_S is placed on the denominator of the equation. On the other hand, AC is placed on the numerator, despite possibly allowing for more water to be held within the material. This is because this properties has been found to not affect the tensile strength and elastic modulus of concrete under spalling temperatures, but allow for comparatively higher escape of water [42], thus improving the material resistance to spalling.

Finally, the actual capacity of macro-porosity to allow vapor transport must be related to its connectivity in addition to its volume. This is reflected in Figures 7.7 and 7.8 that highlight the PP fibre content as a key parameter for spalling prediction. As mentioned previously, the tortuosity of the paste was used as connectivity for the macro-pore space and is introduced as $\Lambda_{(XCT)}$. The author defends the use of this tortuosity parameter in opposition to fibre content because, although indirect, $\Lambda_{(XCT)}$ is a physical measure of the connections between the macro-pores in a given sample. Meanwhile, fibre content does not take into account the influence of fibre diameter, length and aggregate size and content, all of which influence spalling behaviour [43, 44]. Further, samples with the same fiber content can present very different macro-pores connectivity (see Table 7.4). As this is one of the main forms of spalling prevention, the parameter is placed on the numerator. Because tortuosity is measured in small volumes and up-scaling remains a challenge [45], the authors considered the relationship with sample volume (and geometry) non-linear and added a constant C_3 to account for that. This resulted in Equation 7.4:

$$SCI = \frac{\sigma_t \cdot (\Lambda_{(MIP)} - C_1)}{E} \cdot \frac{C_2}{h} \cdot \frac{k \cdot AC}{\alpha \cdot \sqrt{HR}} \cdot \frac{\Lambda_{(XCT)} - 1}{H^{C_3} \cdot \varphi_S} \tag{7.4}$$

In which $C_1 = 0.02$, $C_2 = 180$, $C_3 = 0.17$ and the left hand side of the equation no longer means a critical thermal gradient, but a spalling control index (SCI). The constants were set so a value of $SCI < 1$ denotes spalling and $SCI > 1$ predicts that the studied concrete will not spall under the considered conditions. The value of the constants has been calibrated using the described experiment.

7.4.2. VALIDATION

Although Equation 7.4 correctly predicts whether the samples studied in the experiment of the present chapter would spall or not (Figure 7.10, top), the amount of data was not satisfactory. Hence, five studies [25, 46–49] were selected for the validation of the proposed equation. The main criteria to chose relevant research papers were the publication of heating experiments in which the following parameters were reported: if the samples spalled, the W/C ratio, the volume, the heated area, the polypropylene fibers content and dimensions (if used), the compressive strength, the air content and the heating rate. Because the studied samples were saturated, the search was limited to experiments also using saturated samples.

Ideally, tensile strength and elastic modulus would be part of the searching criteria, however, these values are rarely published after spalling experiments. To circumvent this challenge, the authors estimated tensile strength and elastic moduli for samples lacking these data based on the Eurocode [50]. Within the norm, it is stated that the tensile

strength of concretes of class C50/60 or below can be estimated based on Equation 7.5, while concretes above this class use Equation 7.6. The elastic moduli were estimated using Equation 7.7. Further, these would be the values for the material at room temperature, it would not be feasible to gather enough literature results including mechanical properties at high temperatures. In a review performed by Ma et al (2015) [51], it was estimated that about 25% of the flexural strength and elastic modulus of concrete is lost at a temperature of 250°C, thus, a 0.75 factor was applied to the estimation of these properties.

$$f_{\text{ctm}} = 0.3 \cdot f_{\text{ck}}^{2/3} \tag{7.5}$$

$$f_{\text{ctm}} = 2.12 \cdot ln(1 + (f_{\text{cm}}/10)) \tag{7.6}$$

$$E_{\text{cm}} = 22 \cdot (f_{\text{cm}}/10)^{0.3} \tag{7.7}$$

The heat transfer coefficient between concrete and air was assumed to be 10 W/m^2/K, the thermal conductivity of the samples was set at 1.8 W/m/K, and the coefficient of thermal dilation as 4.5·10^{-5} 1/K. Since $\Lambda_{(\text{MIP})}$ and $\Lambda_{(\text{XCT})}$ were newly proposed parameters, these had to be estimated for all literature samples. For both parameters, regressions were performed using the experiment of this chapter. As expected, $\Lambda_{(\text{MIP})}$ is proportional to W/C ratio, with a logarithmic relation in the shape of Equation 7.8, which yields a $R^2 = 0.9222$. The paste tortuosity, could not be inferred using a single parameter, instead, a combination of multiple fibre properties, air content and compressive strength was necessary. A second order polynomial regression with two variables was used, generating Equation 7.9 with a $R^2 = 0.9911$. The fit of both variables is displayed in Figure 7.9.

$$\Lambda_{(\text{MIP})} = 0.3829 \cdot ln(W/C\ ratio) + 0.7362 \tag{7.8}$$

$$\Lambda_{(\text{XCT})} = 1.194 - 3.034e^{-2} \cdot P_{\text{adj}} - 2.675e^{-3} \cdot f_{\text{ck}} + 2.837e^{-5} \cdot P_{\text{adj}}^2 + 6.955e^{-4} \cdot P_{\text{adj}} \cdot f_{\text{ck}} \tag{7.9}$$

In which the P_{adj} is the polypropylene index divided by the air content of the sample. The concept of PP index was first proposed by Li et al (2021) [7], as a better description of the amount and spacing of PP fibers inside concrete. This index was defined in Chapter 6.

The five selected papers [25, 46–49] contain a total of 102 unique samples that went through heating experiments. These samples varied in volume from 9 dm^3 to 216 dm^3, in air content from 1.6% to 4.2%, in heating rate from 5°C/min to 115°C/min and in PP index from 0 to 4700. Equation 7.4 was used to predict the behaviour of each individual sample, with the results reported in Figure 7.10, bottom.

A total of 93 out of 102 correct predictions was achieved, which is equivalent to 91.18% accuracy. As shown in Figure 7.10, from the 9 incorrect predictions, only 3 belong to samples that did spall when Equation 7.4 indicated a safe situation. The remaining 6 incorrect data points belong to sound samples that were expected to spall.

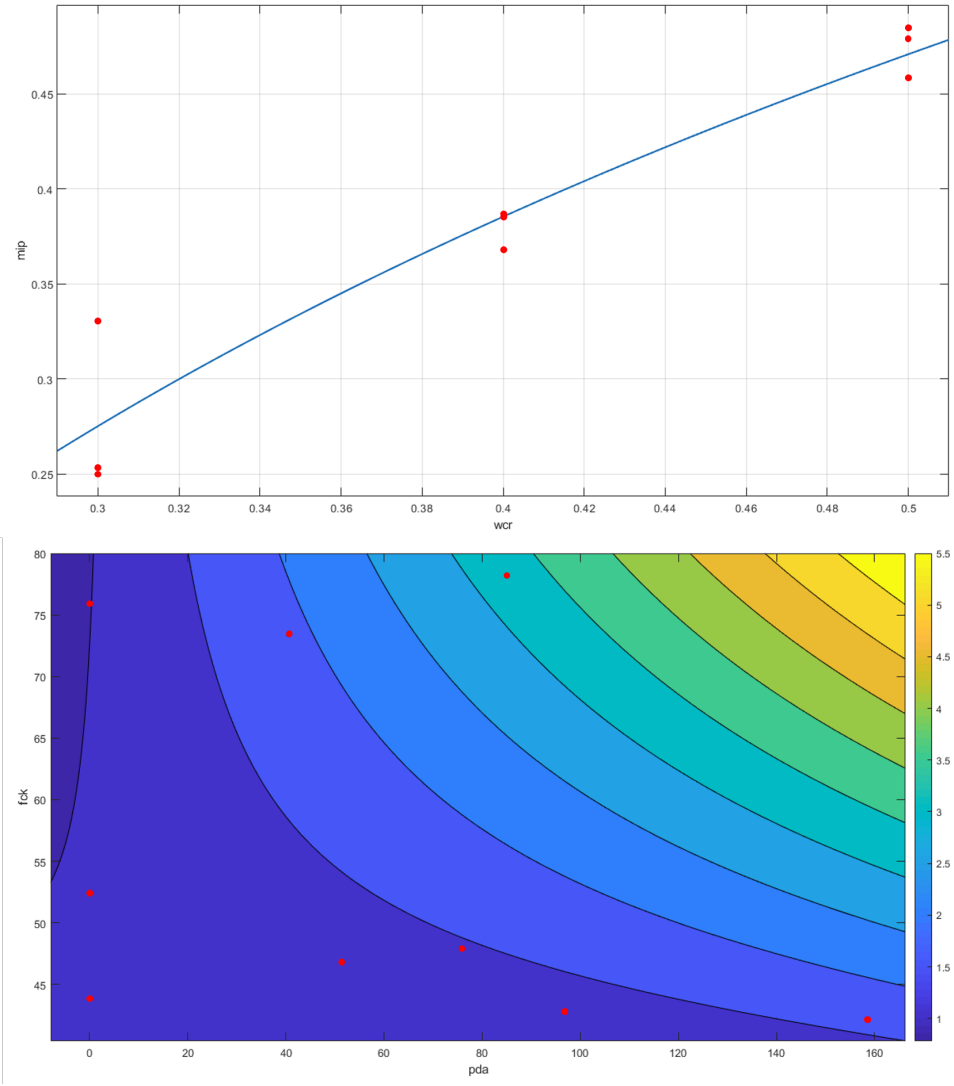

Figure 7.9: Curve fitting of $\Lambda_{(\mathrm{MIP})}$ and $\Lambda_{(\mathrm{XCT})}$.

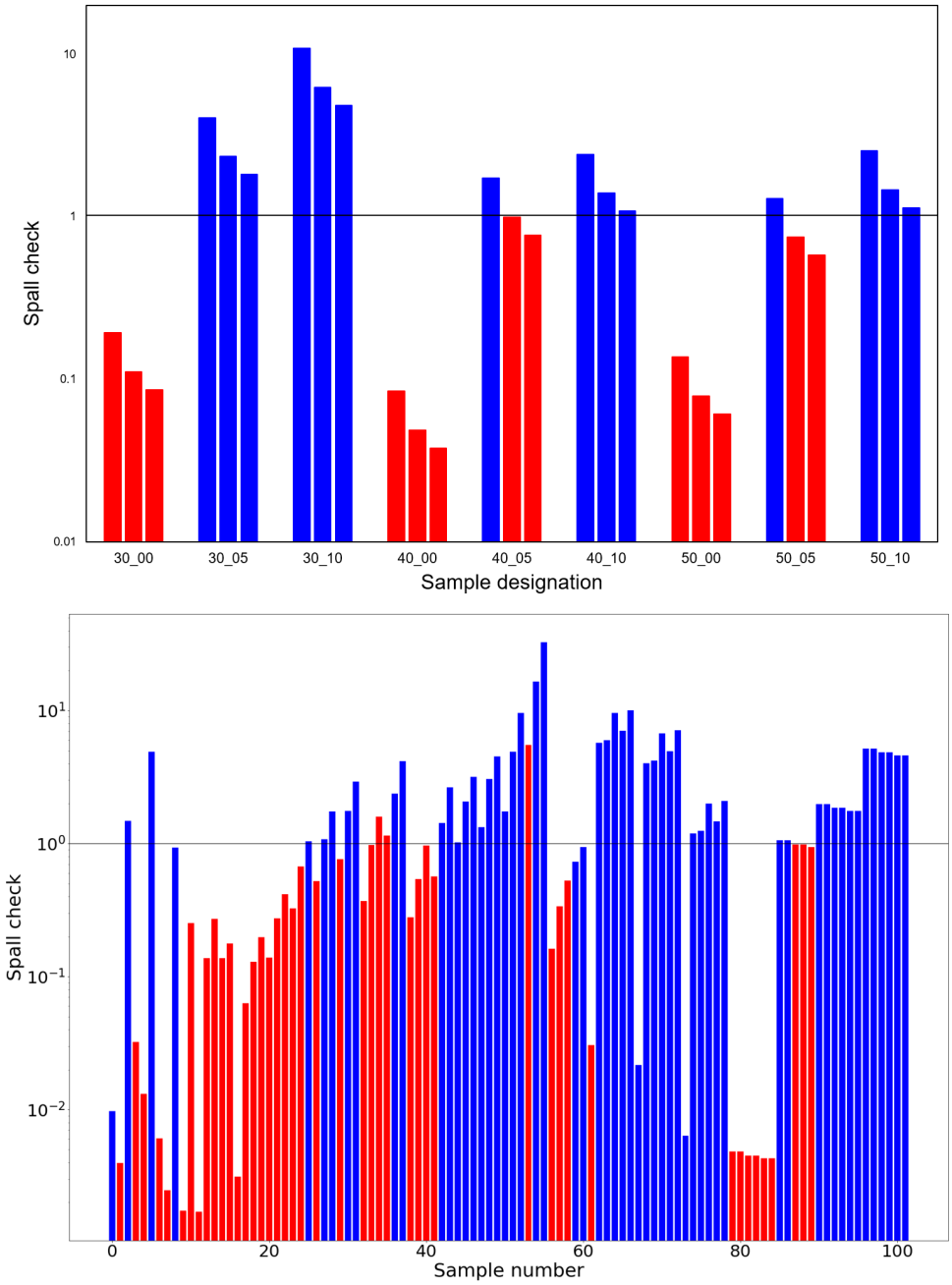

Figure 7.10: Validation of Equation 7.4 using spalling experiments. Blue lines represent samples that did not spall, red lines represent samples that did spall, the black horizontal lines shows the prediction cutoff for spalling. Top: Results from experiment described in this chapter, each mix design has three lines to represent the tests performed at 10°C/min, 30°C/min and 50°C/min, in this order. Bottom: Results from experiments collected from the selected papers [25, 46–49], samples are organized in no particular order.

7.5. DISCUSSION

Although high temperature spalling is a known problem in concrete for nearly a century, the prediction of structural members behaviour against rapid heating is still a challenge. Most standards merely advice a minimum polypropylene fiber content to protect structures from it. However, spalling may affect structures even with high amounts of fibers, depending on physical and geometrical properties of the fiber itself [52, 53]. Alternatively, recent advances in FEM methods aim to couple the TMM and the THM [54–57]. Yet, these use randomly created, often simplified, concrete meso-structures, which do not properly account for mixture variations, such as pore connectivity.

Equation 7.4 reached high accuracy when compared against other laboratory experiments for predicting spalling. However, further work is necessary to predict spalling in actual concrete structures. During fires, the material often experiences one-sided heating, which allows for bigger temperature gradients with faster development. Some works have been published in the shortcomings of sample size and oven heating regarding the study of concrete in high temperatures [49, 58–61], however, this remains as the most accessible option and vast majority of published research.

Another drawback is that concrete in a structure is never fully saturated, it always possesses an inner gradient. This causes a small amount of stress in the structure by default, prior to any thermal loading. Some researchers [41, 62] looked into the influence of different saturation degrees in concrete regarding spalling, but these samples were treated to have a constant saturation through its entirety. The actual gradient found in structures is not only related to the material properties, as it is also linked to the structure design and in which area is the concrete located.

Further, samples were free to expand at the surfaces inside the oven, this was a conscious decision given the goal of focusing in the thermo-hygral mechanism. However, most concrete structures are externally restrained and under loads, which changes the response to high temperatures [63]. Although several works attempted to study spalling in concrete under imposed stress [64–66], these do not account for relaxation of stress. In actual structures, relaxation develops over years of sustained load and increases with temperature [67]. This effect will lessen the stresses caused by the restraining of the material within the structure and should be accounted for.

Still, development in the field of spalling prediction is necessary to achieve prevention. This is a phenomenon that poses great danger for structures with difficult evacuation in the case of fires. Tunnels, for example, can be greatly affected by it, which is not a rare occurrence [68], indeed, most incidents involving trains in tunnels are fire related [69]. Chapter 1 shows the average number of fire incidents (caused by automobiles, trucks or trains) to occur inside tunnels in different countries, and this is still a problem in current society. While the priority is to avoid loss of life, these events also cause great damage to the concrete lining, demanding costly repairs that hinder traffic [52, 70]. Thus, spalling-proof concrete mixtures must be developed and used in these structures.

7.6. CONCLUSIONS

This chapter explored the influence of pore connectivity on concrete resistance against spalling. First, an experiment was proposed in which the microstructure of the samples would be characterized in order to define the connectivity present in the pore space. Then, the samples went through a spalling experiment and an equation was developed to predict which samples would spall. Once the equation correctly predict the experiment, further experiments were collected from literature to validate this work. The analytical equation determines whether a given sample will suffer spalling under fast heating conditions with an accuracy higher than 91.2%, thus, seems a viable alternative for spalling prediction of laboratory concrete.

However, spalling does not depend only on the material, but of a combination of material, structural and thermal parameters. This has been partially argued in Section 7.5 and offers insight on future work. Although functional, Equation 7.4 could be complemented by a research on the influence of saturation gradients within concrete and loaded, reinforced samples. A short recommendation for further studies is provided in Chapter 8.

BIBLIOGRAPHY

[1] P.K. Mehta and P.J.M. Monteiro. *Concrete: Microstructure, Properties, and Materials*. McGraw Hill professional. McGraw-Hill Education, 2006. ISBN: 9780071462891. URL: https://books.google.nl/books?id=3j5EAQAAIAAJ.

[2] T. C. Powers and T. L. Brownyard. "Studies of the Physical Properties of Hardened Portland Cement Paste". In: *ACI Journal Proceedings* 43.9 (Nov. 1946).

[3] Jun Pil Hwang, Moonil Kim, and Ki Yong Ann. "Porosity generation arising from steel fibre in concrete". In: *Construction and Building Materials* 94 (2015), pp. 433–436. ISSN: 0950-0618. DOI: https://doi.org/10.1016/j.conbuildmat.2015.07.044. URL: https://www.sciencedirect.com/science/article/pii/S0950061815300957.

[4] Behlul Furkan Ozel, Şeyma Sakallı, and Yuşa Şahin. "The effects of aggregate and fiber characteristics on the properties of pervious concrete". In: *Construction and Building Materials* 356 (2022), p. 129294. ISSN: 0950-0618. DOI: https://doi.org/10.1016/j.conbuildmat.2022.129294. URL: https://www.sciencedirect.com/science/article/pii/S0950061822029506.

[5] *NEN-EN 196-1:2016 – Methods of testing cement – Part 1: Determination of strength*. Standard. Delft, NL: Nederlands Normalisatie-instituut, May 2016.

[6] Francesco Lo Monte et al. "Assessment of concrete sensitivity to fire spalling: A multi-scale experimental approach". In: *Construction and Building Materials* 212 (2019), pp. 476–485. ISSN: 0950-0618. DOI: https://doi.org/10.1016/j.conbuildmat.2019.03.332. URL: https://www.sciencedirect.com/science/article/pii/S0950061819308402.

[7] Ye Li et al. "Pore pressure build-up and explosive spalling in concrete at elevated temperature: A review". In: *Construction and Building Materials* 284 (2021). ISSN: 09500618. DOI: 10.1016/j.conbuildmat.2021.122818.

[8] *NEN-EN 12390-3:2019 – Testing hardened concrete – Part 3: Compressive strength of test specimens*. Standard. Delft, NL: Nederlands Normalisatie-instituut, July 2019.

[9] *NEN-EN 12390-5:2019 – Testing hardened concrete – Part 5: Flexural strength of test specimens*. Standard. Delft, NL: Nederlands Normalisatie-instituut, July 2019.

[10] *NEN-EN 12390-13:2019 – Testing hardened concrete – Part 13: Determination of secant modulus of elasticity in compression*. Standard. Delft, NL: Nederlands Normalisatie-instituut, Oct. 2019.

[11] Fuyuan Gong et al. “Empirical Estimation of Pore Size Distribution in Cement, Mortar, and Concrete”. In: *Journal of Materials in Civil Engineering* 26.7 (2014), p. 04014023. DOI: 10.1061/(ASCE)MT.1943-5533.0000945. eprint: https://ascelibrary.org/doi/pdf/10.1061/\%28ASCE\%29MT.1943-5533.0000945. URL: https://ascelibrary.org/doi/abs/10.1061/%5C%28ASCE%5C%29MT.1943-5533.0000945.

[12] Bednarska, Dalia and Koniorczyk, Marcin. “Comparison of various methods applied in porous materials microstructure analysis in regard to hardened cement paste”. In: *MATEC Web of Conferences* 282 (2019), p. 02043. DOI: 10.1051/matecconf/201928202043. URL: https://doi.org/10.1051/matecconf/201928202043.

[13] Zhi-Lu Jiang et al. “Pore structure characterization of cement paste by different experimental methods and its influence on permeability evaluation”. In: *Cement and Concrete Research* 159 (2022), p. 106892. ISSN: 0008-8846. DOI: https://doi.org/10.1016/j.cemconres.2022.106892. URL: https://www.sciencedirect.com/science/article/pii/S0008884622001843.

[14] Zhuqing Yu et al. “Relationship between water permeability and pore structure of Portland cement paste blended with fly ash”. In: *Construction and Building Materials* 175 (2018), pp. 458–466. ISSN: 0950-0618. DOI: https://doi.org/10.1016/j.conbuildmat.2018.04.147. URL: https://www.sciencedirect.com/science/article/pii/S095006181830953X.

[15] Ludwig Stelzner et al. “Thermally-induced moisture transport in high-performance concrete studied by X-ray-CT and 1H-NMR”. In: *Construction and Building Materials* 224 (2019), pp. 600–609. ISSN: 0950-0618. DOI: https://doi.org/10.1016/j.conbuildmat.2019.07.065. URL: https://www.sciencedirect.com/science/article/pii/S0950061819317386.

[16] *NEN-EN 1015-7:1998 – Methods of test for mortar for masonry – Part 7: Determination of air content of fresh mortar*. Standard. Delft, NL: Nederlands Normalisatie-instituut, Nov. 1998.

[17] Jie Zhang and George W. Scherer. “Comparison of methods for arresting hydration of cement”. In: *Cement and Concrete Research* 41.10 (2011), pp. 1024–1036. ISSN: 0008-8846. DOI: https://doi.org/10.1016/j.cemconres.2011.06.003. URL: https://www.sciencedirect.com/science/article/pii/S0008884611001645.

[18] J. Schindelin et al. “Fiji: An open-source platform for biological-image analysis”. In: *Nature Methods* 9.7 (2012), pp. 676–682. DOI: https://doi.org/10.1038/nmeth.2019.

[19] Ignacio Arganda-Carreras et al. “Trainable Weka Segmentation: a machine learning tool for microscopy pixel classification”. In: *Bioinformatics* 33.15 (Mar. 2017), pp. 2424–2426. ISSN: 1367-4803. DOI: 10.1093/bioinformatics/btx180. eprint: https://academic.oup.com/bioinformatics/article-pdf/33/15/2424/25157856/btx180.pdf. URL: https://doi.org/10.1093/bioinformatics/btx180.

7

[20] Michael Doube et al. “BoneJ: Free and extensible bone image analysis in ImageJ”. In: *Bone* 47.6 (2010), pp. 1076–1079. ISSN: 8756-3282. DOI: https://doi.org/10.1016/j.bone.2010.08.023. URL: https://www.sciencedirect.com/science/article/pii/S8756328210014419.

[21] MATLAB. *version 9.9.0 (R2020b)*. Natick, Massachusetts: The MathWorks Inc., 2020.

[22] Waldir L. Roque and Richelieu R.A. Costa. “A plugin for computing the pore/grain network tortuosity of a porous medium from 2D/3D MicroCT image”. In: *Applied Computing and Geosciences* 5 (2020), p. 100019. ISSN: 2590-1974. DOI: https://doi.org/10.1016/j.acags.2020.100019. URL: https://www.sciencedirect.com/science/article/pii/S259019742030001X.

[23] Caroline A. Schneider, Wayne S. Rasband, and Kevin W. Eliceiri. “NIH Image to ImageJ: 25 years of image analysis”. In: *Nature Methods* 9 (2012), pp. 671–675. ISSN: 1548-7105. DOI: 10.1038/nmeth.2089. URL: https://doi.org/10.1038/nmeth.2089.

[24] M.B. Dwaikat and V.K.R. Kodur. “Hydrothermal model for predicting fire-induced spalling in concrete structural systems”. In: *Fire Safety Journal* 44.3 (2009), pp. 425–434. ISSN: 0379-7112. DOI: https://doi.org/10.1016/j.firesaf.2008.09.001. URL: https://www.sciencedirect.com/science/article/pii/S0379711208001239.

[25] Mugume Rodgers Bangi and Takashi Horiguchi. “Pore pressure development in hybrid fibre-reinforced high strength concrete at elevated temperatures”. In: *Cement and Concrete Research* 41.11 (2011), pp. 1150–1156. ISSN: 0008-8846. DOI: https://doi.org/10.1016/j.cemconres.2011.07.001. URL: https://www.sciencedirect.com/science/article/pii/S000888461100192X.

[26] Gyeongcheol Choe et al. “Effect of moisture migration and water vapor pressure build-up with the heating rate on concrete spalling type”. In: *Cement and Concrete Research* 116.August 2017 (2019), pp. 1–10. ISSN: 00088846. DOI: 10.1016/j.cemconres.2018.10.021. URL: https://doi.org/10.1016/j.cemconres.2018.10.021.

[27] Pierre Pimienta et al. “Behavior of UHPFRC at High Temperatures”. In: *Designing and Building with UHPFRC*. John Wiley Sons, Ltd, 2011. Chap. 40, pp. 579–600. ISBN: 9781118557839. DOI: https://doi.org/10.1002/9781118557839.ch40. eprint: https://onlinelibrary.wiley.com/doi/pdf/10.1002/9781118557839.ch40. URL: https://onlinelibrary.wiley.com/doi/abs/10.1002/9781118557839.ch40.

[28] Sun Bei and Lin Zhixiang. “Investigation on spalling resistance of ultra-high-strength concrete under rapid heating and rapid cooling”. In: *Case Studies in Construction Materials* 4 (2016), pp. 146–153. ISSN: 2214-5095. DOI: https://doi.org/10.1016/j.cscm.2016.04.001. URL: https://www.sciencedirect.com/science/article/pii/S2214509516300304.

[29] Gai-Fei Peng et al. “Combined curing as a novel approach to improve resistance of ultra-high performance concrete to explosive spalling under high temperature and its mechanical properties”. In: *Cement and Concrete Research* 109 (2018), pp. 147–158. ISSN: 0008-8846. DOI: https://doi.org/10.1016/j.cemconres.2018.04.011. URL: https://www.sciencedirect.com/science/article/pii/S0008884617301886.

[30] T.J. Lu and N.A. Fleck. “The thermal shock resistance of solids”. In: *Acta Materialia* 46.13 (1998), pp. 4755–4768. ISSN: 1359-6454. DOI: https://doi.org/10.1016/S1359-6454(98)00127-X. URL: https://www.sciencedirect.com/science/article/pii/S135964549800127X.

[31] Pierre Kalifa, François-Dominique Menneteau, and Daniel Quenard. “Spalling and pore pressure in HPC at high temperatures”. In: *Cement and Concrete Research* 30.12 (2000). Papers presented at the Symposium on "Transport Properties and Microstructure of Cement-Based Systems", pp. 1915–1927. ISSN: 0008-8846. DOI: https://doi.org/10.1016/S0008-8846(00)00384-7. URL: https://www.sciencedirect.com/science/article/pii/S0008884600003847.

[32] Muhammad Abid et al. “High temperature and residual properties of reactive powder concrete – A review”. In: *Construction and Building Materials* 147 (2017), pp. 339–351. ISSN: 0950-0618. DOI: https://doi.org/10.1016/j.conbuildmat.2017.04.083. URL: https://www.sciencedirect.com/science/article/pii/S0950061817307389.

[33] Takeshi Morita et al. “an Experimental Study on Improvement of Spalling Behavior of High-Strength Concrete Elements Under Fire Attack”. In: *Journal of Structural and Construction Engineering (Transactions of AIJ)* 66.544 (2001), pp. 171–178. DOI: 10.3130/aijs.66.171_3.

[34] F. Lo Monte and R. Felicetti. “Heated slabs under biaxial compressive loading: a test set-up for the assessment of concrete sensitivity to spalling”. In: *Materials and Structures* 50.192 (2017). DOI: https://doi.org/10.1617/s11527-017-1055-1.

[35] Hao Qin et al. “Experimental research on the spalling behaviour of ultra-high performance concrete under fire conditions”. In: *Construction and Building Materials* 303 (2021), p. 124464. ISSN: 0950-0618. DOI: https://doi.org/10.1016/j.conbuildmat.2021.124464. URL: https://www.sciencedirect.com/science/article/pii/S0950061821022212.

[36] Yurong Zhang et al. “Time dependency and similarity of gas permeability of concrete in simulated environment”. In: *Journal of Building Engineering* 51 (2022), p. 104253. ISSN: 2352-7102. DOI: https://doi.org/10.1016/j.jobe.2022.104253. URL: https://www.sciencedirect.com/science/article/pii/S2352710222002662.

[37] Dong Liu et al. “Towards understanding the influence of porosity on mechanical and fracture behaviour of quasi-brittle materials: experiments and modelling”. In: *International Journal of Fracture* 205.1 (May 2017), pp. 57–72. ISSN: 1573-2673.

DOI: 10.1007/s10704-017-0181-7. URL: https://doi.org/10.1007/s10704-017-0181-7.

[38] Fethi Soltani et al. “Relationship between ultrasonic Rayleigh wave propagation and capillary porosity in cement paste with variable water content”. In: *NDT E International* 54 (2013), pp. 75–83. ISSN: 0963-8695. DOI: https://doi.org/10.1016/j.ndteint.2012.12.003. URL: https://www.sciencedirect.com/science/article/pii/S0963869512001648.

[39] Izabela Hager et al. “Effect of Cement Type on the Mechanical Behavior and Permeability of Concrete Subjected to High Temperatures”. In: *Materials* 12.18 (2019). ISSN: 1996-1944. DOI: 10.3390/ma12183021. URL: https://www.mdpi.com/1996-1944/12/18/3021.

[40] Ana Da Luz, M.A.L. Braulio, and Victor Pandolfelli. *F.I.R.E. Compendium Series - Refractory Castable Engineering*. Göller Verlag, Mar. 2015, p. 734. ISBN: ISBN 978-3-87264-004-8.

[41] Marcus Maier, Matthias Zeiml, and Roman Lackner. “On the effect of pore-space properties and water saturation on explosive spalling of fire-loaded concrete”. In: *Construction and Building Materials* 231 (2020), p. 117150. ISSN: 0950-0618. DOI: https://doi.org/10.1016/j.conbuildmat.2019.117150. URL: https://www.sciencedirect.com/science/article/pii/S0950061819326029.

[42] Wasim Khaliq and Farhan Waheed. “Mechanical response and spalling sensitivity of air entrained high-strength concrete at elevated temperatures”. In: *Construction and Building Materials* 150 (2017), pp. 747–757. ISSN: 0950-0618. DOI: https://doi.org/10.1016/j.conbuildmat.2017.06.039. URL: https://www.sciencedirect.com/science/article/pii/S0950061817311807.

[43] Young-Sun Heo et al. “Relationship between inter-aggregate spacing and the optimum fiber length for spalling protection of concrete in fire”. In: *Cement and Concrete Research* 42.3 (2012), pp. 549–557. ISSN: 0008-8846. DOI: https://doi.org/10.1016/j.cemconres.2011.12.002. URL: https://www.sciencedirect.com/science/article/pii/S0008884611003061.

[44] Ye Li et al. “Effect of aggregate size and inclusion of polypropylene and steel fibers on explosive spalling and pore pressure in ultra-high-performance concrete (UHPC) at elevated temperature”. In: *Cement and Concrete Composites* 99 (2019), pp. 62–71. ISSN: 0958-9465. DOI: https://doi.org/10.1016/j.cemconcomp.2019.02.016. URL: https://www.sciencedirect.com/science/article/pii/S0958946518306504.

[45] Ming Wu et al. “A three-dimensional model for quantification of the representative elementary volume of tortuosity in granular porous media”. In: *Journal of Hydrology* 557 (2018), pp. 128–136. ISSN: 0022-1694. DOI: https://doi.org/10.1016/j.jhydrol.2017.12.030. URL: https://www.sciencedirect.com/science/article/pii/S002216941730848X.

[46] N. Algourdin et al. “Influence of polypropylene and steel fibres on thermal spalling and physical-mechanical properties of concrete under different heating rates”. In: *Construction and Building Materials* 259 (2020), p. 119690. ISSN: 0950-0618. DOI: https://doi.org/10.1016/j.conbuildmat.2020.119690. URL: https://www.sciencedirect.com/science/article/pii/S0950061820316950.

[47] Yining Ding et al. “Influence of different fibers on the change of pore pressure of self-consolidating concrete exposed to fire”. In: *Construction and Building Materials* 113 (2016), pp. 456–469. ISSN: 0950-0618. DOI: https://doi.org/10.1016/j.conbuildmat.2016.03.070. URL: https://www.sciencedirect.com/science/article/pii/S0950061816303658.

[48] Young-Sun Heo et al. “Critical parameters of nylon and other fibres for spalling protection of high strength concrete in fire”. In: *Materials and Structures* 44.3 (Apr. 2011), pp. 599–610. ISSN: 1871-6873. DOI: 10.1617/s11527-010-9651-3. URL: https://doi.org/10.1617/s11527-010-9651-3.

[49] G. Debicki, R. Haniche, and F. Delhomme. “An experimental method for assessing the spalling sensitivity of concrete mixture submitted to high temperature”. In: *Cement and Concrete Composites* 34.8 (2012), pp. 958–963. ISSN: 0958-9465. DOI: https://doi.org/10.1016/j.cemconcomp.2012.04.002. URL: https://www.sciencedirect.com/science/article/pii/S0958946512000637.

[50] *EN 1992-1-1 Eurocode 2: Design of concrete structures – Part 1-1: General rules and rules for buildings*. EN. Brussels: CEN, 2011.

[51] Qianmin Ma et al. “Mechanical properties of concrete at high temperature—A review”. In: *Construction and Building Materials* 93 (2015), pp. 371–383. ISSN: 0950-0618. DOI: https://doi.org/10.1016/j.conbuildmat.2015.05.131. URL: https://www.sciencedirect.com/science/article/pii/S0950061815006765.

[52] Cristian Maluk et al. “Experimental study on the fire behaviour of fibre reinforced concrete used in tunnel applications”. In: *Fire Safety Journal* 120 (2021). Fire Safety Science: Proceedings of the 13th International Symposium, p. 103173. ISSN: 0379-7112. DOI: https://doi.org/10.1016/j.firesaf.2020.103173. URL: https://www.sciencedirect.com/science/article/pii/S037971122030134X.

[53] Young-Sun Heo et al. “Synergistic effect of combined fibers for spalling protection of concrete in fire”. In: *Cement and Concrete Research* 40.10 (2010), pp. 1547–1554. ISSN: 0008-8846. DOI: https://doi.org/10.1016/j.cemconres.2010.06.011. URL: https://www.sciencedirect.com/science/article/pii/S0008884610001596.

[54] Yiming Zhang et al. “Model-based risk assessment of concrete spalling in tunnel linings under fire loading”. In: *Engineering Structures* 77 (2014), pp. 207–215. ISSN: 0141-0296. DOI: https://doi.org/10.1016/j.engstruct.2014.02.033. URL: https://www.sciencedirect.com/science/article/pii/S0141029614001266.

[55] Michal Beneš and Radek Štefan. “Hygro-thermo-mechanical analysis of spalling in concrete walls at high temperatures as a moving boundary problem”. In: *International Journal of Heat and Mass Transfer* 85 (2015), pp. 110–134. ISSN: 0017-9310. DOI: https://doi.org/10.1016/j.ijheatmasstransfer.2015.01.050. URL: https://www.sciencedirect.com/science/article/pii/S0017931015000587.

[56] Yiming Zhang et al. “Fast assessing spalling risk of tunnel linings under RABT fire: From a coupled thermo-hydro-chemo-mechanical model towards an estimation method”. In: *Engineering Structures* 142 (2017), pp. 1–19. ISSN: 0141-0296. DOI: https://doi.org/10.1016/j.engstruct.2017.03.068. URL: https://www.sciencedirect.com/science/article/pii/S0141029617310623.

[57] Antonio Caggiano et al. “Meso-scale response of concrete under high temperature based on coupled thermo-mechanical and pore-pressure interface modeling”. In: *Engineering Failure Analysis* 85 (2018), pp. 167–188. ISSN: 1350-6307. DOI: https://doi.org/10.1016/j.engfailanal.2017.11.016. URL: https://www.sciencedirect.com/science/article/pii/S135063071731107X.

[58] Lars Boström, Ulf Wickström, and Bijan Adl-Zarrabi. “Effect of specimen size and loading conditions on spalling of concrete”. In: *Fire and Materials* 31.3 (2007), pp. 173–186. DOI: https://doi.org/10.1002/fam.931. eprint: https://onlinelibrary.wiley.com/doi/pdf/10.1002/fam.931. URL: https://onlinelibrary.wiley.com/doi/abs/10.1002/fam.931.

[59] I. Rickard et al. “Predictive testing for heat-induced spalling of concrete”. In: *Structural Engineering: Providing Solutions to Global Challenges*. International Association for Bridge and Structural Engineering (IABSE). Zurich, Switzerland: International Association for Bridge and Structural Engineering (IABSE), 2015.

[60] Fabio P. Figueiredo et al. “Effects of Recycled Steel and Polymer Fibres on Explosive Fire Spalling of Concrete”. In: *Fire Technology* 55.5 (Sept. 2019), pp. 1495–1516. ISSN: 1572-8099. DOI: 10.1007/s10694-019-00817-9. URL: https://doi.org/10.1007/s10694-019-00817-9.

[61] F.F. Mendonça Filho et al. “Surface effects of molten slag spills on calcium aluminate cement paste”. In: *Materials Design* 217 (2022), p. 110623. ISSN: 0264-1275. DOI: https://doi.org/10.1016/j.matdes.2022.110623. URL: https://www.sciencedirect.com/science/article/pii/S0264127522002441.

[62] M. Maier et al. “An experimental fire-spalling assessment procedure for concrete mixtures”. In: *Construction and Building Materials* 232 (2020), p. 117172. ISSN: 0950-0618. DOI: https://doi.org/10.1016/j.conbuildmat.2019.117172. URL: https://www.sciencedirect.com/science/article/pii/S0950061819326248.

[63] M. B. Dwaikat and V. K. R. Kodur. “Fire Induced Spalling in High Strength Concrete Beams”. In: *Fire Technology* 46.1 (Apr. 2009), p. 251. ISSN: 1572-8099. DOI: 10.1007/s10694-009-0088-6. URL: https://doi.org/10.1007/s10694-009-0088-6.

[64] F. A. Ali, D. O'Connor, and A. Abu-Tair. "Explosive spalling of high-strength concrete columns in fire". In: *Magazine of Concrete Research* 53.3 (2001), pp. 197–204. DOI: 10.1680/macr.2001.53.3.197. eprint: https://doi.org/10.1680/macr.2001.53.3.197. URL: https://doi.org/10.1680/macr.2001.53.3.197.

[65] Carré, H. et al. "Effect of compressive loading on the risk of spalling". In: *MATEC Web of Conferences* 6 (2013), p. 01007. DOI: 10.1051/matecconf/20130601007. URL: https://doi.org/10.1051/matecconf/20130601007.

[66] C. Kahanji, F. Ali, and A. Nadjai. "Explosive spalling of ultra-high performance fibre reinforced concrete beams under fire". In: *Journal of Structural Fire Engineering* 7.4 (Jan. 2016), pp. 328–348. ISSN: 2040-2317. DOI: 10.1108/JSFE-12-2016-023. URL: https://doi.org/10.1108/JSFE-12-2016-023.

[67] T.M. Jeyashree, P.R. Kannan Rajkumar, and K.S. Satyanarayanan. "Developments and research on fire response behaviour of prestressed concrete members – A review". In: *Journal of Building Engineering* 57 (2022), p. 104797. ISSN: 2352-7102. DOI: https://doi.org/10.1016/j.jobe.2022.104797. URL: https://www.sciencedirect.com/science/article/pii/S2352710222008105.

[68] *Technical Report 2016 R35 – Experience with significant incidents in road tunnels*. Tech. rep. PIARC – World Road Association, 2016. URL: http://www.piarc.org.

[69] K. Bergmeister and S. Francesconi. *Causes and Frequency of Incidents in Tunnels*. Tech. rep. 5th Framework Programme of the European Union Competitive and Sustainable Growth, 2004. URL: https://www.cob.nl/document/causes-frequencies-incidents/.

[70] Ying Zhen Li and Haukur Ingason. "Overview of research on fire safety in underground road and railway tunnels". In: *Tunnelling and Underground Space Technology* 81.August (2018), pp. 568–589. ISSN: 08867798. DOI: 10.1016/j.tust.2018.08.013. URL: https://doi.org/10.1016/j.tust.2018.08.013.

IV

FINAL CONSIDERATIONS

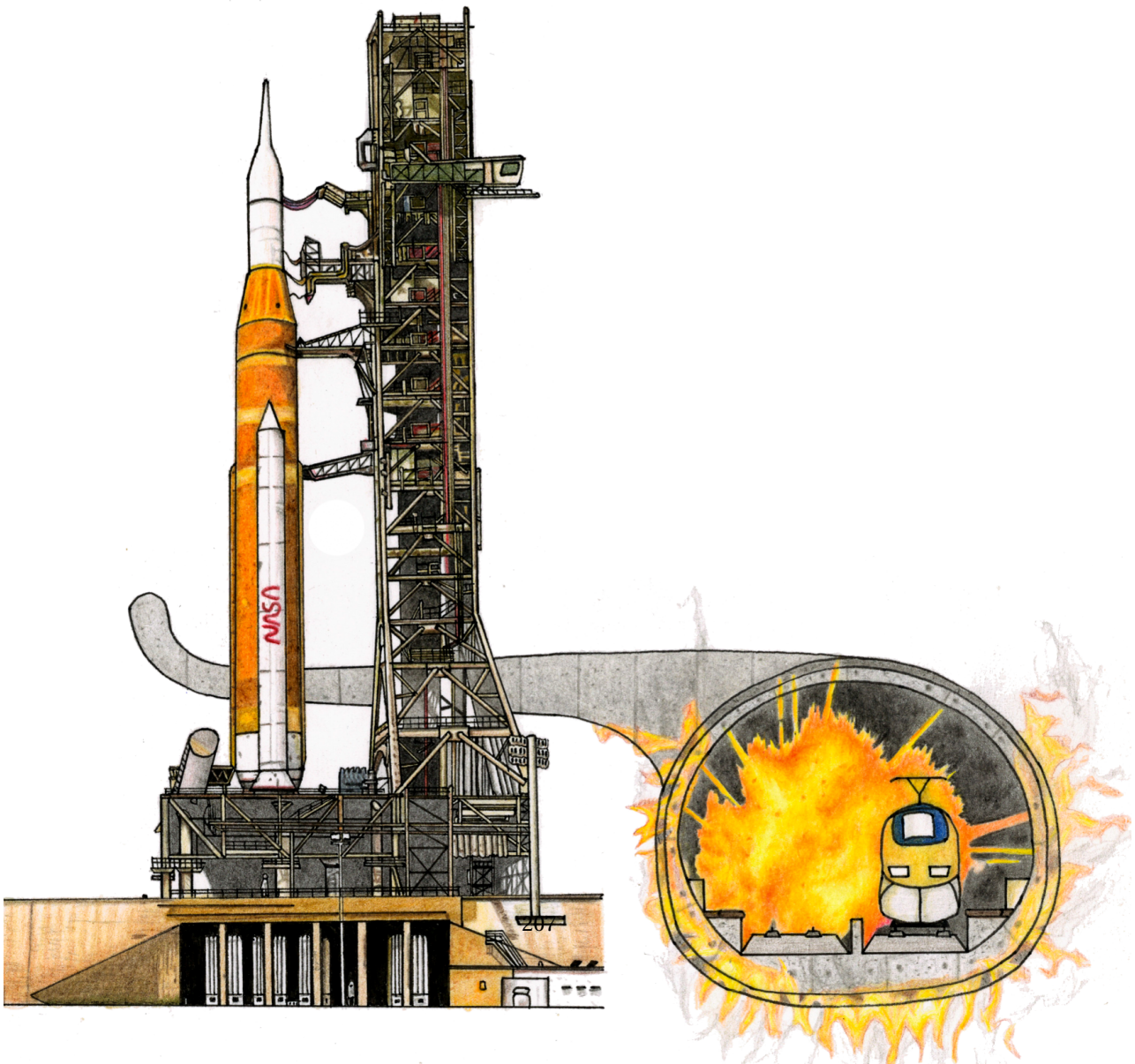

8

Applications & Recommendations

It is so shocking to find out how many people
do not believe that they can learn, and how
many more believe learning to be difficult.

Frank Herbert, Dune

Let's be clear. The planet is not in jeopardy. We are in jeopardy.
We haven't got the power to destroy the planet - or to save it.
But we might have the power to save ourselves.

Michael Crichton, Jurassic Park

This chapter contains suggestions of possible applications to the findings in the previous chapters. These focus on the improvement of materials used on industrial sites and road tunnels. Further, the chapter also collects the author's opinions on how the experimental research of Chapter 7 could be continued and implemented in a numerical model for fast simulation of spalling in concrete. Finally, space shuttle launchpads are pointed out as a potential new field of application for modern refractory concrete research.

8.1. APPLICATIONS

8.1.1. FACTORIES

HIGH temperatures are very common in several industries. Below, a list of some of the main processes involving it:

- Aerospace components manufacturing;
- Aluminium processing;
- Autoclave applications;
- Cement manufacturing;
- Ceramics manufacturing;
- Foundry;
- Glass manufacturing;
- Petrol refining;
- Rubber vulcanization
- Steel manufacturing.

All of these require special equipment, created for the specific temperature and production cycle of each product. On the other hand, factory structures are designed in similar manners in every case. In Chapter 5 it is shown that designs taking into account both mechanical and thermal stresses can provide great economic benefits through the decrease of maintenance needs and pause of production schedule. However, these are fairly specific or even unique situations, thus it should not fall upon the design codes to specify guidelines for every scenario. Rather, civil engineers should consider including thermal consideration for designs when working in industries related to high temperatures. This would require good communication, as the structural engineer would have to be educated towards the intended operation of the factory and determine, besides the class of the concrete, the composing materials.

Because the design of special concrete mixtures is outside of the expertise of most structural engineers, it would be helpful to have guidelines that could guarantee the thermal stability of concrete without requiring a laboratory campaign. This poses a challenge as Chapter 5 demonstrated that even refractory materials can suffer damage due to engineering choices in the actual factory environment.

The first step to produce a refractory concrete is the selection of the binder. A number of options has already been tested and is commercially available, such as, hydratable alumina, phosphate cements, magnesium-silicate-hydrate cements, collidal silica, collodial alumina, etc. However, the industry standard remains calcium aluminate cement (CAC) [1]. This is, in part, because of its application similarities with Portland cement and nearly equal pH [2]. The reasons for this are explained Chapter 2. In a similar manner that certain cement types are recommended for environments with high degrees of

sulphates, specific industrial structures could be considered high risk for thermal shock events and require the use of CAC or another refractory binder. As CAC has been used for several decades [3], guidelines for its application are available in several sources [2, 4, 5]. Further, Chapter 3 showed a detailed analysis of the cement performance in an experiment with a thermal shock of approximately $\Delta T = 1500^{o}C$, as most industries have a similar or smaller temperature gradient, the findings of that chapter could be directly used as general recommendations.

The choice of aggregates, however, would be more challenging. Aggregates are usually selected by their geographical availability [6, 7]. Chapters 2 and 4 discuss some stones with high performance against high temperatures, however, this is far from being an exhaustive list of refractory rocks. In general, basalt, olivine and plutonic rocks are recommended, but specific options could be found by consulting the textbooks of the geographical region of interest [1, 8].

The use of special concrete in certain factory locations is usually not discussed in the design phase, because it incurs an increase in project cost. Calcium aluminate cement is more expensive than Portland cement by mass and the same can be said about refractory aggregates when compared with common river sand, for example. However, Section 5.4 of Chapter 5 demonstrates how the initial material cost might be very misleading when estimating the actual expenditure of a factory. Additionally, the shift in design philosophy would also produce a secondary advantage in the form of sustainability. This is largely based on the positive effects the reduction of repairs cause in the CO_2 footprint of structures [9], as discussed in Chapter 1.

8.1.2. FIRE SAFETY FOR TUNNELS

Road tunnels present a different engineering challenge than factory structures as the main goal is to avoid spalling [10], rather than to conserve a certain degree of mechanical strength after a thermal shock event. This is due the long evacuation time of such structures and much higher risk of human life loss, besides the considerable economic costs [11]. Further, although such events are more rare than in industrial settings, they remain relatively frequent, as shown in Figure 1.1.

The most common way of protecting concrete against high temperature spalling is by the addition of polypropylene (PP) fibres [1, 12–14]. However, Chapters 6 and 7 discuss how our current capacity of predicting spalling is limited. In this context, Equation 7.4 from Chapter 7 could be used as a rough design guideline. By replacing Equations 7.5, 7.6, 7.7, 7.8 and 7.9 into Equation 7.4, one can estimate the minimum PP index for a given mixture and heating condition. This results in Equation 8.1, with Ω shown in Equation 8.2 and Ξ shown in Equation 8.3 for concretes of class 50 or lower and in Equation 8.4 for concretes above class 50.

$$PPI \geq \left[-F_1 \cdot f_{ck} + F_2 \pm \sqrt{F_1^2 \cdot f_{ck}^2 - 2F_1 \cdot F_2 \cdot f_{ck} + F_2^2 - 4F_3(0.194 + \Omega \cdot \Xi \cdot f_{ck})}\right] \cdot \frac{AC}{2F_3} \quad (8.1)$$

$$\Omega = 0.002675 - 0.2042\left(\frac{h \cdot \alpha}{k} \cdot \frac{\sqrt{HR}}{AC}\right) \cdot \left(\frac{H^{C_3} \cdot \phi_S}{0.3829 ln(w/c) + 0.7162}\right) \quad (8.2)$$

$$\Xi = \frac{1}{f_{ck}^{1.36}} \tag{8.3}$$

$$\Xi = \frac{1}{ln(10 + f_{ck}) - 1.6118 f_{ck}} \tag{8.4}$$

All symbols and variables are consistent with what was provided in Chapter 7. The constants are defined as: $F_1 = 6.955 \cdot 10^{-4}$, $F_2 = 3.034 \cdot 10^{-2}$ and $F_3 = 2.837 \cdot 10^{-5}$. This would require the structural engineer to define the desired f_{ck}, w/c ratio and air content in the concrete, all of which the concrete producers can easily control. Additionally, the PP index as output is more useful than a PP dosage, as the dosage can be calculated through Equation 8.5, adapting to whichever PP fibre is available in the area of the project. This is simply the inversion of Equation 6.1, and all variables and units are the same as in Chapter 6.

$$\varphi = \frac{PPI \cdot d}{l} \tag{8.5}$$

This is, however, only a preliminary equation. In Section 7.5 of Chapter 7 the author discusses several shortcomings of it and the lack of full scale experiments. Before including this in the design process, it would be recommended to carry additional experimental work, as discussed in the Section 8.2.

8.1.3. LAUNCHPADS

Conventional launchpads are concrete structures destined to endure exceptional thermal and mechanical loading. In particular, non-military rocket launches have a much bigger mass to transport, which increases the loads in the platform proportionally. In order to help absorbing the energy, the actual concrete is at an angle from the rockets engines, so the propellant can be directed sideways, these are called flame diverters. On top of that, active systems release water during the launch to consume more of the energy and decrease the sound impact on the rocket.

However, as the goals shift to landing and re-launching the rockets, the launch platforms have changed to horizontal concrete structures without water flooding. This is because of the intent of also performing launches outside of Earth. Yet, this has considerably altered both the thermal and mechanical loads, which is now a problem for launch systems.

On the 9th of November 2020, a Starship prototype from Space X performed a firing test on one of such new platforms, this test caused chunks of concrete to fly upwards damaging the structures nearby as well as the rocket turbine [15]. This was not the only incident. In a technical report [16], a committee at NASA has informed that their refractory concrete has become susceptible to failure during modern launches, with the possibility of damaging the space shuttles, the ground support equipment and even endangering the safety of employees. The report further found that among the available options at the time (2013), refractory concrete still presented the best performance, however requiring maintenance.

This is a niche area of application that still requires additional research. While the present thesis focused on the thermal performance of such materials, launchpads are

also subjected to ablation and erosion. The same report [16] also identified the poor testing of materials as a key problem in evaluating or developing better solutions. This is in agreement with what was observed in Chapters 2 and 6, as very few spalling experiments use a controlled setting of direct exposure to flames (such as of a blowtorch) and this is usually performed without mechanical loading [17–19]. In the case of launch-pads, the loading occurs in the same direction of the flame emission, which requires a large-scale experimental setup.

Finally, because there is only a very small amount of commercial products available for this application, it also presents a business opportunity for research carried out in this topic. Although space launches are not very frequent, they have increased at an exponential rate in the past decade, surpassing an amount previously only seen during the cold war (see Figure 8.1). Considering the recent boom of commercial endeavours to use orbital space and further destinations, this trend is expected to increase, more than doubling the market size [20]. Thus, this field seems attractive for novel research efforts using the current developments in high strength refractory concrete.

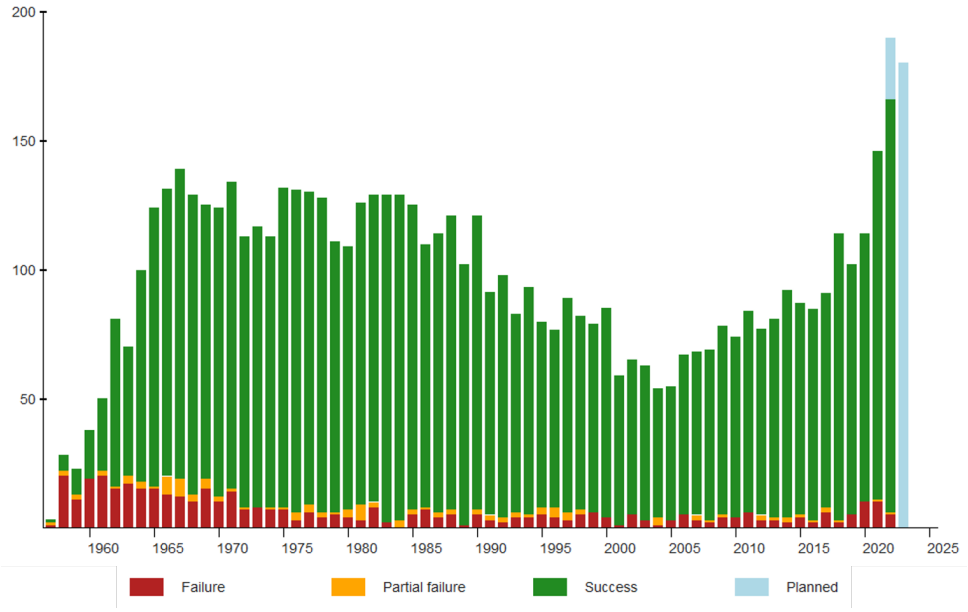

Figure 8.1: Frequency of failed and successful space launches per year, data source: [21].

8.2. RECOMMENDATIONS FOR FUTURE RESEARCH

8.2.1. PREDICTION OF SPALLING THROUGH ANALYTICAL EQUATION

Chapter 7 focused on exploring the influence of pore connectivity on spalling and how to quantify it. One of the main outcomes of that chapter was Equation 7.4, which proved that the quantification method was effective through the Validation section. However, the equation can only be used to predict spalling in samples with specific parameters (i. e. fully saturated samples). This is due to the focus of the experimental campaign in highlighting the contribution of pore connectivity to the phenomenon of spalling. An extension of this experiment, focusing on the other parameters of Equation 7.4 could potentially improve the prediction power to include any laboratory sample.

The extension of the experiment could be divided in three campaigns:

1. Determine the influence of the saturation degree on the samples;
2. Determine the influence of the volume to heated area ratio on the samples;
3. Determine the influence of the change of aggregates on the samples.

Because the base experiment already possessed three variables (w/b ratio, pp content and heating ratio), it is likely the follow up campaigns would have to eliminate one these to keep the amount of samples manageable. For example, it would be interesting in campaign 1 to maintain the fibre content fixed as 0.00% while varying the saturation degree of each sample, creating a testing matrix similar to the one presented in Figure 7.7. The saturation levels could be controlled using the mass differences between saturated samples and samples dried at 105°C until mass balance was achieved. Once the minimum saturation necessary for the occurrence of spalling was identified, the polypropylene content could be increased to explore the relationship between the PP density and water volume for a given mixture. The outcome would likely improve the use of Equation 7.4 as a design recommendation tool by determining the amount of polypropylene needed following Equation 8.1.

In order to further improve the understanding of the effect of the saturation degree on spalling of concrete, experiments could be carried out with considerably larger samples that would present moisture gradients previous to heating. As previously discussed, real structures are not dry or saturated, but present different gradients in each member, which cause small stresses in the concrete. Then, ϕ_S in Equation 7.4 would no longer be a constant and likely replaced by Equation 8.6, with x representing the depth in the sample and d_{tot} the total thickness of the sample. For multi-directional heating, it would be better to use $d/2$.

$$\phi_S = \int_0^{d_{\text{tot}}} \phi_x \, dx \tag{8.6}$$

Although creating moisture gradients within laboratory samples is simple, controlling such gradients to generate reproducible results isn't. Because of the semi-random pore structure of concrete, the rate of water loss is not the same for samples with the same mixture [22, 23]. Further, reliably measuring moisture profiles is also challenging, as the main method still involves drilling the sample and testing the collected powder

material. These challenges currently pose an obstacle for the extension of laboratory results into full structural predictors. As such, the author considers this as a very fertile topic for future research.

The second campaign is deemed useful because it could further explore the effect of the TMM, which was less studied in Chapter 7. The validation attempted to correct this by showing the application of the equation in samples of varying sizes, which presented very distinct volume to area of heating ratios. However, the actual size of the samples tested in the selected studies [24–28] varied from 9 to 216 dm^3, which would be equivalent cubes of sides from 20 cm to 60 cm. These are already samples considerably larger than the ones used for the experiment in Chapter 7, but the area of heating was fixed.

For a new experiment, it would be interesting to set a fixed volume and change the shape of the samples, so a correlation between the area of heating and spalling resistance could be explored. This could be achieved by testing a series of rectangular prisms with varying height and cross-section. Figure 8.2 shows a sketch of the proposed series of samples, if a cube with 30 cm side was chosen as starting point, the other samples would have a height of 5, 10, 20, 40, 60, 80 and 100 cm. For simplicity, all samples could be saturated and a single mixture design could be studied. Once a critical volume to area of heating ratio was identified, this experiment could be repeated with the same H/L ratios for varying volumes, further clarifying the influence of the size factor on spalling. Additionally, the variation of saturation degree and PP content could highlight the transition between spalling processes governed by vapour pressure development or thermal gradients and bring the experiments very close to real field conditions.

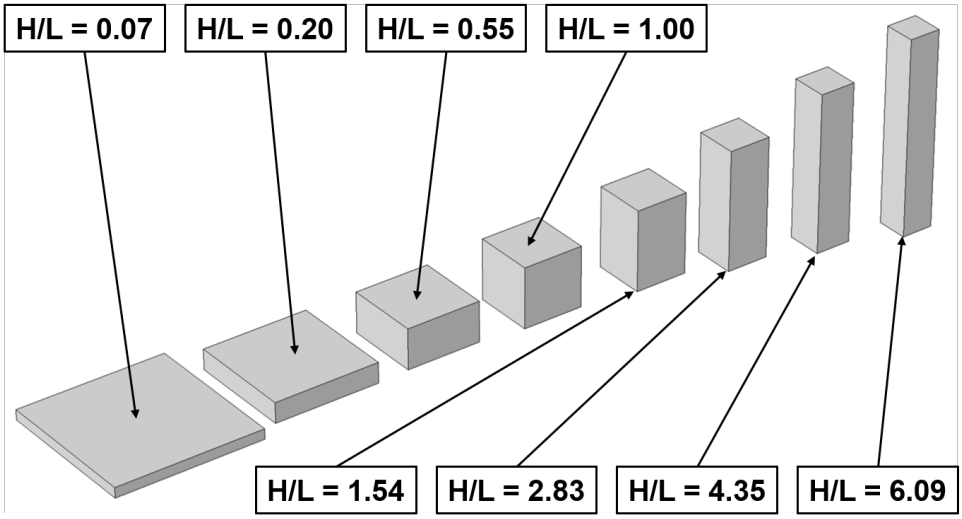

Figure 8.2: Sketch of samples to study the influence of the variation of area to a fixed volume, H/L stands for the ratio between the height H of a sample and its side length L.

Another point of interest would be the test of equal mixtures using different aggregates. In Chapter 2 a brief description was given of aggregates performance during rapid heating. However, aggregates also influence the thermal dilation [29–31] and thermal

conductivity [32–34] of concrete. Because Equation 2.23 was initially developed for solid, homogeneous materials, it assumes a linear relation between thermal dilation and conductivity with the material resistance to cracking. This assumption usually holds for concrete because most studies only use one type of aggregate per experiment (see Chapter 7 experiment and validation sections). Nevertheless, it is known that the thermal dilation of concrete is not linear [35, 36], as shown in Figure 4.7. Thus, a systematic study of samples using several types of aggregates could clarify the influence of these properties on spalling. The author believes this could require a small correction factor, that could be incorporated in the coefficient $C2$ of Equation 7.4.

Finally, if Portland cement is eventually replaced by a carbonatable cement, concrete would likely retain the mechanical properties better as decomposition of the main binder phase would start at 750°C instead of 300°C (see Chapter 2). Because of the low thermal conductivity of concrete [29], this difference could prove useful for the necessary time to evacuate a structure. However, very few studies regarding carbonated Portland cement or carbonatable calcium silicate cement exposure to high temperatures are available. Design guidelines would be necessary taking into account the effect of mixture not only in mechanical properties, but also in dimensional stability.

8.2.2. MODELLING OF SPALLING

The lattice model has been used in concrete for a long time [37] and the description of it and its three dimensional application can be found elsewhere [38]. Although initially developed to describe the fracture processes caused by mechanical stresses in concrete, this model has been extended to predict cracking due corrosion [39], chloride ingress [40], capillary absorption [41], buckling during 3D printing [42], among others. Some of these extensions directly benefit the creation of a spalling model as cracking due corrosion happens in a similar manner than the TMM of spalling (albeit in different time scales) and capillary absorption present the basis of water transport necessary for the THM of spalling. Further, the ANM model [43] allows for the use of realistically shaped aggregates, which can influence the water escape path and, thus, the raise of hydraulic stresses.

Recently, Lottman (2017) [44] developed a 2D lattice model for the prediction of spalling in concrete that attempted to couple the TMM and THM. This work tackled some issues mentioned throughout this thesis, such as the assumption of concrete as a solid, homogeneous and isotropic material. It also tried to include the difference in material through the study of two cases, one of concrete class C25/30 and another of concrete class C90/105. This model showed that the cracks developed in concrete during service were enough to release all water during a fire, making the THM negligible. Spalling would occur due to the buckling of concrete members caused by the TMM. These results are in opposition of experimental evidence of concrete spalling through THM while enduring compressive loads [45–47]. Moreover, the model neglected to take into account any influence of aggregates aside from their physical blockage of water transport. Additionally, the cases of concrete class C25/30 and C90/105 had the same microstructure, aggregate distribution and paste content, which is unrealistic. Finally, the anisotropy, heterogeneity and porosity of the material were chosen as fixed parameters for all concretes.

The work of Lottman (2017) [44] presented many important insights for the coupling of TMM and THM, and development of a fully functional spalling 2D model, but used porosity and permeability as the only non-mechanical properties of the material. As mentioned in Section 7.5, this is a common challenge in current finite element models trying to couple the different mechanisms of spalling. Although modelling was outside of the scope of this thesis, the author believes that the implementation of some of the findings of Chapter 7 could improve the model proposed by Lottman (2017) [44] and solve the neglect of THM issue.

The estimation of stresses caused by TMM seem accurate and require no adjustment. For the estimation of stresses due THM, the drying front would build up stresses similar to what was found in experiments using pore pressure gages, following Equation 2.24, as it was shown in Li et al (2021) [48] (see Figure 8.3). This is in agreement with the magnitude of stresses found in the model proposed by Lottman, however, when one crack occurred in the system, the gas pressures would revert to atmospheric pressure almost immediately. This could be improved by replacing the porosity by air content and both, average pore diameter and permeability by pore connectivity. The connectivity could be used in a bilinear relation in which micropores connectivity could still cause pressure buildup after a crack released water vapour concentrated in macropores. Further, σ_{THM} could receive a penalty based on the total pore connectivity of the concrete. For a given value of $\Lambda_{(XCT)} + \Lambda_{(MIP)}$, $\sigma_{THM} \rightarrow 0$. This threshold would have to be determined by testing samples with very high W/B ratios and very high PP indexes or very widespread cracking.

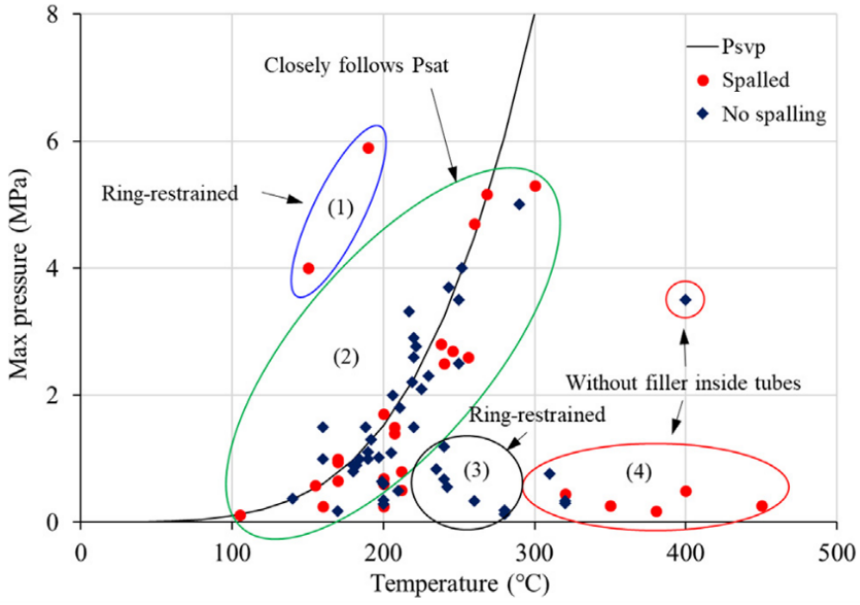

Figure 8.3: Relationship between maximum pore pressure and the saturated vapor pressure. Extracted from [48].

Because the material's properties are considered static for the duration of the simulation, relaxation could be considered instant, being applied in the next time step as it was suggested previously [49]. Finally, aggregates could be considered non-inert, by adding their expansion based on composition. Indeed, a two- or three-class aggregate classification system should be enough to account for its thermal behaviour [14, 45, 50–52]. Validation experiments could be carried out on granite and basalt samples, for example.

8.2.3. DEVELOPMENT OF HIGH STRENGTH REFRACTORY CONCRETE

Refractory concrete is usually designed for applications such as lining of kilns and ovens, where the material has to resist hundreds or thousands of high temperature cycles [1], but its mechanical resistance is usually not of concern. Although less common, applications in which the mechanical properties of refractory concrete are important exist, as it was demonstrated in Chapter 5. However, the development of very high strength refractory concrete is almost non-existent, as the material usually has to sacrifice the mechanical properties to endure higher temperatures [53, 54].

In this context, the findings in Chapter 4 could be of some importance, as both dunite and microgabbro retained very high compressive strength after being exposed to a temperature of 900°C. In fact, dunite has displayed a nearly 80% increase in resistance, with both rocks showing a compressive strength above 140 MPa after said temperature. Additionally, to the knowledge of the author, the results from dunite were previously unreported.

Research should be carried out on the possibility of using these stones as aggregates for the production of high strength refractory concrete post heating. Given its similar coefficient of thermal dilation to concrete (see Figure 4.7), these stones could go through firing after the concrete is already cast, so both the binder and aggregates suffer the initial shrinkage from chemical shift together. Such material could become an excellent option for all the applications suggested in the previous section. In particular, the high hardness of the stones could improve the resistance to ablation and erosion, as required on launchpads.

Nevertheless, these rocks are not a regular type of aggregate found in any supplier, and furthermore, are usually not provided in small batches. Thus, a cost analysis would need to be performed considering the transport and crushing energy to convert the rocks to concrete aggregates before this is considered a sound engineering solution, even if the experimental results point to a high strength refractory concrete.

8.2.4. PREDICTION OF CYCLIC THERMAL SHOCK PERFORMANCE

Finally, most applications discussed on this chapter require materials that endure repeated exposure to thermal shock and high temperatures. However, due to the limited capacity of prediction of materials performances, very few experiments aim to determine the long term behaviour of materials in cyclic thermal shock environments. This is a field most often explored in the refractories community, where the main concern is chemical equilibrium and high temperature corrosion [55, 56]. For concrete, this is a knowledge gap.

Assuming a material does not spall and retain a certain degree of mechanical properties after exposure to high temperatures, one could approach the determination of its

service-life with an approach similar to what was proposed by Yu et al (2017) [57] for freeze-thaw fatigue. This is fitting as these authors already propose a frame of reference for fatigue failure due temperature cycles. Naturally, the experiment would have to be adapted to high temperature thermal shock.

Figure 8.4 shows a sketch of how the experiment was envisioned. As in freeze-thaw testing, the main tool for concrete analysis would be ultrasonic pulse signals. To perform the temperature cycles, rather than putting the concrete inside an oven, a steel plate could be pre-heated to a certain temperature and then placed on top of a rectangular concrete slab. The size and temperature of the steel plate should be equivalent to the amount of heat desired per cycle. The ultrassonic sensors would be embedded in the slab, thus it is recommended to use transducers with a aggregate coating (see top right corner of Figure 8.4). Because temperature affects the ultrasonic transmission within solids [58], a preliminary experiment in which the slab is slowly heated while pulse signals are continuously recorded should be performed as means to create a baseline. Additionally, a laser thermometer could be used to determine the cooling rate of the selected steel plate at the local laboratory environmental temperature. Finally, during the cycles the laser thermometer could be pointed at the location of one of the sensors for temperature correction.

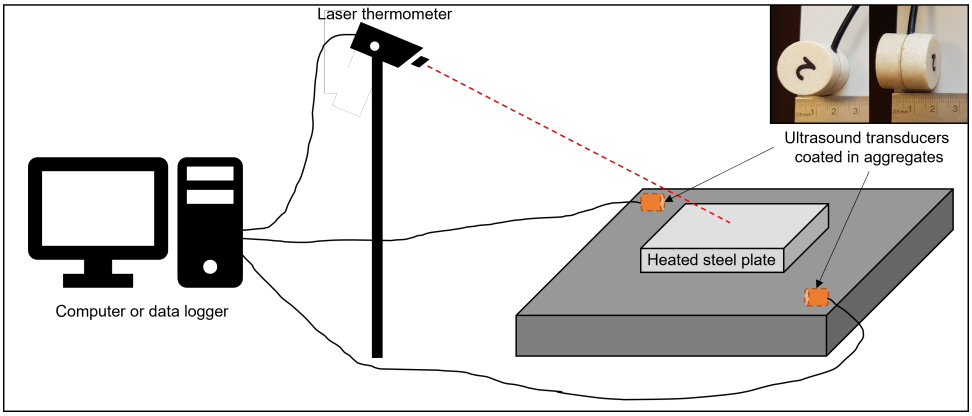

Figure 8.4: Sketch of experimental setup for cyclic thermal analysis of concrete.

The shift in pulse signal could be potentially correlated to macro-cracks formation or the deterioration of mechanical properties, as it was proven elsewhere [59]. Macro-cracks formation could be inspected through visual appreciation or X-ray tomography, however, the size of the sample would limit the tomography resolution to a minimal of several millimeters. The deterioration of mechanical properties would require the destructive testing of the samples after a set number of cycles, which would require considerable more repeated samples. Still, results of such experiment could provide a way of creating guidelines for the estimation of service-life of structures repeatedly exposed to thermal shock events. This would be a relatively novel field of study for concrete and could benefit factories from the industries mentioned above.

BIBLIOGRAPHY

[1] Ana Da Luz, M.A.L. Braulio, and Victor Pandolfelli. *F.I.R.E. Compendium Series - Refractory Castable Engineering*. Göller Verlag, Mar. 2015, p. 734. ISBN: ISBN 978-3-87264-004-8.

[2] J. Bensted. "Calcium Aluminate Cements". In: *Structure and performance of cements*. Ed. by J. Bensted and P. Barnes. London: CRC Press, 2002. Chap. 13, pp. 114–139.

[3] Karen L. Scrivener, Jean-Louis Cabiron, and Roger Letourneux. "High-performance concretes from calcium aluminate cements". In: *Cement and Concrete Research* 29.8 (1999), pp. 1215–1223. ISSN: 0008-8846. DOI: https://doi.org/10.1016/S0008-8846(99)00103-9. URL: https://www.sciencedirect.com/science/article/pii/S0008884699001039.

[4] H.F.W. Taylor. *Cement Chemistry*. Thomas Telford, 1997. ISBN: 9780727725929. URL: https://books.google.nl/books?id=1BOETtwi7mMC.

[5] H. Ideker J. et al. "Calcium Aluminate Cements". In: *Lea's Chemistry of Cement and Concrete*. Ed. by P.C. Hewlett and M. Liska. Oxford: Butterworth-Heinemann, 2019. Chap. 13, pp. 713–782.

[6] L.A. Bauer. *Materiais De Construção - Vol. 1*. LTC, 2000. ISBN: 9788521612490.

[7] P.K. Mehta and P.J.M. Monteiro. *Concrete: Microstructure, Properties, and Materials*. McGraw Hill professional. McGraw-Hill Education, 2006. ISBN: 9780071462891. URL: https://books.google.nl/books?id=3j5EAQAAIAAJ.

[8] S.R. Bragança and C.P. Bergmann. "Materiais Refratários e Abrasivos". In: *Materiais de Construção Civil*. Ed. by G.C. Isaia. São Paulo: IBRACON, 2010. Chap. 20, pp. 619–655.

[9] Eduardo Peris Mora. "Life cycle, sustainability and the transcendent quality of building materials". In: *Building and Environment* 42.3 (2007), pp. 1329–1334. ISSN: 0360-1323. DOI: https://doi.org/10.1016/j.buildenv.2005.11.004. URL: http://www.sciencedirect.com/science/article/pii/S0360132305004737.

[10] K. Sakkas et al. "In-situ fire test to assess tunnel lining fire resistance". In: *Tunnelling and Underground Space Technology* 85 (2019), pp. 368–374. ISSN: 0886-7798. DOI: https://doi.org/10.1016/j.tust.2019.01.002. URL: https://www.sciencedirect.com/science/article/pii/S0886779818304863.

[11] D. de Silva et al. "Structural safety assessment of concrete tunnel lining subjected to fire". In: *Fire Safety Journal* 134 (2022), p. 103697. ISSN: 0379-7112. DOI: https://doi.org/10.1016/j.firesaf.2022.103697. URL: https://www.sciencedirect.com/science/article/pii/S0379711222001746.

[12] A. Bentur and S. Mindess. *Fibre Reinforced Cementitious Composites, Second Edition*. Modern Concrete Technology. Taylor & Francis, 2006. ISBN: 9780203088722. URL: https://books.google.nl/books?id=zqJbJ4rNXvEC.

[13] I. Marković. *High-performance Hybrid-fibre Concrete: Development and Utilisation*. DUP Science, 2006. ISBN: 9789040726217. URL: https://books.google.nl/books?id=B4ZgZlB75mYC.

[14] C.A. Britez and C.N. Costa. "Ações do Fogo nas Estruturas de Concreto". In: *Concreto: Ciência e Tecnologia*. Ed. by G.C. Isaia. São Paulo: IBRACON, 2011. Chap. 29, pp. 1029–1068.

[15] L. Kanayama and A. Beil. "SpaceX continues forward progress with Starship on Starhopper anniversary". In: *NASASpaceFlight* (Aug. 28, 2021). URL: https://www.nasaspaceflight.com/2021/08/starship-starhopper/ (visited on 11/16/2022).

[16] L.M. Calle et al. *Refractory Materials for Flame Deflector Protection System Corrosion Control: Similar Industries and/or Launch Facilities Survey*. Tech. rep. Report N.: NASA/TM-2013-217910. National Aeronautics and Space Administration (NASA), Jan. 2013. URL: https://ntrs.nasa.gov/citations/20130014277.

[17] Rodgers Bangi Mugume and Takashi Horiguchi. "Prediction of spalling in fibre-reinforced high strength concrete at elevated temperatures". In: *Materials and Structures* 47.4 (Apr. 2014), pp. 591–604. ISSN: 1871-6873. DOI: 10.1617/s11527-013-0082-9. URL: https://doi.org/10.1617/s11527-013-0082-9.

[18] L Missemer et al. "Fire spalling of ultra-high performance concrete : From a global analysis to microstructure investigations". In: *Cement and Concrete Research* 115.April 2018 (2019), pp. 207–219. ISSN: 0008-8846. DOI: 10.1016/j.cemconres.2018.10.005. URL: https://doi.org/10.1016/j.cemconres.2018.10.005.

[19] Fabio P. Figueiredo et al. "Effects of Recycled Steel and Polymer Fibres on Explosive Fire Spalling of Concrete". In: *Fire Technology* 55.5 (Sept. 2019), pp. 1495–1516. ISSN: 1572-8099. DOI: 10.1007/s10694-019-00817-9. URL: https://doi.org/10.1007/s10694-019-00817-9.

[20] *Space Launch Services Market Size, Share COVID-19 Impact Analysis*. Tech. rep. Report ID: FBI101931. Fortune Business Insights, May 2022. URL: https://www.fortunebusinessinsights.com/industry-reports/space-launch-services-market-101931.

[21] J.C. McDowell. *Jonathan's space report Launch Logs*. Tech. rep. 2019. URL: https://planet4589.org/index.html.

[22] J. Bret Robertson and M. Tyler Ley. "Determining the water to cement ratio of fresh concrete by evaporation". In: *Construction and Building Materials* 242 (2020), p. 117972. ISSN: 0950-0618. DOI: https://doi.org/10.1016/j.conbuildmat.2019.117972. URL: https://www.sciencedirect.com/science/article/pii/S0950061819334257.

8

[23] Angel Padilla et al. “Correlating damage and cracking with air (gas) permeability in concrete using the Brazilian tension test”. In: *Construction and Building Materials* 348 (2022), p. 128616. ISSN: 0950-0618. DOI: https://doi.org/10.1016/j.conbuildmat.2022.128616. URL: https://www.sciencedirect.com/science/article/pii/S0950061822022735.

[24] Mugume Rodgers Bangi and Takashi Horiguchi. “Pore pressure development in hybrid fibre-reinforced high strength concrete at elevated temperatures”. In: *Cement and Concrete Research* 41.11 (2011), pp. 1150–1156. ISSN: 0008-8846. DOI: https://doi.org/10.1016/j.cemconres.2011.07.001. URL: https://www.sciencedirect.com/science/article/pii/S000888461100192X.

[25] N. Algourdin et al. “Influence of polypropylene and steel fibres on thermal spalling and physical-mechanical properties of concrete under different heating rates”. In: *Construction and Building Materials* 259 (2020), p. 119690. ISSN: 0950-0618. DOI: https://doi.org/10.1016/j.conbuildmat.2020.119690. URL: https://www.sciencedirect.com/science/article/pii/S0950061820316950.

[26] Yining Ding et al. “Influence of different fibers on the change of pore pressure of self-consolidating concrete exposed to fire”. In: *Construction and Building Materials* 113 (2016), pp. 456–469. ISSN: 0950-0618. DOI: https://doi.org/10.1016/j.conbuildmat.2016.03.070. URL: https://www.sciencedirect.com/science/article/pii/S0950061816303658.

[27] Young-Sun Heo et al. “Critical parameters of nylon and other fibres for spalling protection of high strength concrete in fire”. In: *Materials and Structures* 44.3 (Apr. 2011), pp. 599–610. ISSN: 1871-6873. DOI: 10.1617/s11527-010-9651-3. URL: https://doi.org/10.1617/s11527-010-9651-3.

[28] G. Debicki, R. Haniche, and F. Delhomme. “An experimental method for assessing the spalling sensitivity of concrete mixture submitted to high temperature”. In: *Cement and Concrete Composites* 34.8 (2012), pp. 958–963. ISSN: 0958-9465. DOI: https://doi.org/10.1016/j.cemconcomp.2012.04.002. URL: https://www.sciencedirect.com/science/article/pii/S0958946512000637.

[29] C.S. Neto. “Agregados Naturais, Britados e Artificiais para Concreto”. In: *Concreto: Ciência e Tecnologia*. Ed. by G.C. Isaia. São Paulo: IBRACON, 2011. Chap. 7, pp. 233–260.

[30] N. Algourdin et al. “Effect of fine and coarse recycled aggregates on high-temperature behaviour and residual properties of concrete”. In: *Construction and Building Materials* 341 (2022), p. 127847. ISSN: 0950-0618. DOI: https://doi.org/10.1016/j.conbuildmat.2022.127847. URL: https://www.sciencedirect.com/science/article/pii/S0950061822015203.

[31] Víctor Revilla-Cuesta et al. “Self-compacting concrete with recycled concrete aggregate subjected to alternating-sign temperature variations: Thermal strain and damage”. In: *Case Studies in Construction Materials* 17 (2022), e01204. ISSN: 2214-5095. DOI: https://doi.org/10.1016/j.cscm.2022.e01204. URL: https://www.sciencedirect.com/science/article/pii/S2214509522003369.

[32] Vito Francioso, Carlos Moro, and Mirian Velay-Lizancos. “Effect of recycled concrete aggregate (RCA) on mortar’s thermal conductivity susceptibility to variations of moisture content and ambient temperature”. In: *Journal of Building Engineering* 43 (2021), p. 103208. ISSN: 2352-7102. DOI: https://doi.org/10.1016/j.jobe.2021.103208. URL: https://www.sciencedirect.com/science/article/pii/S2352710221010664.

[33] Weiwen Quan et al. “Efficient numerical model for effective thermal conductivity of concrete with aggregates of different morphologies and imperfect interfaces”. In: *International Journal of Heat and Mass Transfer* 185 (2022), p. 122358. ISSN: 0017-9310. DOI: https://doi.org/10.1016/j.ijheatmasstransfer.2021.122358. URL: https://www.sciencedirect.com/science/article/pii/S0017931021014575.

[34] Lucen Hao et al. “Thermal conductivity of 3D printed concrete with recycled fine aggregate composite phase change materials”. In: *Journal of Cleaner Production* 364 (2022), p. 132598. ISSN: 0959-6526. DOI: https://doi.org/10.1016/j.jclepro.2022.132598. URL: https://www.sciencedirect.com/science/article/pii/S0959652622021977.

[35] Tayfun Uygunoğlu and İlker Bekir Topçu. “Thermal expansion of self-consolidating normal and lightweight aggregate concrete at elevated temperature”. In: *Construction and Building Materials* 23.9 (2009), pp. 3063–3069. ISSN: 0950-0618. DOI: https://doi.org/10.1016/j.conbuildmat.2009.04.004. URL: http://www.sciencedirect.com/science/article/pii/S0950061809001159.

[36] I. Hager. “Behaviour of cement concrete at high temperature”. In: *Bulletin of the Polish Academy of Sciences: Technical Sciences* 61.No 1 (2013), pp. 145–154. DOI: 10.2478/bpasts-2013-0013.

[37] H.E.J.G. Schlangen. “Experimental and numerical analysis of fracture processes in concrete”. PhD thesis. Delft University of Technology, 1993.

[38] G. Lilliu. “3D analysis of fracture processes in concrete”. PhD thesis. Delft University of Technology, 2007.

[39] Branko Šavija et al. “Cracking of the concrete cover due to reinforcement corrosion: A two-dimensional lattice model study”. In: *Construction and Building Materials* 44 (2013), pp. 626–638. ISSN: 0950-0618. DOI: https://doi.org/10.1016/j.conbuildmat.2013.03.063. URL: https://www.sciencedirect.com/science/article/pii/S0950061813002730.

[40] Branko Šavija, José Pacheco, and Erik Schlangen. “Lattice modeling of chloride diffusion in sound and cracked concrete”. In: *Cement and Concrete Composites* 42 (2013), pp. 30–40. ISSN: 0958-9465. DOI: https://doi.org/10.1016/j.cemconcomp.2013.05.003. URL: https://www.sciencedirect.com/science/article/pii/S0958946513000899.

[41] Anmol Singla et al. “Modelling of capillary water absorption in sound and cracked concrete using a dual-lattice approach: Computational aspects”. In: *Construction and Building Materials* 320 (2022), p. 125826. ISSN: 0950-0618. DOI: https://doi.org/10.1016/j.conbuildmat.2021.125826. URL: https://www.sciencedirect.com/science/article/pii/S0950061821035595.

[42] Ze Chang et al. “3D concrete printing: Lattice modeling of structural failure considering damage and deformed geometry”. In: *Cement and Concrete Composites* 133 (2022), p. 104719. ISSN: 0958-9465. DOI: https://doi.org/10.1016/j.cemconcomp.2022.104719. URL: https://www.sciencedirect.com/science/article/pii/S0958946522003122.

[43] Hau-Kit Man and Jan G. M. van Mier. “Size effect on strength and fracture energy for numerical concrete with realistic aggregate shapes”. In: *International Journal of Fracture* 154.1 (Nov. 2008), pp. 61–72. ISSN: 1573-2673. DOI: 10.1007/s10704-008-9270-y. URL: https://doi.org/10.1007/s10704-008-9270-y.

[44] B.B.G. Lottman. “The spalling mechanism of fire exposed concrete”. PhD thesis. Delft University of Technology, 2017.

[45] K D Hertz. “Limits of spalling of fire-exposed concrete”. In: *Fire Safety Journal* 38 (2003), pp. 103–116.

[46] R. Jochen and M. Christoph. “The influence of pore size distribution and the chemical composition of cement paste on the explosive spalling of concrete”. In: *5th International Workshop on Concrete Spalling due to Fire Exposure*. RISE Research Institute of Sweden. Borås, Sweden: RILEM, 2017.

[47] Francesco Lo Monte, Roberto Felicetti, and Chiara Rossino. “Fire spalling sensitivity of high-performanceconcrete in heated slabs under biaxial compressive loading”. In: *Materials and Structures* 52.1 (Jan. 2019), p. 14. ISSN: 1871-6873. DOI: 10.1617/s11527-019-1318-0. URL: https://doi.org/10.1617/s11527-019-1318-0.

[48] Ye Li et al. “Pore pressure build-up and explosive spalling in concrete at elevated temperature: A review”. In: *Construction and Building Materials* 284 (2021). ISSN: 09500618. DOI: 10.1016/j.conbuildmat.2021.122818.

[49] E. Schlangen, E.A.B. Koenders, and K. van Breugel. “Influence of internal dilation on the fracture behaviour of multi-phase materials”. In: *Engineering Fracture Mechanics* 74.1 (2007). Fracture of Concrete Materials and Structures, pp. 18–33. ISSN: 0013-7944. DOI: https://doi.org/10.1016/j.engfracmech.2006.01.033. URL: https://www.sciencedirect.com/science/article/pii/S0013794406000452.

[50] Qianmin Ma et al. “Mechanical properties of concrete at high temperature—A review”. In: *Construction and Building Materials* 93 (2015), pp. 371–383. ISSN: 0950-0618. DOI: https://doi.org/10.1016/j.conbuildmat.2015.05.131. URL: https://www.sciencedirect.com/science/article/pii/S0950061815006765.

[51] Jin-Cheng Liu, Kang Hai Tan, and Yao Yao. "A new perspective on nature of fire-induced spalling in concrete". In: *Construction and Building Materials* 184 (2018), pp. 581–590. ISSN: 0950-0618. DOI: https://doi.org/10.1016/j.conbuildmat.2018.06.204. URL: https://www.sciencedirect.com/science/article/pii/S0950061818316118.

[52] T.M. Jeyashree, P.R. Kannan Rajkumar, and K.S. Satyanarayanan. "Developments and research on fire response behaviour of prestressed concrete members – A review". In: *Journal of Building Engineering* 57 (2022), p. 104797. ISSN: 2352-7102. DOI: https://doi.org/10.1016/j.jobe.2022.104797. URL: https://www.sciencedirect.com/science/article/pii/S2352710222008105.

[53] W E Lee et al. "Castable refractory concretes". In: *International Materials Reviews* 46.3 (2001), pp. 145–167.

[54] M Nouri-khezrabad et al. "Nano-bonded refractory castables". In: *Ceramics International* 39.4 (2013), pp. 3479–3497. ISSN: 0272-8842. DOI: 10.1016/j.ceramint.2012.11.028. URL: http://dx.doi.org/10.1016/j.ceramint.2012.11.028.

[55] Z. Ignaszak and P. Popielarski. "Contribution to Thermal Properties of Multi-Component Porous Ceramic Materials Used in High-Temperature Processes in the Foundry Industry". In: *Heat and Mass Transfer in Porous Media*. Ed. by J.M.P.Q. Delgado. Berlin, Heidelberg: Springer Berlin Heidelberg, 2012, pp. 187–218. ISBN: 978-3-642-21966-5. DOI: 10.1007/978-3-642-21966-5_8. URL: https://doi.org/10.1007/978-3-642-21966-5_8.

[56] J. Poirier and M. Rigaud. *FIRE Compendium Series: Corrosion of refractories : the fundamentals*. F.I.R.E. compendium series. Göller Verlag, 2017. ISBN: 9783872640062. URL: https://books.google.nl/books?id=rDwqswEACAAJ.

[57] Hongfa Yu, Haoxia Ma, and Kun Yan. "An equation for determining freeze-thaw fatigue damage in concrete and a model for predicting the service life". In: *Construction and Building Materials* 137 (2017), pp. 104–116. ISSN: 0950-0618. DOI: https://doi.org/10.1016/j.conbuildmat.2017.01.042. URL: https://www.sciencedirect.com/science/article/pii/S0950061817300557.

[58] J.L. Rose. *Ultrasonic Waves in Solid Media*. Ultrasonic Waves in Solid Media. Cambridge University Press, 2004. ISBN: 9780521548892. URL: https://books.google.nl/books?id=DEtHDJJ-RS4C.

[59] Manda Ramaniraka et al. "Effect of Interfacial Transition Zone on diffuse ultrasound in thermally damaged concrete". In: *Cement and Concrete Research* 152 (2022), p. 106680. ISSN: 0008-8846. DOI: https://doi.org/10.1016/j.cemconres.2021.106680. URL: https://www.sciencedirect.com/science/article/pii/S000888462100329X.

9

RETROSPECTION, CONCLUSIONS AND FINAL CONSIDERATIONS

No one really starts anything new, Mrs. Nemur. Everyone builds on other men's failures. There is nothing really original in science. What each man contributes to the sum of knowledge is what counts.

Daniel Keyes, Flowers for Algernon

... anyone who thinks one book has all the answers hasn't read enough books.

Brian K. Vaughn, Saga

This is a concluding chapter explaining the scientific and technical implications of the research findings for society in considerable detail.

9.1. RETROSPECTION

THE main aim of this thesis was to develop a predictive method to determine if a material would suffer high temperature spalling under certain heating conditions. This was necessary to design a structural concrete that would not be affected by it, and could be installed in a factory setting. Due to schedule demands from the industrial partners of the project, the design of the material became the first part of the thesis, while the prediction of spalling was researched later. Because each of these tasks demanded a multi-level approach, the following works were conducted:

In Chapter 2 a review of the main effects and chemical changes caused by high temperature was performed in the conventional building materials, followed by some novel materials being currently explored. This aided in the pre-selection of material to be tested during the project. Further, the chapter also reviewed the current understanding of high temperature spalling, the causes and the main methods of avoidance. This was the starting point for Chapters 6 and 7.

In Chapters 3 and 4 the binder and stones to be used in the project were pre-selected and tested in conditions similar to what is present at the factory of the industrial partners. A new experimental setup had to be developed in order to match the heating conditions and perform such observations. Typical analytical chemistry and microscopy techniques were employed to study the microstructural changes in the materials, with focus on how this could affect the stress state of the concrete. Finite element modelling was used to explain some of the behaviour of the samples and predict performance on a large scale setting.

In Chapter 5 the materials explored in the previous chapters were used to design four test elements that would be installed at the studied factory location. Such elements would require to follow all codes for precast concrete elements that are subjected to hoisting operations. To design such elements, the PhD candidate spent time in the factory determining the actual load cases and performing a historical review of the factory operation and how the load cases evolved. After installation of the test elements, the research team was allowed access to the area of operation for observation of the elements twice, one after 6 months of factory operation and one after 1 year of factory operation. The inspections showed that the test elements had a much better performance than the current method of protection used and the test was considered successful.

In Chapters 6 and 7 attempts were made to advance the knowledge in spalling prediction. Initially, because of the high amount of influencing parameters, it was decided to try a machine learning approach. Before testing algorithms, a large database of concrete samples that went through spalling experiments was necessary. Such database was developed by taking note of over 40 relevant features in experiments that included concrete samples going through spalling tests. Over one thousand unique combination of parameters were collected and annotated regarding the sample resistance to spalling. Several architectures were attempted to use machine learning for the prediction of concrete spalling, but the algorithms just fell short of 90% accuracy. It was hypothesized that this was due the incomplete information provided regarding the microstructure of samples. For this reason, the next chapter was dedicated to the exploration of the pores structure and connectivity within mortar on their spalling. It culminated on an analytical equation that could predict spalling in laboratory samples and achieved a 91% accuracy

when validated with experiments from literature.

In Chapter 8 a review of possible applications for the findings of the other chapters is provided and recommendations for extensions of the research performed. Because the present thesis focused on an industrial problem, many of the outcomes could be used to aid in other factories that also deal with high temperature issues. The spalling prediction could also be used for the benefit of road tunnel structures, or even rearranged to work as a design guideline, as shown in this chapter. Furthermore, launchpads are pointed out as a relatively new field of interest in which this research would fit well. Finally, recommendations for improvement of spalling prediction, both, through further development of the proposed equation or through numerical methods is offered. A suggestion on how to pursue a continuation of the work carried in Chapter 4 is also provided.

9.2. GENERAL CONCLUSIONS

Although conclusions are provided in every chapter, these are restricted to the corresponding work. In this section, some general conclusions on this research topic are given:

- **Special applications require special experimental setups**
  The conditions to which structures are submitted in factories are fairly rare and accordingly, literature is scarce. The standard experiments for concrete submitted to high temperatures involve heating a sample in an oven and studying the changes afterwards, which is motivated by the investigation of remaining properties after a fire event. However, in Chapter 3, the first section is dedicated to explaining why this would be a poor performance predictor to industrial setting that include non-fire related high temperature events. The former justifies the different test method used in Chapters 3 and 4. This allowed for the study of the interaction between the molten material and the proposed surface protection, which resulted on some assumptions regarding the type and rate of high temperature chemistry to occur in the actual setting of the case study. Similarly, for different factories, experimental setups should include the contact of the sample with the product in question at high temperatures whenever possible. This would allow to extend the investigation into chemical reactions often unavailable anywhere else, besides the effects of temperature in the structural material.

- **Upscaling requires more engineering than scientific work**
  When designing the test elements from Chapter 5, many of the complications were related to logistics and practical limitations, not to the properties of the elements. Furthermore, most meeting with the design committee focused on detailing of reinforcement based on normal temperature concrete codes. Finally, it is the opinion of the author that the stones in the hybrid elements eventually fractured due to a design flaw, not a material one. Such challenges are common for materials destined to be used in high temperature environments. To overcome many of this situation, most industrial refractory concrete is currently sprayed, avoiding the need of considerations regarding dynamic loads, or redundant reinforcement. Although it was necessary to produce precast elements for this

thesis, the future application of the material would benefit from casting through the wet gunning method.

- **Testing of concrete spalling needs better reporting**
  While studying for the writing of Chapter 2 and searching for papers for the creation of the database in Chapter 6, it became clear that spalling experiments need better detailing of its own experimental parameters. Figures 6.2 and 6.4 show several hundreds of samples with unreported aggregates size, type or lading state of the samples. These are all features that severely influence spalling behaviour. Moreover, tens of papers were not added to the database for lacking fundamental information regarding the used material, such as, W/C ratio, mixture design, fibre content and dimensions, or heating parameters. This is likely due to the somewhat still controversial determination of main parameters influencing spalling in concrete. However, considering the results shown in Figure 6.9, most parameters should be reported, as they all have varying degrees of influence in spalling.

- **The complexity of cement porosity is a formidable obstacle to spalling research**
  In addition to the previous conclusion, Chapter 6 found the microstructure to be the least reported feature of concrete in spalling research. This is in big part due to the sheer complexity of it, but also because it became somewhat acceptable to use W/C ratio as a replacement for information in cement microstructure. This is often not enough for spalling, as porosity affects the concrete behaviour differently depending on its size and distribution. Chapter 7 presents some evidence that W/C ratio is a suitable indication of the amount and connectivity of capillary porosity, but not of macro-porosity, which is more important regarding the THM of spalling. The influence of macro-porosity in spalling was quantified through microtomography, but this incurs a considerable amount of data per sample that would not be possible to make available in publications without the creation of a dedicated server. A correlation between the connectivity of the macro-porosity was created with air content, compressive strength and fibres dimensions and content on the samples. However, these properties are also often not reported. Although the multi-scale effect of porosity in spalling requires the employment of more than one analytical technique for its analysis, this is an essential feature of samples missing in the study of concrete spalling and remains one of the main obstacles to further the knowledge in this field.

- **Spalling is both a material and a structural phenomenon**
  When concrete is a part of a structure, it experiences several circumstances that small laboratory samples do not. Some examples are stress relaxation, large moisture gradients, eccentric loading, prestressing, among others. Although these also influence spalling behaviour, they are very difficult to control in a laboratory setting. This is such a challenge that many of the research published exploring one of these circumstances overlook all others and several material parameters. In this regard, the continual advancement of computational methods to simulate spalling in concrete is a very promising manner of bridging the gap currently placed between material and structural research of this phenomenon.

9.3. FINAL CONSIDERATIONS

This was a challenging PhD topic with so many interesting research possibilities that the selection of specific paths was a task in itself. Eventually, the research questions posed in Chapter 1 served as guidelines on how to address the defined problem and how to limit the curiosity and will to investigate all aspects of the subject. After the writing of the present thesis, these questions can now be answered and are presented below.

1 **Which materials and proportion can produce a spalling resistant concrete respecting the logistics constraints of application in steel factories?**
A concrete mixture was provided in Chapter 5 for elements that survived over one year of factory operation in critical locations with very few damage and no signs of spalling.

1.1 **Can oven heating simulate the reaction of concrete to spilled molten steel?**
The work performed in Chapter 3 shows that oven heating is insufficient to simulate such reaction.

1.2 **What W/C ratio would perform better in conditions usually found in steel factories?**
Based on the results of Chapter 3 a W/C ratio of 0.40 was selected due to the risk of flooding in the area studied, combined with the use of calcium aluminate cement.

1.3 **Could plutonic rocks act as a protection layer to the concrete receiving high temperature spills?**
The selected rocks showed outstanding performance at high temperatures in Chapter 4 and resisted the loads at the factory better than the conventional repair material in Chapter 5. Depending on the cost of installation, this might be a competitive solution to monolithic concrete.

1.4 **Would a hybrid concrete/stone design perform better than monolithic concrete?**
The inspections performed at the steel factory revealed that monolithic concrete elements performed better than hybrid concrete/stone panels.

1.5 **What is the durability of the proposed solution?**
Unfortunately, the limited access of the PhD candidate to the test elements prevented the estimation of their durability. Nevertheless, all panels had over 60% integrity, with the monolithic elements presenting very few damage only in small locations. Optimistically, this could indicate a very long durability for the monolithic elements.

2 **Given a certain mixture design and composition of concrete, is it possible to predict if spall will occur for a determined thermal load?**
Chapter 7 shows that this is possible for saturated laboratory samples with over 90% of accuracy. Still, the full prediction of spalling requires many other considerations discussed in that Chapters 6, 7, 8 and 9.

2.1 **Which are the key physical or mechanical properties governing the occurrence of spalling in concrete?**
Many of the governing parameters of the phenomenon were identified through the exploration of the somewhat extensive database reported in Chapter 6. These were identified as polypropylene use, content and dimensions; sample volume; concrete heating conditions; compressive strength; moisture content; confinement; curing; and aggregates type, size and content. However, Chapter 7 shows that other properties, such as porosity details, can also govern the process.

2.2 **Why are spalling results so inconsistent across different laboratories?**
This was largely attributed to unreported details in the tested samples, such as pore connectivity, that can cause early spalling.

2.3 **How much loading and confinement affect the material behaviour towards spalling?**
The analysis of the database showed that confinement severely increases the likelihood of spalling. While the influence of loading was found to be of less significance, this might be due the low amount of research found on it.

2.4 **How can the contribution of concrete porosity be accounted?**
Chapter 7 offers a method to classify concrete porosity into two categories and estimate the contribution of each one to spalling. This is done using a combination of mercury intrusion porosimetry, air content determination and X-ray microtomography.

2.5 **Can pore connectivity be quantified and used as a spalling predictor?**
The results cited in the previous answer were treated to estimate pore connectivity at different scales and then predict spalling using Equation 7.4. The quantification of pore connectivity is definitely possible in the context of pores relevant to spalling failure of concrete. The use of this for the prediction of the phenomenon, on the other hand, was only partially proven.

Finally, this thesis started stating the importance of sustainable development for society and civil engineering in particular. Then, a clear correlation was offered between the increase in durability of structures and the reduction of environmental impact by the construction industry. This is of notable importance to structures subjected to high temperatures, as many strategies rely on repair or even replacement after a single event. The effort to better understand and predict spalling, was taken to aid in the design of a durable material against thermal shock. In this context, the entire thesis was aimed at the improvement of concrete durability against this form of deterioration, ultimately for the promotion of more sustainable designs. This is aligned with the author's view of the high importance of the current climate crisis and the need for the combined effort of the scientific community to tackle it in all fields of industry simultaneously.

A

APPENDIX A: STRUCTURAL DESIGN OF CASE STUDY PANELS

A

A.1. REINFORCEMENT & STONES ATTACHMENT

Although the panels were the test samples developed by TU Delft, the design of the reinforcement was done by the engineering department of steel factory. This was a requirement based on previous experience of concrete trials at the studied location. The details for the reinforcement of the monolithic concrete panels are displayed in Figure A.1, while the details for the concrete-stone hybrid panels are in Figure A.2.

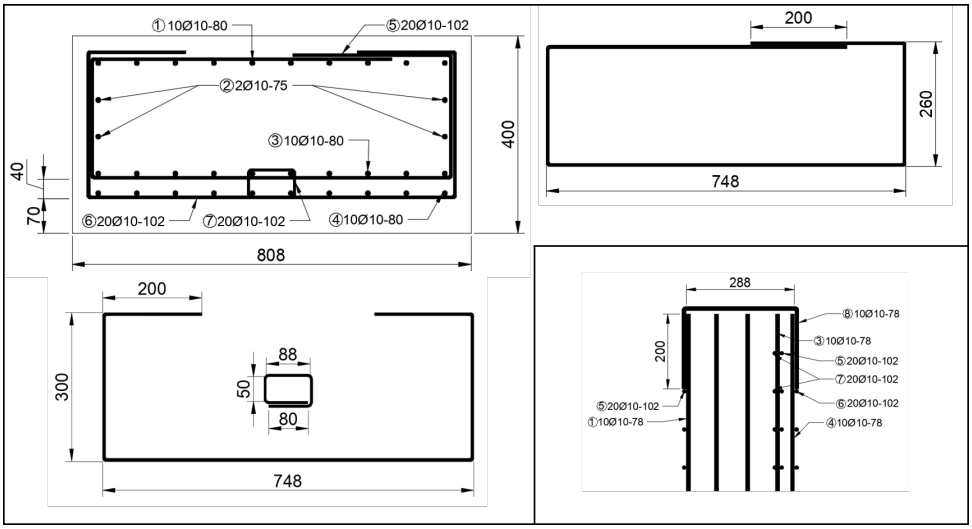

Figure A.1: Details of reinforcement used for monolithic concrete panels, units in mm.

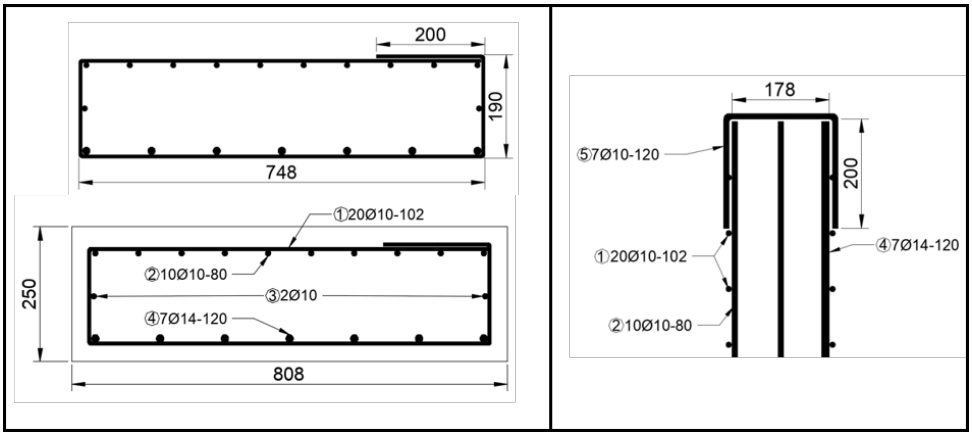

Figure A.2: Details of reinforcement used for concrete-stone hybrid panels, units in mm.

All panels were reinforced with construction steel B500. In the monolithic concrete panels, a basalt mesh BAS MESH 400 from Basaltex ®was placed in the face of the panels

during casting. These meshes possessed a window size of 35 mm x 28 mm and a weight of 400 g/m^2. The meshes received a concrete cover of 15 mm.

The dimensions of the panels and the used stone blocks were adapted based on the availability of large pieces of dunite. The stone blocks were cut into 36 x 36 x 15 cm cuboids. The dimensions of the panels were decided as approximately 2.2 x 0.8 x 0.4 m, this would allow for two columns of stone blocks, each with six blocks. For logistic reasons, it was necessary to cut one block in each column in two and use half block on top and half block in the bottom. To test both stones under the same conditions, it was decided to put one column of each stone in each panel. Figure A.3 shows the final design of the panels.

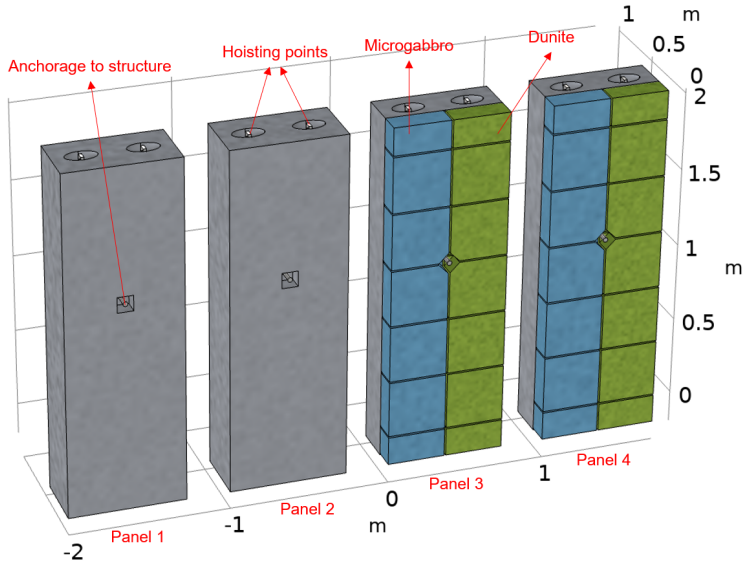

Figure A.3: Sketch of for panels designed for placement in steel factory.

The initial attachment of the stone blocks was envisioned using L-profiles of steel embedded in the concrete. These profiles would have holes, which would allow steel pins to pass, connecting the stones without a rigid connection to allow for free dilation. However, the engineering department of the steel factory requested the addition of steel anchors grouted in the stones as a rigid connection. Both attachments were used as depicted in Figure A.4. It was also requested that TU Delft would prove the strength of the grouted anchors.

Two pull-out tests were performed to ensure the adherence of the embedded steel bar to the stone blocks. These tests were performed in microgabbro blocks with dimensions of 180 x 180 x 146 mm. For the first test, a hole of 16 mm diameter and 48 mm height was drilled in the microgabbro cube and a ribbed steel bar with 12 mm diameter and 120 mm height was grouted to the hole. After 7 days, the sample was tested through the uniaxial pulling of the bar while the block was locked in a steel frame with sufficiently high elastic modulus for its deformation to be considered negligible. The second test was

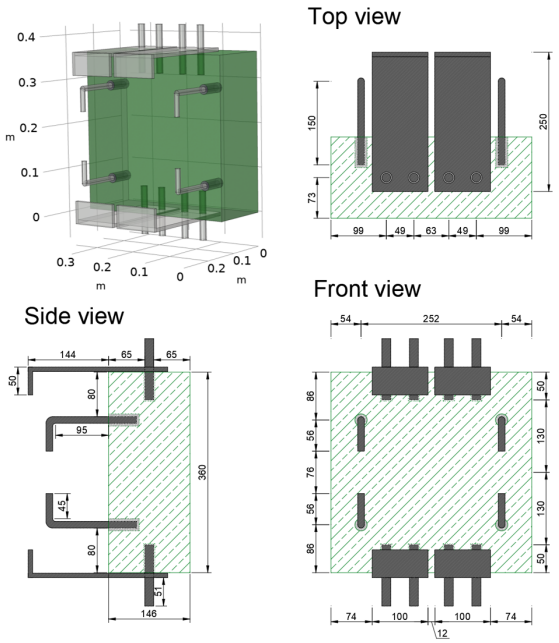

Figure A.4: Sketch of the attachment of the stone blocks in the concrete of the test panels, units in mm.

performed using the same setup, however, the drilled hole possessed 18 mm diameter and 54 mm height. The results are displayed in Figure A.5. The sample with a 16 mm hole had a peak strength of 24.66 kN with a calculated shear strength of 4.85 MPa. The sample with a 18 mm hole had a peak strength of 27.22 kN, with a shear strength of 4.25 MPa.

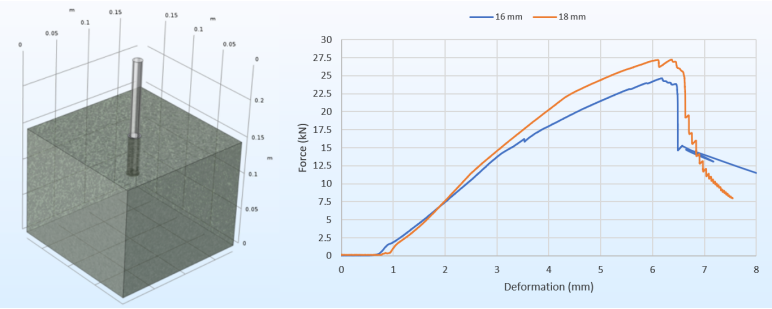

Figure A.5: Sketch and results of pull-out tests.

A.2. HOISTING

In order to handle the panels upon delivery in the factory, it was requested to provide a proof of safety regarding the hoisting of such elements. The calculation is shown below:

A.2.1. KNOWN VALUES:

- The dimensions of the segments are 0.8 x 0.4 x 2.23 m;
- The specific weigt of the segments are considered $25 kN/m^3$ in accordance with DIN 1055-1 [1];
- The adhesion of the mould is considered $2 kN/m^2$ as per oiled, varnished wooden planed boards;
- The maximum angle of lifting is taken as 60, thus giving a chain sling coefficient of 1.16;
- Number of anchor elements per segment is 2;
- The capacity of each individual anchor is equivalent to 49.82 kN.

A.2.2. CRANE FACTORS:

- De-moulding = 1.1;
- Pitching = 1.3;
- Transport at TU Delft = 1.65;
- Transport at factory = 2.5.

A.2.3. MAIN LOADS

Segments deadweight = 0.8 *0.4*2.23*25
Segments deadweight = **17.84 kN**
Adhesion to the mould = 0.8*2.23*2
Adhesion to the mould = **3.58 kN**

A.2.4. LOADS AT THE ANCHORS

De-moulding + pitching = $\frac{(17.84+3.57)/2*1.1*1.3*1.16}{2}$
De-moulding + pitching = **8.88 kN**
Transport at TU Delft = $\frac{17.84*1.65*1.16}{2}$
Transport at TU Delft = **17.07 kN**
Transport at factory = $\frac{17.84*2.5*1.16}{2}$
Transport at factory = **25.87 kN**

A.2.5. MINIMUM ELEMENT THICKNESS (AS DEFINED BY ANCHOR SUPPLIER)

B = 180+10+40
B = 230 mm

A.2.6. PANELS HEIGHT

The maximum height of a panel for edge lifting (pitching) considering a thickness of 250 mm or superior and a strength of the concrete of 35 MPa or superior is recommended as 5,50 meters.

A.2.7. PULL-OUT TEST

The strength of the anchoring system was tested with a scaled concrete sample (made from the mixture in Table 5.1) as shown in Figure A.6. Because the panels were moved from horizontal position to vertical position, two tests were performed, one with the anchors in the direction of the pullout forces and one with the anchor at 90 degrees from the direction of the pullout forces. The test also assumed the worst case scenario on a number of conditions (e. g. the anchors do not have contribution from usual reinforcement, the thickness of the sample is inferior to the test segments).

The concrete used for the sample was tested after one week of casting with no curing. Additionally, compression tests were performed on 100 mm side cubes for quality control, results are found in Table A.1. The built-in anchors were of the type TPA-FS from HALFEN, with a maximum load of 5 tons.

Table A.1: Results of uniaxial compression tests at 7 days.

Sample	Strength (MPa)	Remarks
1	81.99	–
2	81.86	–
3	80.89	–
4	85.01	–
5	75.26	Not compacted

Peak load at test direction > **150 kN**
Peak load at 90 degrees > **50 kN**

A.2.8. RING CLUTCHES AND ANGLE OF LIFTING

The Ring clutches to be used during transportation of the test segments should match the ones using the pullout tests. The product used during the test was TPA-R1 5,0t from HALFEN. Its dimensional specifications are found in Table A.2. This system has the advantage of using removable ring clutches that can be applied for each segment.
The geometry of application of the anchors in the actual test segments can be seen in Figure A.8, as the distance between anchors is 40 cm and the angle used in the calcula-

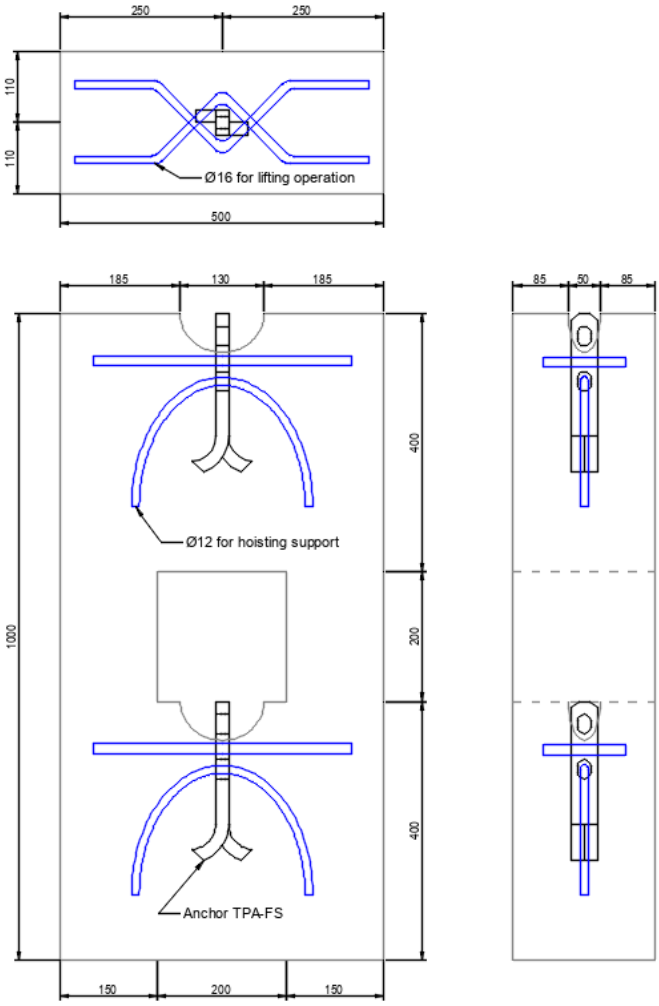

Figure A.6: Geometry of sample used for pullout tests, units in mm.

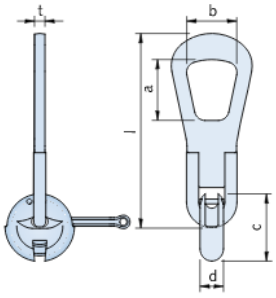

Figure A.7: Ring clutch used during transportation.

Table A.2: TPA-R1 5,0t dimensional specifications.

Detail	Size (mm)
l	330
a	86
b	65
c	105
d	36
t	16

tions was 60, the minimum allowed length of anchor cables in 40 cm. For safety, 1 meter was recommended.

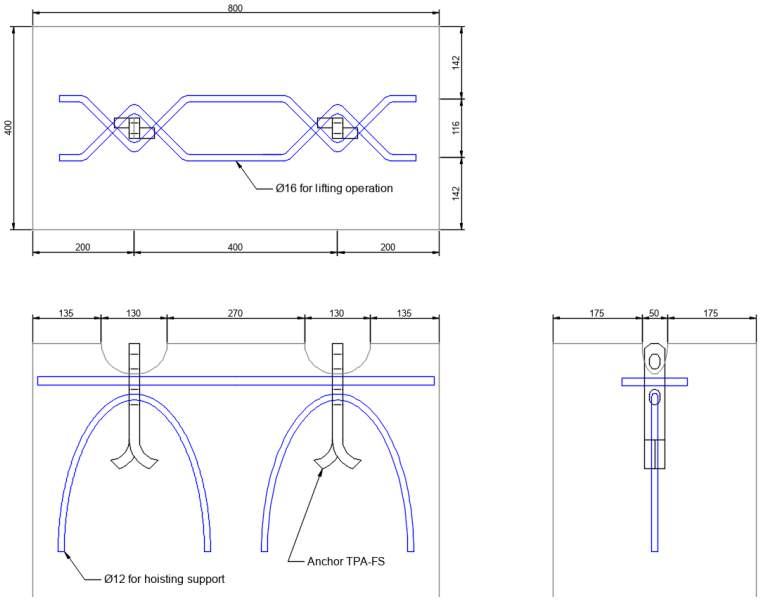

Figure A.8: Details of anchors placement in test panels, units in mm.

A.3. CONCLUSION

The proposed design was in accordance with all the predicted loads. The testing of the anchors proved its capacity to be more than 5 times superior to what was necessary for both the lifting and the transport operation following the factory's safety factor of 2.5. The segments height and thickness were also acceptable, thus it was not expected to perceive any damage during the transport and installation of the test segments, given normal operation standards were respected.

CURRICULUM VITÆ

Fernando FRANÇA DE MENDONÇA FILHO

31-01-1990 Born in Belém, Brazil.

EDUCATION

1996–2006 Primary and middle School
Colégio Moderno, Belém

2005–2007 High School
Colégio Moderno, Belém

2008–2013 Bachelor of Science in Civil Engineering
Universidade da Amazônia

2013–2017 Master of Science in Structural Engineering
Technische Universiteit Delft
Thesis: The Effect of Carbonation and Compressive Stresses on Chloride Ingress in Reinforced Mortars
Promotor: Dr. O. Çopuroğlu

2018–2024 PhD. Civil Engineering
Technische Universiteit Delft
Thesis: Thermal Shock Damage in Building Materials
Promotor: Dr. O. Çopuroğlu

COURSES AND CERTIFICATIONS

2017	Image and modelling of (reactive) fluid transport in geomaterials
2018	Sensitization and prevention of risks in laboratory work
2018	Machine learning with Python
2018	COMSOL multiphysics modelling
2019	Concrete microscopy
2021	COMSOL heat transfer in material processing
2021	Physics with industry
2022	Lime based materials for repairing historic Structures
2022	Corrosion science and corrosion control for infrastructure
2022	Multi-Scale modelling course for concrete

List of Publications

Journal papers

1. **F.F. Mendonça Filho** & O. Çopuroğlu, *Development of concrete resistant to thermal and impact deterioration in factory setting*, Case Studies in Construction Materials, in review.

2. **F.F. Mendonça Filho**, L. de Vilder, E. Schlangen & O. Çopuroğlu, *An analytical equation to predict mortar spalling at laboratory scale*, Construction and Building Materials, Construction and Building Materials (accepted for publication).

3. B. Chen, J. Chen, **F.F. Mendonça Filho**, Y. Sun, M.B. van Zijl, O. Çopuroğlu & G. Ye, *Characterization and mechanical removal of metallic aluminium (Al) embedded in weathered municipal solid waste incineration (MSWI) bottom ash for application as supplementary cementitious material*, Waste Management 176 (2024).

4. M. Nedeljkovic, N. Tošić, P.E. Holthuizen, **F.F. Mendonça Filho**, O. Copuroglu, E. Schlangen, S. Fennis, *Non-destructive screening methodology based on handheld XRF for the classification of concrete: cement type-driven separation*, Materials and Structures 56, 54 (2023).

5. **F.F. Mendonça Filho**, C. Romero Rodriguez, E. Schlangen & O. Çopuroğlu, *Surface effects of molten slag spills on calcium aluminate cement paste*, Materials & Design 217, 110623 (2022).

6. **F.F. Mendonça Filho**, C. Romero Rodriguez, E. Schlangen & O. Çopuroğlu, *Plutonic Rocks as Protection Layers to Concrete Exposed to Ultra-High Temperature*, Materials 15, 3490 (2022).

7. **F.F. Mendonça Filho**, O. Copuroglu, E. Schlangen & B. Šavija, *Determination of Loss of Reinforcement Due to Corrosion through X-ray Computer Micro-Tomography*, Materials 14, 893 (2021).

8. Y. Chen, O. Çopuroğlu, C. Romero Rodriguez, **F.F. de Mendonça Filho** & E. Schlangen, *Characterization of air-void systems in 3D printed cementitious materials using optical image scanning and X-ray computed tomography*, Materials Characterization 173, 110948 (2021).

9. C.L. Justino de Lima, F.A. Veer, H. Zhang, **F.F. Mendonça Filho**, O. Çopuroğlu & R. Nijsse, *Thermal, optical and mechanical properties of new glass compositions containing fly ash*,European Journal of Glass Science and Technology. Part A, 62, 96–108 (2021).

10. C. Romero Rodríguez, **F.F. Mendonça Filho**, S. Chaves Figueiredo, E. Schlangen & B. Šavija, *Fundamental investigation on the frost resistance of mortar with microencapsulated phase change materials*,Cement and Concrete Composites, 113, 103705 (2020).

11. C. Romero Rodríguez, **F.F. Mendonça Filho**, L. Mercuri, Y. Gan, E. Rossi, G. Anglani, P. Antonaci, E. Schlangen & B. Šavija, *Chemo-physico-mechanical properties of the interface zone between bacterial PLA self-healing capsules and cement paste*,Cement and Concrete Research, 138, 106228 (2020).

12. H. Morillas, **F.F. Mendonça Filho**, H. Derluyn, M. Maguregui, D. Grégoire & J.M. Madariaga, *Decay processes in buildings close to the sea induced by marine aerosol: Salt depositions inside construction materials*,Science of The Total Environment, 721, 137687 (2020).

13. **F.F. Mendonça Filho**, H. Morillas, H. Derluyn, M. Maguregui & D. Grégoire, *In-situ versus laboratory characterization of historical site in marine environment using X-ray fluorescence and Raman spectroscopy*, Microchemical Journal, 147, 905–913 (2019).

14. B. Šavija, M. Luković, G.M.G. Kotterman, S.C. Figueiredo, **F.F. Mendonça Filho** & E. Schlangen, *Development of ductile cementitious composites incorporating microencapsulated phase change materials*, International Journal of Advances in Engineering Sciences and Applied Mathematics, 9, 169–180 (2017).

Book chapters

1. **F.F. Mendonça Filho**, Y. Chen & O. Çopuroğlu, *Nano-modification in digital manufacturing of cementitious composites*, Recent Advances in Nano-Tailored Multi-Functional Cementitious Composites, Ed. M. Şahmaran, F. Shaikh & G. Yıldırım, Woodhead Publishing Series in Civil and Structural Engineering, ISBN:978-0-323-85229-6 (2022).

2. E. Schlangen, B. Šavija, S.C. Figueiredo, **F.F. Mendoça Filho** & M. Luković, *Mechanical Properties of Ductile Cementitious Composites Incorporating Microencapsulated Phase Change Materials*, Strain-Hardening Cement-Based Composites, Ed. V. Mechtcherine, V. Slowik & P. Kabele, Springer Netherlands, ISBN:978-94-024-1194-2 (2018).

Conference papers

1. **F.F. Mendonca Filho** & O. Copuroglu, *Re-curing of calcium aluminate cements post contact with molten slag*, 17th Euroseminar on Microscopy Applied to Building Materials, University of Toronto, Toronto, Canada (2019).

2. C. Romero Rodriguez, S.C. Figueiredo, **F.F. Mendonca Filho**, E. Schlangen & B. Savija, *Frost damage progression studied through X-Ray tomography in mortar with Phase Change Materials*, 10th International Conference on Fracture Mechanics of Concrete and Concrete Structures, Université de Pau et des Pays de l'Adour, Bayonne, France (2019).

3. **F.F. Mendonca Filho**, J. Pacheco & O. Copuroglu, *Semi- and full quantitative EDS microanalysis of chlorine in reinforced mortars subjected to chloride ingress and carbonation*, 15th Euroseminar on Microscopy Applied to Building Materials, Delft University of Technology, Delft, The Netherlands (2015).

4. M.R. de Rooij & **F.F. Mendonca Filho**, *Dealing with uncertainty in material characterization of concrete by education*, 15th Euroseminar on Microscopy Applied to Building Materials, Delft University of Technology, Delft, The Netherlands (2015).

5. **F.F. Mendonca Filho**, M. Mira & J.Z.R. Silva Junior, *The Influence of Non-Destructive Test of Ultrasound in the Evaluation of Properties of Structural Concrete (in Portuguese)*, 53° Congresso Brasileiro do Concreto, IBRACON, Florianopolis, Brazil (2011).

6. **F.F. Mendonca Filho** & J.Z.R. Silva Junior, *The Introduction of Fibres to Self-compacting Concrete using the Materials of Belem (in Portuguese)*, 53° Congresso Brasileiro do Concreto, IBRACON, Florianopolis, Brazil (2011).

7. M.D.V. Paumgartten, J.Z.R. Silva Junior, P.L.S. Gomes, **F.F. Mendonca Filho** & A.D.P. Pinheiro Filho, *Self-compacting concrete using materials from the region of Belem (in Portuguese)*, 52° Congresso Brasileiro do Concreto, IBRACON, Fortaleza, Brazil (2010).